IITRI Project M6103
Final Report

DEBRIS FORMATION AND TRANSLATION

Distribution of this Document is Unlimited

Prepared for
Department of the Army
Office of the Secretary of the Army
Office of Civil Defense

OCD-PS-64-201 Work Unit 3322B

IITRI Project M6103
Final Report

DEBRIS FORMATION AND TRANSLATION

Distribution of this Document is Unlimited

Prepared for
Department of the Army
Office of the Secretary of the Army
Office of Civil Defense

OCD-PS-64-201 Work Unit 3322B

IIT Research Institute
Technology Center
Chicago, Illinois 60616

IITRI Project M6103

Final Report

DEBRIS FORMATION AND TRANSLATION

SUMMARY

by
Ralph L. Barnett
James F. Costello
David I. Feinstein

Prepared for

Department of the Army
Office of the Secretary of the Army
Office of Civil Defense

OCD-PS-64-201
Work Unit 3322B

November 1966

DEBRIS FORMATION AND TRANSLATION SUMMARY

INTRODUCTION

This report represents a systematic effort to examine the physical basis for predicting the final location of blast-initiated debris. There are three principal sources of this debris:

- Frangible structural elements, such as masonry wall panels.
- Nonfrangible structural elements, such as building frames and wood or metal siding and roofing.
- Building contents.

The first two categories require a method to predict the loads at which they will come apart and the kinds of pieces into which they will break, or more generally, a method of failure prediction. Chapters Two and Three of this report deal with this problem.

Presuming a knowledge of the failure modes, the important question from a postattack point of view is: how much of these elements end up obstructing the adjacent roadway? More particularly, there is interest in the weight-size-composition, height, and total volume of matter in the desired right-of-way. Chapter Four is concerned with the construction of a computer-oriented model to predict the distribution of "loose particles", that is, structural fragments and building contents. Also in Chapter Four, assorted loose ends are tied up concerning the finer points associated with the transport model.

A summary of the state-of-the-art in debris prediction is shown in Table 1, an examination of which will show that with the results given in this report, the theoretical basis for debris prediction is pretty well covered. However, a few holes still exist. The most noticeable is the restriction of the fragmentation model to homogeneous wall panels. Further modification will be required to be able to handle nonhomogeneous wall panels.

Since a great number of walls (including those made of brick), are in this category, such an extension would be desirable.

Table 1
SUMMARY OF DEBRIS-PREDICTION

Debris Source	Method of Failure Prediction	Method of Final Location Prediction
Frangible Structural Elements	Fragmentation Theory	Transport Model
Nonfrangible Structural Elements	Limited Plasticity	Continuity (Frames) Transport Model (Siding and Roofing)
Building Contents	Not Applicable	Transport Model (Plus overturning and sliding analysis for diffraction-sensitive items.)

NONFRANGIBLE STRUCTURAL ELEMENTS

Debris resulting from the effects of blast on nonfrangible structural elements, such as beams and columns, seems worthy of consideration in any attempt to provide meaningful inputs for postattack recovery planning. This follows from the fact that while elements of this sort have a smaller volume of potential debris than frangible ones, the resulting "particles" will be larger, more cumbersome, and hence, more demanding, pound for pound, in any clean-up effort. With this motivation, we have striven to develop an analytical procedure capable of predicting the size and weight distribution of the debris deposited, in a nuclear blast environment, by elements which have some ductility. Such elements will be denoted as nonfrangible to distinguish them from frangible (or brittle) ones, such as

unreinforced wall panels, which have no capacity to absorb energy beyond their yield points.

For all practical purposes, the load-response behavior of nonfrangible structural elements can be divided into two categories, based on the plastic regions of their stress-strain diagrams. The response is either sufficiently ductile to allow the use of an elastic-perfectly plastic model or the amount of strain that can be accommodated is limited, requiring a "limited plasticity" model. The former case, which has been thoroughly investigated over the last twenty years, is generally applicable to steel-framed structures. The latter case, which is appropriate for reinforced-concrete structures, was considered and the effect of the limited ductility was demonstrated.

Finally, a small series of experiments on model frames was devised to check the validity of the limited-plasticity model and verify the hypothesis that any energy supplied to a frame in excess of that necessary to cause collapse is taken up by rotations of the plastic hinges to the extent of their capacities and acceleration of the mechanism, rather than in secondary damage between hinges. The information gained from this series of experiments was qualitative in nature.

Some conclusions about the utility of the theories and techniques demonstrated are:

- The limited-plasticity theory provides a realistic approach for predicting blast-induced debris from nonfrangible structural elements in a manner which is consistent with, and indeed an extension of, design procedures.
- Recourse to modern computer-oriented analysis techniques overcomes the prohibitive computational complexity which heretofore has inhibited applications of limited plasticity.

- Models of reinforced-concrete structures, constructed at low cost from inexpensive materials, can be used to provide meaningful answers to questions about debris production which characteristically involve gross behavior such as the collapse mode.

FRAGMENTATION OF FRANGIBLE STRUCTURAL ELEMENTS

The frangible plate structure represents a significant debris producing element in the form of wall panels and a vital source of dangerous missiles in the form of plate glass. The fragmentation characteristics of such structures are studied in this section using a pragmatic approach which blends results from statistical fracture theory with those recently obtained by IITRI on an experimental study of dynamically-loaded plaster plates (Ref. 1). The work extends the considerations of two previous investigations on beam fragmentation to the plate (Ref. 2 and 3).

The general fragmentation algorithm consists of four steps:

- Determine the maximum dynamic stresses throughout the plate.
- Compute the probability of fracture initiation throughout the plate.
- Divide the plate into appropriate regions based on crack propagation.
- Compute the distribution of fragment "sizes."

Three computational procedures are described for determining the distribution of fragment sizes. Each of these methods begins by dividing a plate into regions or strips formed by the principal stress trajectories. These strips independently fracture or remain intact and the combination of fracture and

nonfracture determines the geometry and number of fragments. The first computation scheme, the combination method, considers individually each of the possible 2^n combinations of failure and nonfailure of the strips where n is the total number of strips. This method provides the specific description and quantity of every possible fragment, and in addition, it details the various possible mixtures of large and small fragments. It unfortunately, is very time consuming even with the aid of very large computers.

If we are not interested in how the various fragments are mixed together, we can adopt a very efficient procedure called the fragment group method, for calculating the total number of every possible type of fragment. Here, there are only $(n/2)(n+1)$ combinations of fragment groups to be considered. Although the increased efficiency of the method of fragment groups is considerable, an even faster method can be used if we again settle for less information. The final method, called the method of runs, determines the number of identical contiguous nonfractured strips. It will not furnish information about fragment geometry; only fragment weights.

TRANSPORT MODEL

In order to represent the effect of debris transport and subsequent distribution, it is necessary to move from a problem space consisting of the real world to a more abstract mathematical model. This abstraction consists of representing the initial condition of possible debris as a series of lumped masses at levels above ground. Each lumped mass is characterized by a unique particle size distribution. The particle size, in turn, has weight and shape attributes associated with it. The trajectory model assumes two ideal initial conditions. These are:

- Zero failure time of fragmented elements.
- An initial particle velocity of zero.

These assumptions were made, initially, due to a lack of knowledge concerning any other possible values.

A study concerning these parameters has since been made and is reported. The result of this study indicates that the initial assumptions are well grounded.

SINBAD (Simulation Investigation of Nuclear Blast Associated Debris) is a problem-oriented computer language that deals with the problem of postattack structural debris. In a previous investigation (Ref.3) debris profile curves (i.e., height of debris versus distance thrown) were developed for a free-standing masonry panel wall. Several analyses, both manual and computerized, were utilized to predict the profile of a single wall. The present study is a refinement of the previous techniques and is extended to include any grouping of walls subjected to a frontal shock. It is now also possible to determine the size distribution and a measure of the momentum of the debris at any point in the profile. The language is expandable and in its entirety will include frame response as well as the interior contents of the structure. The flow diagram indicates the general computational scheme. The boxes that are now dotted are components that will be added to the system at a later time.

REFERENCES

1. Liber, T., Experimental Study of Fragmentation of Structural Wall Panels, for OCD, Contract No. OCD-PS-64-50, October 1966.

2. Ahlers, E. B., Debris Clearance Study, OCD Contract No. OCD-OS-62-202, Subtask 3322A; IIT Research Institute Project No. M264, September 1963.

3. Feinstein, D. I., Debris Distribution, Task 3322B for Office of Civil Defense, Washington, D.C., August 1965.

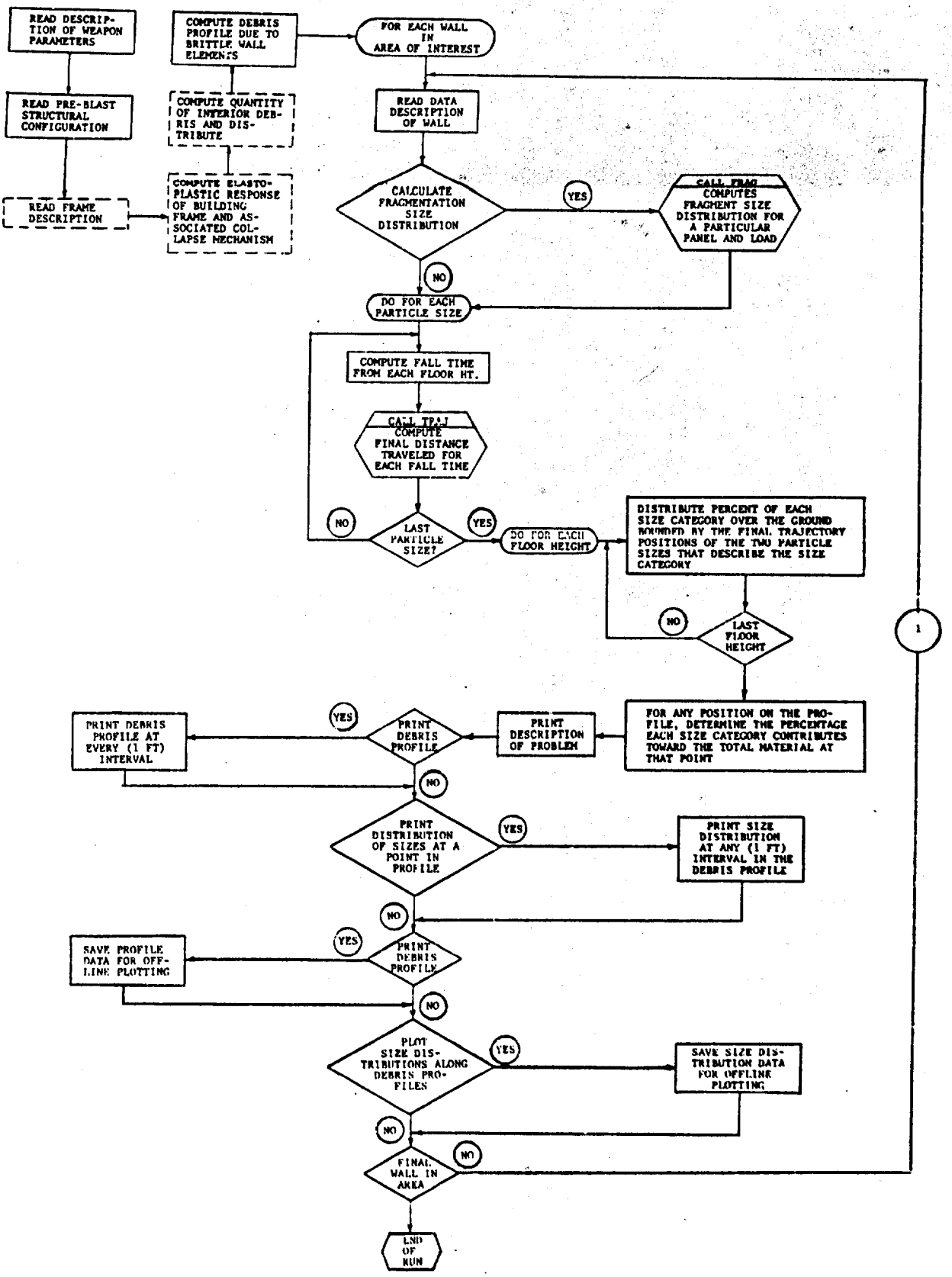

COMPUTATIONAL FLOW GRAPH FOR SINBAD

IIT RESEARCH INSTITUTE
Technology Center
Chicago, Illinois 60616

IITRI Project M6103

Final Report

DEBRIS FORMATION AND TRANSLATION

by

Ralph L. Barnett
James F. Costello
David I. Feinstein

Prepared for

Department of the Army
Office of the Secretary of the Army
Office of Civil Defense

OCD-PS-64-201
Work Unit 3322B

November 1966

FOREWORD

This is the Final Report on the research performed under Subcontract No. B-70942(4949 A-34)-US, "Debris Formation and Translation". The major topics investigated were:

- Debris generated by nonfrangible structural elements.
- Fragmentation of plate-type elements.
- Trajectory of debris particles.

Limited investigations were also performed on selected topics relevant to debris prediction.

Respectfully submitted,

J. Costello
Associate Research Engineer

R. L. Barnett
Program Manager

APPROVED:

C. A. Miller
Assistant Director of Research
Mechanics Research Division

DEBRIS FORMATION AND TRANSLATION

by

Ralph L. Barnett
James F. Costello
David I. Feinstein

ABSTRACT

A comprehensive view is taken of the physical models required to estimate volumes and heights of blast-initiated debris. Particular emphasis and development is directed toward three areas: the fragmentation of frangible elements, the failure of elements with limited ductility, and the transport of debris particles by blast winds. Computer programs to handle the computations involved in these three models have been written.

CONTENTS

CONTENTS (Contd)

ILLUSTRATIONS

ILLUSTRATIONS (Contd)

ILLUSTRATIONS (Cont'd)

TABLES

CHAPTER ONE
INTRODUCTION

1.1 PERSPECTIVE OF DEBRIS PREDICTION

This report represents a systematic effort to examine the physical basis for predicting the final location of blast-initiated debris. There are three principal sources of this debris:

- Frangible structural elements, such as masonry wall panels.
- Nonfrangible structural elements, such as building frames and wood or metal siding and roofing.
- Building contents.

The first two categories require a method to predict the loads at which they will come apart and the kinds of pieces into which they will break, or more generally, a method of failure prediction. Chapters Two and Three of this report deal with this problem.

Presuming a knowledge of the failure modes, the important question from a postattack point of view is: how much of these elements end up obstructing the adjacent roadway? More particularly, there is interest in the weight-size-composition, height, and total volume of matter in the desired right-of-way. Chapter Four is concerned with the construction of a computer-oriented model to predict the distribution of "loose particles", that is, structural fragments and building contents. Also in Chapter Four, assorted loose ends are tied up concerning the finer points associated with the transport model.

A summary of the state-of-the-art in debris prediction is shown in Table 1, an examination of which will show that with the results given in this report, the theoretical basis for

Table 1

SUMMARY OF DEBRIS-PREDICTION

Debris Source	Method of Failure Prediction	Method of Final Location Prediction
Frangible Structural Elements	Fragmentation Theory	Transport Model
Nonfrangible Structural Elements	Limited Plasticity	Continuity (Frames) Transport Model (Siding and Roofing)
Building Contents	Not Applicable	Transport Model (Plus overturning and sliding analysis for diffraction-sensitive items.)

debris prediction is pretty well covered. However, a few holes still exist. The most noticeable is the restriction of the fragmentation model to homogeneous wall panels. Further modification will be required to be able to handle nonhomogeneous walls. Since there are a great number of walls in this category, which includes those made of brick, such an extension would be desirable.

CHAPTER TWO
DEBRIS GENERATED BY NONFRANGIBLE STRUCTURAL ELEMENTS

2.1 INTRODUCTION

Debris resulting from the effects of blast on nonfrangible structural elements, such as beams and columns, seems worthy of consideration in any attempt to provide meaningful inputs for postattack recovery planning. This follows from the fact that while elements of this sort have a smaller volume of potential debris than frangible ones, the resulting "particles" will be larger, more cumbersome, and hence, more demanding, pound for pound, in any clean-up effort. With this motivation, we have striven to develop an analytical procedure capable of predicting the size and weight distribution of the debris deposited, in a nuclear blast environment, by elements which have some ductility. Such elements will be denoted as nonfrangible to distinguish them from frangible (or brittle) ones, such as unreinforced wall panels, which have no capacity to absorb energy beyond their yield points.

For all practical purposes, the load-response behavior of nonfrangible structural elements can be divided into two categories, based on the plastic regions of their stress-strain diagrams. This distinction is shown in Fig. 1 for a bending member where moment corresponds to stress and rotation to strain. The response is either sufficiently ductile to allow the use of an elastic-perfectly plastic model or the amount of strain that can be accommodated is limited, requiring a "limited-plasticity" model. The former case, although rather thoroughly investigated over the last 20 years, is of little interest for debris-prediction purposes. The latter model, however, has considerable applicability (Ref. 1). In the first place, the removal of both metal and wooden siding from building frames can be formulated as a limited plasticity problem since the mode of failure involves both rupture at connections and tearing apart of the

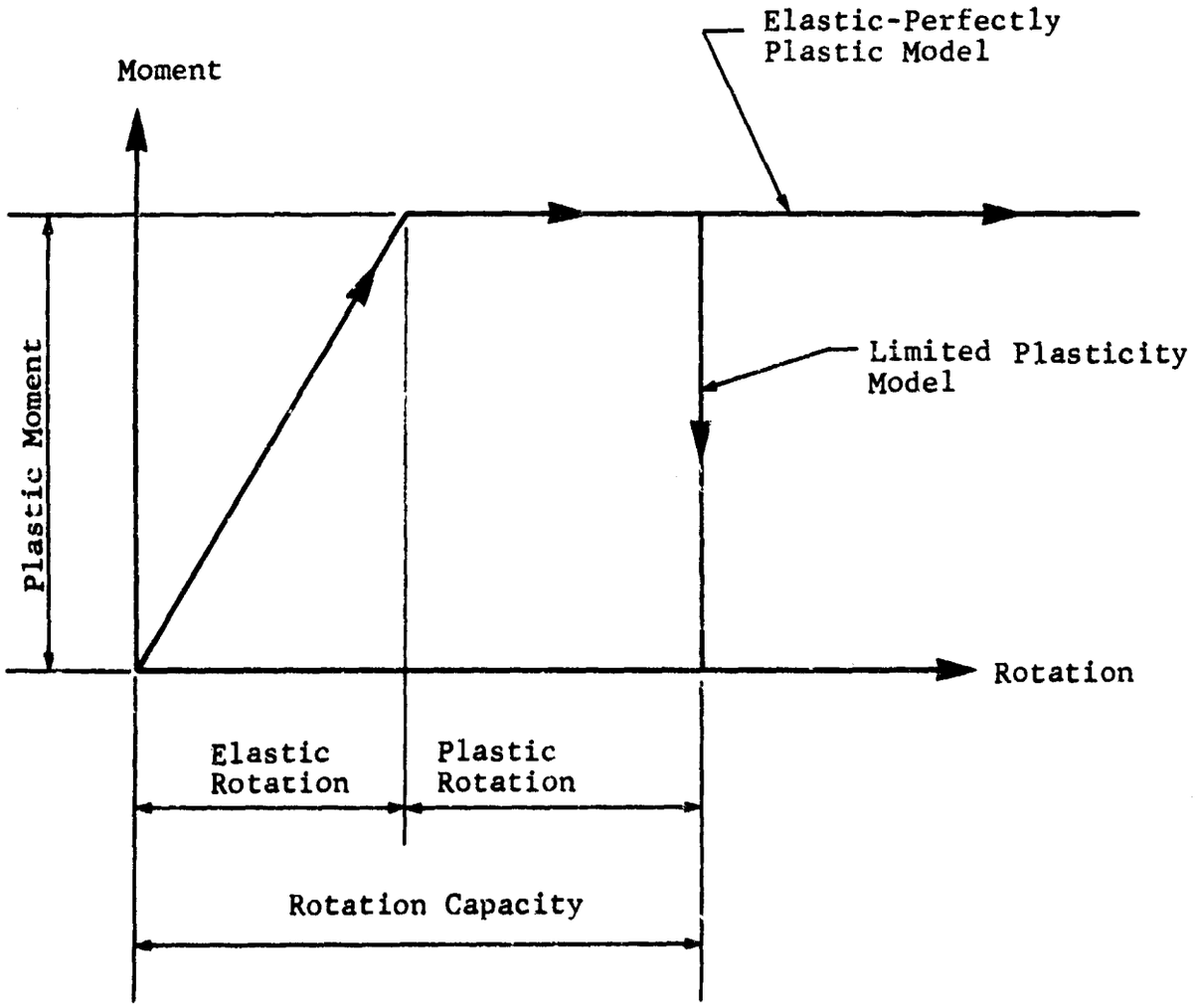

Fig. 1 ELASTIC-PERFECTLY PLASTIC AND LIMITED ROTATION MODELS

panels after large deformations. This aspect was not treated in detail in this portion of the research effort, but rather, attention was focused on the more difficult application to the collapse of reinforced concrete frames. However, the goal of this study was an ability to predict the locations on a reinforced concrete frame at which the inelastic rotations will be sufficiently large for the reinforcing steel to be exposed. The steel can be cut at these points and the structure dismantled. This corresponds to a first (or ready-made) level of debris clearance. Attempts to break the structure into smaller pieces will require chipping away the concrete in order to sever the reinforcement.

2.2 LIMITED PLASTICITY OF FRAMES

The behavior of reinforced concrete frames is still quite a controversial subject (Ref. 2). One point of view insists that for multistory frames in particular, the loss of stiffness due to the beam-column effect must be considered in ultimate load calculations and is supported by experiments on model frameworks (Ref. 3 through 6). However, an analysis of this sort neglects the support given by walls and floors and is bound to be overly conservative when applied to complete buildings. Even in an examination of blast-load effects on framed buildings, where the walls are considered to have been removed by the diffraction loading, beam-column effects are important only in tall, slender frames. We will concentrate on the simpler theory which is applicable to the great majority of buildings. Another basic item of contention is the choice of a model to represent the flexural behavior of reinforced concrete. One side demands that "strain-softening" (i.e., resistance increasing to a maximum and then decreasing smoothly as the deformation increases) be included in the model. (Consult the papers by Barnard and Rosenblueth in Ref. 2). The other, and preponderant, viewpoint expressed in the paper of Baker and Amarakone, also in Ref. 2, adopts a limited-plastic model of

the type shown in Fig. 1. We have gone along with the majority in using the straight-line model for limited plasticity. The reasoning on our part was simple since we are concerned with the plastic moment, rotation capacity, and energy absorption (which is the area under the curve). Thus, whatever the exact shape of the moment-rotation curve may be, a la Bernard and Rosenbleuth, we can pick three straight-line segments which will match those salient characteristics. (This is done at the expense of accuracy in the "elastic rotation" which we do not care about.)

Once the moment at a section becomes equal to the plastic moment, a "plastic hinge" is formed and the rotation increases at constant moment. If we postulate a limited rotation capacity, the behavior beyond that amount is like a "real hinge" and rotation increases, but no moment is transmitted across the section. Clearly then, if the rotation at a point in a loaded structure exceeds the capacity at that point, the ultimate load which can be carried will be the same as would be indicated by an analysis of a modified structure that had a real hinge at the point in question. Moreover, and of greater interest from the debris removal aspect, the hinge pattern will differ in general from that found under an assumption of unlimited rotation capacity.

In order to have the ability to assess rapidly the magnitudes of the inelastic rotations encountered in a large framed structure, a computational method, first suggested by Wang (Ref. 7) as a limit analysis procedure, was programmed for IIT Research Institute (IITRI) 7094 computer. Basically, the approach is to perform a sequence of elastic analyses on the structure. Consider a given structure and loading pattern. If an elastic analysis is performed, and the location of maximum moment determined, the load factor can be adjusted to cause a plastic hinge to form at that point. Then, after adjusting the moments at all nodes in accordance with this load factor, the remaining moment resistances can be found. Next, an elastic analysis

performed on a structure which is identical with the original one (except for a pin inserted at the location of the plastic hinge) will indicate the node having the maximum moment. A load factor can then be found which will induce a moment at that point equal to its remaining moment resistance, implying the formation of a plastic hinge. This process is repeated until a collapse mechanism is formed. The sum of the load factors for all cycles is the ultimate load factor.

This method may seem roundabout, and perhaps it is, but it is well suited for the exceptionally efficient computer solutions utilizing matrix algebra, since the modifications can be performed automatically during the analysis. Also, the inelastic rotations can be computed at each stage, permitting inclusion of the effect of limited rotation capacity. The basis for the calculations is the well-known deflection method, where, using matrix notation, the member end-rotations, $\{\phi\}$, and moments $\{M\}$, are vectors related by the stiffness matrix S,

$$\{M\} = S\{\phi\} \tag{1}$$

The external forces, $\{P\}$, are related to the end moments by the beam and bent equations,

$$\{P\} = A\{M\}. \tag{2}$$

It follows that the external displacements, $\{X\}$, are related to the end rotations by

$$\{\phi\} = A^T\{X\}, \text{ where } A^T \text{ is the transpose of A.} \tag{3}$$

The procedure for solution is to use Eqs. (1), (2), and (3) to solve for the displacements,

$$\{X\} = \left[A\,S\,A^T\right]^{-1}\{P\}, \tag{4}$$

and then to compute the end moments by

$$\{M\} = \left[S\, A^T\right]\{X\}. \tag{5}$$

If the stiffness matrix of the original structure is designated as S_o, the end rotations at the end of the first cycle and corresponding to the formation of the first plastic hinge, computed by either Eq. (1) or (3) as

$$\{\phi\} = \left[S_o\right]^{-1}\{M\} \tag{6}$$

will be identical. After subsequent cycles, during which the stiffness matrix of the structure has been modified, the inelastic rotation at the nodes H will be given by the difference

$$\{H\} = \left[S_o\right]^{-1}\{M\} - A^T\{X\}. \tag{7}$$

A listing of the FORTRAN IV computer program is given in Appendix A.

2.3 RESULTS OF FRAME STUDIES

A limited-plasticity analysis of a framed structure can give results which will differ from those of a standard limit analysis in three areas:

- the ultimate load carried,
- the total energy absorbed, and
- the final collapse mode.

Two example problems were run to demonstrate these disparities. The first example demonstrates the reductions in both ultimate load and energy-absorption due to limited rotation capacity. The frame analyzed is shown in Fig. 2 along with the notation consistent with the computer program. As can be seen in Fig. 3, an elastic-perfectly plastic (i.e., "limit") analysis will indicate collapse at a load factor of 3000. Now, for purposes of

L = 10

All members have: $M_p = 6 \times 10^3$

$EI = 18 \times 10^5$

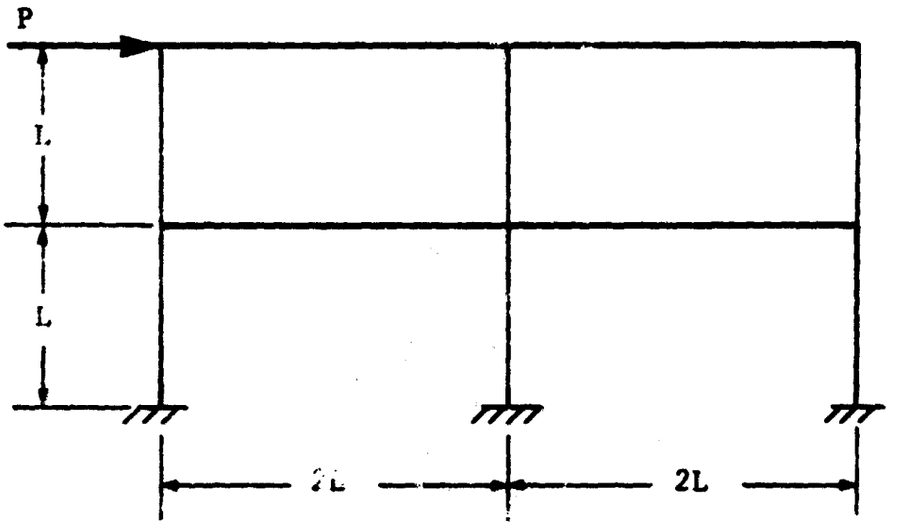

(a) Dimensions and Loading

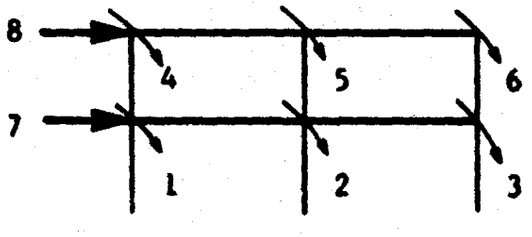

(b) External Force - Displacement Notation

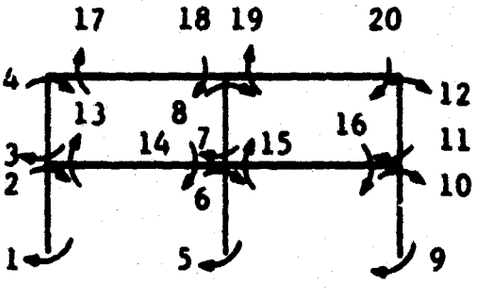

(c) Internal Moment - Rotation Notation

Fig. 2 FRAME USED IN SAMPLE PROBLEM

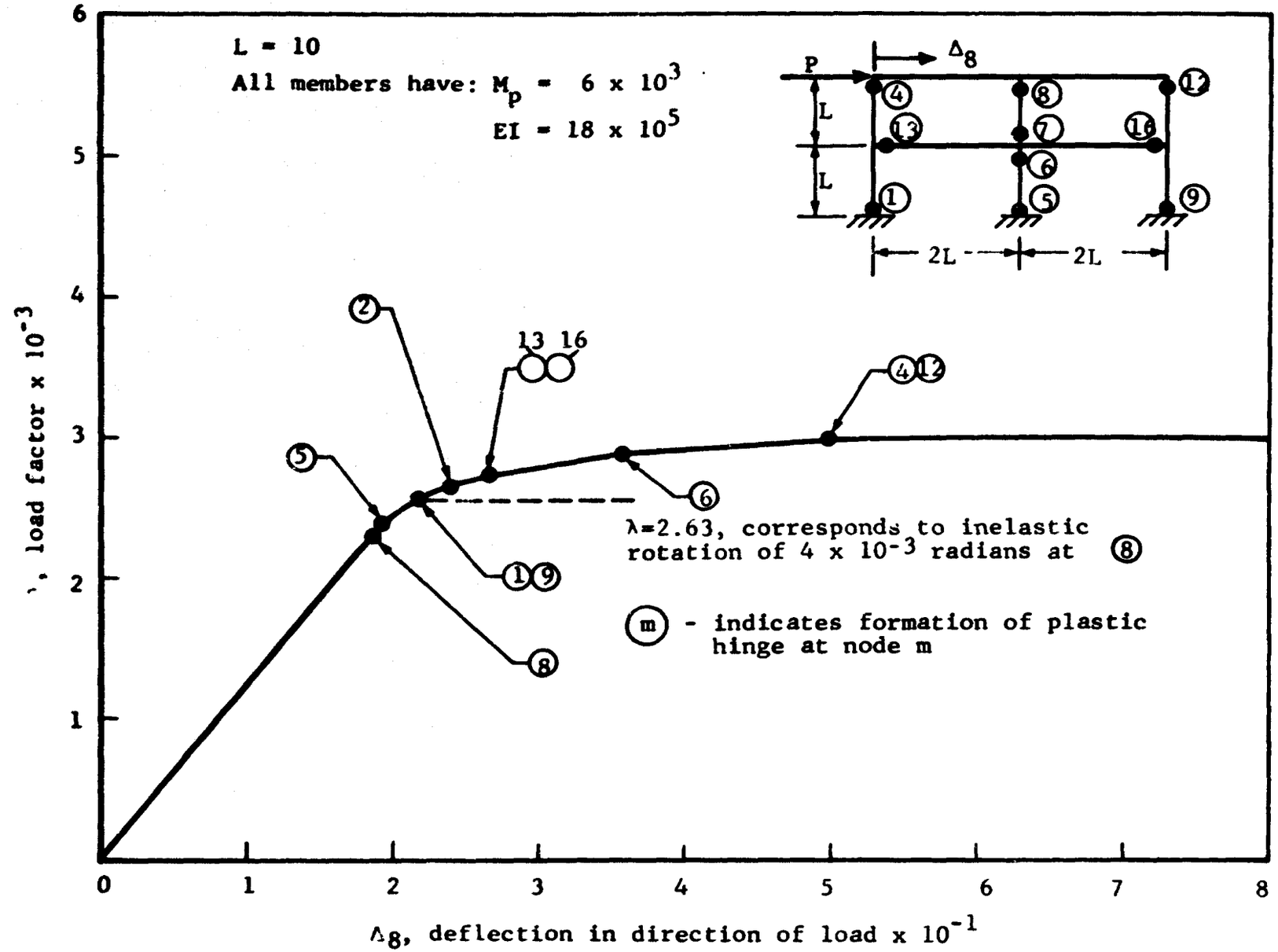

Fig. 3 ELASTIC-PLASTIC ANALYSIS OF ORIGINAL FRAME

illustration, say that the inelastic rotation capacity at all nodes is 0.004 radian. An examination of the computer output for this problem, which is displayed as Appendix B, will show that with this restriction the inelastic rotation at node 8 becomes critical. A linear interpolation between load factors and hinge rotations allows us to fix the load factor consistent with the rotation constraint at 2630.

To find the energy absorbing capacity of the frame, we consider the load which can be supported by the frame under imposed deformation. When the rotation capacity at node 8 is exceeded, the load which can be sustained is that associated with the same deformation in a frame, identical with the original frame except for a real hinge at node 8. An elastic-perfectly plastic analysis can be run on such a frame and the effects of the rotation constraints found. In this manner, a series of modified frames can be considered and the solid curve shown in Fig. 4 constructed. The area under this curve is a measure of the energy which can be absorbed by the frame in question.

To illustrate the possibility of restrictions on rotation capacity leading to a different collapse mode, the frame shown in Fig. 5, 6, and 7 was analyzed. Since node 16 proved to be critical in this case, it was assumed that its rotation capacity would be exceeded while that of all other nodes would not. The structure was then analyzed with a real hinge inserted at node 16. The results are shown in Fig. 8 and 9. It can be seen that not only is the collapse load lowered, but also the mode of collapse differs, since dead loads are included. In the previous example, since only side-on loads acted, the collapse had to be in a side sway mode.

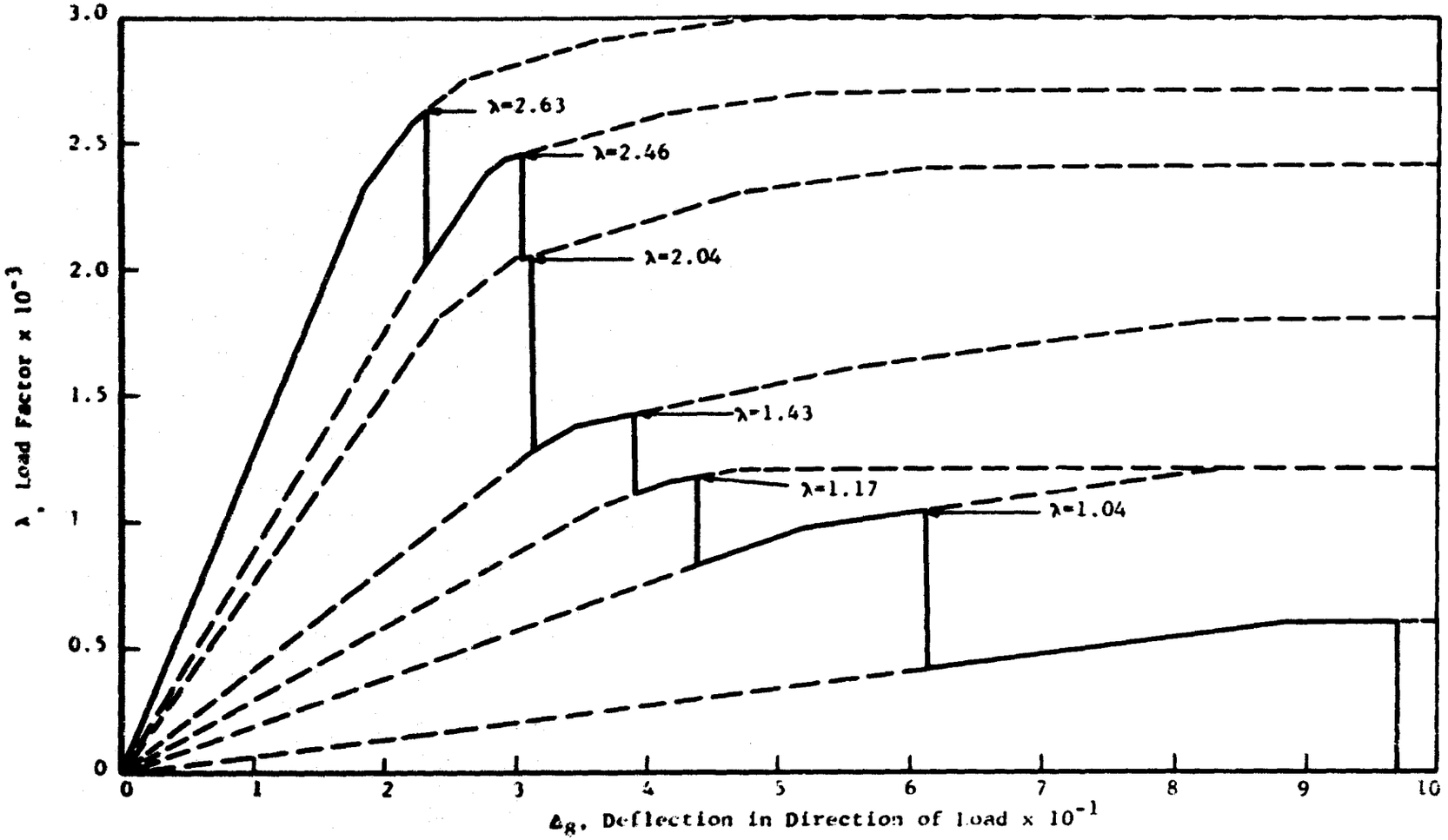

Fig. 4 ENERGY-ABSORBING CAPACITY OF FRAME

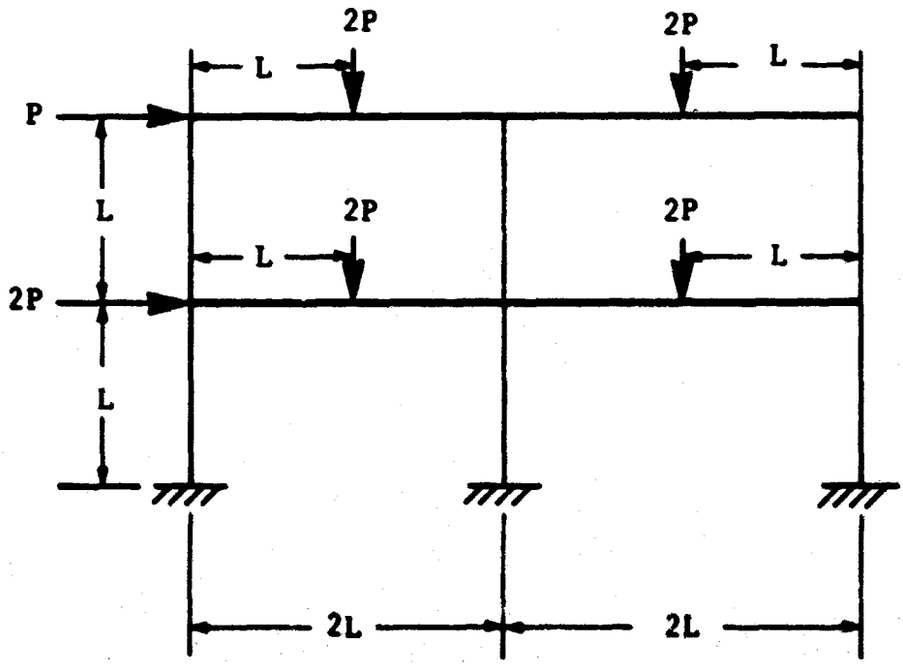

All members have the same stiffness, EI, and plastic moment, PM.

Fig. 5 LOADING AND GEOMETRY FOR SAMPLE PROBLEM

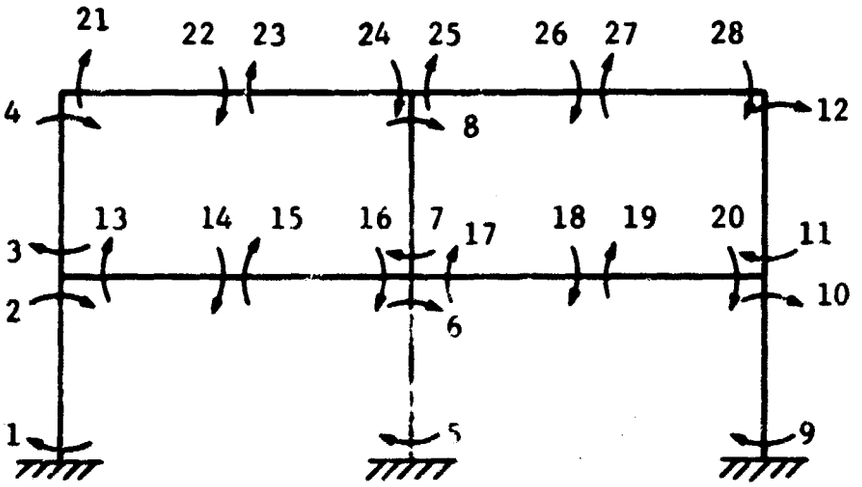

Fig. 6 POSITIVE DIRECTIONS FOR END MOMENTS AND ROTATIONS

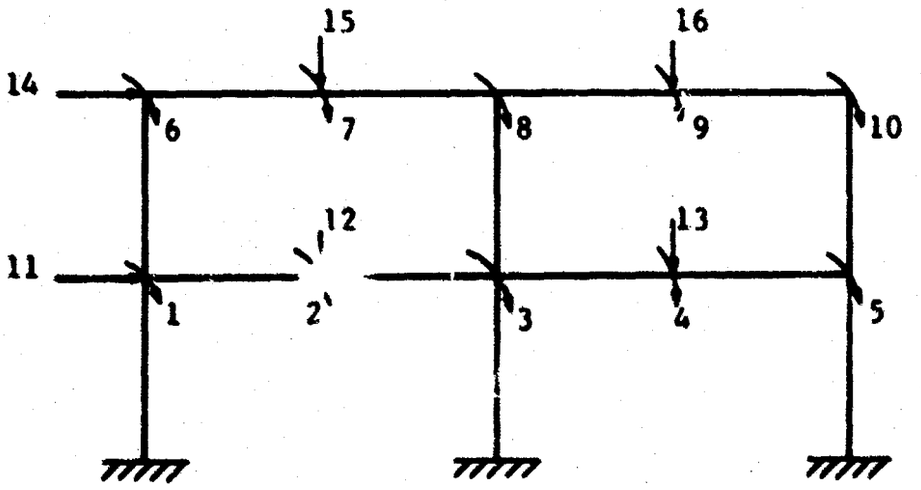

Fig. 7 POSITIVE DIRECTIONS FOR EXTERNAL FORCES AND DISPLACEMENTS

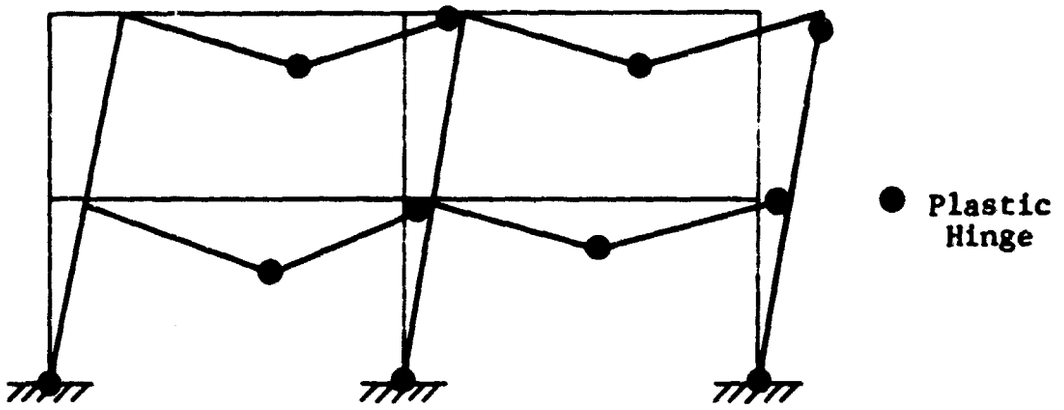

Fig. 8 COLLAPSE MECHANISM FOR CASE NO. 1, $P_u = 950$

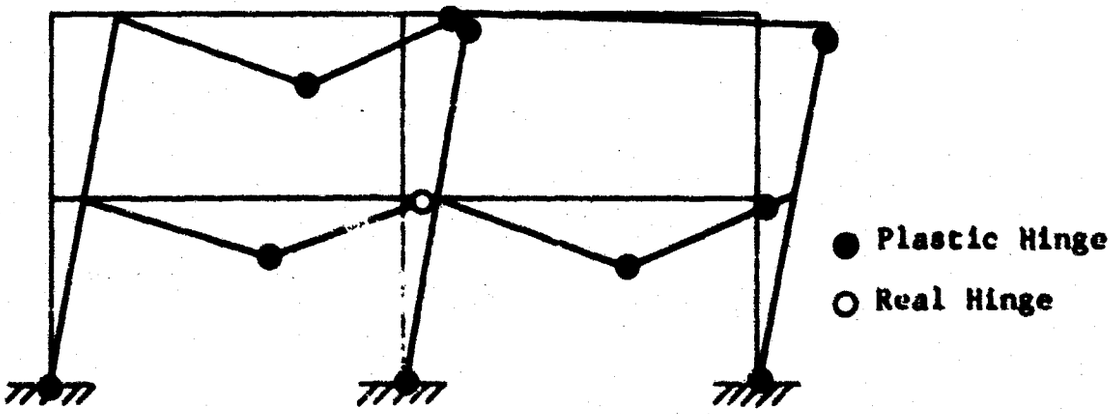

Fig. 9 COLLAPSE MECHANISM FOR CASE NO. 2, $P_u = 840$

2.4 QUALITATIVE FRAME EXPERIMENTS

A small series of experiments on model frames was devised to check the validity of the limited-plasticity model and verify the hypothesis that any energy supplied to a frame in excess of that necessary to cause collapse is taken up by rotations of the plastic hinges to the extent of their capacities and acceleration of the mechanism rather than in secondary damage between hinges The information to be gained from this series of experiments was qualitative in nature.

The geometry of the frames tested is shown in Fig. 10. The materials used were Hydrostone plaster and a soft wire reinforcement. The mold used to case the frames is displayed in Fig. 11. Due to the small percentage of reinforcement, about 1 percent, the behavior of the frames was governed almost entirely by the reinforcement. Static collapse load predictions are shown in Fig. 12 and the observed collapse loads in Fig. 13 and 14. Since the objectives were qualitative in nature, the static collapse tests were performed in a Riehle testing machine for ease of load application. The fact that the load scale on this machine only permitted readings to the nearest 10 lb was still sufficient to show satisfactory agreement between prediction and observation. Further verification of the limited-plasticity theory was gained from the static collapse test on the single-story frame. The history of the failure was as follows:

- At a load somewhat below 100 lb, cracks became visible at the column bases.
- Deformation continued without increase in load at about 100 lb.
- As deformation increased, the load fell suddenly to about 50 lb.
- After further deformation at this level, the load fell to zero.

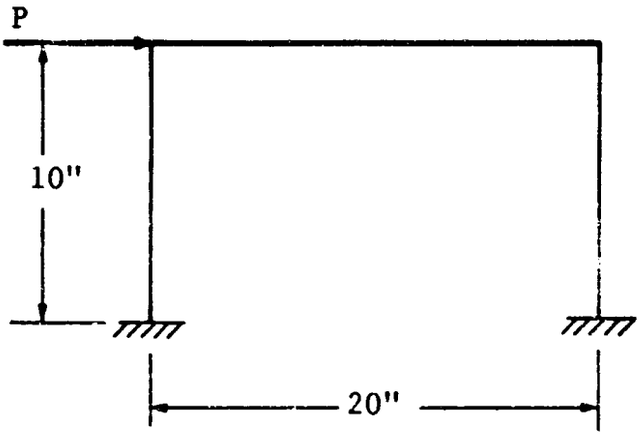

Single-Story Frame

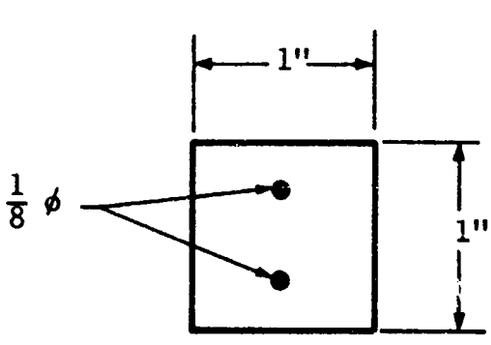

Cross Section
(uniform)

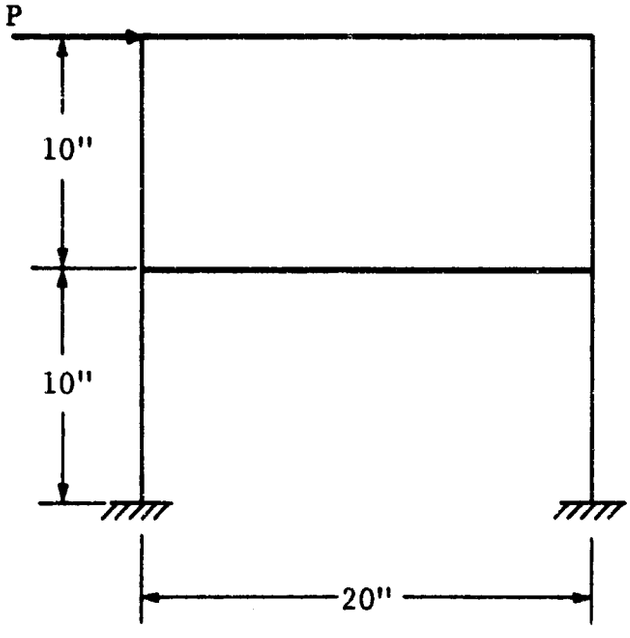

Two-Story Frame

Fig. 10 TEST FRAMES

Fig. 11 MOLD FOR MODEL FRAMES

$M_p = T_u(d + d') - ca = T_u(d' + d)$

Since the moment due to the compressive force is negligible.

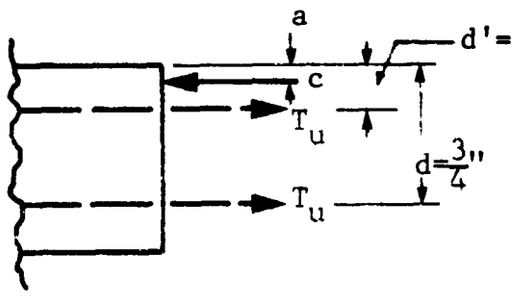

Test data indicate $T_u = 240\#$

$\therefore M_p = 240\ (\frac{1}{4} + \frac{3}{4}) = 240$ in.#

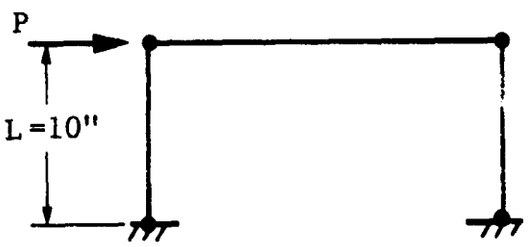

$$P_u = \frac{4M_p}{L} = \frac{4(240)}{10} = 96\#$$

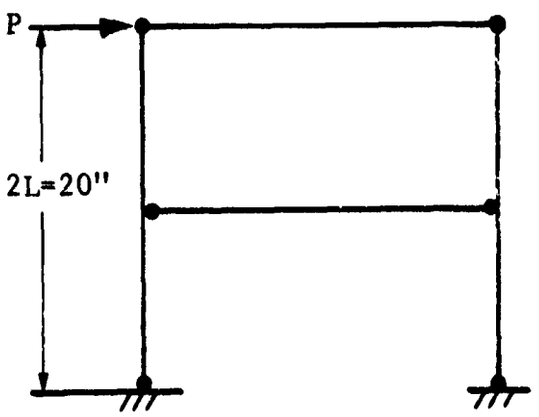

$$P_u = \frac{3M_p}{L} = \frac{3(240)}{10} = 72\#$$

Fig. 12 STATIC COLLAPSE LOAD PREDICTION

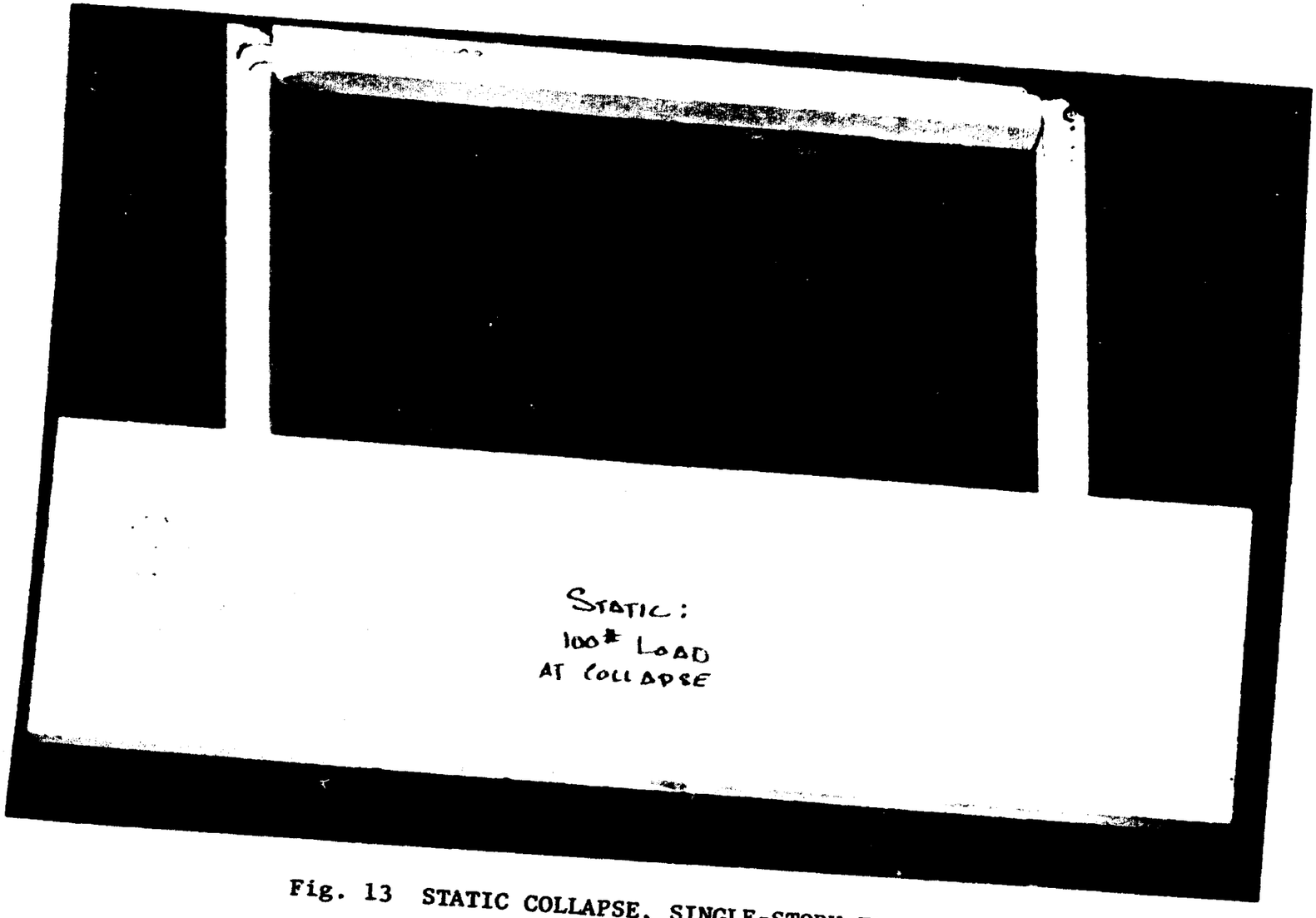

Fig. 13 STATIC COLLAPSE, SINGLE-STORY FRAME

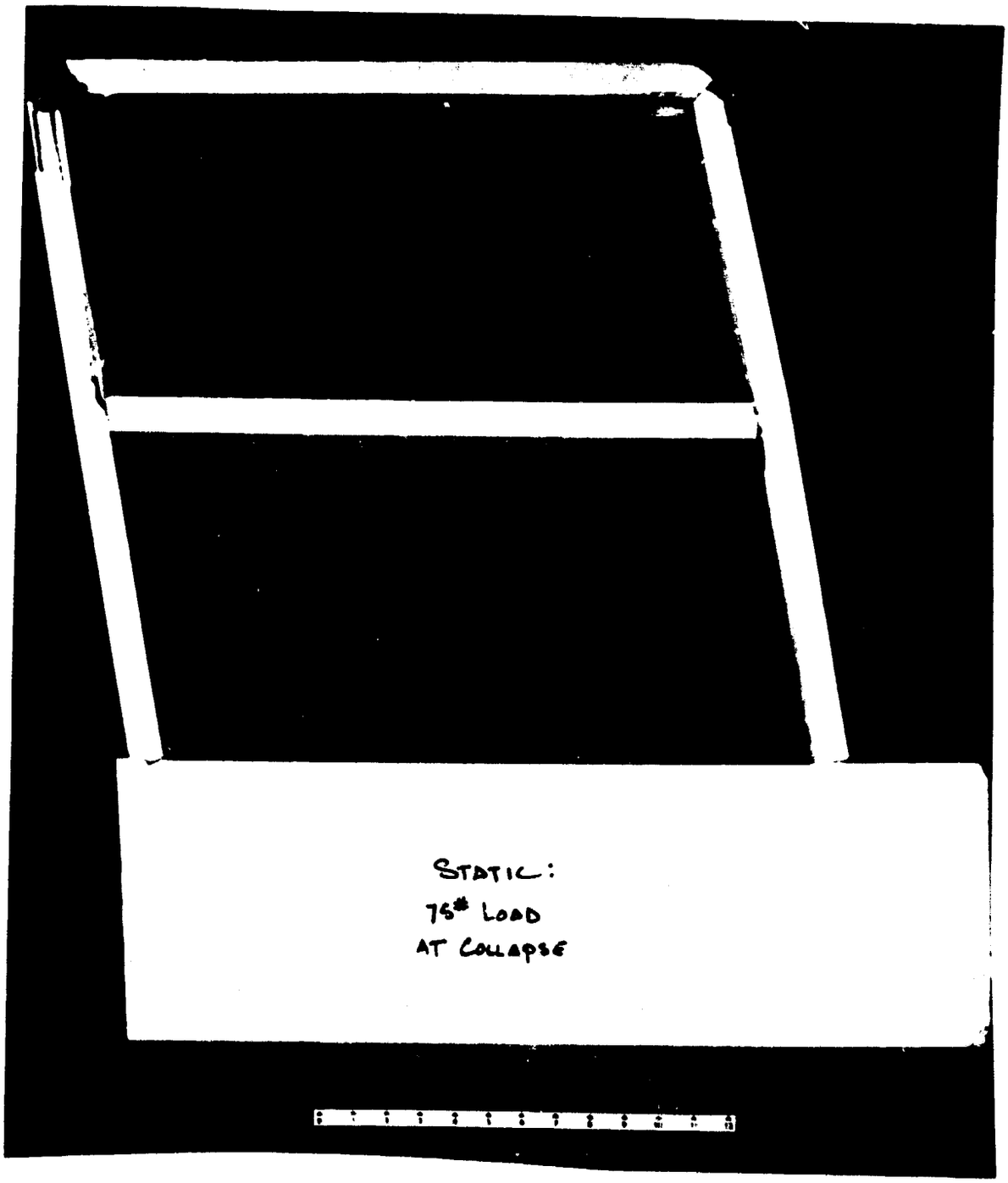

Fig. 14 STATIC COLLAPSE, TWO-STORY FRAME

This sequence of events is consistent with a limited-plasticity formulation shown in Fig. 15.

Finally, dynamic collapse tests were performed on both single-story and two-story frames. Since the behavior of frames in a high-yield blast environment is, for all intents and purposes, solely dependent on response to drag loadings of durations much greater than the natural period of the structure, a dynamic loading fixture was devised to produce a load pulse as shown in Fig. 16. Loads, both slightly greater than the observed static collapse loads and more than twice as much, were applied in this fashion. The collapse modes and amounts of damage at the hinges were comparable in all cases, as was predicted. The responses of the four frames tested under impact are shown in Fig. 17 through 20.

2.5 CONCLUSIONS

Some conclusions about the utility of the theories and techniques demonstrated in this chapter are appropriate:

- The limited-plasticity theory provides a realistic approach for predicting blast-induced debris from nonfrangible structural elements in a manner which is consistent with, and indeed an extension of, design procedures.
- Recourse to modern computer-oriented analysis techniques overcomes the prohibitive computational complexity which heretofore has inhibited applications of limited plasticity.
- Models of reinforced-concrete structures, constructed at low cost from inexpensive materials, can be used to provide meaningful answers to questions about debris production which characteristically involve gross behavior such as the collapse mode.

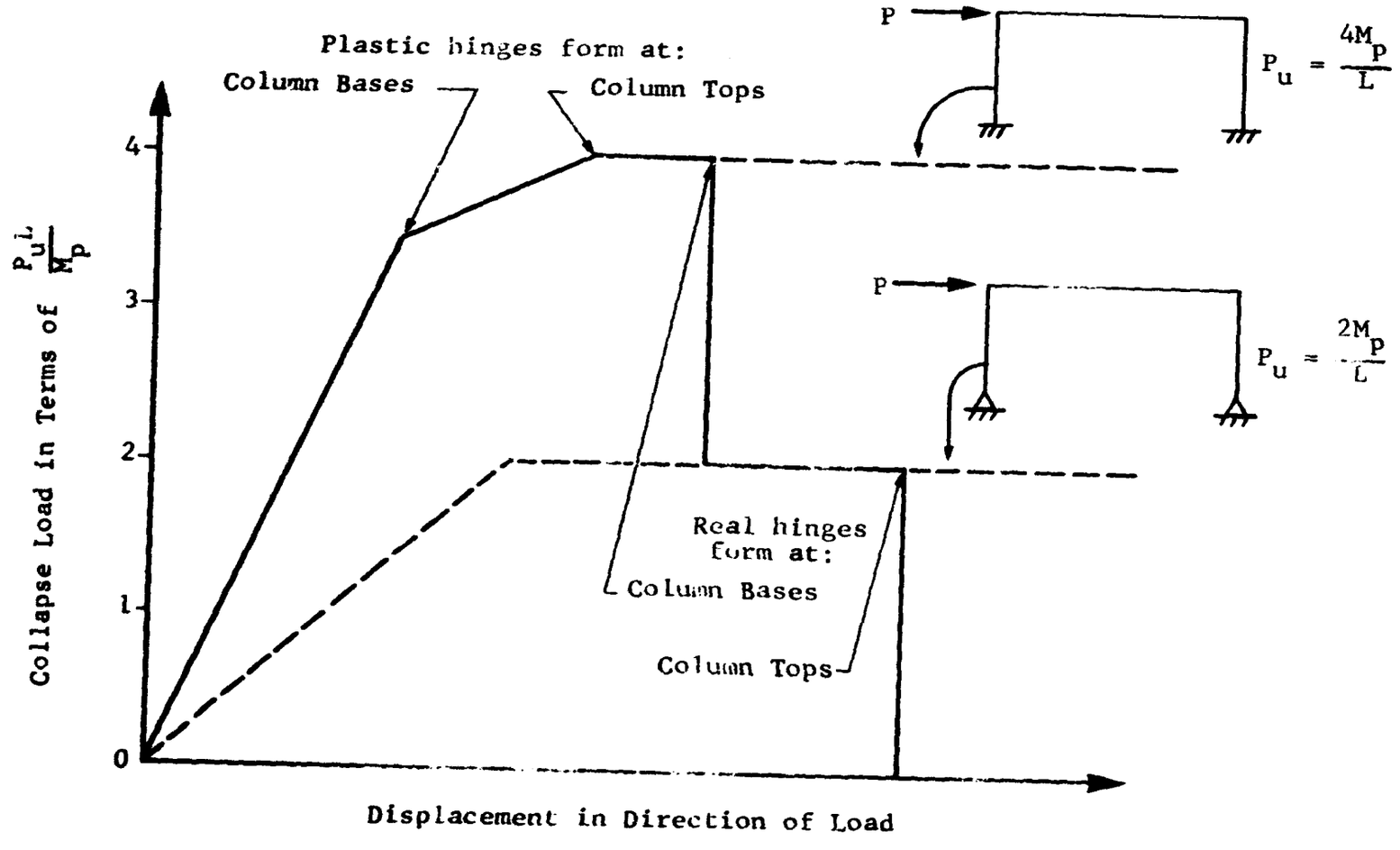

Fig. 15 LIMITED-PLASTICITY BEHAVIOR OF TEST FRAME

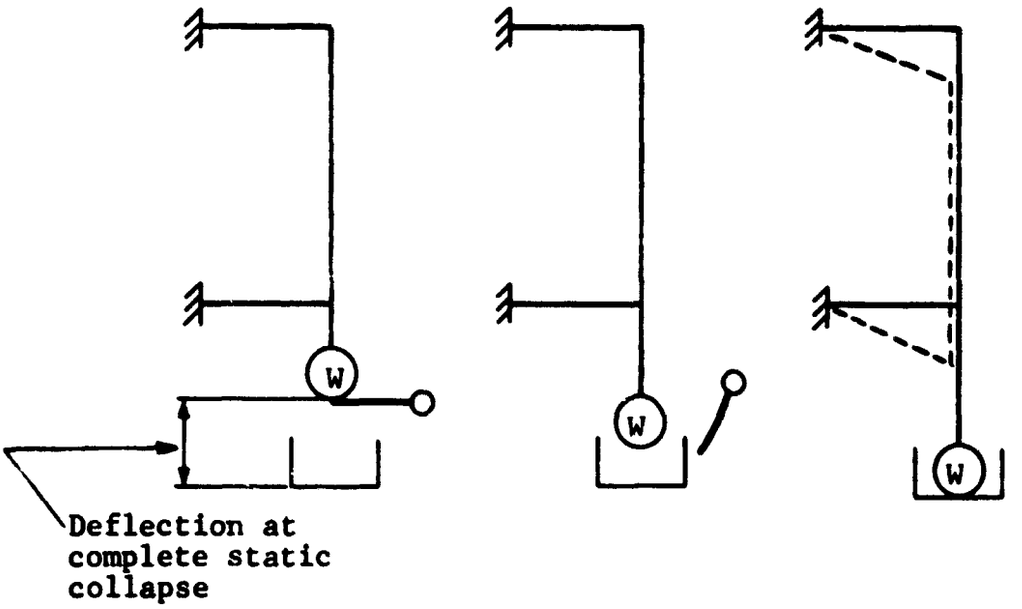

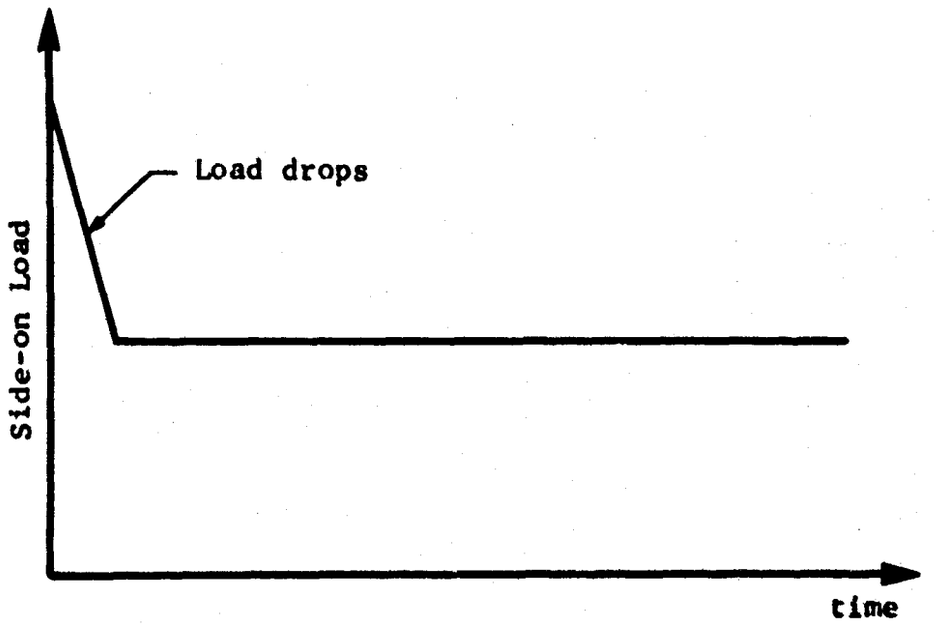

Fig. 16 DYNAMIC LOADING OF TEST FRAMES

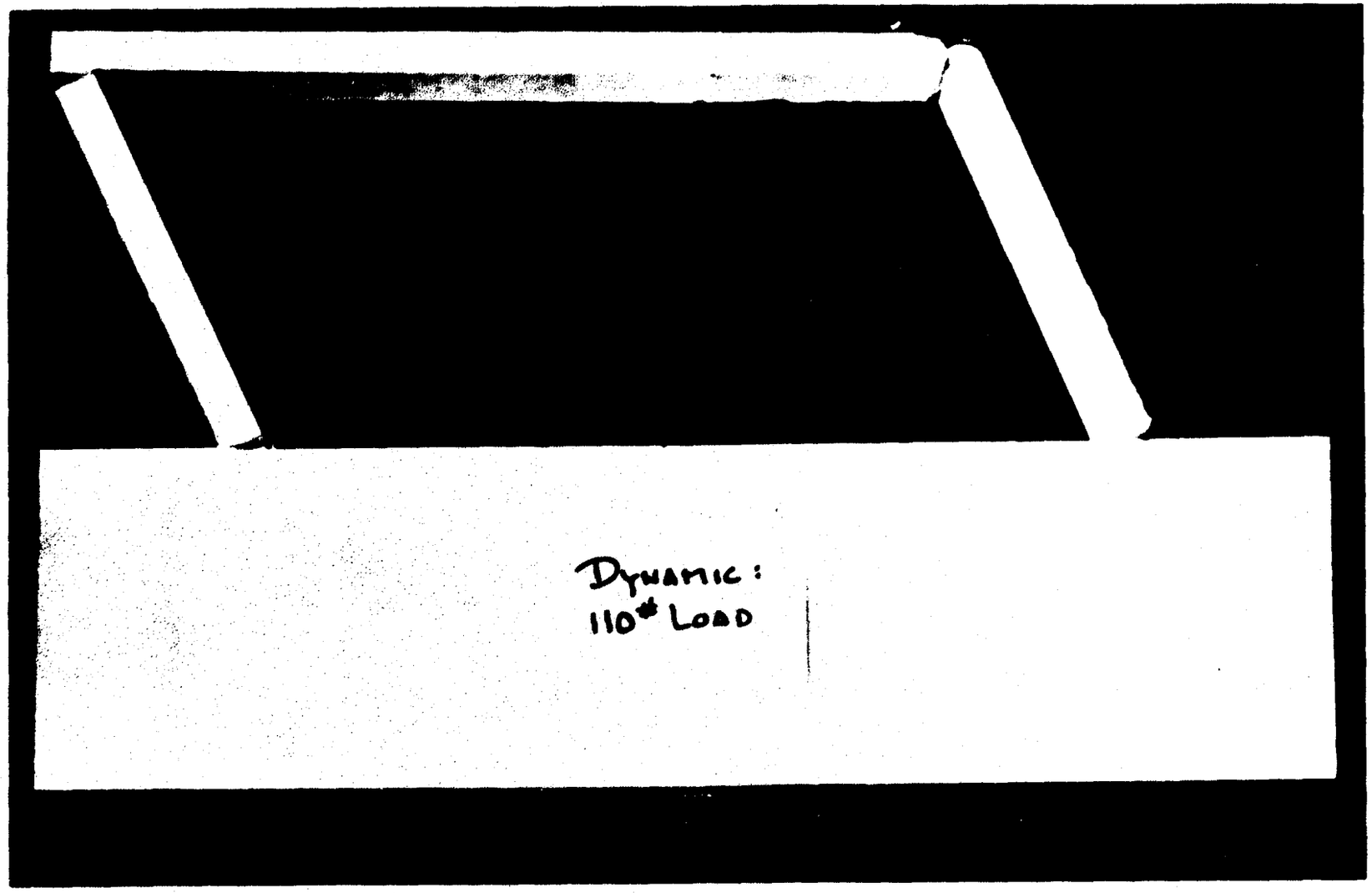

Fig. 17 DYNAMIC COLLAPSE, SINGLE-STORY FRAME

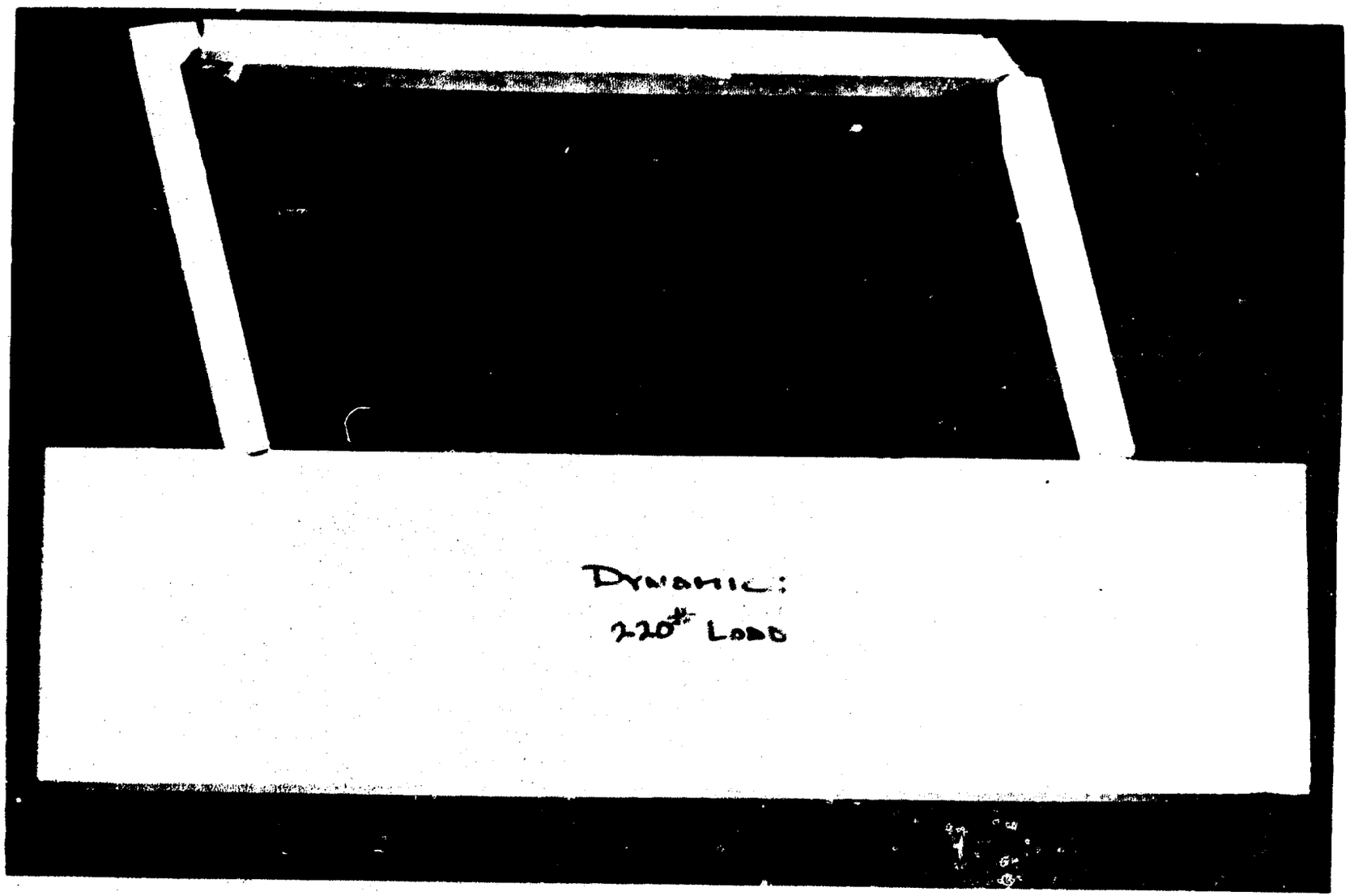

Fig. 18 DYNAMIC COLLAPSE, SINGLE-STORY FRAME

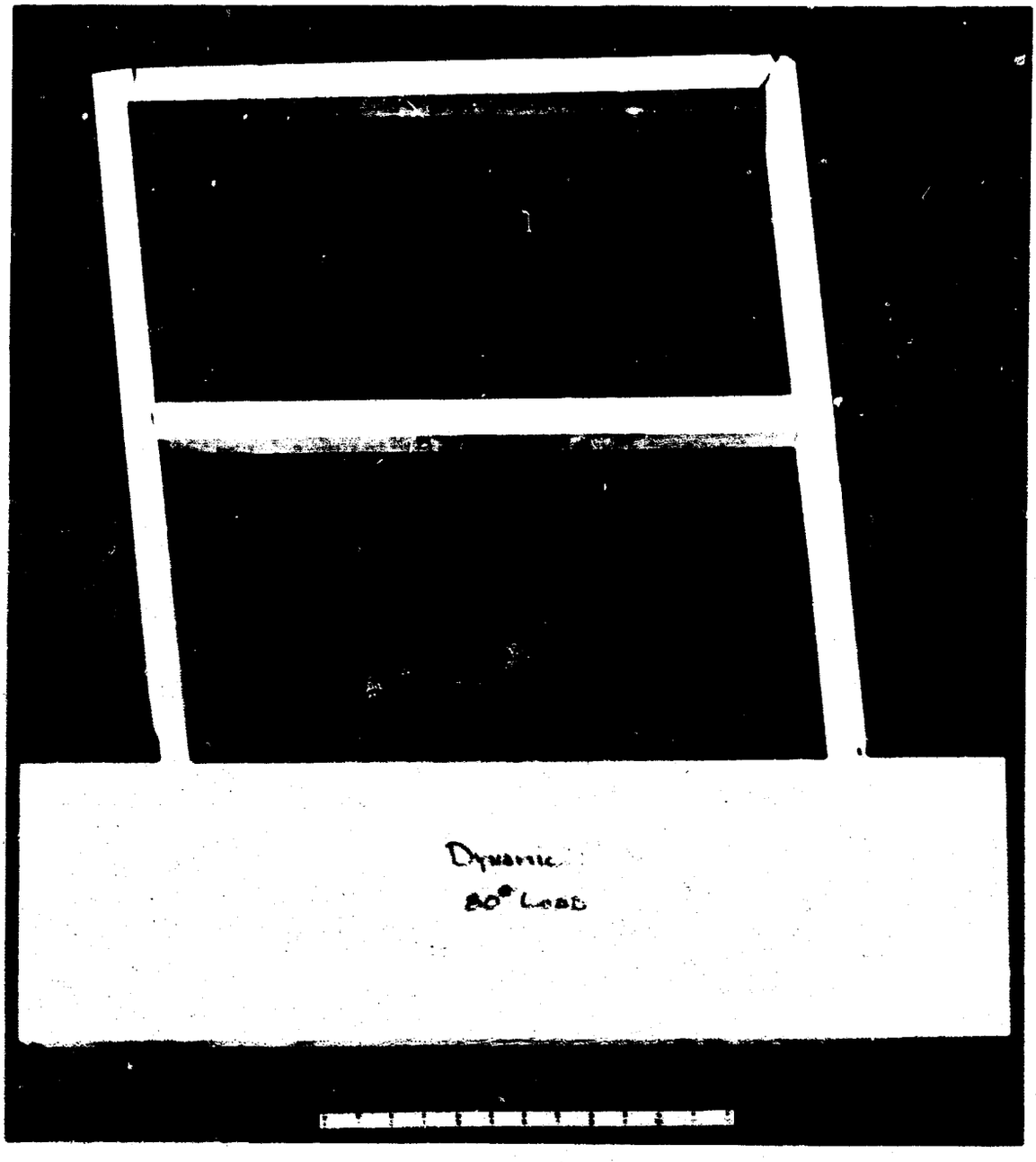

Fig. 19 DYNAMIC COLLAPSE, TWO-STORY FRAME

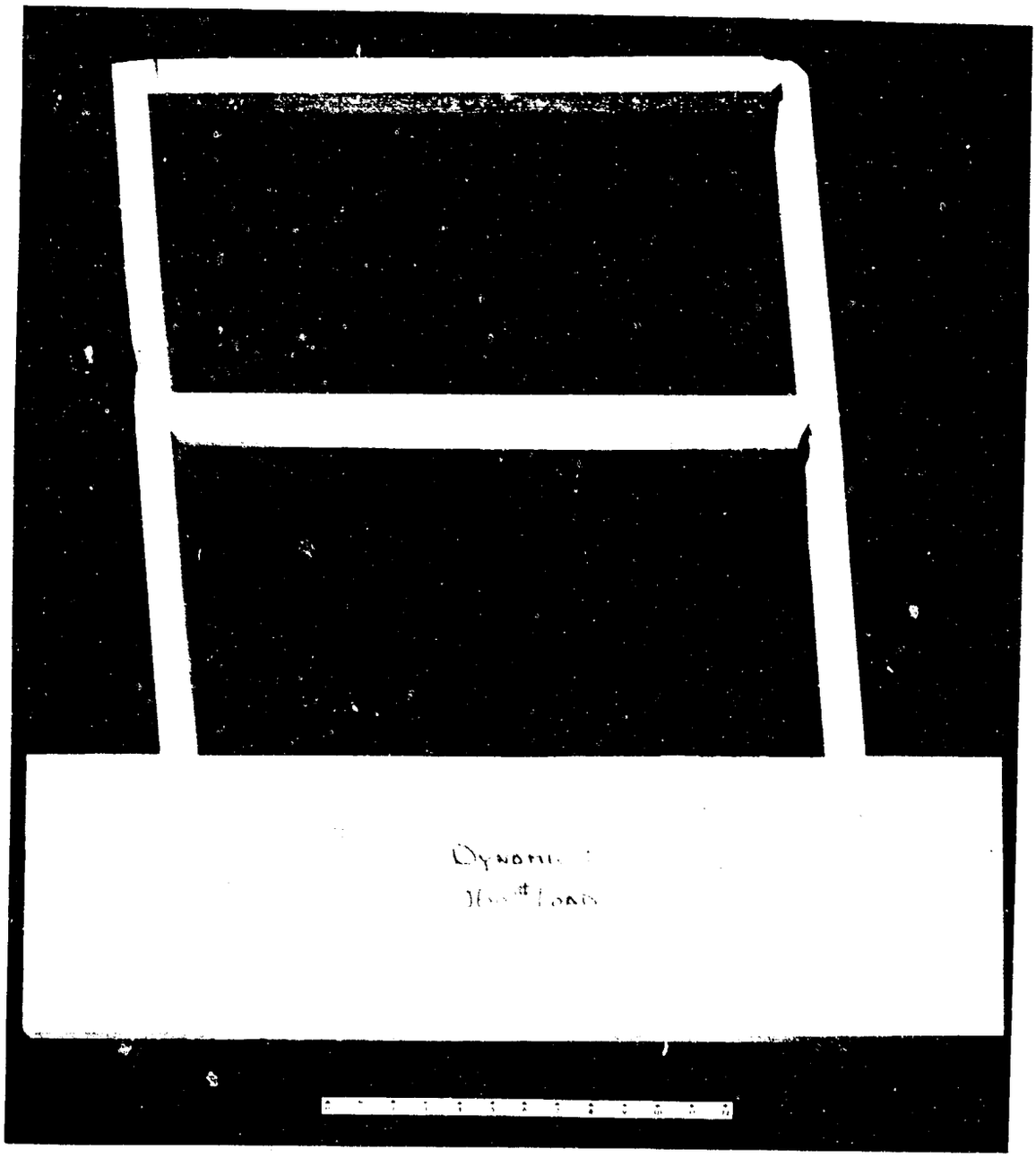

Fig. 20 DYNAMIC COLLAPSE, TWO-STORY FRAME

CHAPTER THREE
PLATE FRAGMENTATION

3.1 INTRODUCTION

The frangible plate structure represents a significant debris producing element in the form of wall panels and a vital source of dangerous missiles in the form of plate glass. The fragmentation characteristics of such structures are studied in this section using a pragmatic approach which blends results from statistical fracture theory with those recently obtained by IITRI on an experimental study of dynamically-loaded plaster plates (Ref. 8). The work we shall describe extends the considerations of two previous programs on beam fragmentation to the plate (Ref. 9 and 10).

In the first of these programs, the statistical nature of the problem is established together with the physical assumptions underlying the basic computational scheme. Essentially, the method considers separately every possible combination of crack patterns. As such, it provides a description of the distribution of fragment shapes and masses, and in addition, it can be used to characterize the mixture of different fragments. Unfortunately, the computational time for this program is very great even for large computers. In the second beam fragmentation program, a very efficient and rapid computation method related to the theory of runs was proposed which described only the fragment size distribution - the original locations of the fragments cannot be determined nor are they required for beam response. As we shall see, this additional information may be useful for describing the fragmentation of plates.

The general fragmentation algorithm consists of four steps:

- Determine the maximum dynamic stresses throughout the plate.

- Compute the probability of fracture initiation throughout the plate.
- Divide the plate into appropriate regions based on crack propagation.
- Compute the distribution of fragment "sizes."

Each of these steps is discussed in the following subsections.

3.2 DYNAMIC STRESS ANALYSIS

To decide whether or not fracture will initiate at a point in a dynamically loaded plate, we must first know the "worst" stress state that can occur at the point. This is a straightforward determination when no fractures occur throughout the load history. If, on the other hand, fractures do develop during the loading process, the problem is considerably more complicated. Even for a material with a deterministic strength we would have to consider changing boundary conditions, the speed of crack growth, and the direction of crack propagation. For a brittle material with statistically distributed strength, the number of combinations requiring analysis would truly be enormous.

To extricate ourselves from this forbidding prospect, we have introduced the assumption that the maximum dynamic stresses are independent of the fracture characteristics of the structure. The following comments are relevant to this approximation:

1. No experimental evidence has been sought to examine the validity of this assumption for different types of dynamic loading.
2. The unloading that accompanies the first fracture of a slowly loaded statically determinate beam usually precludes a second fracture.

3. Multiple fractures invariably occur on a rapidly loaded statically determinate beam.

4. The more severe the dynamic loading the smaller the fragment size and the greater the number of fragments.

5. Under such an assumption the various possible fracture patterns are stochastically independent.

6. Crack velocity is substantially below the velocity of elastic disturbances.

7. The actual stress magnitudes in a structure will usually be equal to or lower than those computed for a dynamically equivalent plate with infinite strength. This implies that we will experience fewer crack initiations and larger pieces than we might predict.

Consistent with our principal assumption of independence, i.e. 5 (above), we shall proceed to calculate the maximum stresses occurring in a rectangular simply-supported plate subject to uniform load across its surface but varying in time. The coordinate system and plate dimensions are shown in Fig. 21. Conventional small deformation theory is used and the plate is assumed to be homogeneous and isotropic.

As a specific example, we have chosen a simply-supported rectangular plate with an exponentially decaying load, $q = p_o \exp\left[-\mu t\right]$. The initial velocities and displacements are taken to be zero. The deflection for such a plate is described in Section 9.5 of Ref. 11 where their general deflection expression, Eq. (8), can be specialized by taking $q = p_o \exp(-\mu t)$ and $f = g = 0$. Then, using Eq. (10) of this reference, we obtain after a simple integration the required plate deflection:

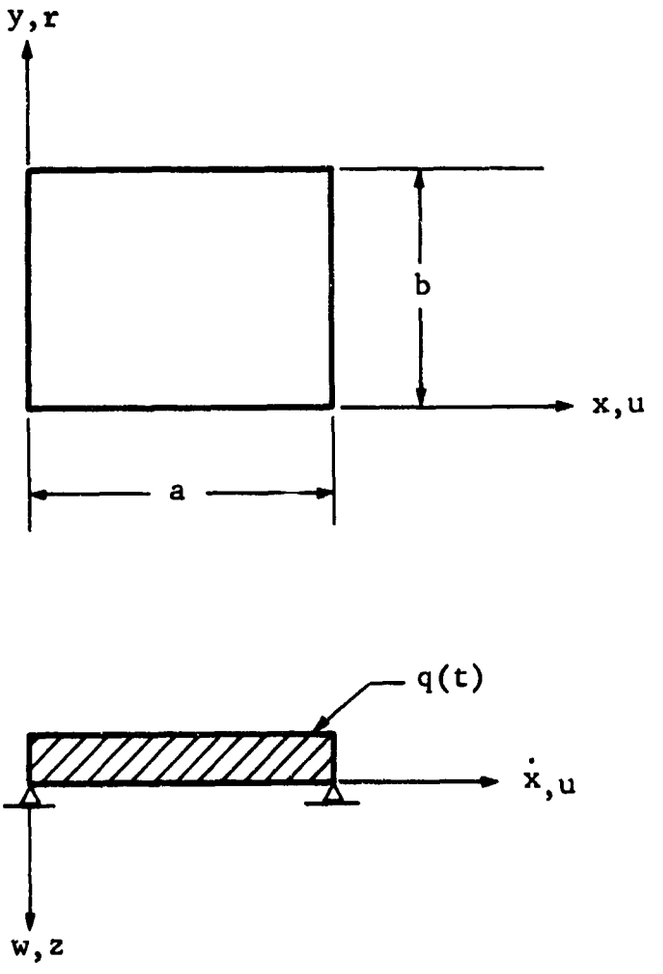

Fig. 21 PLATE COORDINATES AND DIMENSIONS

$$w(x,y,t) = \left(\frac{16\ p_o g}{a\ b\ h\ \gamma}\right) \sum_{m=1,3\ldots} \sum_{n=1,3,\ldots} \frac{1}{\beta_m \alpha_n (w_{nm}^2 + \mu^2)}$$

$$\left\{ \sin(\alpha_n x)\ \sin(\beta_m y) \left[\exp(-\mu t) + \frac{\mu}{w_{mn}} \sin(w_{mn} t) - \cos(w_{mn} t) \right] \right\} \quad (8)$$

where

$$\alpha_n = \frac{n\pi}{a}$$

$$\beta_m = \frac{m\pi}{b}$$

$$w_{nm}^2 = \left[\alpha_n^2 + \beta_m^2 \right]^2 \frac{Eh^2 g}{12(1-\nu^2)\gamma}$$

h = plate thickness
E = Young's modulus
ν = Poisson's Ratio
γ = weight density
g = acceleration of gravity.

The resulting moments can be found by substituting Eq. (8) into the following which relate moments to deflections.

$$M_{xx} = \frac{-Eh^3}{12(1-\nu^2)} \left[\frac{\partial^2 w}{\partial x^2} + \nu \frac{\partial^2 w}{\partial y^2} \right] \quad (a)$$

$$M_{yy} = \frac{-Eh^3}{12(1-\nu^2)} \left[\frac{\partial^2 w}{\partial y^2} + \nu \frac{\partial^2 w}{\partial x^2} \right] \quad (b) \quad (9)$$

$$M_{xy} = \frac{-Eh^3(1-\nu)}{12(1-\nu^2)} \frac{\partial^2 w}{\partial x \partial y} \quad (c)$$

It is then possible to find the principal moments from:

$$M_1, M_2 = 1/2 \left[M_{xx} + M_{yy} \right] \pm \sqrt{\left[\frac{M_{xx} - M_{yy}}{2} \right]^2 + M_{xy}^2}. \quad (10)$$

Since the principal stresses are related to the principal moments by

$$S_{1,2} = \frac{6}{h^2} M_{1,2} , \qquad (11)$$

we can find the magnitudes and directions of the principal stresses in the plate at any time.

Because of the arduous summations involved, Eqs. (8) through (11) were programmed for the IBM 7094 digital computer. A particular problem, that of a square plate 15 in. on a side and 1/2 in. thick, was run and the resulting contours of maximum principal stress are shown in Fig. 22 for P_o = 5 psi and $\mu = 2 \text{ sec}^{-1}$. The curves are the contours at the time when the stress at the center of the plate (which, of course, is the maximum stress in a simply-supported plate) is a maximum, i.e., t = 0.001958 sec. The maximum stresses are very closely approximated by the stresses associated with the contour lines in Fig. 22 because the plate deflects predominantly in the first mode.

3.3 PROBABILITY OF FRACTURE INITIATION

Using the principal stresses calculated by the methods of the previous subsection, we shall address ourselves to the problem of establishing the probability that fracture will initiate in a typical subdivision of the plate shown in Fig. 23. These subdivisions are identified by the integers running from 1 to 120 and their associated bending moments are calculated at their centroids. Figure 24 shows a subdivision from which we have extracted a slice which is subjected to the principal stresses $(S_1, S_2, 0)$. Before we can establish its reliability, it is necessary that a theory be developed for multiaxial stress fields.

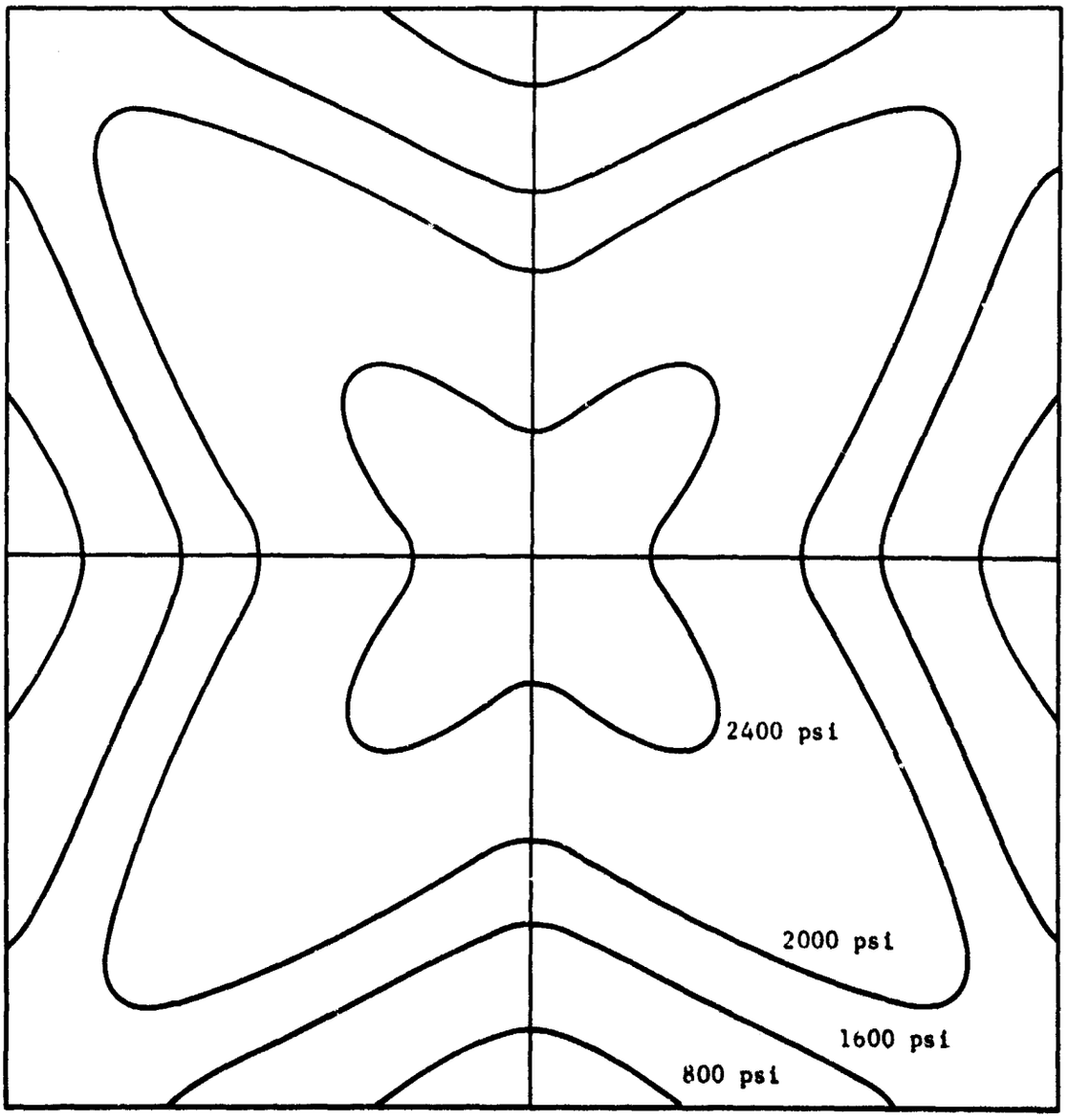

Note: a = b = 15 inches
h = 1/2 inch

Fig. 22 LINES OF CONSTANT MAXIMUM STRESS

3.3.1 Combined Stress Theory

In his classic paper of 1939 (Ref. 12), Weibull developed an expression for the fracture probability of a brittle material under a polyaxial stress state. Using a different point of view, we shall expand on his brief statistical treatment of this combined stress problem and extend our results to cases of varying mechanical and thermal loading, and to materials which cannot be represented by the Weibull distribution function.

Briefly, it is our objective to establish a fracture surface, i.e., to find a relationship among the strengths achieved under various stress states. The usual approach to this problem in either brittle or ductile materials is to find a property common to all stress states that will indicate failure or nonfailure. In ductile materials the distortion energy represents such a property, since incipient flow occurs in any stress state in which the distortion energy is equal to the distortion energy obtained in a tension specimen at yield. Stated in another way, we can correlate yielding under any stress state with the distortion energy. Our approach for brittle materials is completely analogous - we shall try to find a property that will correlate with the reliabilities associated with the various possible combined stress conditions.

To avoid the "size effect" problem observed in the strength of brittle elements, (i.e., increasing fracture stress with decreasing volume) we shall begin our study by considering a finite unit volume ΔV of fixed size. We assume that both the material and the stress state in this unit volume are homogeneous and that the materials used in all the unit volumes to be considered have been drawn from the same population. In addition, we shall restrict the study to brittle materials that are statistically isotropic, i.e., the distribution of strengths obtained from an indefinitely large number of unit volumes will be identical in every direction.

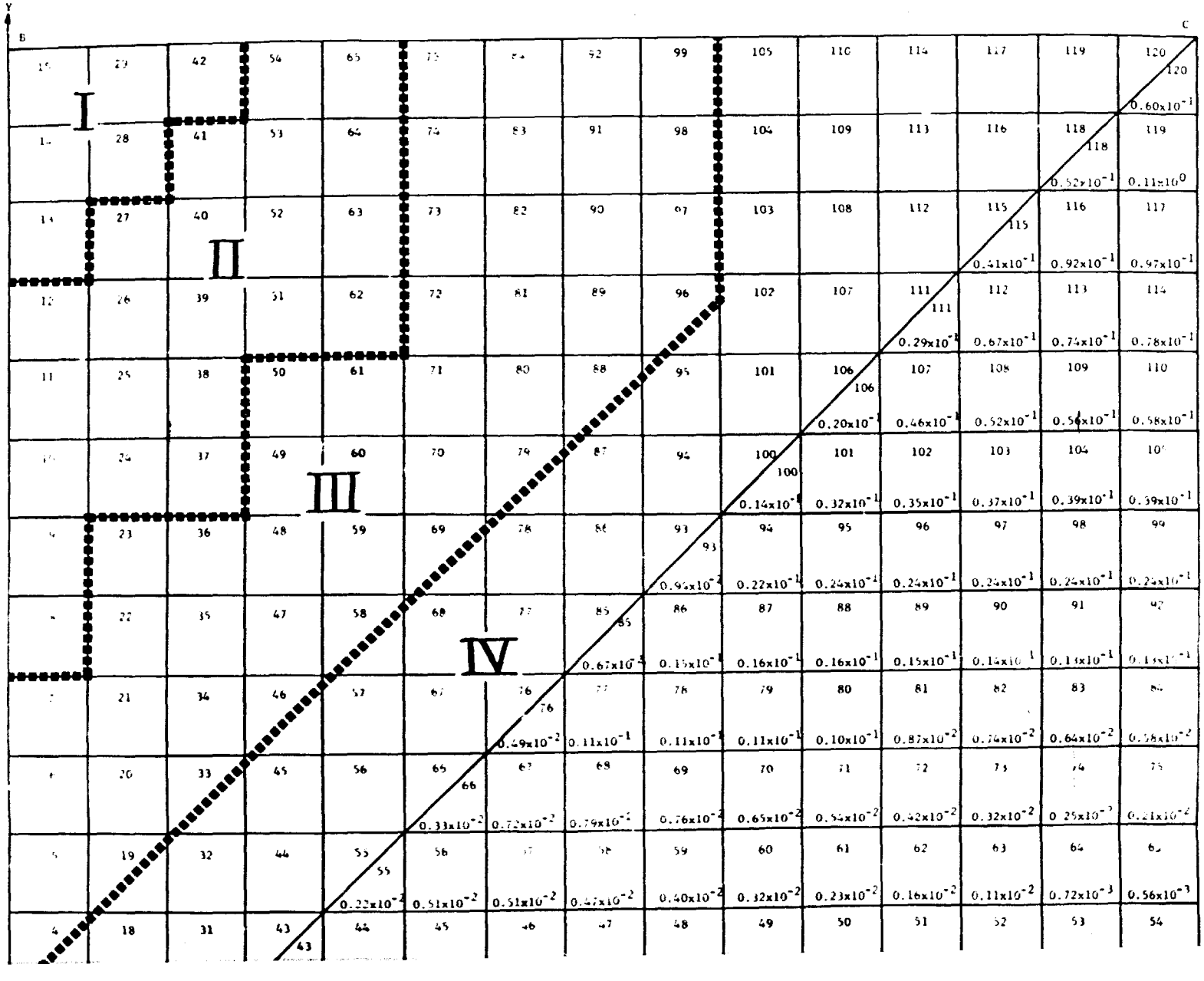
Y
B
C
I
II
III
IV

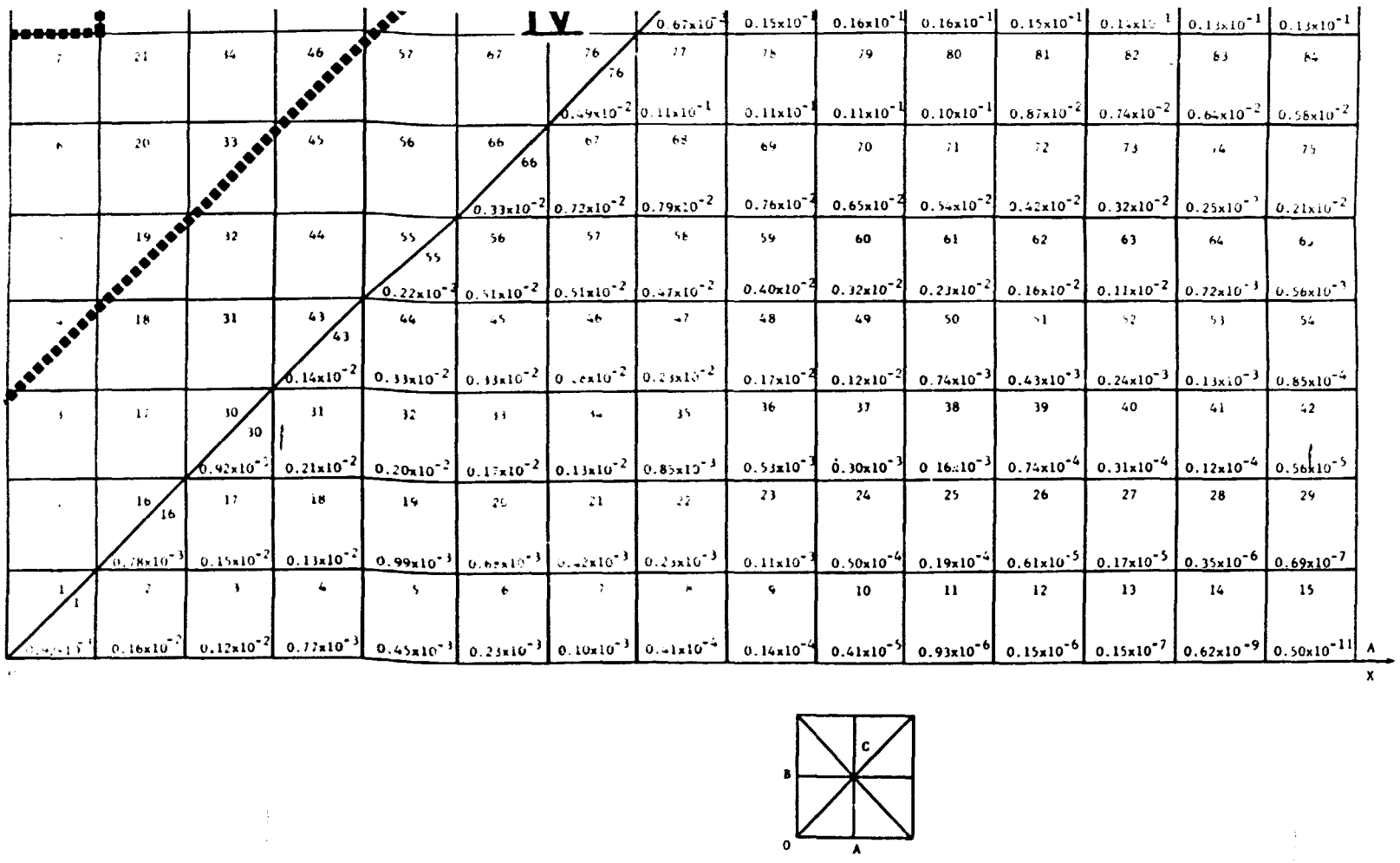

Fig. 23 PLATE SUBDIVISIONS SHOWING THEIR RISK OF RUPTURE VALUES

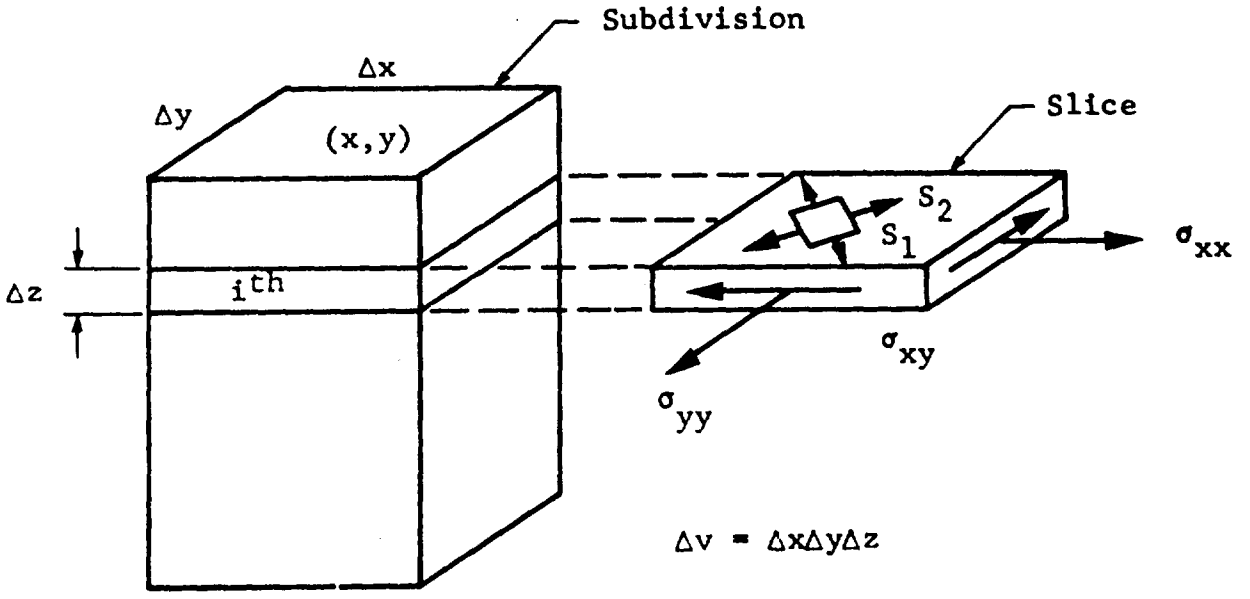

Fig. 24 TYPICAL PLATE SUBDIVISION

We shall assume that the principal stresses S_1, S_2, S_3 which act on a basic unit volume are proportional to a load factor S, that is,

$$S_1 = \alpha S$$
$$S_2 = \beta S \qquad (12)$$
$$S_3 = \gamma S$$

where α, β, γ are constants which define the stress state. The strength of a basic element will be taken as the maximum load factor that it can equilibrate. Failure of the unit element is represented by its inability to equilibrate the applied loading. It is important to point out that it is possible for cracks to initiate and propagate within the unit volume without causing failure of the element. Materials in which cracks can be arrested or which provide alternative load paths when local failures occur are classified as parallel or series-parallel materials. If a local failure necessarily leads to overall failure, the associated material is called a series or "weakest link" material. One can advantageously adopt an infinitesimal unit volume for the series material and, as we shall subsequently discuss, combined stress testing is greatly simplified in this case.

Only the tensile or cohesive mode of failure will be considered in this investigation. We shall assume that neither compressive nor shear stresses influence the strength of a brittle material. The potential usefulness of this tension criterion is a consequence of two observations; first, that the shear strength of brittle materials is usually an order of magnitude greater than the tensile strength, and, second, that it is extremely difficult to eliminate tensile stresses from prototype or laboratory elements. Almost every structural failure of a brittle component can be attributed to the presence of some distribution of tensile stresses.

3.3.2 Two-Dimensional Theory Heuristic Development

When we attempt to describe the statistical fracture strength of a unit volume of material under a uniaxial stress state, the axial stress (strain) is the only reasonable choice for the statistical variate. Taking a general form for any cumulation distribution function, we can write the fracture probability F for the uniaxial stress state as

$$F(\sigma) = 1 - \exp\left[-\frac{\Delta V}{v}\, g(\sigma)\right] \tag{13}$$

where ΔV is the specified volume of the basic unit element, v is a volume of unity, and σ is the axial stress. The delineation of the constant $\Delta V/v$ does not affect the generality of this expression and in the special case of a series material it provides a convenient representation. If we examine the strength of a unit volume of an isotropic material under a general homogeneous stress state, it follows that failure will depend only on the three principal stresses acting on the unit. Thus, the probability of failure of the unit volume can be designated as $F(S_1,S_2,S_3)$ where the three principal stresses are taken as the statistical variates. For this case we shall take Eq. (13) in the form

$$\frac{-\ell_n\left[1-F(S_1,S_2,S_3)\right]}{\Delta V/v} = g(S_1,S_2,S_3) \tag{14}$$

For a specified reliability (1-F), we note that Eq. (14) becomes $g(S_1,S_2,S_3)$ = constant, which defines our fracture surface.

On the basis that failure is caused only by tensile stresses, it seems reasonable to look for the function g within the collection of all possible tensile stresses which can occur at any point in the unit volume. In the plane stress problem we can relate the normal stress σ_n acting in any direction to the principal stresses through the expression

$$\sigma_n = S_1 \cos^2\theta + S_2 \sin^2\theta \tag{15}$$

where θ is the angle between σ_n and S_1. As θ sweeps through all values from $-\pi/2$ to $\pi/2$, Eq. (15) describes every possible normal stress acting at a point. The normal stresses associated with the various directions described by θ are shown in Fig. 25 for several different stress states. The question, now, is what are the distinguishing features of these figures that will reflect the differences they cause in a material's response?

The most obvious first guess is to differentiate among these stress states by comparing the areas associated with the tensile normal stresses. However, this approach does not reflect the possibility that the magnitude of the stresses may have a different influence than their extent or distribution. For example, hydrostatic and pure tension stress states are depicted in Fig. 26 that lead to the same area but where one peak stress is twice the other. Experience indicates that the pure tension state is the more critical. This suggests that we "weight" the ordinates in these figures and then compare the areas of the weighted normal stress-theta diagrams.

Assuming a statistically isotropic material, the weighting should be independent of the orientation θ of the normal stress. We might use for example a power function to modify the normal stresses, i.e., $D\sigma_n^k$ where D and k are constants. This alteration results in the dashed curve shown on the left side of Fig. 27. If the normal stress distribution for several stress states were weighted in this fashion, we could compare the areas of the resulting curves, that is,

$$g(S_1,S_2) = \text{Area} = D \int_{\sigma_n \geq 0} \sigma_n^k \, d\theta \qquad (16)$$

where the integration extends over those values of θ where the normal stress is non-negative. Because of symmetry we need consider only the positive normal stresses in the interval zero to $\pi/2$. To account for the possibility that tensile stresses below a certain magnitude σ_ℓ may not cause failure, we may choose to weight the difference $(\sigma_n-\sigma_\ell)$ as shown in the right half of Fig. 27.

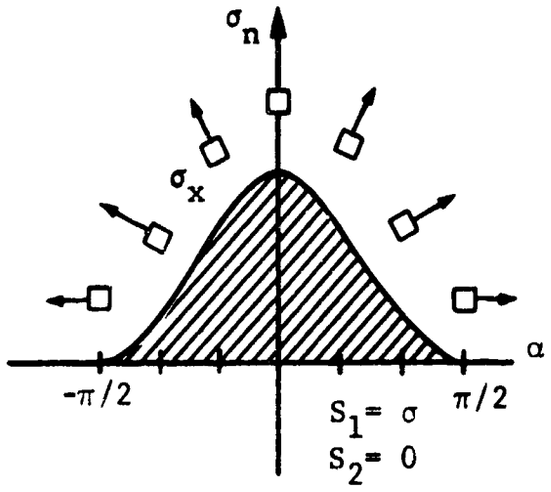

Pure Tension

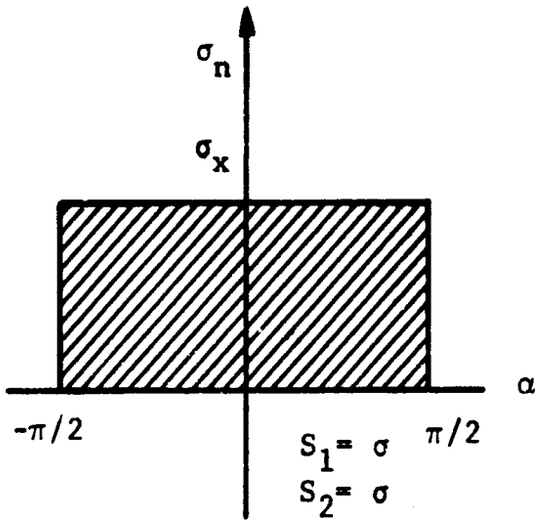

Hydrostatic Tension

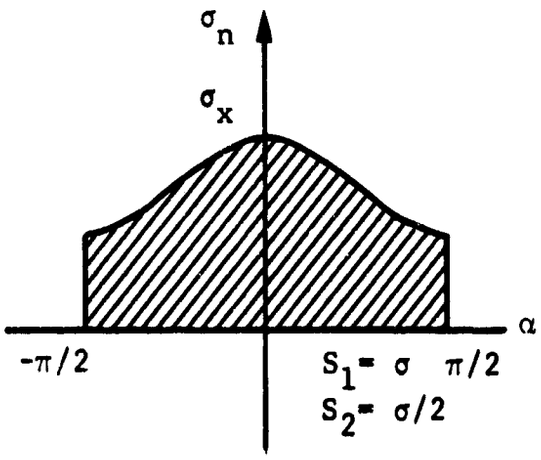

Biaxial Tension

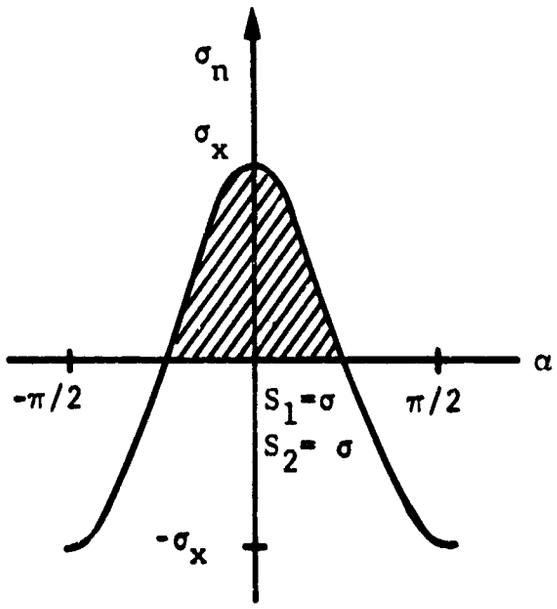

Pure Shear

Fig. 25 NORMAL STRESS DISTRIBUTIONS FOR VARIOUS STRESS STATES

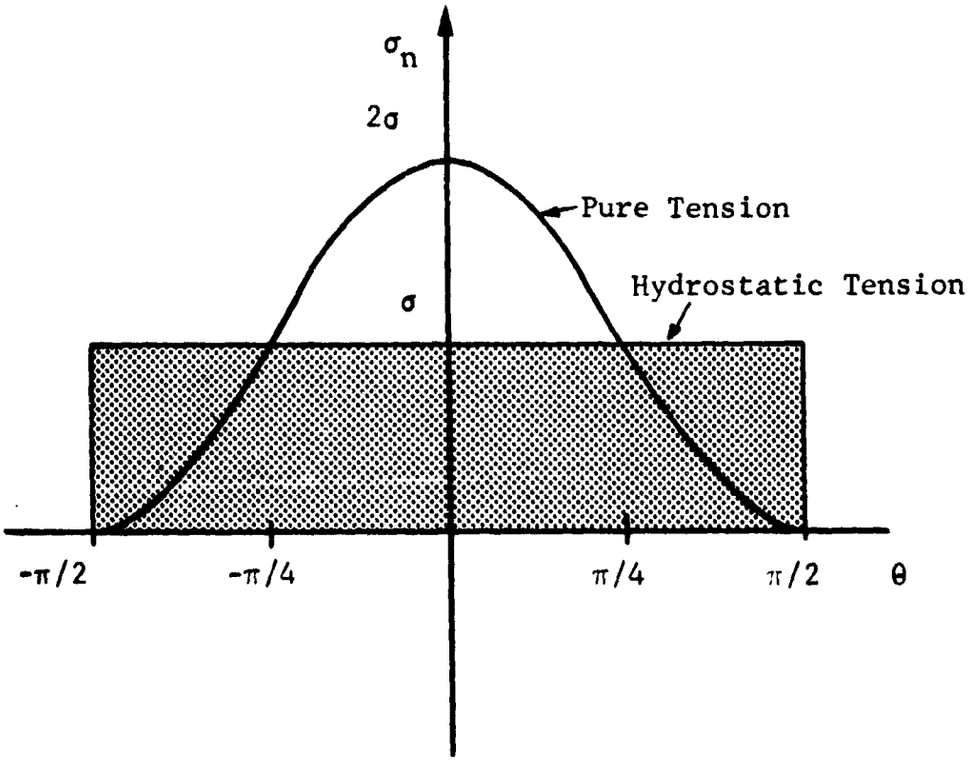

Fig. 26 EQUAL AREAS, UNEQUAL MAXIMUM STRESSES

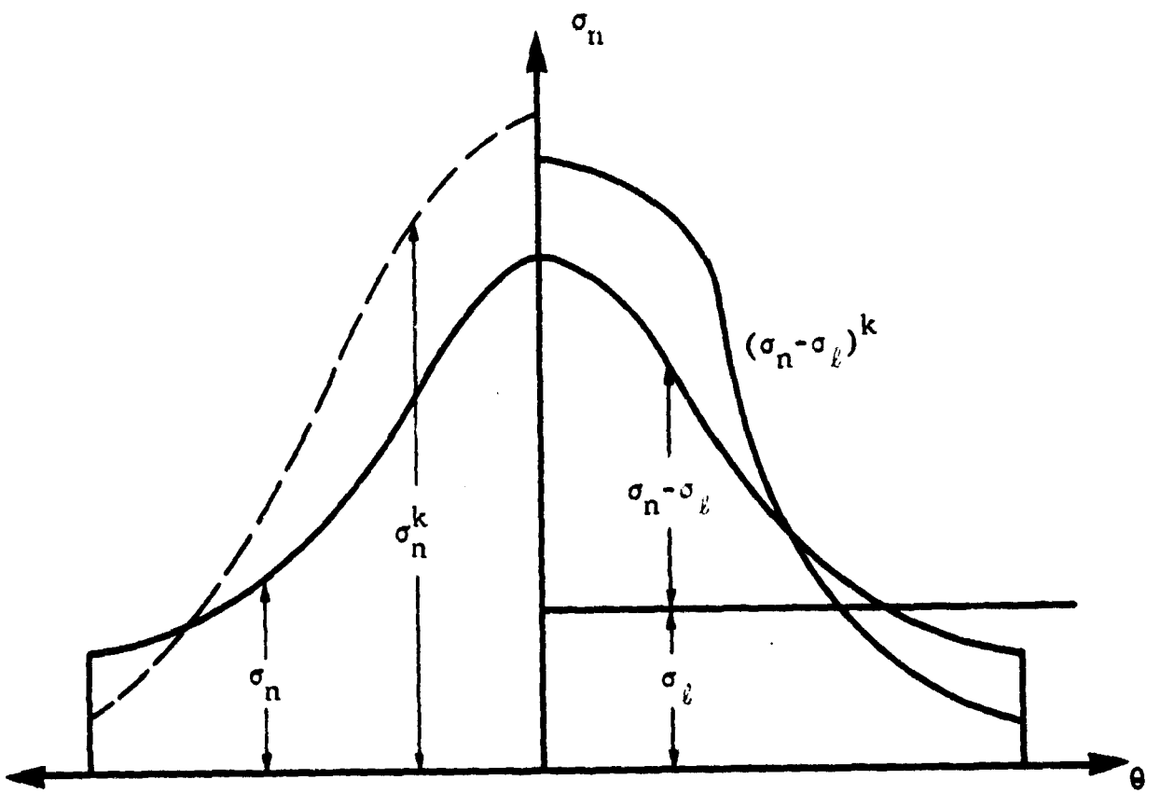

Fig. 27 "WEIGHTED" NORMAL STRESS DIAGRAM

The associated area is given by

$$g(S_1,S_2) = \text{Area} = D \int_{\sigma_n \geq \sigma_\ell} (\sigma_n - \sigma_\ell)^k \, d\theta \, . \qquad (17)$$

Certainly, the use of a power function to weight the normal stress-theta diagrams is completely arbitrary and there are many other ways of manipulating and distorting such curves. Our problem is to find a weighting function that will reflect the influence of stress state on the reliability of a unit volume. Denoting the weighting function by f, the fracture probability becomes

$$F(S_1,S_2) = 1 - \exp\left[- \frac{\Delta V}{V} \int_{\sigma_n \geq \sigma_\ell} f(\sigma_n - \sigma_\ell) \, d\theta \right]. \qquad (18)$$

We are now in a position to describe certain guidelines for the selection of f. First, to account for the possible existence of a zero fracture probability stress σ_ℓ, we must take

$$f = f(\sigma_n - \sigma_\ell) \qquad \sigma_n \geq \sigma_\ell \geq 0$$

$$f = 0 \qquad \sigma_n \leq \sigma_\ell \, .$$

The latter condition implies that both $S_1 \leq \sigma_\ell$ and $S_2 \leq \sigma_\ell$, and that in such cases F = 0. At the other extreme, we expect that fracture is a certainty when either S_1 or S_2 is positive and unbounded; hence, F = 1 implies that

$$f \rightarrow \infty \text{ when } S_i \rightarrow + \infty.$$

Furthermore, we would expect on physical grounds that the failure probability would increase continuously with increasing principal stresses, thus,

f ... continuous and monotone increasing.

Finally, f must be chosen in such a way that the associated $F(S_1,S_2)$ fits the cumulative distribution curve obtained from fracture tests conducted using various stress states. In particular, it is necessary that fracture data obtained under pure tension be represented by $F(S_1,0)$.

Typical examples of admissible forms for the weighting function f are the following:

$$f = \left(\frac{\sigma_n-\sigma_\ell}{\sigma_o}\right)^k \tag{19}$$

$$f = \exp\left[a(\sigma_n-\sigma_\ell)\right] - 1 \tag{20}$$

$$f = \exp\left\{\exp\left[a\ (\sigma_n-\sigma_\ell)\ \right] - 1\right\} - 1 \tag{21}$$

$$f = A(\sigma_n-\sigma_\ell) + B(\sigma_n-\sigma_\ell)^2 + C(\sigma_n-\sigma_\ell)^3 + \ldots$$
$$A \geq 0,\ B \geq 0,\ C \geq 0 \tag{22}$$

where a, k, A, B, C, σ_o, and σ_ℓ are constants of the material.

3.3.3 Three-Dimensional Theory

The extension of our theory given in Eq. (18) to three dimensions requires that we appropriately distort the surface formed by the normal stress vector in three dimensions. This vector is given in the polar coordinates as

$$\sigma_n = \cos^2\phi(S_1\cos^2\psi + S_2\sin^2\psi) + S_3\sin^2\phi \qquad (23)$$

where the angles ϕ and ψ are defined in Fig. 28a. A typical surface representing the focus of normal stress vectors is shown in Fig. 28b for a biaxial tension field. A weighted surface is formed by $f(\sigma_n-\sigma_\ell)$ and its volume can be introduced into the general distribution function to give

$$F(S_1,S_2,S_3) = 1-\exp\left[-\frac{\Delta V}{V}\iiint_{\sigma_n\geq\sigma_\ell} f(\sigma_n-\sigma_\ell)dV\right]. \qquad (24)$$

Specializing to the form of f given in Eq. (19) and using polar coordinates, the failure probability F is given by

$$F = 1-\exp\left[-\frac{1}{3}\frac{\Delta V}{V}\int_0^{\pi/2}d\psi\int_{\phi_L}^{\phi_U}\cos\phi\,d\phi\left(\frac{\sigma_n-\sigma_\ell}{\sigma_o}\right)^{3k}\right] \qquad (25)$$

where we find three cases:

1) $S_1 \geq S_2 \geq \sigma_\ell$

$$\phi_L = 0;\ \phi_U = \cos^{-1}\sqrt{\frac{\sigma_\ell}{S_1\cos^2\psi+S_2\sin^2\psi}}$$

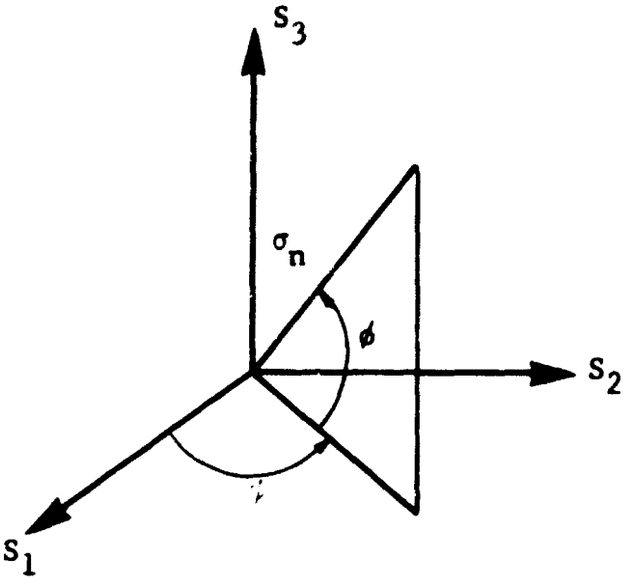

a) Coordinate System

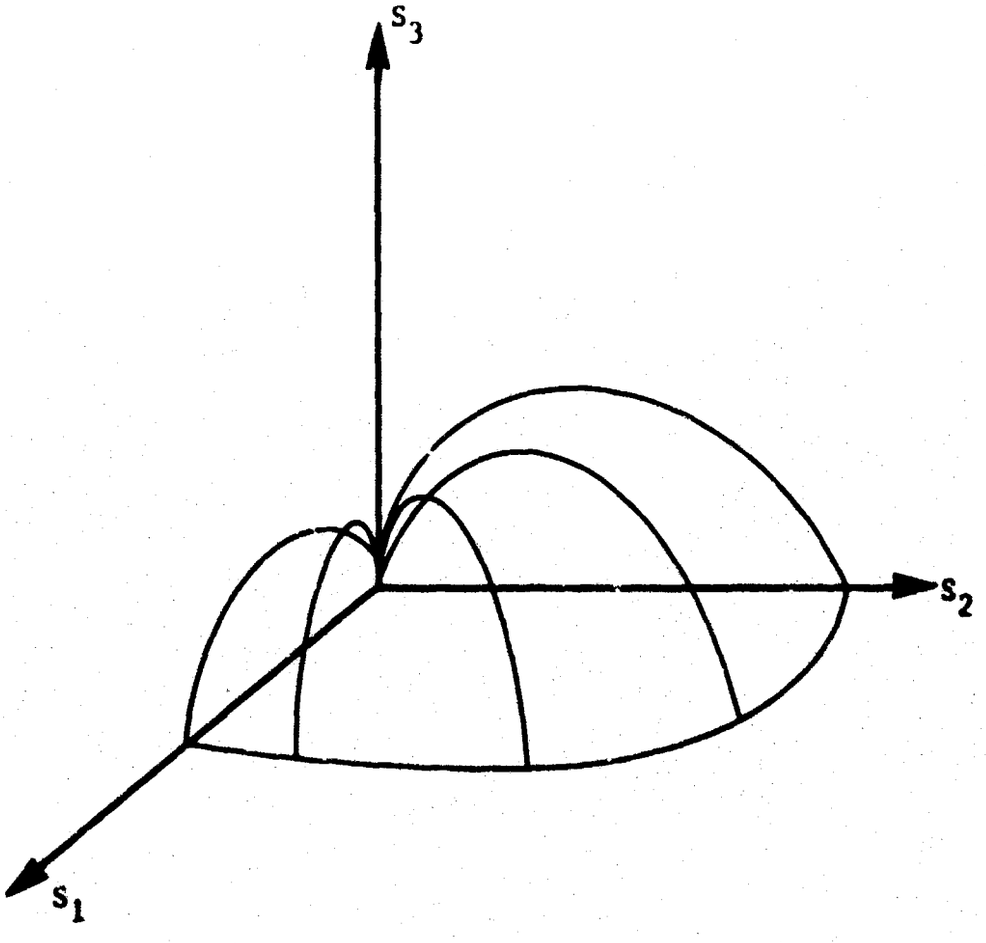

b) General Biaxial Tension

Fig. 28 NORMAL STRESS SURFACE IN THREE DIMENSIONS

2) $S_1 \geq \sigma_\ell$, $S_2 \leq \sigma_\ell$

$$\phi_L = \cos^{-1} \sqrt{\frac{S_1-\sigma_\ell}{S_1-S_2\cos^2\psi}} \; ; \; \phi_U = \pi/2$$

3) $S_1 \leq \sigma_\ell$, $S_2 \leq \sigma_\ell$

$$\phi_L = 0, \; \phi_U = 0 \quad (F = 0) \; .$$

Equation (25) can be written in the form

$$1 - F = e^{-B} \tag{26}$$

where the "risk of rupture" B is given by the negative of the term within the square brackets of Eq. (25). The risk of rupture B was evaluated numerically for each slice of every plate subdivision indicated in Fig. 23. Specifically, the following data was used:

Plate size:	15 x 15 x 1/2 in.
Overpressure:	P_o = 5 psi
Pressure decay:	μ = 2 sec^{-1}
Statistical parameters:	k = 3
	σ_o = 1500 psi
	σ_ℓ = 50 psi

Now, a value of B_i for the ith slice shown in Fig. 24 enables us through Eq. (26) to establish the probability that no fracture will initiate in the slice, $(1-F_i)$. The probability that no fracture will initiate in the entire subdivision $(1-F_S)$, requires the simultaneous survival of each slice, thus,

$$(1-F_S) = (1-F_1)(1-F_2)\ldots(1-F_n) = \prod_{i=1}^{n} (1-F_i) \tag{27}$$

where n is the total number of slices. Substituting Eq. (26) into this equation we obtain

$$(1-F_S) = \exp(-B_S) = \exp\left(-\sum_{i=1}^{n} B_i\right) . \qquad (28)$$

Therefore, the risk of rupture of a "big piece" is equal to the sum of the risk of ruptures of its component "small pieces". The sum of the slice risk of ruptures for each plate subdivision is tablulated in Table 2, together with its centroid coordinates and maximum principal bending stresses. These risk of rupture values are displayed in Fig. 23 by the lower number in each subdivision.

3.4 PLATE EXPERIMENTS

One of the most difficult aspects of the plate fragmentation problem concerns the question of crack propagation. Crack initiation was the concern of the previous two subsections. In the beam problem, when a crack initiated within the beam volume this always resulted in a fracture surface which was roughly perpendicular to the beam axis. When a crack initiates within a plate, its direction of travel is not obvious. Furthermore, we meet a new problem when many cracks are propagating because one crack crossing the path of a second crack will generally arrest the second crack. We are faced, therefore, with the "who got there first" problem. In the face of these complications, we examined the results of experiments conducted with Hydrostone plaster plates under dynamic loadings. The experiments conducted at IITRI (Ref. 8), were supposed to demonstrate characteristic crack patterns that would provide the needed propagation information for our fragmentation analysis. If no patterns were obtained, our analysis procedure would have to be abandoned, and indeed, the hope of developing a rational prediction scheme would be pretty gloomy. Fortunately, patterns did emerge from these tests and we shall very briefly summarize the findings which are described in detail in Ref. 8.

3.4.1 Description of Drop Test

It has been shown in Ref. 8 that the response of a plate under any uniform time-dependent loading can be made identical to that achieved in a drop test when the appropriate support deceleration is imposed. To produce the dynamic load in our drop test facility, the plate support was mounted on the drop table as shown in Fig. 29. The idea was to drop the table and suddenly decelerate it, which would load the plate mounted on the supports (as shown in Fig. 30) with downward acting inertia body forces. To increase the downward loading, sand was piled onto the plate and held in place by the box device in Fig. 31. The results of a typical drop test are illustrated in Fig. 32 where the fragments are held intact by masking tape on their upper surface.

To check out the symmetry of the drop test loading, two plastic plates were stress coated and dropped from different heights. As can be observed from Fig. 33 and 34, the loading is excellent and a pattern of principal directions is obtained which is not unlike that obtained for the pressure loading $q = p_o \exp[-\mu t]$ as shown in Fig. 22.

3.4.2 Results and Conclusions

Typical examples of the crack outlines obtained for five different size Hydrostone plaster plates are shown in Fig. 35. We first observe that these cracks form a pattern. Second, by comparing the crack pattern on the square plates to the stress coat patterns of Fig. 33 and 34 we see that for the most part the cracks propagate along the principal direction trajectories. Further examination of the square plates indicates that the central pattern forms first. In all of the cases, cracks occur along 45 deg lines at the corners.

On the basis of these observations, we shall postulate the formation of the primary fracture mode shown in Fig. 36a and the secondary fracture mode shown in Fig. 36c. The strips in the secondary mode are intended to approximate the principal stress trajectories.

Table 2

PRINCIPAL STRESSES AND RISKS OF RUPTURE
(P_o = 5 psi; μ = 2 sec^{-1})

I	X(I)	Y(I)	S1(I)	S2(I)	BDv(I)
1	0.33333333E 00	0.14666667E 00	0.18462893E 04	-0.18171205E 04	0.92048060E-03
2	0.74999999E 00	0.25000000E 00	0.18413438E 04	-0.17527666E 04	0.15775269E-02
3	0.12500000E 01	0.25000000E 00	0.18018105E 04	-0.16667018E 04	0.11767227E-02
4	0.17500000E 01	0.25000000E 00	0.17364895E 04	-0.15600733E 04	0.77354835E-03
5	0.22500000E 01	0.25000000E 00	0.16491553E 04	-0.14388426E 04	0.44895240E-03
6	0.27500000E 01	0.25000000E 00	0.15433849E 04	-0.13008348E 04	0.22951261E-03
7	0.32500000E 01	0.25000000E 00	0.14236622E 04	-0.11571118E 04	0.10341446E-03
8	0.37500000E 01	0.25000000E 00	0.12944717E 04	-0.10089843E 04	0.40989199E-04
9	0.42499999E 01	0.25000000E 00	0.11591054E 04	-0.85777081E 03	0.14132072E-04
10	0.47499999E 01	0.25000000E 00	0.10182966E 04	-0.70272936E 03	0.40844197E-05
11	0.52499999E 01	0.25000000E 00	0.87190847E 03	-0.54482000E 03	0.92639029E-06
12	0.57499999E 01	0.25000000E 00	0.72127274E 03	-0.38586947E 03	0.15020885E-06
13	0.62499999E 01	0.25000000E 00	0.56815604E 03	-0.22644656E 03	0.14834068E-07
14	0.67499999E 01	0.25000000E 00	0.41279781E 03	-0.66573882E 02	0.82346323E-09
15	0.72499999E 01	0.25000000E 00	0.25734172E 03	0.90746543E 02	0.49608078E-11
16	0.83333333E 00	0.66666666E 00	0.18858777E 04	-0.16422514E 04	0.78266261E-03
17	0.12500000E 01	0.75000000E 00	0.18969709E 04	-0.15131230E 04	0.14871994E-02
18	0.17500000E 01	0.75000000E 00	0.18747640E 04	-0.13688094E 04	0.12818827E-02
19	0.22500000E 01	0.75000000E 00	0.18251703E 04	-0.12128436E 04	0.99227943E-03
20	0.27500000E 01	0.75000000E 00	0.17517588E 04	-0.10500757E 04	0.68344243E-03
21	0.32500000E 01	0.75000000E 00	0.16584436E 04	-0.88573476E 03	0.41737803E-03
22	0.37500000E 01	0.75000000E 00	0.15509397E 04	-0.72197433E 03	0.22813417E-03
23	0.42499999E 01	0.75000000E 00	0.14341238E 04	-0.55770200E 03	0.11256317E-03
24	0.47499999E 01	0.75000000E 00	0.13100667E 04	-0.39115191E 03	0.49765560E-04
25	0.52499999E 01	0.75000000E 00	0.11777147E 04	-0.22455278E 03	0.19027528E-04
26	0.57499999E 01	0.75000000E 00	0.10384200E 04	-0.60504936E 02	0.61078177E-05
27	0.62499999E 01	0.75000000E 00	0.89520396E 03	0.10188647E 03	0.16678019E-05
28	0.67499999E 01	0.75000000E 00	0.74957175E 03	0.26065458E 03	0.35215909E-06
29	0.72499999E 01	0.75000000E 00	0.61113625E 03	0.40472310E 03	0.69224218E-07
30	0.13333333E 01	0.11666667E 01	0.19496411E 04	-0.13473393E 04	0.91595651E-03
31	0.17500000E 01	0.12500000E 01	0.19720676E 04	-0.11687179E 04	0.20581433E-02
32	0.22500000E 01	0.12500000E 01	0.19605316E 04	-0.98416479E 03	0.19990756E-02
33	0.27500000E 01	0.12500000E 01	0.19201556E 04	-0.79873373E 03	0.16968604E-02
34	0.32500000E 01	0.12500000E 01	0.18546199E 04	-0.61773271E 03	0.12673375E-02
35	0.37500000E 01	0.12500000E 01	0.17705390E 04	-0.44159624E 03	0.85087321E-03
36	0.42499999E 01	0.12500000E 01	0.16743179E 04	-0.26693905E 03	0.52518809E-03
37	0.47499999E 01	0.12500000E 01	0.15688734E 04	-0.91304420E 02	0.29964329E-03
38	0.52499999E 01	0.12500000E 01	0.14525193E 04	0.81277130E 02	0.15950005E-03
39	0.57499999E 01	0.12500000E 01	0.13267167E 04	0.24774379E 03	0.73723334E-04
40	0.62499999E 01	0.12500000E 01	0.11959053E 04	0.41008265E 03	0.31068480E-04
41	0.67499999E 01	0.12500000E 01	0.10627763E 04	0.56506731E 03	0.12277633E-04
42	0.72499999E 01	0.12500000E 01	0.94368334E 03	0.69410158E 03	0.55806919E-05
43	0.18333333E 01	0.16666667E 01	0.20304975E 04	-0.96224950E 03	0.13962859E-02
44	0.22500000E 01	0.17500000E 01	0.20576119E 04	-0.75333245E 03	0.32807431E-02
45	0.27500000E 01	0.17500000E 01	0.20495605E 04	-0.55007759E 03	0.32857081E-02
46	0.32500000E 01	0.17500000E 01	0.20110427E 04	-0.35643891E 03	0.28746090E-02
47	0.37500000E 01	0.17500000E 01	0.19522367E 04	-0.17081314E 03	0.22428475E-02
48	0.42499999E 01	0.17500000E 01	0.18780040E 04	0.12175735E 02	0.16506640E-02
49	0.47499999E 01	0.17500000E 01	0.17923908E 04	0.19455238E 03	0.11717954E-02
50	0.52499999E 01	0.17500000E 01	0.16932440E 04	0.37051053E 03	0.74029474E-03
51	0.57499999E 01	0.17500000E 01	0.15824420E 04	0.55719437E 03	0.43121718E-03
52	0.62499999E 01	0.17500000E 01	0.14656572E 04	0.69800034E 03	0.23965600E-03
53	0.67499999E 01	0.17500000E 01	0.13468354E 04	0.84725901E 03	0.13247059E-03
54	0.72499999E 01	0.17500000E 01	0.12427802E 04	0.96363689E 03	0.85292475E-04
55	0.23333333E 01	0.21666667E 01	0.21148779E 04	-0.52733936E 03	0.22136323E-02
56	0.27500000E 01	0.22500000E 01	0.21393420E 04	-0.31031530E 03	0.51475524E-02
57	0.32500000E 01	0.22500000E 01	0.21290173E 04	-0.10741397E 03	0.51400328E-02
58	0.37500000E 01	0.22500000E 01	0.20938562E 04	0.85626457E 02	0.47708076E-02
59	0.42499999E 01	0.22500000E 01	0.20421898E 04	0.27520680E 03	0.39984915E-02
60	0.47499999E 01	0.22500000E 01	0.19769110E 04	0.46199524E 03	0.31580695E-02
61	0.52499999E 01	0.22500000E 01	[illegible]	[illegible]	[illegible]

[illegible]

54	0.72499999E 01	0.17500000E 01	0.12427802E 04	0.96363689E 03	0.85292475E-04

56	0.27500000E 01	0.22500000E 01	0.21393420E 04	-0.31031530E 03	0.51475524E-02
57	0.32500000E 01	0.22500000E 01	0.21290173E 04	-0.10741397E 03	0.51400328E-02
58	0.37500000E 01	0.22500000E 01	0.20938562E 04	0.85626457E 02	0.47708076E-02
59	0.42499999E 01	0.22500000E 01	0.20421898E 04	0.27520689E 03	0.39984915E-02
60	0.47499999E 01	0.22500000E 01	0.19769110E 04	0.46199524E 03	0.31580695E-02
61	0.52499999E 01	0.22500000E 01	[illegible]	[illegible]	[illegible]
54	0.72499999E 01	0.17500000E 01	0.12427802E 04	0.96363689E 03	0.85292475E-04
55	0.23333333E 01	0.21666667E 01	0.21148779E 04	-0.52733936E 03	0.22136323E-02
56	0.27500000E 01	0.22500000E 01	0.21393420E 04	-0.31031530E 03	0.51475524E-02
57	0.32500000E 01	0.22500000E 01	0.21290173E 04	-0.10741397E 03	0.51400328E-02
58	0.37500000E 01	0.22500000E 01	0.20938562E 04	0.85626457E 02	0.47708076E-02
59	0.42499999E 01	0.22500000E 01	0.20421898E 04	0.27520689E 03	0.39984915E-02
60	0.47499999E 01	0.22500000E 01	0.19769110E 04	0.46199524E 03	0.31580695E-02
61	0.52499999E 01	0.22500000E 01	0.18956642E 04	0.63897826E 03	0.23150734E-02
62	0.57499999E 01	0.22500000E 01	0.18007313E 04	0.80434344E 03	0.15886256E-02
63	0.62499999E 01	0.22500000E 01	0.16984847E 04	0.96246449E 03	0.10643750E-02
64	0.67499999E 01	0.22500000E 01	0.15924616E 04	0.11053530E 04	0.72302434E-03
65	0.72499999E 01	0.22500000E 01	0.15025429E 04	0.12121824E 04	0.55565598E-03
66	0.28333333E 01	0.26666667E 01	0.21884867E 04	-0.85414144E 02	0.33338824E-02
67	0.32500000E 01	0.27500000E 01	0.22059818E 04	0.12519310E 03	0.77996037E-02
68	0.37500000E 01	0.27500000E 01	0.21950389E 04	0.32438920E 03	0.78629684E-02
69	0.42499999E 01	0.27500000E 01	0.21659227E 04	0.51891333E 03	0.73887997E-02
70	0.47499999E 01	0.27500000E 01	0.21208598E 04	0.70759016E 03	0.65366024E-02
71	0.52499999E 01	0.27500000E 01	0.20576591E 04	0.88363314E 03	0.63858839E-02
72	0.57499999E 01	0.27500000E 01	0.19790207E 04	0.10467551E 04	0.41922129E-02
73	0.62499999E 01	0.27500000E 01	0.18918114E 04	0.12012841E 04	0.32215710E-02
74	0.67499999E 01	0.27500000E 01	0.17982038E 04	0.13377354E 04	0.25105218E-02
75	0.72499999E 01	0.27500000E 01	0.17187174E 04	0.14379604E 04	0.21397624E-02
76	0.33333333E 01	0.31666667E 01	0.22451846E 04	0.34074501E 03	0.48566310E-02
77	0.37500000E 01	0.32500000E 01	0.22591315E 04	0.54536884E 03	0.10922549E-01
78	0.42499999E 01	0.32500000E 01	0.22518136E 04	0.74246384E 03	0.11340134E-01
79	0.47499999E 01	0.32500000E 01	0.22269076E 04	0.93057965E 03	0.11049922E-01
80	0.52499999E 01	0.32500000E 01	0.21813639E 04	0.11043933E 04	0.10048476E-01
81	0.57499999E 01	0.32500000E 01	0.21191705E 04	0.12645182E 04	0.86783057E-02
82	0.62499999E 01	0.32500000E 01	0.20466408E 04	0.14141895E 04	0.74164806E-02
83	0.67499999E 01	0.32500000E 01	0.19648912E 04	0.15445554E 04	0.63833777E-02
84	0.72499999E 01	0.32500000E 01	0.18934509E 04	0.16401999E 04	0.58177307E-02
85	0.38333333E 01	0.36666667E 01	0.22928068E 04	0.75207062E 03	0.66891843E-02
86	0.42499999E 01	0.37500000E 01	0.23074479E 04	0.94919829E 03	0.15272208E-01
87	0.47499999E 01	0.37500000E 01	0.23016573E 04	0.11348878E 04	0.16239796E-01
88	0.52499999E 01	0.37500000E 01	0.22742726E 04	0.13054990E 04	0.16133015E-01
89	0.57499999E 01	0.37500000E 01	0.22286291E 04	0.14612678E 04	0.15254879E-01
90	0.62499999E 01	0.37500000E 01	0.21703588E 04	0.16045638E 04	0.14221207E-01
91	0.67499999E 01	0.37500000E 01	0.21008741E 04	0.17287414E 04	0.13221391E-01
92	0.72499999E 01	0.37500000E 01	0.20364794E 04	0.18202000E 04	0.12630400E-01
93	0.43333333E 01	0.41666666E 01	0.23395702E 04	0.11432714E 04	0.94020686E-02
94	0.47499999E 01	0.42500000E 01	0.23536819E 04	0.13257308E 04	0.21819148E-01
95	0.52499999E 01	0.42500000E 01	0.23444277E 04	0.14918554E 04	0.23541474E-01
96	0.57499999E 01	0.42500000E 01	0.23153196E 04	0.16411798E 04	0.24123146E-01
97	0.62499999E 01	0.42500000E 01	0.22718578E 04	0.17767371E 04	0.24209267E-01
98	0.67499999E 01	0.42500000E 01	0.22152149E 04	0.18937426E 04	0.23946910E-01
99	0.72499999E 01	0.42500000E 01	0.21584209E 04	0.19797549E 04	0.23676847E-01
100	0.48333333E 01	0.46666666E 01	0.23840477E 04	0.15030367E 04	0.13603513E-01
101	0.52499999E 01	0.47500000E 01	0.23934497E 04	0.16629365E 04	0.31813479E-01
102	0.57499999E 01	0.47500000E 01	0.23877522E 04	0.18040838E 04	0.34994295E-01
103	0.62499999E 01	0.47500000E 01	0.23527548E 04	0.19311413E 04	0.37423159E-01
104	0.67499999E 01	0.47500000E 01	0.23093638E 04	0.20391316E 04	0.38824894E-01
105	0.72499999E 01	0.47500000E 01	0.22613572E 04	0.21184919E 04	0.39411122E-01
106	0.53333333E 01	0.51666666E 01	0.24175728E 04	0.18140185E 04	0.15787830E-01
107	0.57499999E 01	0.52500000E 01	0.24221472E 04	0.19466244E 04	0.46489703E-01
108	0.62499999E 01	0.52500000E 01	0.24096056E 04	0.20640192E 04	0.52368242E-01
109	0.67499999E 01	0.52500000E 01	0.23797750E 04	0.21617022E 04	0.56343137E-01
110	0.72499999E 01	0.52500000E 01	0.23408348E 04	0.22340273E 04	0.58343065E-01
111	0.58333333E 01	0.56666666E 01	0.24477541E 04	0.20691088E 04	0.28614962E-01
112	0.62499999E 01	0.57500000E 01	0.24443062E 04	0.21754025E 04	0.67267102E-01
113	0.67499999E 01	0.57500000E 01	0.24285282E 04	0.22420222E 04	0.74437296E-01
114	0.72499999E 01	0.57500000E 01	0.23992977E 04	0.23261338E 04	0.78192167E-01
115	0.63333333E 01	0.61666666E 01	0.24612808E 04	0.22692939E 04	0.40539843E-01
116	0.67499999E 01	0.62500000E 01	0.24612589E 04	0.23438865E 04	0.91836811E-01
117	0.72499999E 01	0.62500000E 01	0.24437966E 04	0.23970472E 04	0.97392396E-01
118	0.68333333E 01	0.66666666E 01	0.24738933E 04	0.24045943E 04	0.52404368E-01
119	0.72499999E 01	0.67500000E 01	0.24706819E 04	0.24455529E 04	0.11214711E 00
120	0.73333333E 01	0.71666666E 01	0.24795791E 04	0.24725691E 04	0.59932956E-01

Figure 35 provides typical fracture patterns of rectangular panels with length-to-width ratios of approximately 2, 3, and 4. The fracture patterns are generally what would be expected. As the length to width ratio of the plate increases, the performance of the plate appears to approach that of one supported on the two long sides only. The "square" center section of a square plate associated with the primary failure mode apparently rather rapidly degenerates from a square through a rectangular phase and into essentially a line. Figure 35, for example, tends to indicate that for even a length-to-width ratio of 2, the center section has almost entirely degenerated. Thus, the prediction of the primary fracture mode for rectangular plates may be simpler than for square plates. It would appear to follow from the degeneration of the plate's center region to a line that debris fragment sizes might be derived on the basis of the procedures for the secondary fracture mode alone.

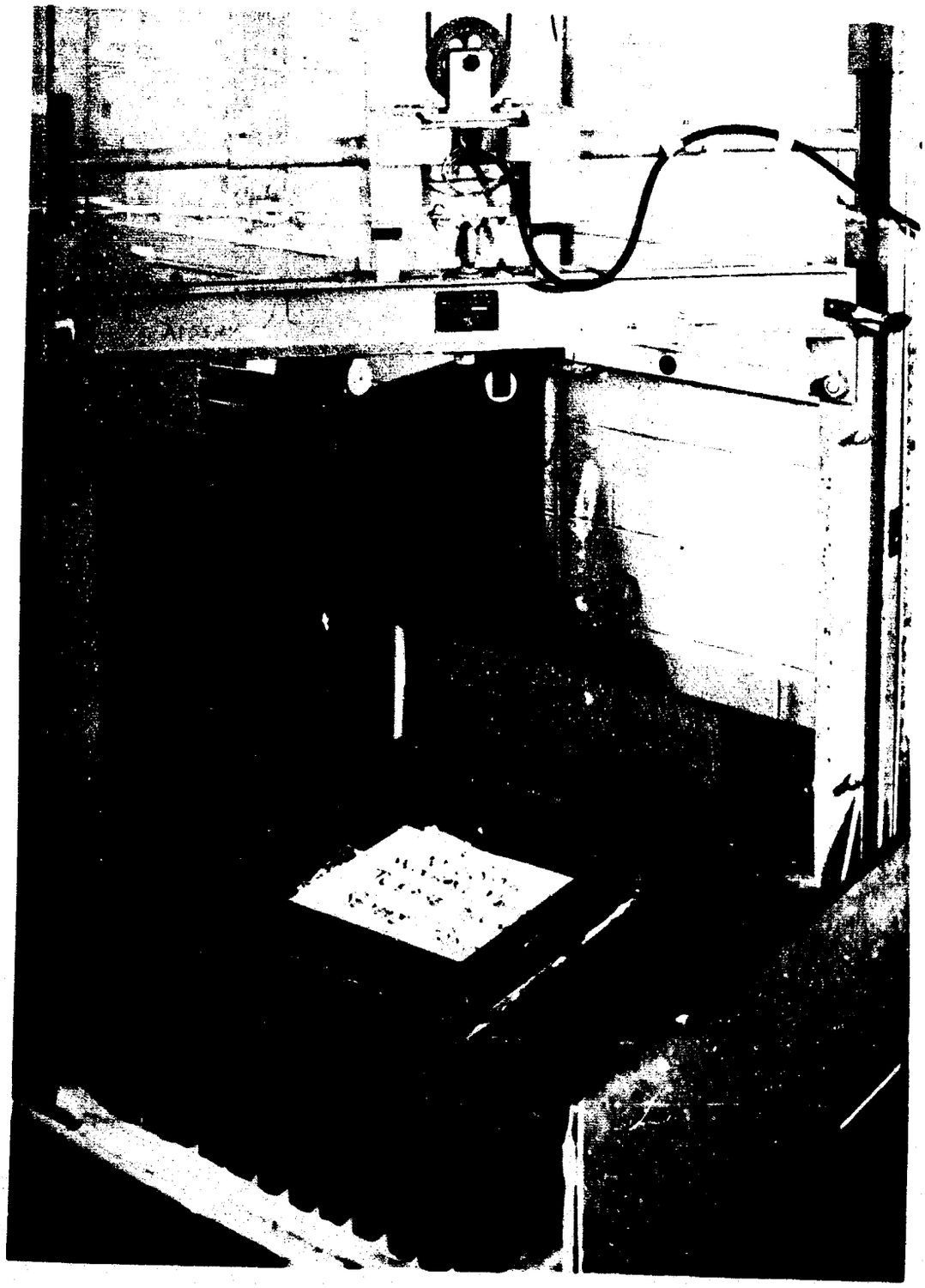

Fig. 29 DROP TABLE

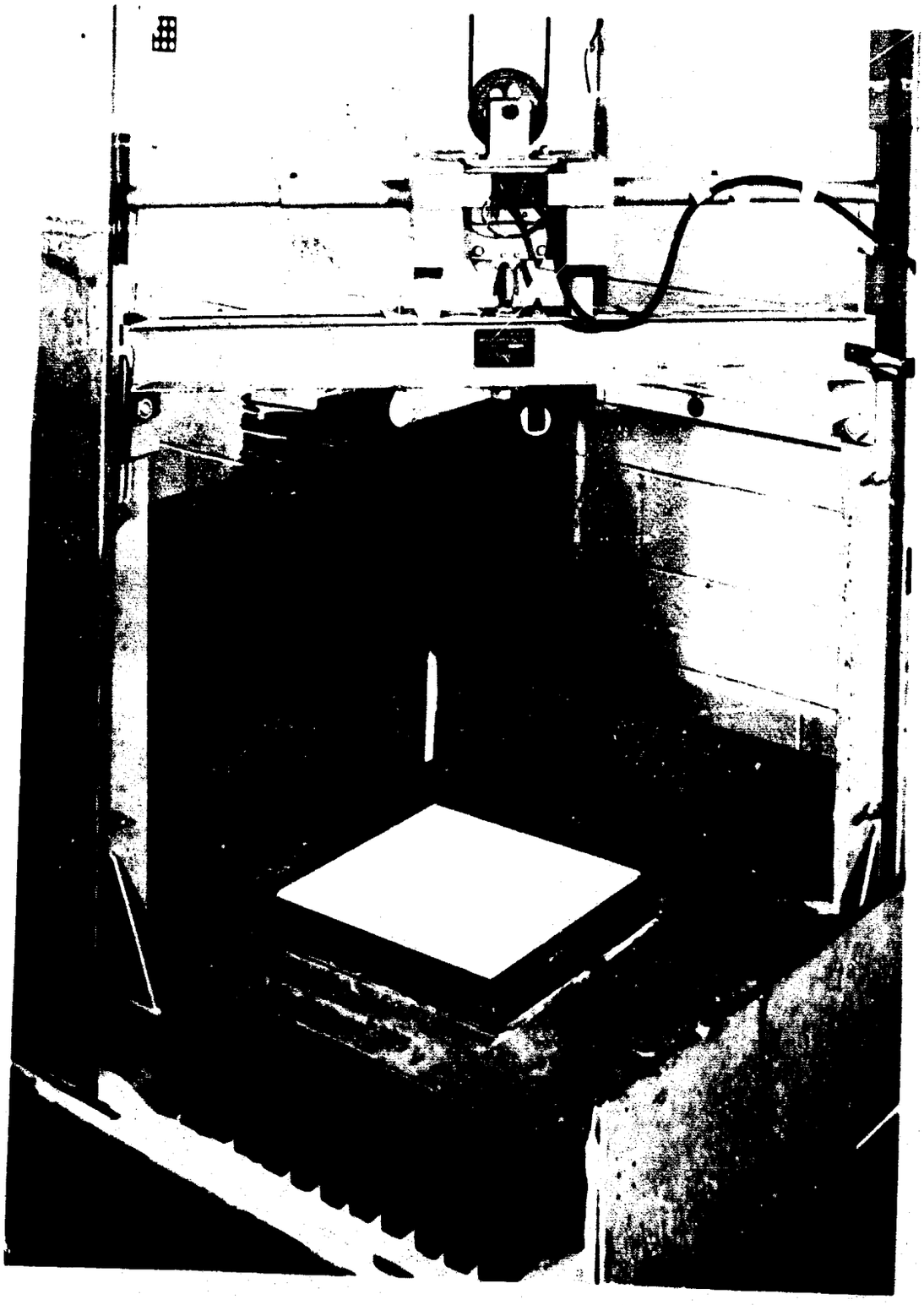

Fig. 30 HYDROSTONE PLASTER PLATE MOUNTED ON DROP TABLE

Fig. 31 PLASTER PLATE TEST WITH SAND OVERBURDEN

Fig. 32 TYPICAL PLATE FRAGMENTATION

Fig. 33 STRESS COAT PATTERN (Drop Height 36 in., Total Uniform Sand Load 40 lbs)

Fig. 34 STRESS COAT PATTERN (Drop Height 18 in., Total Uniform Sand Load 40 lbs)

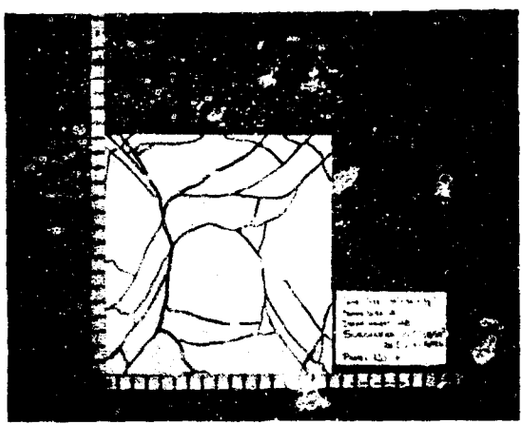

16 x 16 (1:1)

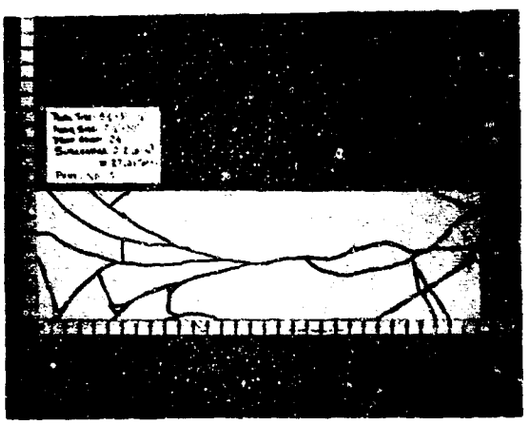

8.5 x 31 (~1:4)

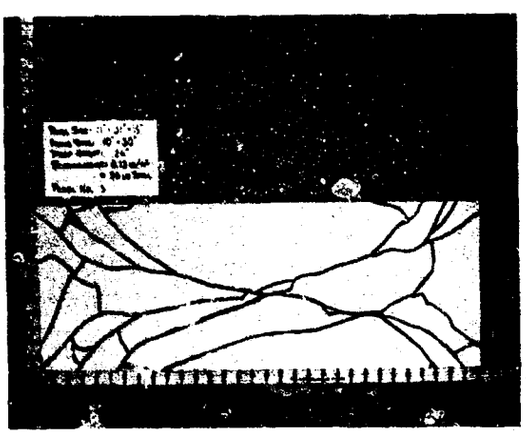

11 x 31 (~1:3)

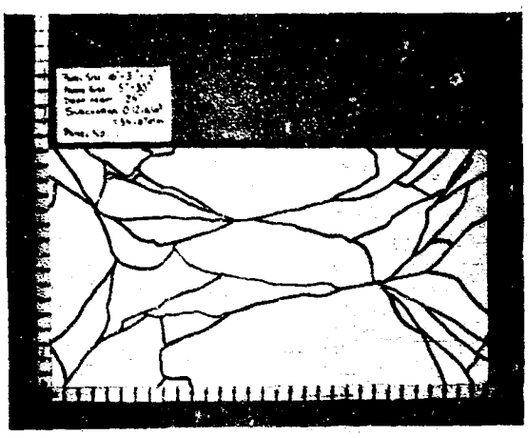

16 x 31 (~1:2)

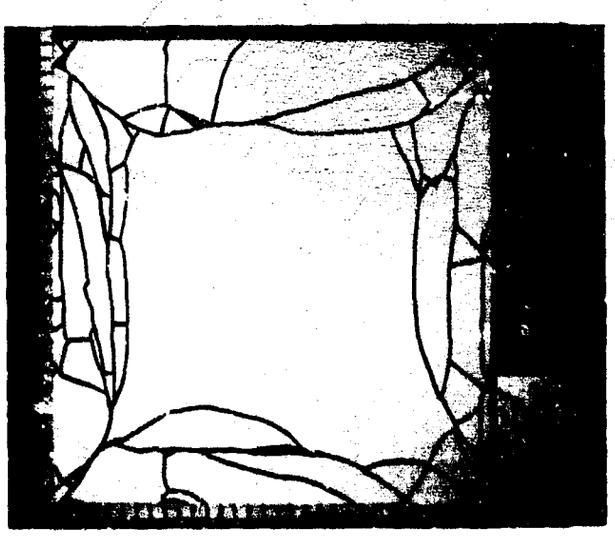

31 x 31 (1:1)

Fig. 35 TYPICAL FRACTURE PATTERNS FOR PLASTER PLATES

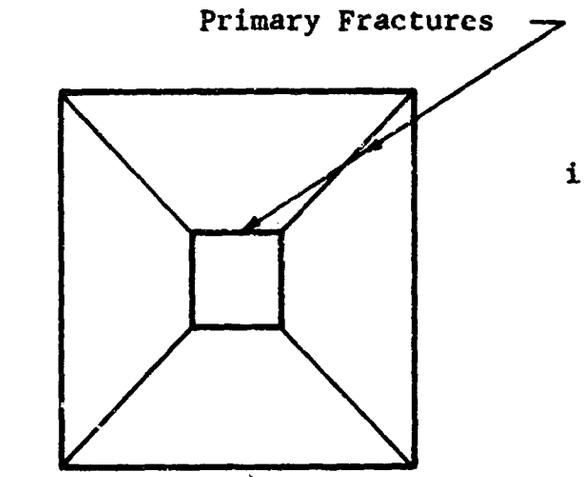

a. Primary Fracture Pattern

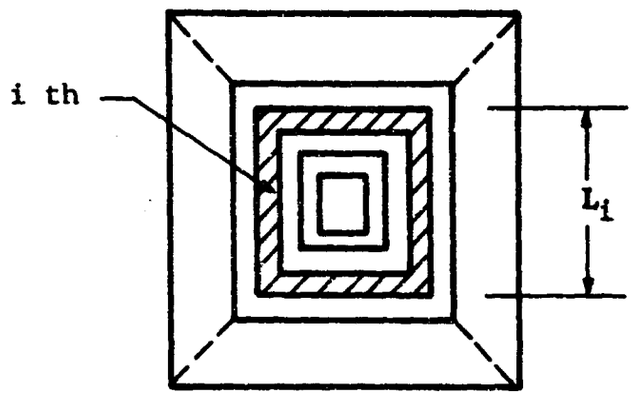

b. Unit Elements - Primary Mode

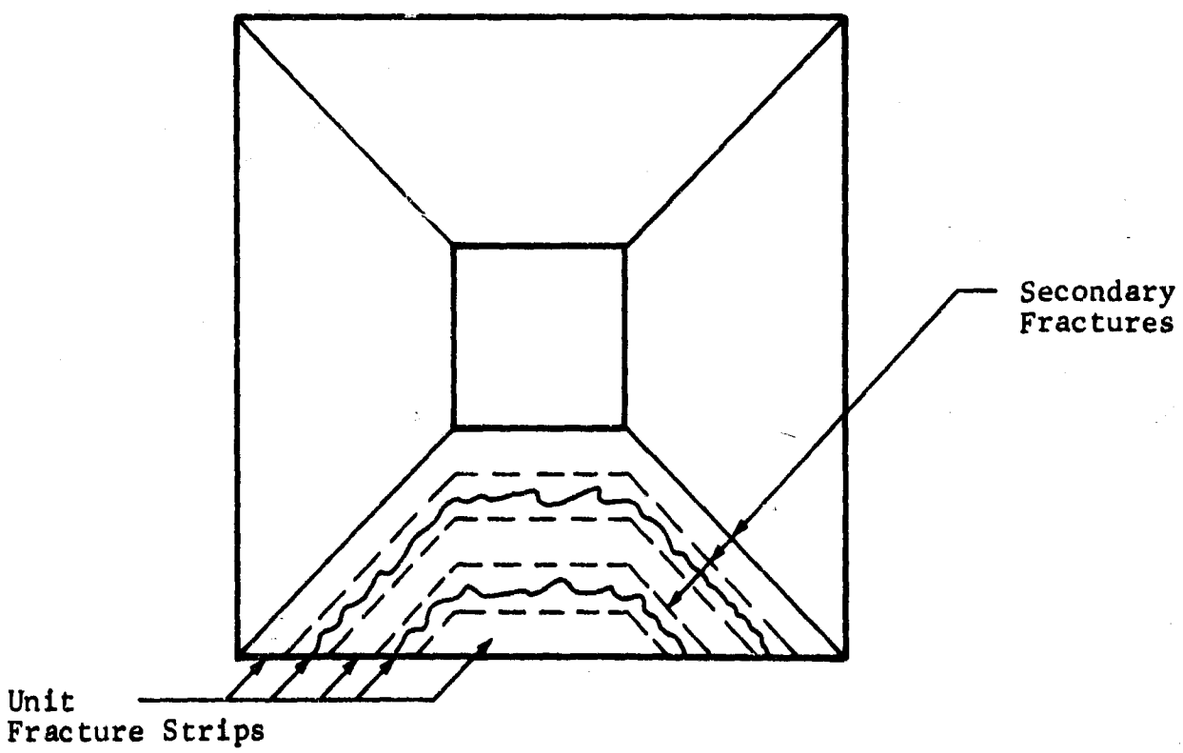

c. Secondary Fracture Pattern

Fig. 36 FRACTURE PATTERNS FOR A SQUARE PLATE

3.5 FRAGMENTATION ANALYSIS

Before we describe the methods for defining primary and secondary fragments we must first establish the probability that a crack will initiate within an arbitrary region of a plate. Consider the triangular area enclosed by OBC for the square plate of Fig. 23. Assume that the principal stress trajectories suggest that the area be subdivided into the four strips identified by the Roman numerals shown in the figure. Note that strip II contains the plate subdivisions, 8, 9, 10, 11, 12, 24, 25, 26, 27, 37, 38, 39, 40, 41, 51, 52, 53, 54, 62, 63, 64 and 65. The risk of rupture for strip II, B_{II}, is equal to the sum of the risks of rupture associated with the preceding sequence of subdivisions, i.e.,

$$B_{II} = B_8 + B_9 + \ldots + B_{64} + B_{65} = 0.00558$$

Now, the probability that a crack will initiate in strip II is simply

$$F_{II} = 1\text{-}e^{-BII} = 1\text{-}e^{-0.00558}$$

We may now consider the primary mode.

3.5.1 Primary Fracture Mode

To establish the size of the central square fracture pattern we will divide the central region of the plate into the imaginary square strips shown in Fig. 36b. The failure probability F_i of each of the strips will be computed and the length L_i associated with the largest F_i or B_i will be taken as the size of the square pattern.

In Fig. 37 we have computed one-eighth of the risk of rupture for each of the square strips shown in Fig. 36b. The maximum occurs in the strip containing the subdivisions 111, 112, 113, and 114. Clearly then, this defines the primary fracture mode. We note in passing that the maximum stresses decrease as we move away from the center and that the primary strip volumes increase as we move from the center. This explains why we find a relative maximum between the center and the edges.

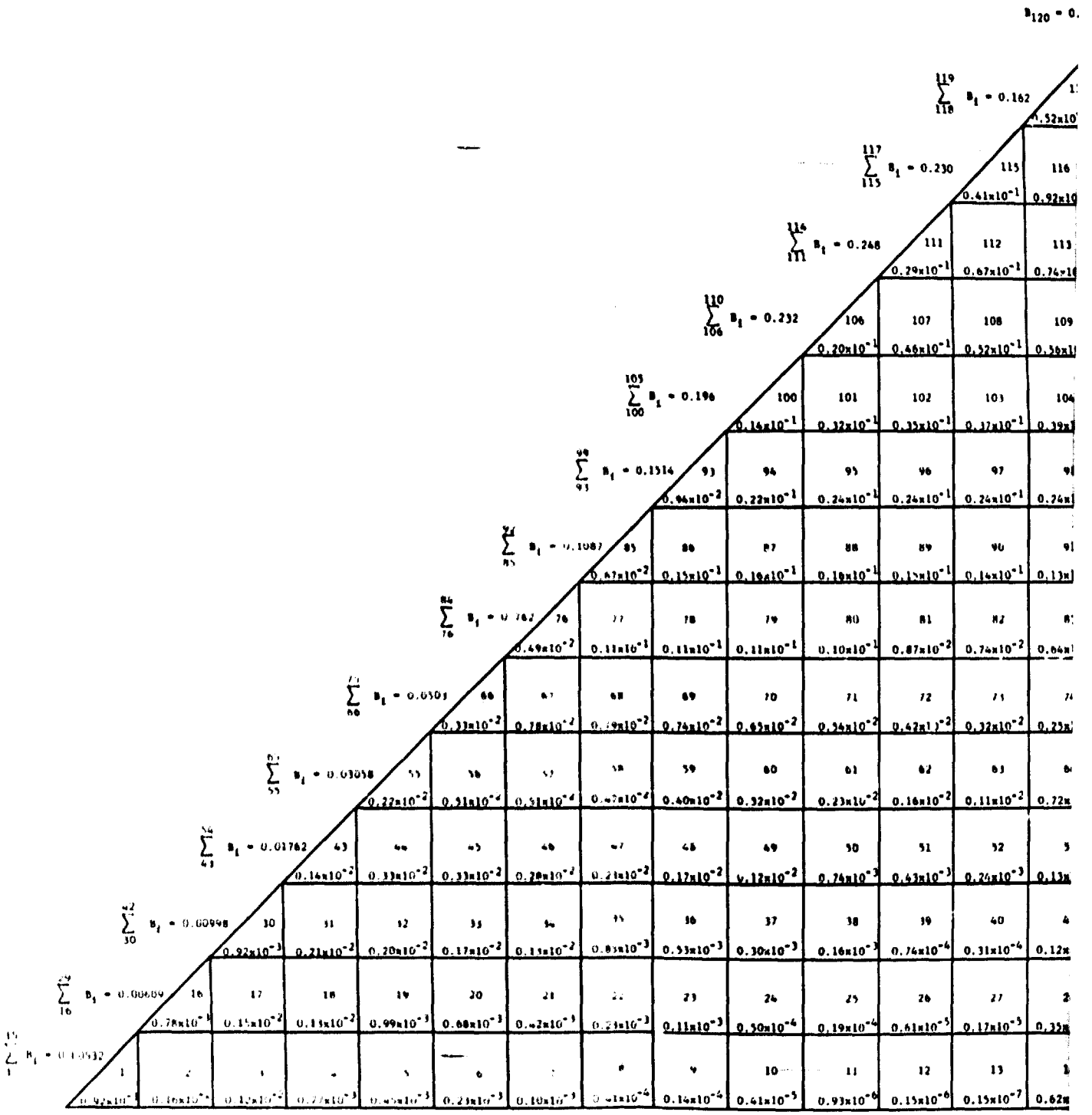

Fig. 37 RISKS OF RUPTURE ALONG HORIZONTAL STRIPS, PRIMARY MODE

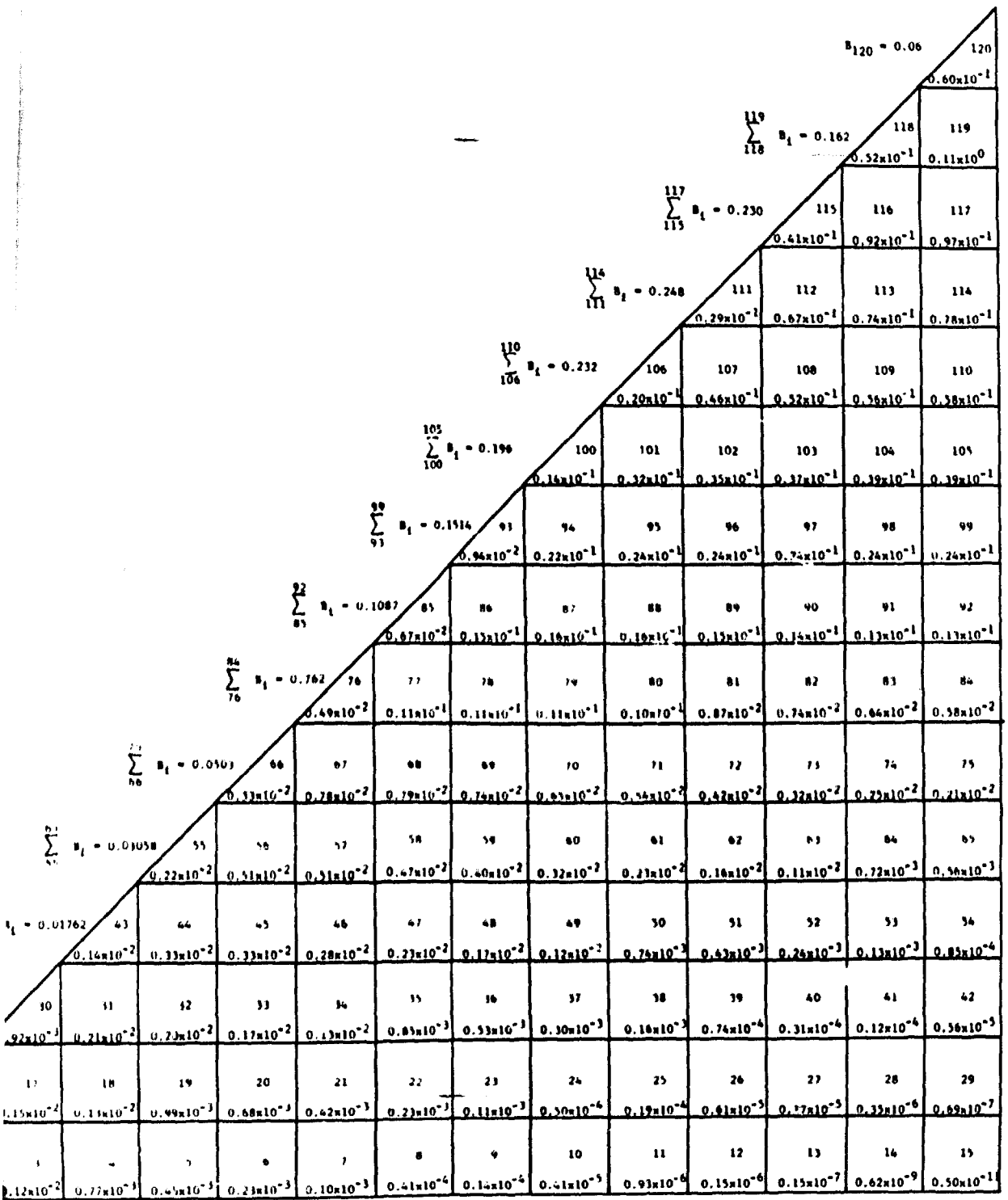

Fig. 37 RISKS OF RUPTURE ALONG HORIZONTAL STRIPS, PRIMARY MODE

We observed from the various replications of drop tests on square plates that the size of the center square remained fairly constant. If large variations would have occurred the probability of getting a size L_i is simply F_i.

3.5.2 Secondary Fracture Mode

Using the hypothesis that the secondary cracks will follow the principal stress trajectories, we can divide the trapezoidal regions formed by the primary cracks, into the fracture strips shown in Fig. 38. Each of these strips will independently fracture or remain intact in exactly the same manner previously described for beam fragmentation. Specifically, the simply supported plate gives rise to the same problem solved for the simply supported beam.

There are three methods available for dealing with secondary plate fractures. We begin each method by numbering the strips as shown in Fig. 38. Then, using the same technique employed to find the probability of fracture initiation in strip II of Fig. 23, we can find the fracture probability of each of the n strips indicated in Fig. 36, F_m. Finally, we observe that the periphery ABCD is a free boundary. We may now consider each method separately.

3.5.2.1 Combination Method

This method, which is described in Ref. 9, considers individually each of the possible 2^n combinations of failure and nonfailure of the strips. If F_i is the fracture probability of the ith strip and S_i the associated survival probability (note: $S_i = 1-F_i$), then the following combinations of fracture and survival tabulated in Table 3 are possible in a four-strip plate.

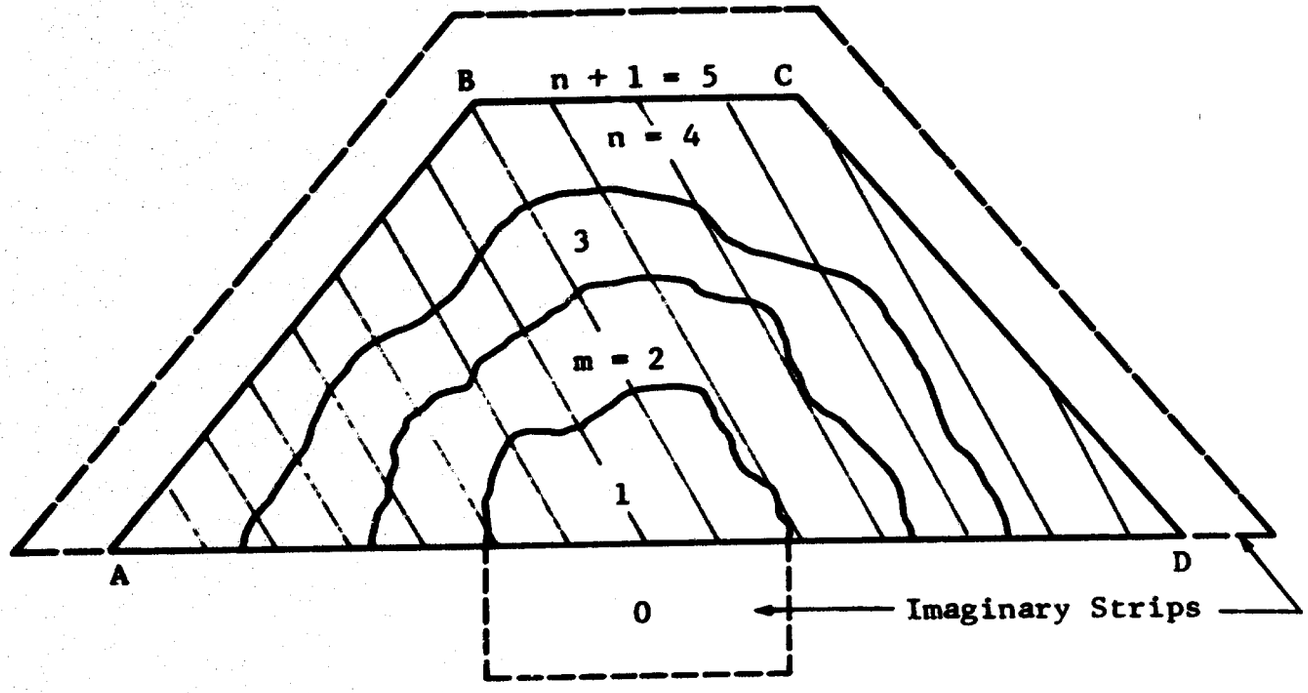

Fig. 38 NUMBERING SYSTEM FOR PLATE STRIPS

Table 3

POSSIBLE COMBINATIONS IN A FOUR-STRIP TRAPEZOID

Combinations			
$S_1S_2S_3S_4$	$S_1S_2S_3F_4$	$S_1F_2F_3S_4$	$F_1F_2S_3F_4$
$F_1S_2S_3S_4$	$F_1F_2S_3S_4$	$S_1F_2S_3F_4$	$F_1S_2F_3F_4$
$\underline{S_1F_2S_3S_4}$	$F_1S_2F_3S_4$	$S_1S_3F_3F_4$	$S_1F_2F_3F_4$
$S_1S_2F_3S_4$	$F_1S_2S_3F_4$	$F_1F_2F_3S_4$	$F_1F_2F_3F_4$

Each of these products represent the probability that the represented combination will occur. The sum of these probabilities will, of course, equal unity.

Now, let us examine a typical combination, say the underlined one, and describe its significance to the fragmentation problem. First, if n plates are dynamically loaded, 4n trapezoids will give rise to secondary fractures. Consequently, the number of times the underlined combination will occur is $4n(S_1F_2S_3S_4)$. Associated with this particular combination is the mixture of the two fragments (strip 1) and (strips 3 + 4). An examination of Table 3 indicates that these two fragments can arise from other combinations; for example, strip (3 + 4) is formed by both $S_1F_2S_3F_4$ and $F_1F_2S_3S_4$. It is a simple matter of bookkeeping to accumulate the number of times each possible fragment occurs. On the other hand, it is very time consuming to consider each of the 2^n possible combinations which generate the various fragments.

The type and efficiency of debris removal equipment will be influenced in a significant way by the composition of the debris. By studying the more frequently occurring combinations of fracture and nonfracture, it is possible to estimate the character of a mixture of fragments. The combination which appears most frequently is associated with the following probability.

$$P_{max} = \prod_{i=1}^{n} \max(F_i, S_i) \qquad (29)$$

If $F_i \neq 0.5$ this combination is unique.

3.5.2.2 Fragment Group Method

If we are not interested in how the various fragments are mixed together, we can adopt a very efficient procedure for calculating the total number of every possible type of fragment. In an n-strip plate segment there are $(n/2)(n+1)$ possible combinations of contiguous strips. Each of these combinations represent a possible fragment. We can easily display these combinations as shown in Table 4 for a four-strip trapezoid. The fragments are designated by the numbers of the strips contained in the fragment. For example, fragment 2,3 is composed of the strips 2 and 3 in Fig. 38. To obtain this fragment, it is clear from this figure that strips 1 and 4 must fracture, and strips 2 and 3 must not fracture. The probability of this happening is represented as the probability of simultaneously getting fracture in strips 1 and 4 and getting no fracture in strips 2 and 3, i.e., $F_1S_2S_3F_4$.

As another example, we see that fragment 1,2 can be realized by survival of strips 1 and 2 followed by fracture in strip 3. It does not matter whether strip 4 fractures or not. Thus, the probability of obtaining fragment 1,2 in a trapezoid is simply $(S_1S_2F_3 \cdot 1)$. The total number of fragments "1,2" realized from n plate experiments is $4n(S_1S_2F_3)$.

If a fragment is composed of strips k, k+1, ...,k+ℓ, the probability of its occurrence in a trapezoid, $P_{k,k+1,\ldots,k+\ell}$, is given by

$$P_{k,k+1,\ldots,k+\ell} = F_{k-1} F_{k+\ell+1} \prod_{i=k}^{i=k+\ell} (1-F_i) \qquad (30)$$

where the fracture probabilities F_0 and F_{n+1} represent the imaginary strips shown in Fig. 38.

For a trapezoid with a free boundary, $F_o = F_{n+1} = 1$, a fixed boundary condition is represented by $F_o = 1$. Until the fracture pattern is known, we cannot comment on the shape, location or behavior of the n+1 strip in the fixed boundary plate.

Table 4

NUMBER AND TYPE OF FRAGMENTS IN FOUR-STRIP TRAPEZOID

Fragment Designation	Probability of Occurrence-Trapezoid
1	S_1F_2
2	$F_1S_2F_3$
3	$F_2S_3F_4$
4	F_3S_4
1,2	$S_1S_2F_3$
2,3	$F_1S_2S_3F_4$
3,4	$F_2S_3S_4$
1,2,3	$S_1S_2S_3S_4$
2,3,4	$F_1S_2S_3S_4$
1,2,3,4	$S_1S_2S_3S_4$

3.5.2.3 Method of Runs

By considering every one of the possible 2^n distinct fracture patterns, the method of combinations provides the specific description and quantity of every possible fragment, and in addition, it details the various possible mixtures of large and small fragments. The method of fragment groups sacrifices this latter information, but it increases the computational efficiency enormously. For example, if the number of strips n is equal to 20, the combination method considers $2^n = 1,048,576$ distinct fracture patterns; the method of fragment groups will consider at most all of the possible fragment combinations, $(n/2)(n+1)=2010$.

Although the increased efficiency of the method of fragment groups is considerable, an even faster method can be used if we settle for less information. This method, called the method of runs, was described in Ref. 7 for the fragmentation of beams. The procedure as developed is not directly applicable to the plate problem. To see this we shall consider the general problem of describing the fragments resulting from fractures in strips 1 and 3. For the beam we would say that we had a one-unit piece between units 1 and 3 and between unit 3 and the support; that is, units 2 and 4 remain intact. Therefore, for this combination we would have recorded two "one-unit" pieces. In the plate, a glance at Fig. 38 indicates that strips 2 and 4 are different and we cannot claim generally that we have two one-unit strips.

With this in mind, we shall begin our approach by selecting strips with equal areas as shown in general in Fig. 39a or in particular in Fig. 39b. Now, every one-strip, two-strip, and r-strip fragment (or run) has the same mass.

This choice of equal strip areas reduces the fragmentation problem exactly to that described for beams in Ref.10. For example, to find the total number of two-unit runs in the four strips shown in Fig. 39b, we observe that a two-unit strip can occur in two ways: two nonfailure strips followed by a failure at either end or two nonfailure preceded and followed by failures. The probability that these events will take place is given by:

$(1-F_1)(1-F_2)F_3 \cdot 1$	two-unit fragment, bottom
$(1-F_4)(1-F_3)F_2 \cdot 1$	two-unit fragment, top
$F_1(1-F_2)(1-F_3)F_4$	two-unit fragment, middle

The sum of these individual probabilities is the total probability of obtaining a two-unit fragment from one trapezoid in the plate.

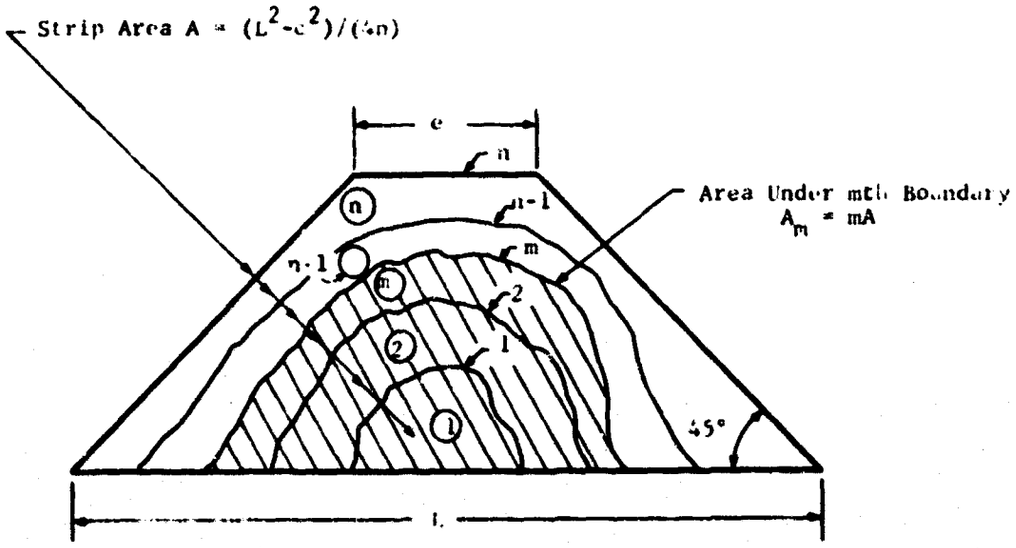

a) Arbitrary Strip Geometry

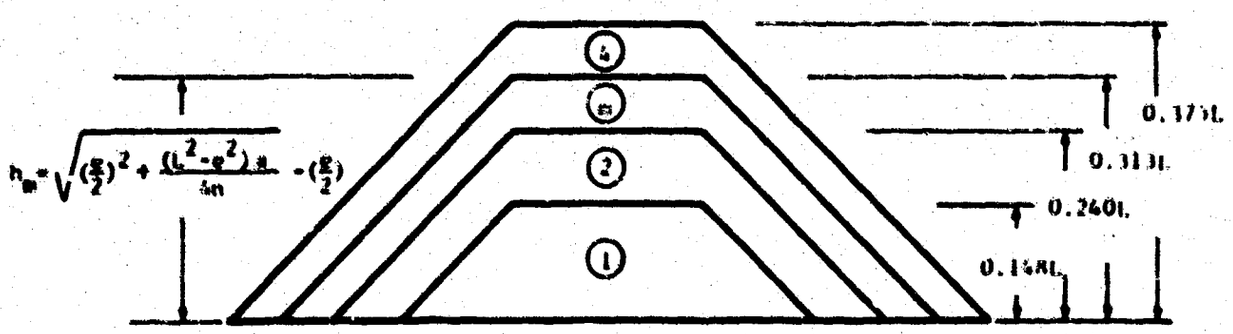

b) Specific Strip Geometry

Fig. 39 GEOMETRIC PROPERTIES FOR EQUAL STRIP AREAS

The general formula for calculating the probability that a run of r equal area strips will occur in a trapezoid is given by

$$P_{(r)} = \sum_{k=1}^{n-\ell} P_{k,k+1,\ldots,k+\ell} \tag{31}$$

or

$$P_{(r)} = \sum_{k=1}^{n-r+1} F_{k-1}\, F_{k+r} \prod_{i=k}^{k+r-1} (1-F_i) \tag{32}$$

where F_o and F_{n+1} are the fracture probabilities in the two imaginary strips shown in Fig. 38. Here, $F_o = F_{n+1} = 1$. Computing the fragmentation from this formula is very rapid and inexpensive; however, we know only the weight characteristics of the fragments, not their geometry or their mixture.

As a final comment we should note that the propagation of a crack is at best a temperamental and sensitive phenomenon. One should not be surprised if a single crack branches into two cracks, or if an occasional crack propagates across the principal stress trajectories. These pecularities will produce a larger number of small fragments and a smaller number of large fragments than predicted.

CHAPTER FOUR
TRAJECTORY OF DEBRIS PARTICLES

4.1 DESCRIPTION OF THE PHYSICAL MODEL

In order to represent the effect of debris transport and subsequent distribution, it is necessary to move from a problem space consisting of the real world to a more abstract mathematical model. This abstraction consists of representing the initial condition of possible debris as a series of lumped masses at levels above ground. Each lumped mass is characterized by a unique particle size distribution. The particle size, in turn, has weight and shape attributes associated with it. The trajectory model assumes two ideal initial conditions. These are:

- Zero failure time of fragmented elements.
- An initial particle velocity of zero.

These assumptions were made, initially, due to a lack of knowledge concerning any other possible values. A study concerning these parameters has since been made and is reported at the conclusion of this chapter. The result of this study indicates that the initial assumptions are well grounded.

4.2 INTRODUCTION TO SINBAD

SINBAD (Simulation Investigation of Nuclear Blast Associated Debris) is a problem-oriented computer language that deals with the problem of postattack structural debris. In a previous investigation (Ref. 10) debris profile curves (i.e., height of debris versus distance thrown) were developed for a free-standing masonry panel wall. Several analyses, both manual and computerized, were utilized to predict the profile of a single wall. The present study is a refinement of the previous techniques and is extended to include any grouping of walls subjected to a frontal shock. It is now also possible to determine the size distribution and a measure of the momentum of the debris at any point in the profile. The language is expandable and in its entirety will

include frame response as well as the interior contents of the structure. The flow diagram illustrated in Fig. 40 indicates the general computational scheme. The boxes that are now dotted are components that will be added to the system at a later time. The remaining sections of this chapter describe the input language and sample problems run on the program.

4.2.1 Input Language

The form of the input to the SINBAD processor differs significantly from most other computer programs. Format and ordering of card input have been almost eliminated; they have been replaced by a set of commands consistent with postattack terminology. The fact that a group of characters starts with a letter is sufficient to recognize a word. Similarly, a number indicates numerical data; a decimal point distinguishes a decimal number from an integer; and a blank or a comma after a group of characters indicates the end of the group.

The input commands may be data descriptors, data to be stored, or more generally information about the input process. A data descriptor (e.g., YIELD or OVERPRESSURE) communicates to the system that the number that follows is to be associated with that command. Data to be stored consist of the numerical data associated with data descriptors. Commands such as WEAPON PARAMETERS, PREBLAST STRUCTURAL CONFIGURATION and SOLVE actually control the internal flow of the program. Table 5 contains the dictionary of available commands. Each command occupies a separate input card in the data and a card may be continued by placing a dollar sign ($) in the first column of the following cards. Each input card is printed on the system output before the solution phase of the processor takes over. It is possible to put comment cards into the input phase simply by placing an asterisk (*) in column 1 of the card. This card is simply echo printed, but otherwise ignored. Table 6 illustrates a set of commands that is sufficient to describe a debris problem. Once the problem has been initially described for one wall and solved, it is necessary to change only those parameters which one wishes to vary in any subsequent wall or problem.

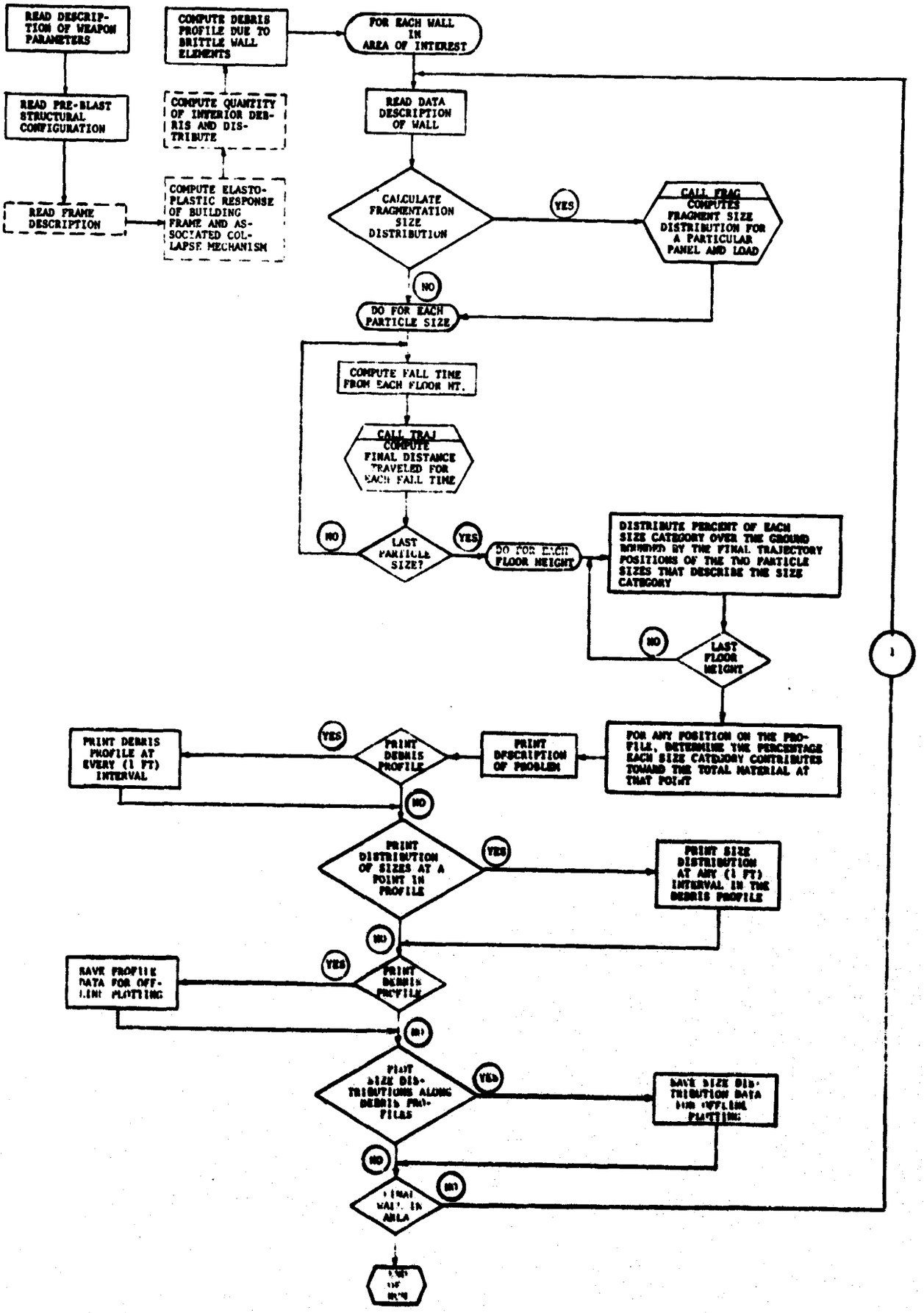

Fig. 40 COMPUTATIONAL FLOW GRAPH FOR SINBAD

Table 5

DICTIONARY OF PROCESS COMMANDS AND DATA DESCRIPTORS

Process Commands	Data Descriptor
WEAPON PARAMETERS	YIELD
	OVERPRESSURE
	GROUND ZERO DISTANCE
PREBLAST STRUCTURAL CONFIGURATION	WALL HEIGHT
	HEIGHT BETWEEN FLOORS
	SPACE BETWEEN WALLS
	NORMALIZING FACTOR
FRAGMENTATION CHARACTERISTICS	NUMBER OF PARTICLE SIZES
	PARTICLE SIZES
	PERCENTAGE BY SIZE
	ACCELERATION COEFFICIENT
COMPUTE FRAGMENTATION CHARACTERISTICS	BEAM REPRESENTATION
	LENGTH
	DEPTH
	WIDTH
	STRESSO
	STRESSU
OUTPUT	PROFILE DISTRIBUTION
	LOCATIONS
	DISTANCES FROM FIRST WALL
	VELOCITY DESCRIPTION
	DEBRIS PROFILE PLOT
SOLVE	

Table 6

A SUFFICIENT SET OF COMMANDS AND INPUT TO SPECIFY A DEBRIS PROBLEM TO SINBAD

```
WEAPON PARAMETERS
YIELD 5000 KT
OVERPRESSURE 10 PSI
PREBLAST STRUCTURAL CONFIGURATION
WALL HEIGHT 40 FLOORS
HEIGHT BETWEEN FLOORS 10 FEET
DISTANCE OF WALL FROM INITIAL WALL 50 FEET
NORMALIZING FACTOR 1.0
FRAGMENTATION CHARACTERISTICS
NUMBER OF PARTICLE SIZES 5
PARTICLE SIZES 2.0, 4.0, 6.0, 8.0, 10.0 INCHES
PERCENTAGE BY SIZE 0.05, 0.32, 0.16, 0.32, 0.05
ACCELERATION COEFFICIENT 0.0
OUTPUT
PROFILE DISTRIBUTION
DISTRIBUTION OF SIZES
LOCATIONS 3
DISTANCES FROM FIRST WALL 50, 150, 300 FEET
DEBRIS PROFILE PLOT
SIZE DISTRIBUTION PLOT
SOLVE
WEAPON PARAMETERS
OVERPRESSURE = 20.0 PSI
SOLVE
```

The command SOLVE terminates the input phase of the processor and transfers control to the computational section. When the specified problem is solved and the answer printed, control is automatically returned to the input phase. Each of the data descriptors will now be discussed in detail.

- The process command WEAPON PARAMETERS has three data descriptors: YIELD, OVERPRESSURE, and GROUND ZERO DISTANCE. The YIELD is the weapon size in kilotons, and is used in conjuction with either the OVERPRESSURE (psi) or GROUND ZERO DISTANCE (ft) to specify an overpressure-distance relationship. This relationship is presently based on a mach region surface burst assumption, however, as the overall system is modular in concept, airburst and regular reflection capabilities could be included with only some additional effort. Again, it is only necessary to specify either the OVERPRESSURE or the GROUND ZERO DISTANCE. Knowledge of one of these parameters, along with YIELD, is sufficient to determine the other.

- PREBLAST STRUCTURAL CONFIGURATION consists of four data descriptors that describe the wall under investigation. WALL HEIGHT gives the total number of floors (i.e., panels) in the wall. HEIGHT BETWEEN FLOORS is the panel height in feet. SPACE BETWEEN WALLS is the distance in feet of the wall presently being investigated from the last previously investigated wall. If only one wall, or the initial wall in a multiwall configuration is being investigated, this descriptor is unnecessary. Finally, a NORMALIZING FACTOR descriptor is included to account for the normalization of the debris profile curve.

This normalization has been explained in the previous report (Ref.10) and it suffices to say that this descriptor is usually the product of an individual panel's length and thickness. If the NORMALIZING FACTOR is unity, then the subsequent debris profile will be normalized by a unit width volume (i.e., the product of the length and thickness, sq ft, of an individual panel).

- The process commands FRAGMENTATION CHARACTERISTICS of COMPUTE FRAGMENTATION CHARACTERISTICS describe the type of particles that result due to panel fragmentation. This report will only include a description of the FRAGMENTATION CHARACTERISTICS process command since the computational model of panel fragmentation is only in a formative stage at present. The panel fragmentation model, based on a beam analogy that was developed in the previous report, has been included in the present system but has not been utilized. This was done because its use was considered marginal in light of the work done on panel fragmentation as discussed in Chapter Three. Thus, the data descriptors listed under COMPUTE FRAGMENTATION CHARACTERISTICS are consistent with the input necessary for that previous fragmentation analysis. The data descriptor NUMBER OF PARTICLE SIZES indicates the number of different size particles resulting from panel fragmentation. PARTICLE SIZES is the descriptor of an array of the individual particle sizes in inch units and each is separated by a comma. This array is listed in descending order of size. In a similar manner, PERCENTAGE BY SIZE is a corresponding array of the percentages of an individual panel falling into each of the previously described particle sizes. ACCELERATION COEFFICIENT describes the shape and orientation in flight of an individual debris projectile.

Under normal usage this parameter is set equal to zero and the program assumes a sphere of an equivalent volume radius. If it is desired to investigate other shapes with several orientations, then ACCELERATION is equal to 2 x mass/projected area in units of lb/sq in.

- The process descriptor OUTPUT controls the type of printed and computed output that can be obtained from the system. PROFILE DESCRIPTION indicates that a record of debris height as a function of distance from an initial wall is desired. The next two data descriptors are utilized to obtain the percent by size range at each desired location in the debris profile. LOCATIONS is the number of points in the debris profile where a size distribution breakdown is wanted. DISTANCES FROM FIRST WALL is the array of distances in feet from the initial wall to the points in the debris profile where a size distribution is desired. VELOCITY DESCRIPTION generates three output relationships: cumulative debris momentum, minimum debris momentum, and maximum debris momentum as a function of distance from the initial wall in feet. These relationships are normalized by the mass of an individual panel and are actually momentum per unit length along the debris profile. This will be further developed in the following section. The data descriptor DEBRIS PROFILE PLOT results in the machine plotting of the different relations previously outputed in printed form.

- The process command SOLVE transfers control from the input phase to the computational mode.

The process commands and data descriptors described above and in Table 5 can be inputed in any order, however, the order outlined in Table 6 seems to be logical.

Once a problem has been initially defined it is only necessary to re-specify those data descriptors that change in any subsequent problem. This is also illustrated in Table 6 by the change in overpressure from 10 to 20 psi.

4.3 MOMENTUM ANALYSIS

One of the primary effects of nuclear associated structural debris is the tertiary effect it has on the unsheltered population. It has been shown (Ref. 13) that whereas one may survive from free-field prompt effects of a nuclear explosion, (i.e., blast, thermal and radiation) he may still be highly vulnerable to high-speed flying debris projectiles. In order to measure the effectiveness of this type of phenomenology the projectile's mass as well as its speed must be included. This is accomplished by describing the projectile's momentum per unit length over the debris profile.

The trajectory analysis that was utilized to find the final position of flying debris also yields the projectile's final speed. Figure 41 illustrates how a normalized momentum per unit length is determined. A size range is specified by two projectile sizes. Each of these sizes has a final speed associated with it as well as a final horizontal displacement from its original position. The normalized momentum per unit length is determined by:

$$\bar{M} = \frac{\left| Z_i \frac{V_j + V_{j+1}}{2} \right|}{x_j - x_{j+1}} \qquad (33)$$

where

$\bar{M}$ is the normalized debris momentum per unit length

Z_i is the percent of debris falling into size range i which is composed of particle sizes falling between sizes j and j+1

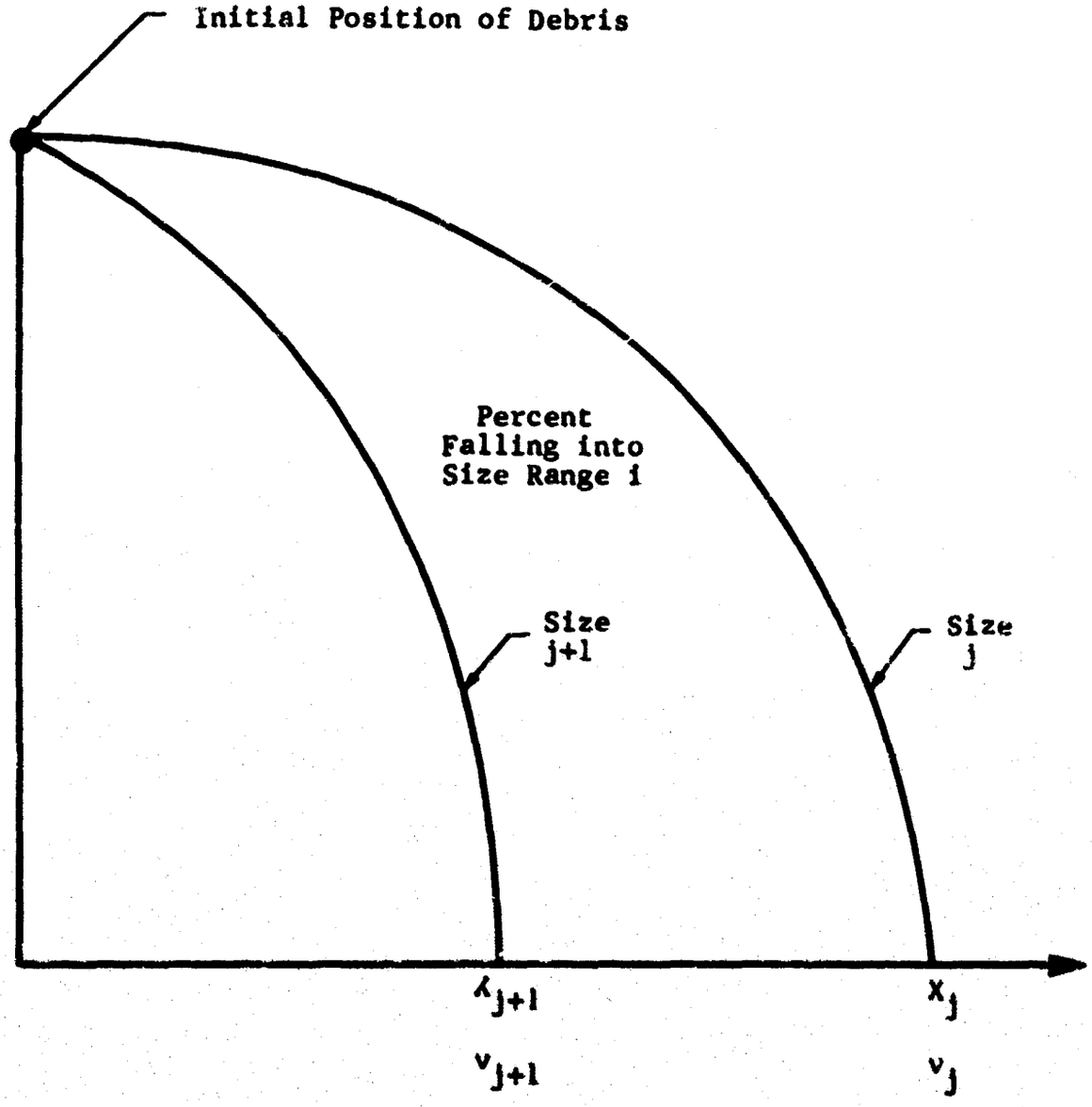

Fig. 41 FORMULATION OF MASS NORMALIZED MOMENTUM PER UNIT LENGTH

V_j, V_{j+1} are the speeds (i.e., magnitude of velocities) of projectile size j and j+1 respectively

x_j, x_{j+1} are the final displacements of the debris particles from their initial position.

If $\bar{M}$ is multiplied by the mass of one panel then the actual momentum per unit length may be obtained. However, $\bar{M}$ is presently left in a mass normalized condition because this allows for window openings in the panel and variation in material properties. Presently $\bar{M}$ is utilized to form three different relationships:

- Mass normalized cumulative debris momentum per unit length along the profile.
- Mass normalized minimum debris momentum per unit length along the profile.
- Mass normalized maximum debris momentum per unit length along the profile.

Once the value of $\bar{M}$ has been determined, it is applied along the length of profile determined by x_j and x_{j+1}. In the case of cumulative momentum, all the individual $\bar{M}$ for all size ranges and for all floor heights are accumulated along x. This gives an indication of the amount of projectiles and their total effect along the debris profile. The minimum momentum relationship along the profile consists of the minimum momentum of any single size range at each x location (i.e., every foot) along the debris profile. The maximum momentum is likewise the maximum effect of any single size range acting along the debris profile. The maximum and minimum momentum relationships along the debris profile establish bounds on the individual projectile's momentum. Whereas the maximum and minimum momentum bounds give the effect of individual projectiles, the cumulative momentum is some indication of the effect of many projectiles landing at any one spot along the debris profile. These relationships, when coupled with available biological data as to impact, are sufficient to estimate the casualties caused by flying structural debris.

4.4 SAMPLE PROBLEMS

Two example problems were run on SINBAD to illustrate the system versatility. The results of these problems are only presented to demonstrate the problem solving capability of the system. They are not meant to illustrate actual debris situations. The first problem is illustrated in Fig. 42 and includes four free-standing frangible walls all of the same length. No shielding of one wall by another is assumed to take place since the example is designed to show the superposition procedure alone. The time to fragmentation of all walls is assumed to be zero as is the initial velocity of all fragments. In this problem all calculated parameters (i.e., debris profile, size distributions at selected points in the profile, and momentum) were printed first for one wall, then two, three and finally all four walls. The input to the problem is also printed and both it and the output are displayed as Appendix C. Plots of the profiles resulting from the different wall combinations are illustrated in Fig. 43 through 46. All profile distances are relative to the first wall and the remaining walls are located down wind of the first wall. It may be seen that this example illustrates that multiple wall configurations may be studied and that the walls can have different structural configurations.

The second sample problem which is independent of the first example demonstrates how a variation of parameters study on the aerodynamic properties of a single brick may be carried out conveniently with the system. A free-standing wall, 40 floors at 400 ft high, consisting of only a single size particle (i.e., a masonry brick with nominal dimensions of 2-1/4 x 3-3/4 x 8 in.) is exposed to a 1 MT weapon. The brick has essentially three orientations: side-on, face-on and end-on. The aerodynamic properties of these three orientations have been documented previously (Ref. 14). Five separate cases were run on SINBAD. These included:

- A volume equivalent sphere.
- Side-on orientation.
- Face-on orientation.
- End-on orientation.
- The numerical average of cases 2, 3 and 4.

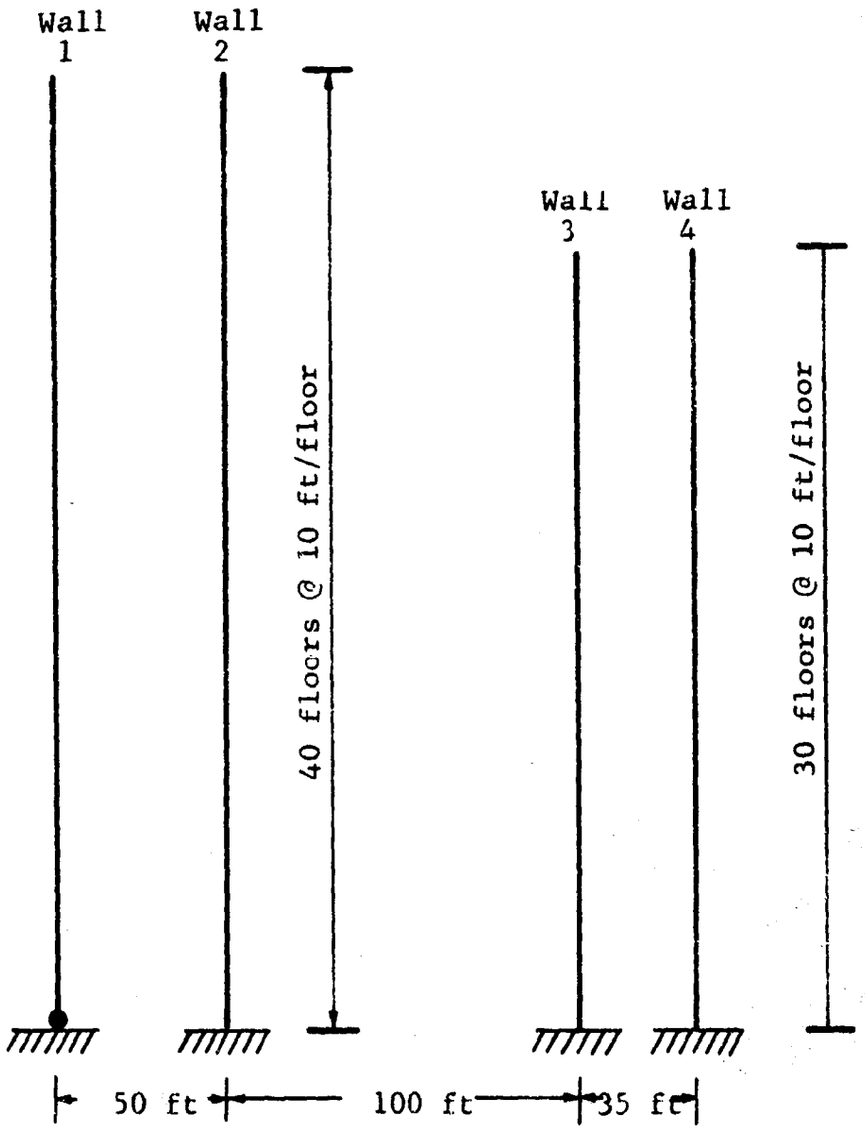

Fig. 42 STRUCTURAL CONFIGURATION FOR SAMPLE PROBLEM 1

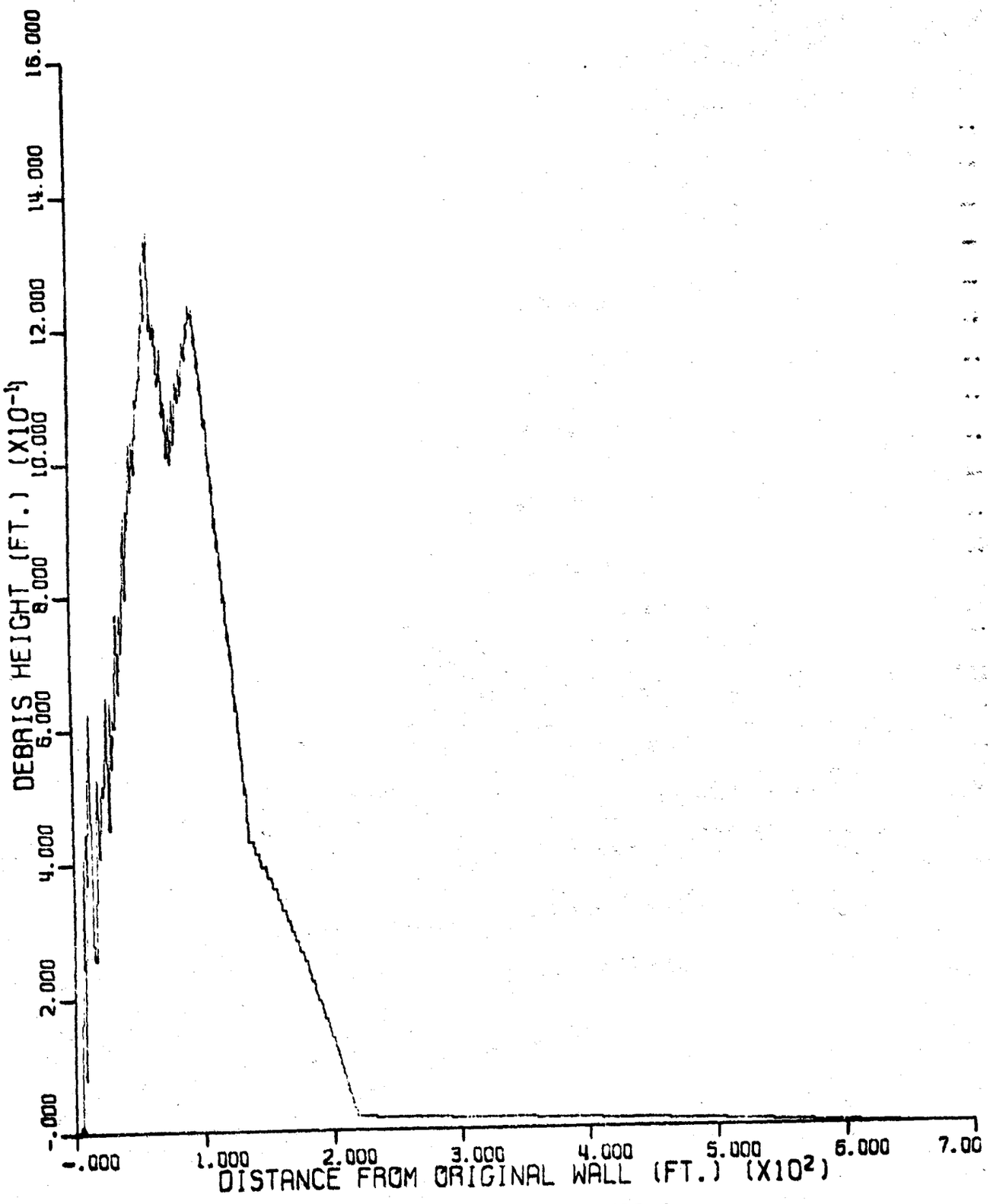

Fig. 43 DEBRIS HEIGHT OF WALL 1

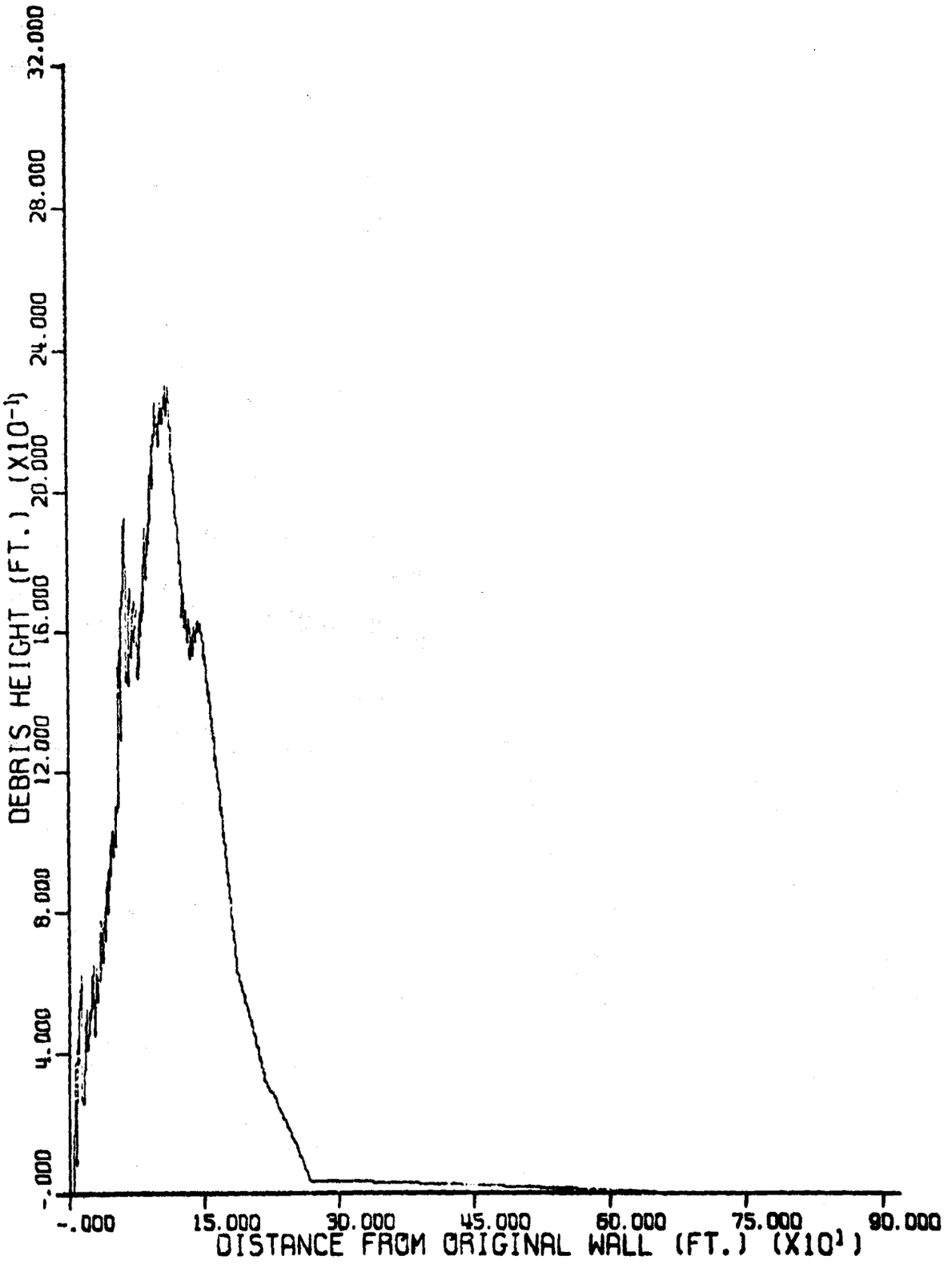

Fig.44 DEBRIS HEIGHT OF WALLS 1 AND 2

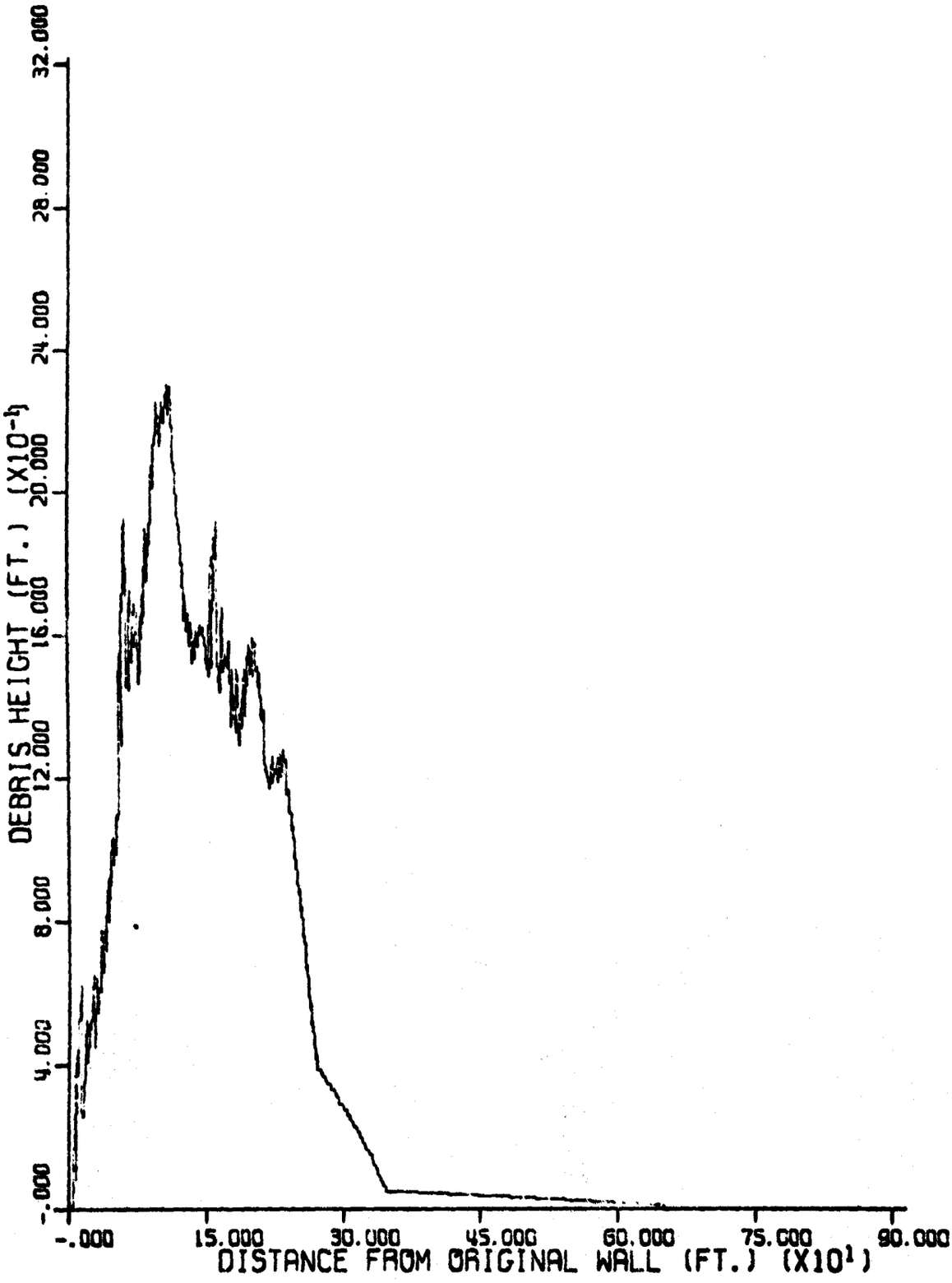

Fig. 45 DEBRIS HEIGHT OF WALLS 1, 2, AND 3

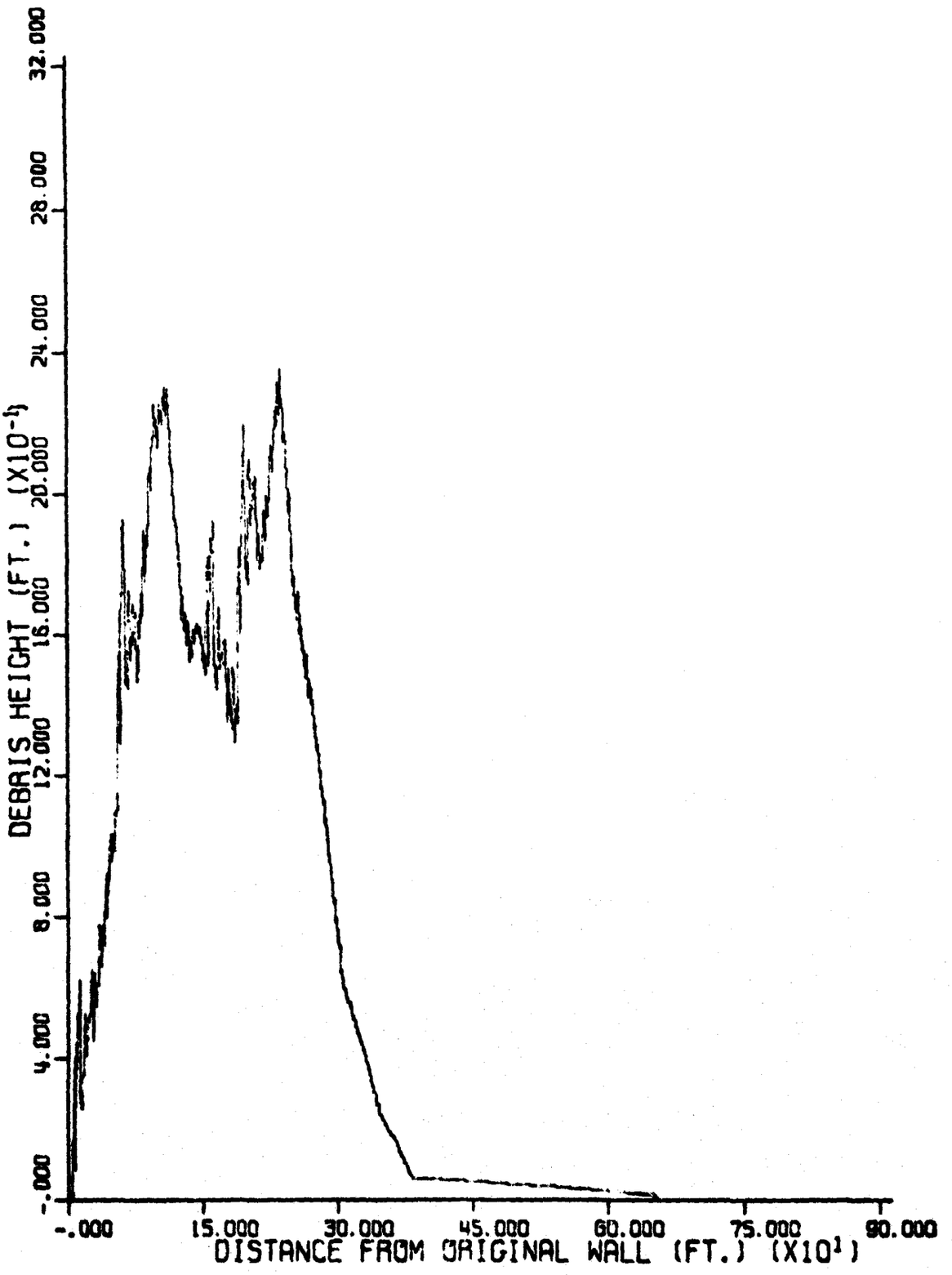

Fig. 46 DEBRIS HEIGHT OF WALLS 1, 2, 3 AND 4

The results of the analysis are summarized in Fig. 47 through 51 for debris profiles, Fig. 52 through 56 for normalized cumulative debris momentum, and Fig. 57 through 61 for maximum and minimum bounds on normalized debris.

It is perhaps interesting to note the almost exact correspondence between cases 1 and 5 of this problem. This is to be expected since an object with the dimensions of a brick is not very different in shape from a spherical object when an average orientation is assumed. Larger objects with more extreme dimensional variation will probably not display this similarity.

The two examples presented were to show the versatility of SINBAD. Thus it is difficult to draw specific conclusions as to debris dispersal from these two problems. The second example however, does illustrate that maximum cumulative debris occurs at the same point down range as maximum debris depth. This fact is substantiated by Table 7. Intuitive reasoning would lead to this same conclusion since the point of maximum debris height is more than likely the point where the most individual particles fall. The maximum momentum of an individual particle falls much closer to the wall than the maximum cumulative momentum.

Table 7

SUMMARY OF RESULTS OF EXAMPLE PROBLEM 2

Particle Type	Maximum Height	Distance @ Maximum Height	Maximum Distance
Sphere (Fig. 47)	0.72	210	380
Side-on (Fig. 48)	0.60	250	480
Face-on (Fig. 49)	0.52	290	560
End-on (Fig. 50)	1.25	110	220
Average (Fig. 51)	0.73	190	370

Particle Type	Momentum	
	Cumulative	Distance
Sphere (Fig. 52)	26	210
Side-on (Fig. 53)	22	250
Face-on (Fig. 54)	19	290
End-on (Fig. 55)	44	110
Average (Fig. 56)	27	190

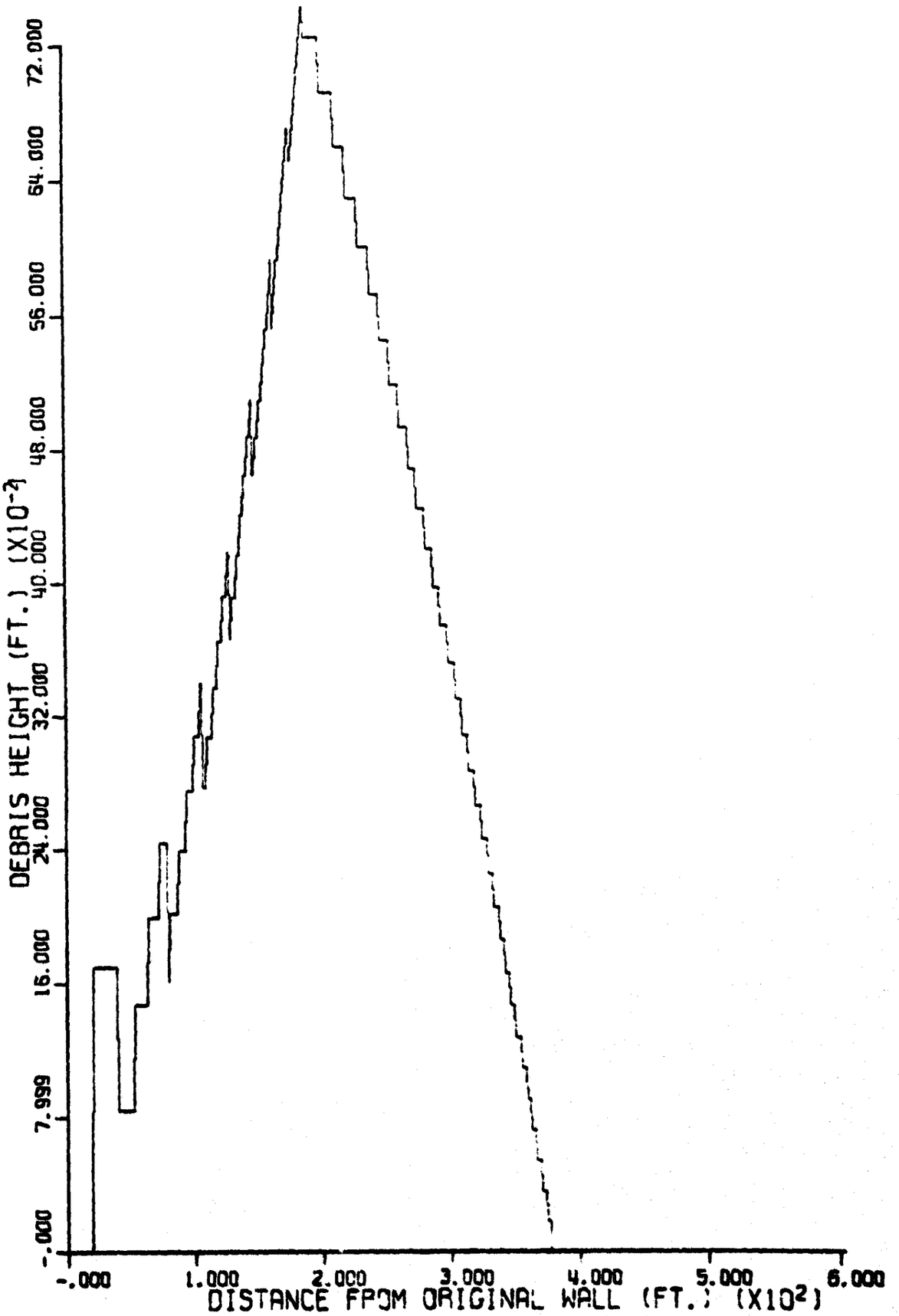

Fig.47 DEBRIS PROFILE OF EQUIVALENT SPHERICAL BRICK PARTICLE

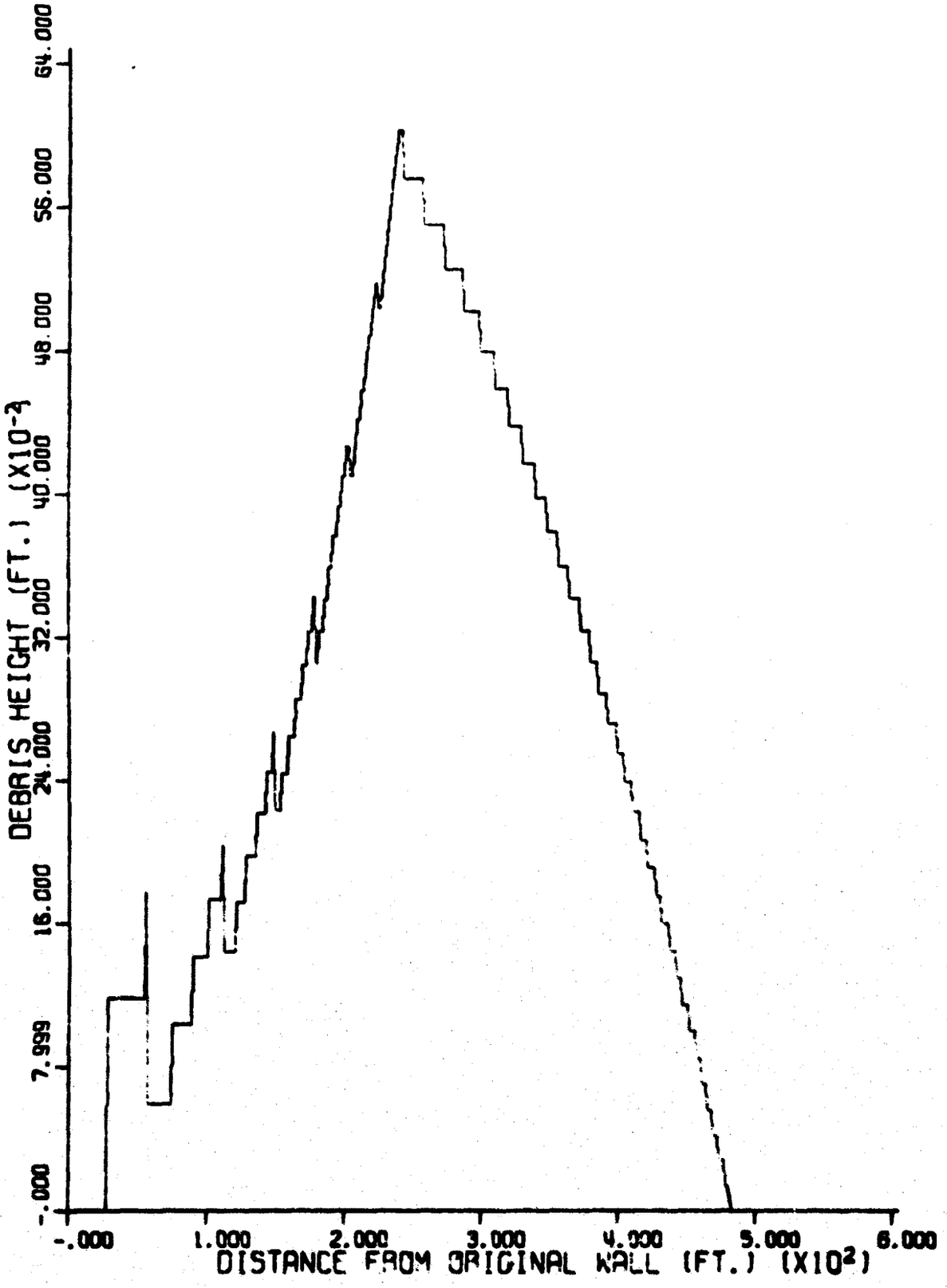

Fig.48 DEBRIS PROFILE OF BRICK PARTICLE IN SIDE-ON ORIENTATION

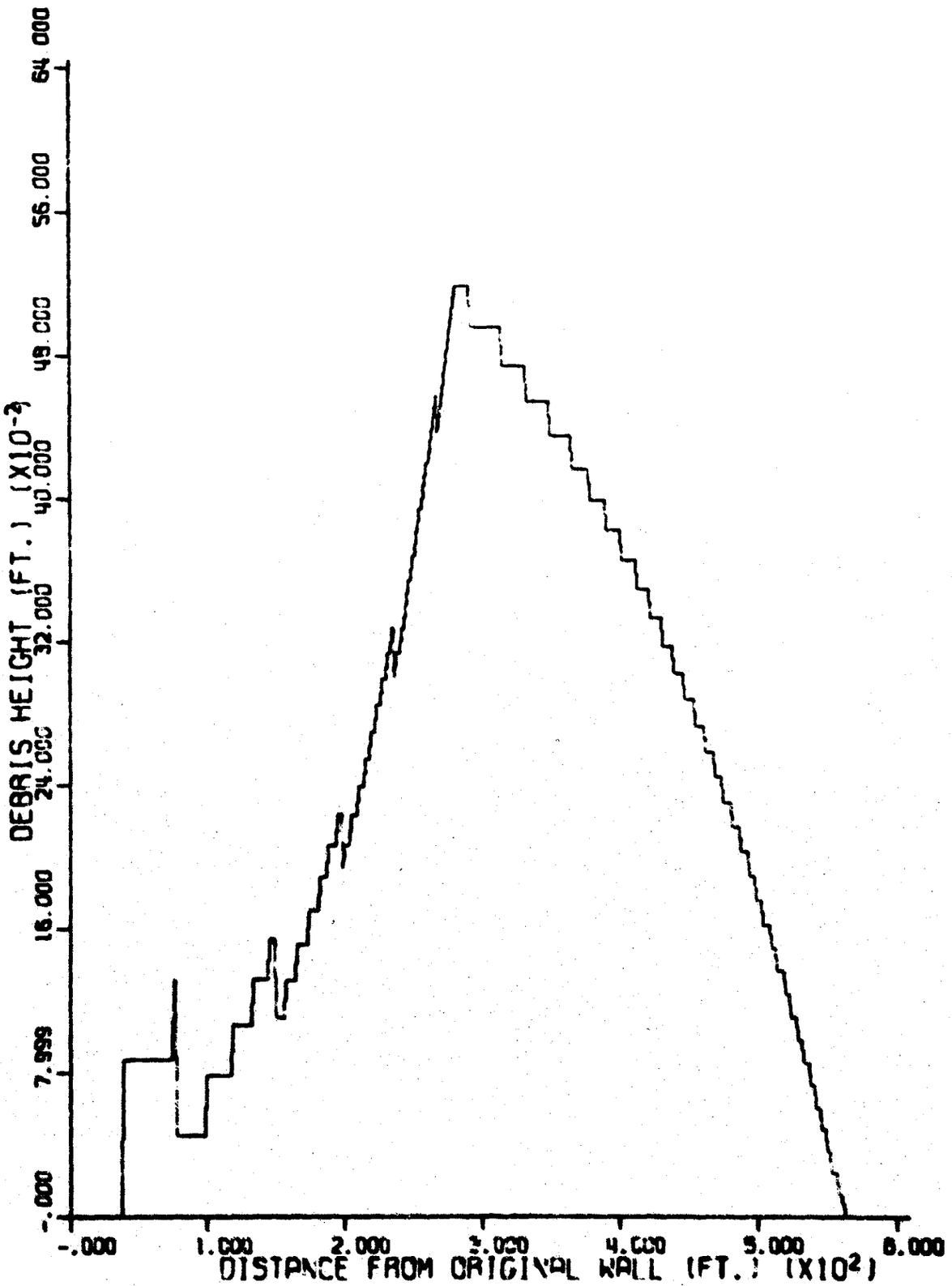

Fig. 49 DEBRIS PROFILE OF BRICK PARTICLE IN FACE-ON ORIENTATION

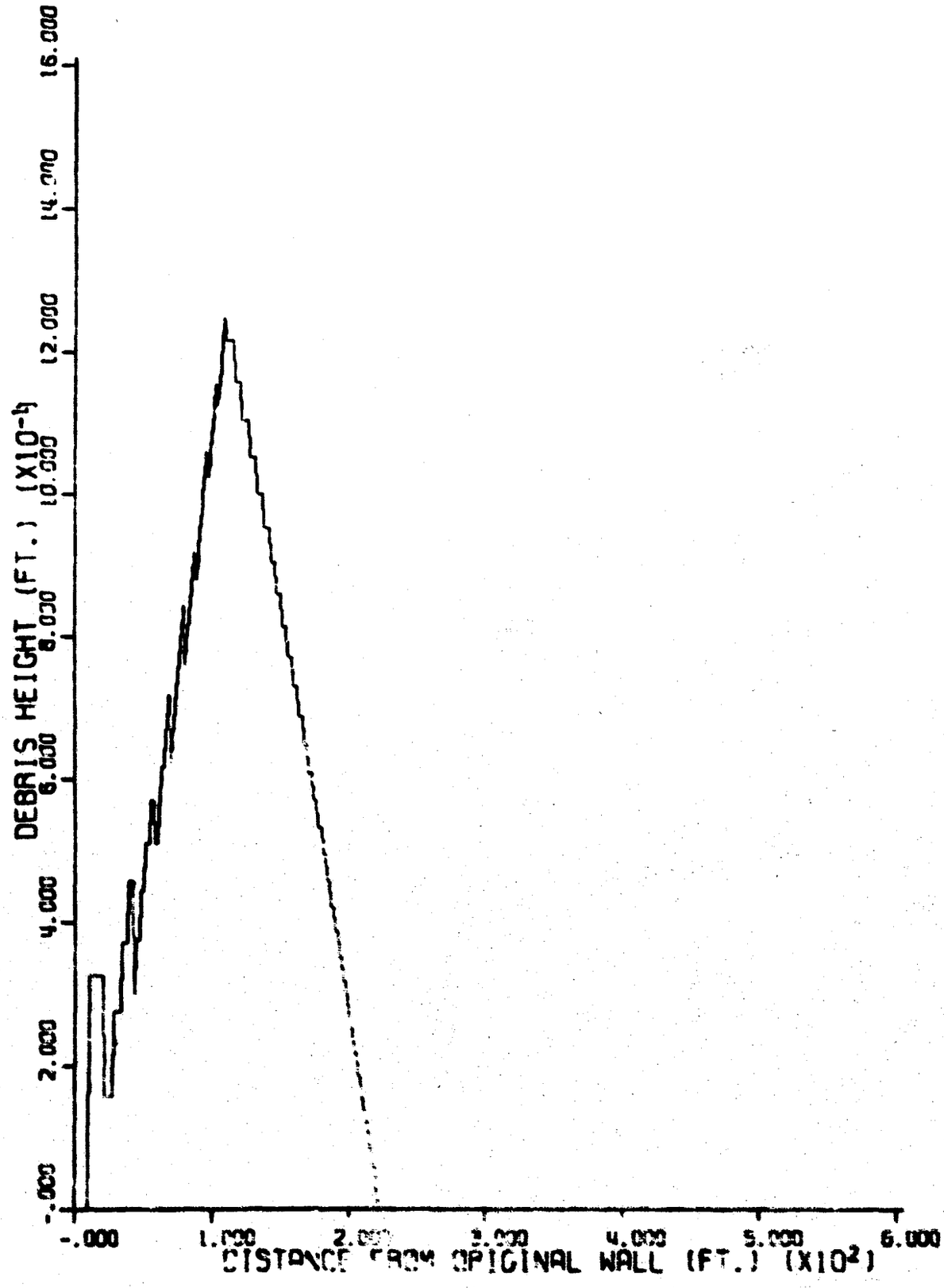

Fig. 50 DEBRIS PROFILE OF BRICK PARTICLE IN END-ON ORIENTATION

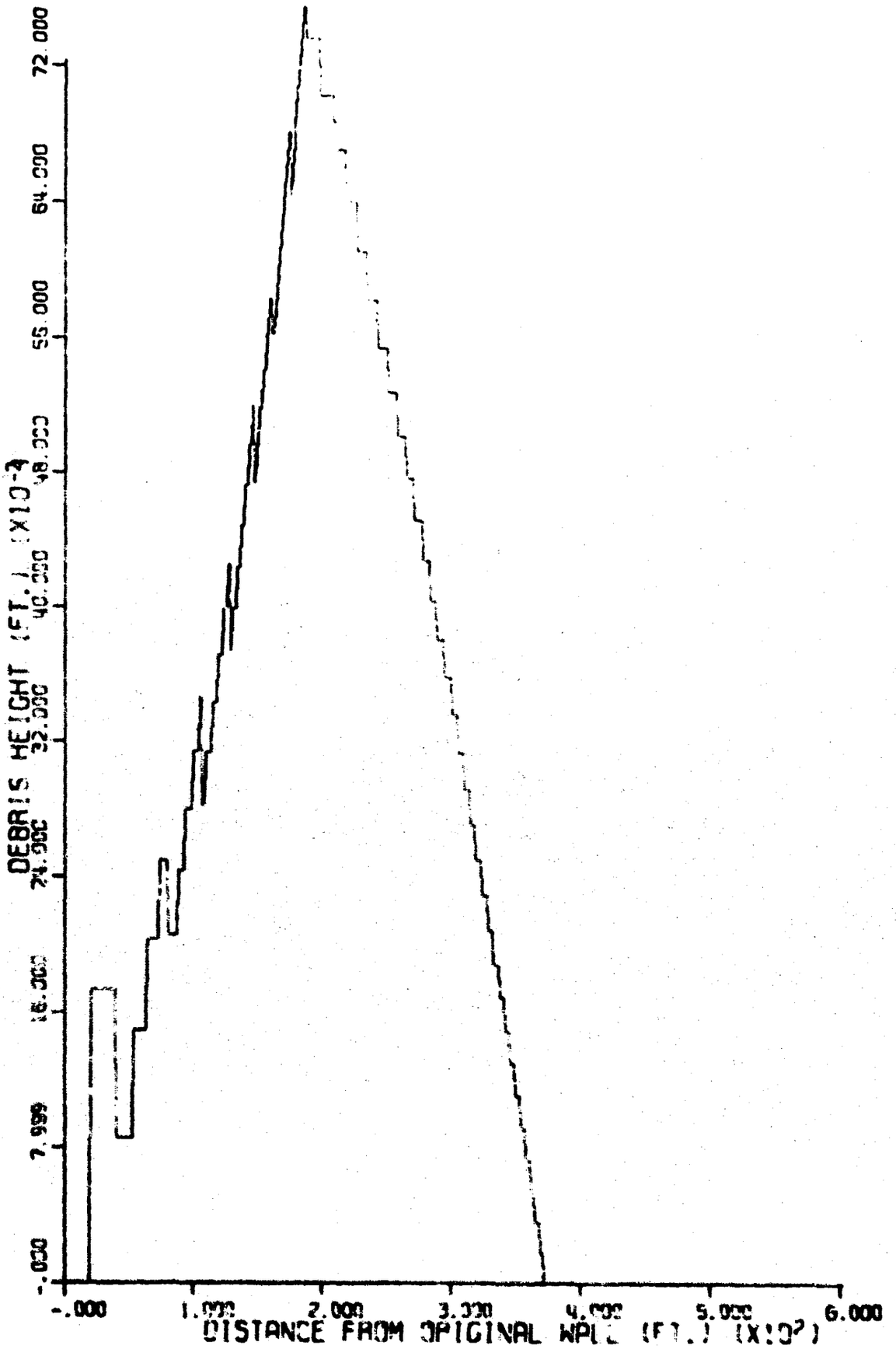

Fig. 51 DEBRIS PROFILE OF BRICK PARTICLE IN AVERAGE ORIENTATION

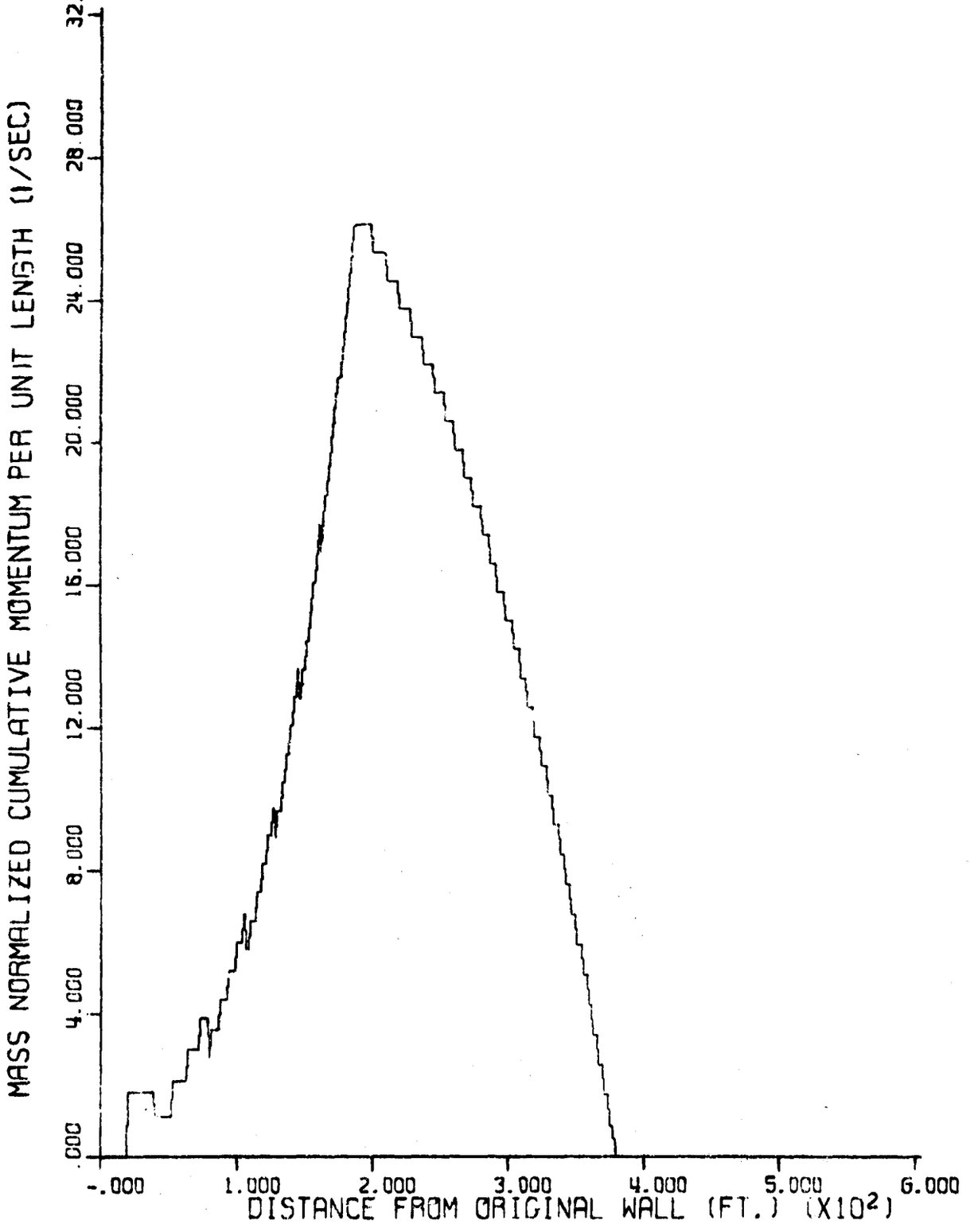

Fig. 52 CUMULATIVE MOMENTUM ALONG DEBRIS PROFILE FOR EQUIVALENT SPHERICAL PARTICLE

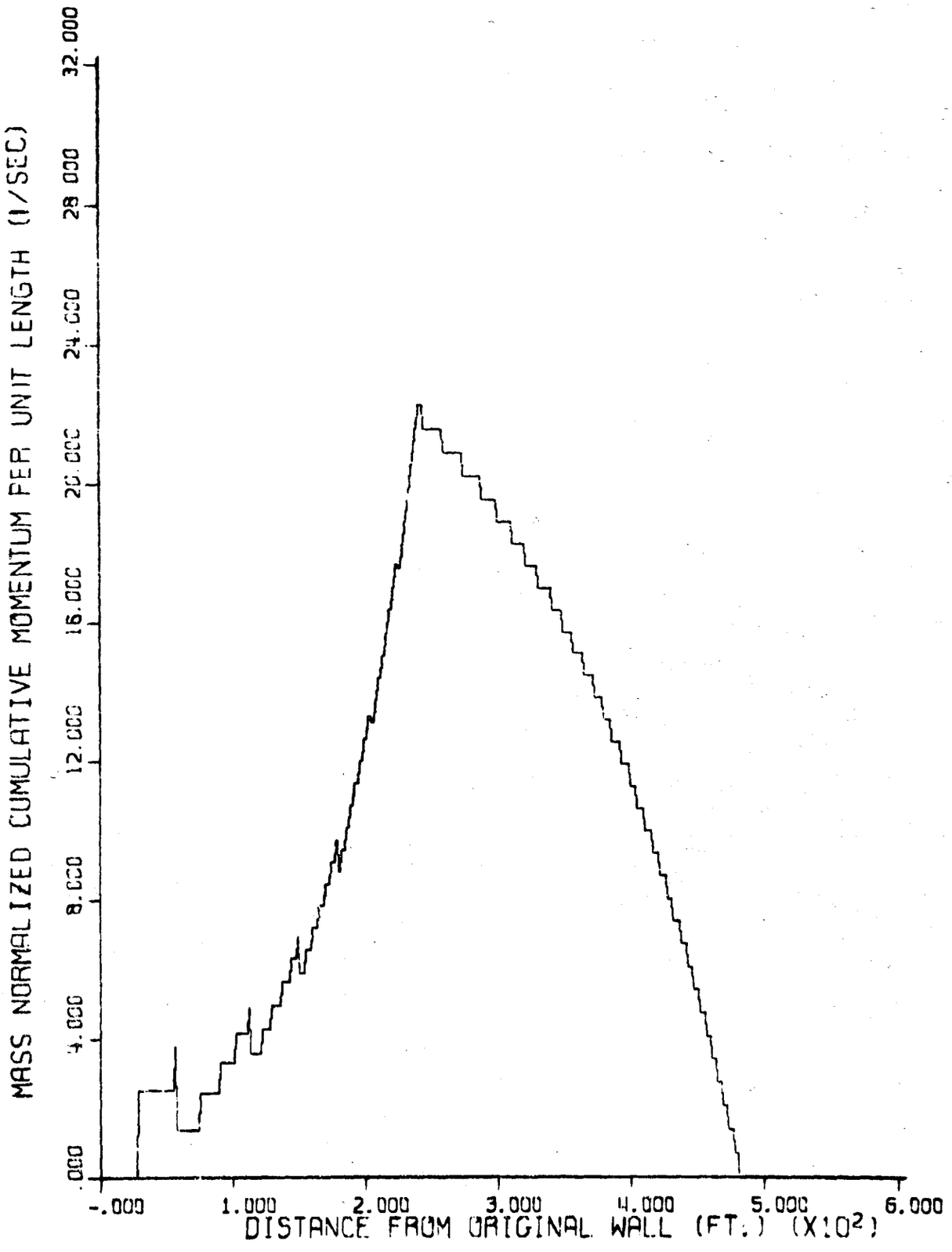

Fig. 53 CUMULATIVE MOMENTUM ALONG DEBRIS PROFILE FOR SIDE-ON ORIENTATION

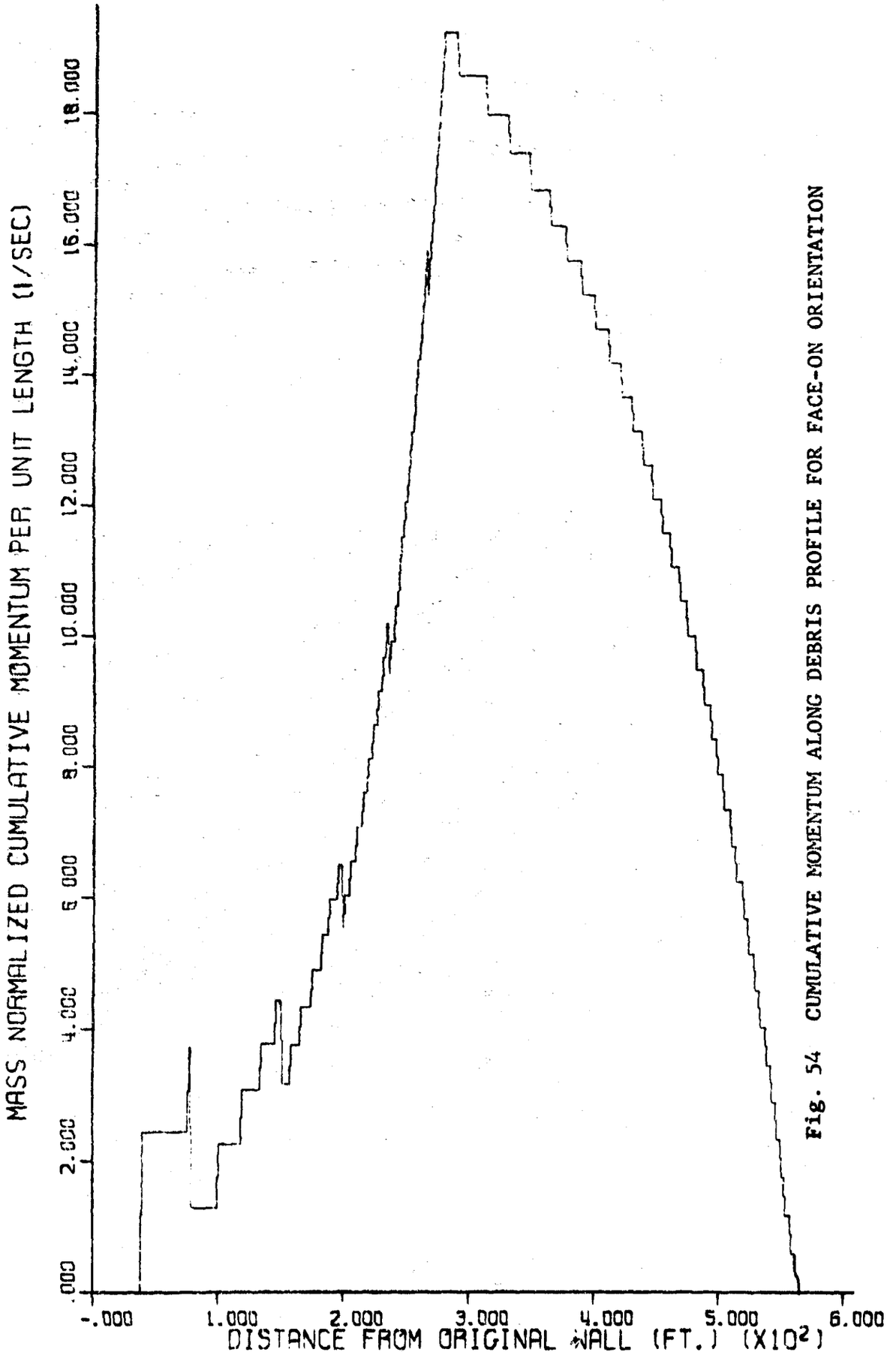

Fig. 54 CUMULATIVE MOMENTUM ALONG DEBRIS PROFILE FOR FACE-ON ORIENTATION

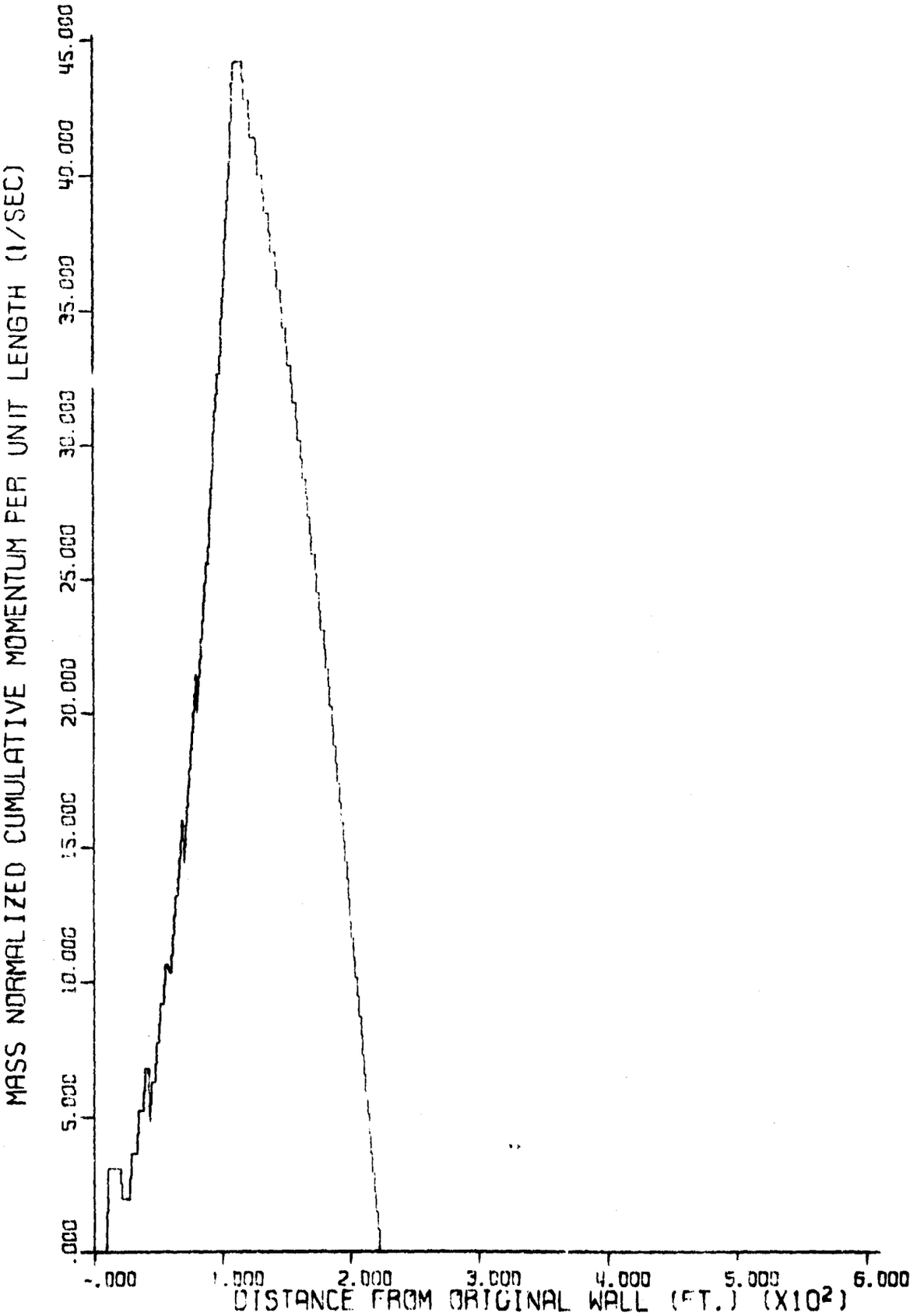

Fig. 55 CUMULATIVE MOMENTUM ALONG DEBRIS PROFILE FOR END-ON ORIENTATION

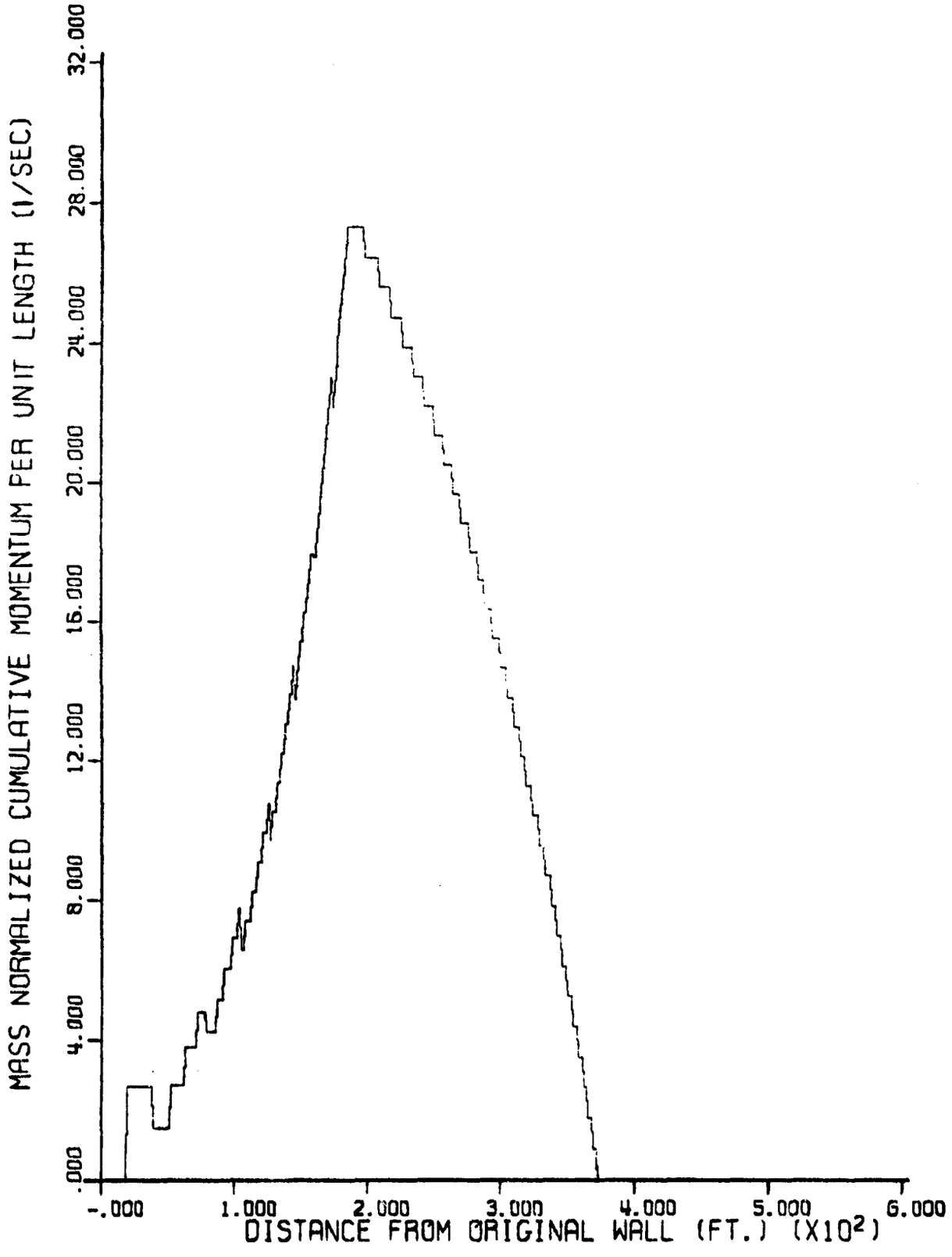

Fig. 56 CUMULATIVE MOMENTUM ALONG DEBRIS PROFILE FOR AVERAGE ORIENTATION

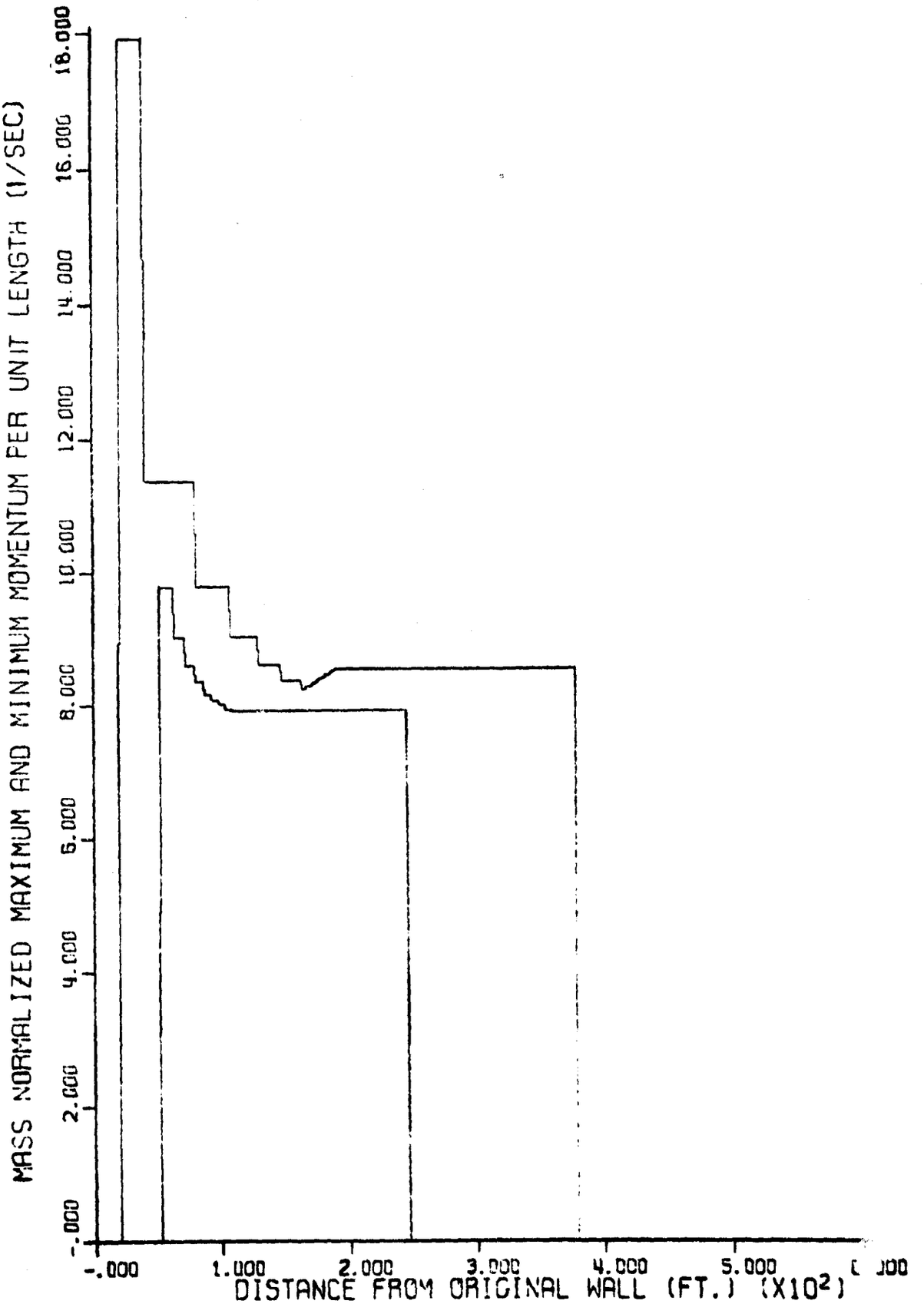

Fig. 57 MAXIMUM AND MINIMUM MOMENTUM ALONG DEBRIS PROFILE FOR EQUIVALENT SPHERICAL PARTICLE

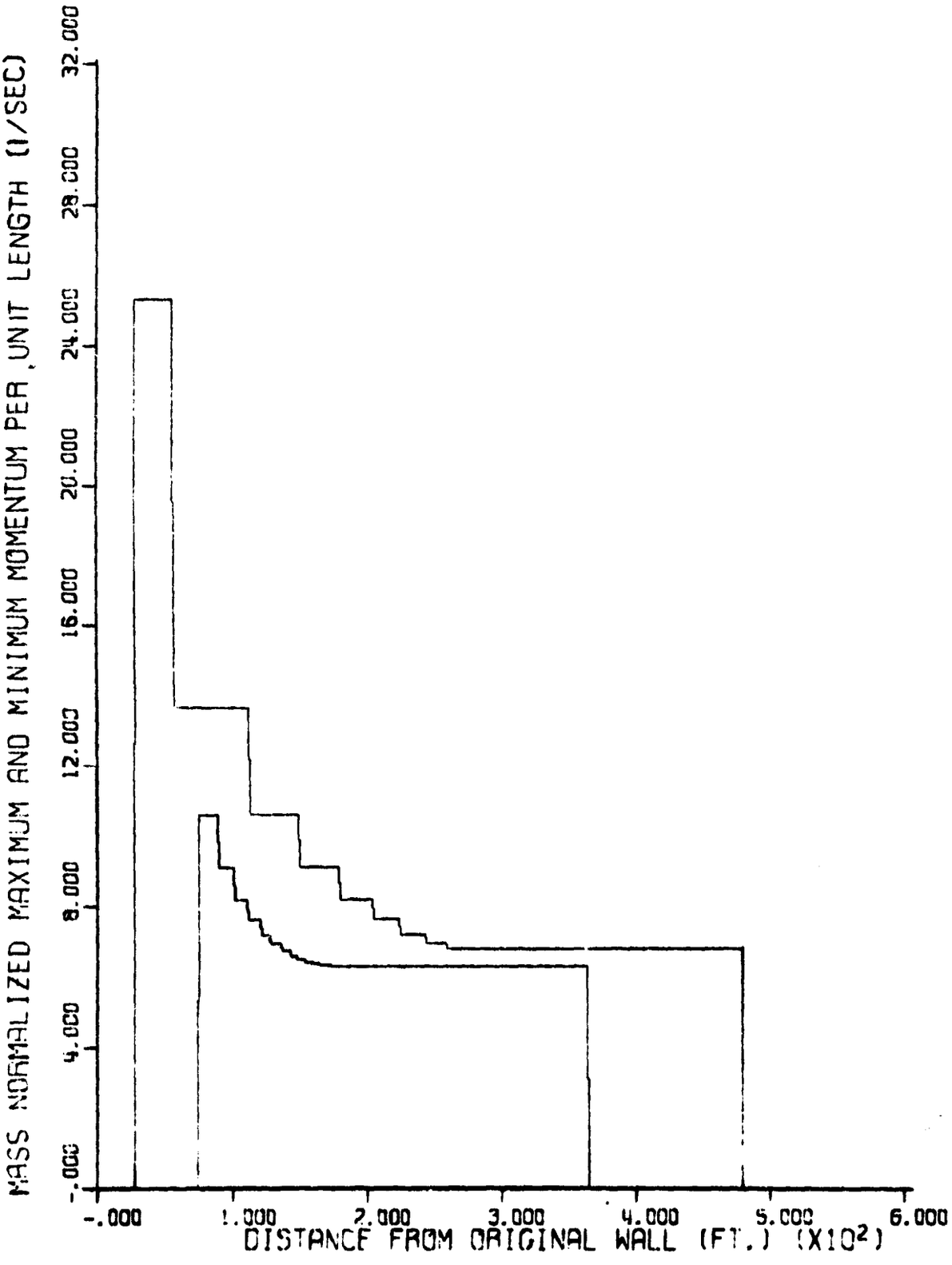

Fig. 58 MAXIMUM AND MINIMUM MOMENTUM ALONG DEBRIS PROFILE FOR SIDE-ON ORIENTATION

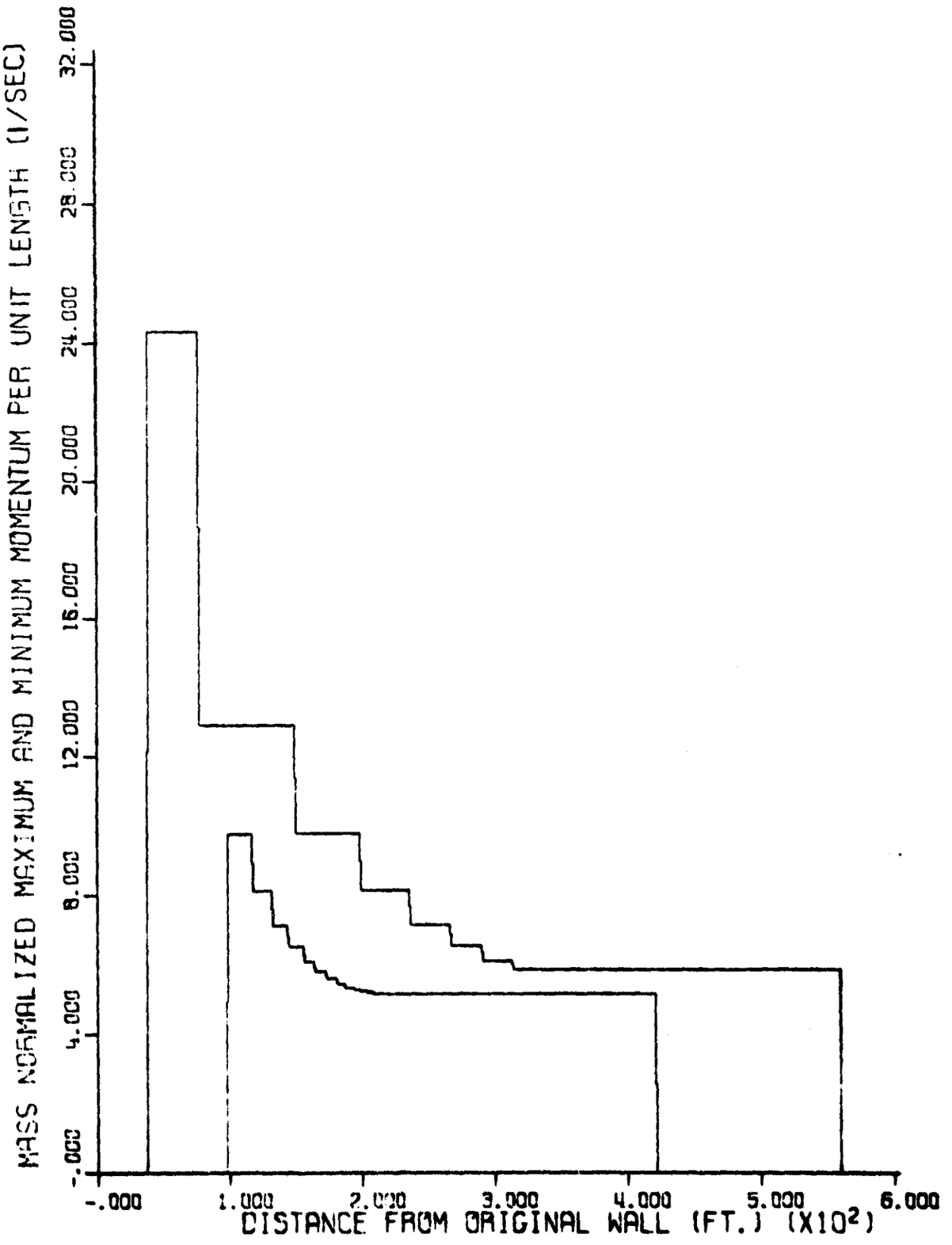

Fig. 59 MAXIMUM AND MINIMUM MOMENTUM ALONG DEBRIS PROFILE FOR FACE-ON ORIENTATION

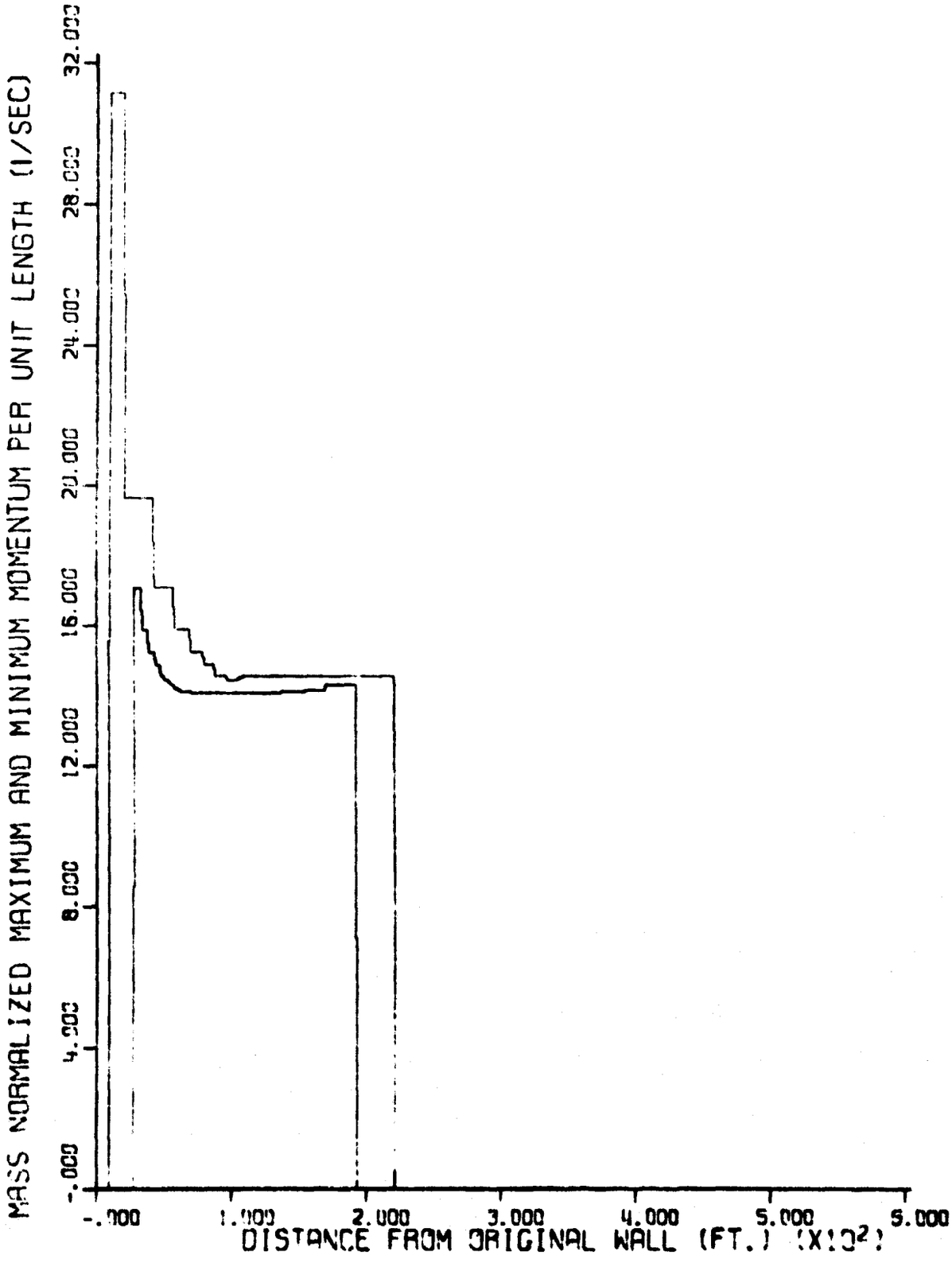

Fig. 60 MAXIMUM AND MINIMUM MOMENTUM ALONG DEBRIS PROFILE FOR END-ON ORIENTATION

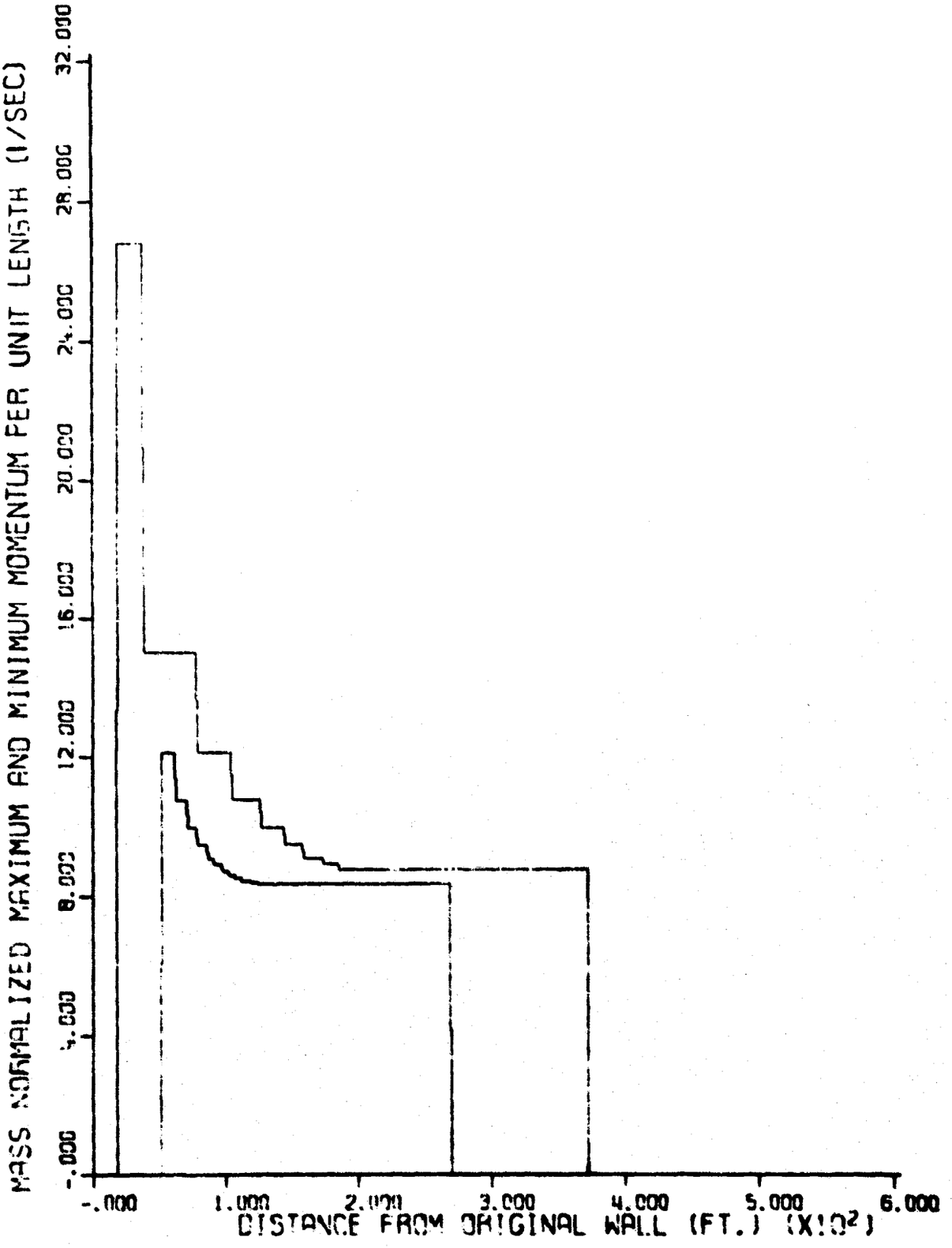

Fig. 61 MAXIMUM AND MINIMUM MOMENTUM ALONG DEBRIS PROFILE FOR AVERAGE ORIENTATION

4.5 FRAGMENTATION DELAY TIMES AND INITIAL VELOCITIES

As previously mentioned, the trajectory analysis used in the SINBAD code is based on the assumptions of zero initial velocity and zero fragmentation time. The trajectory analysis is essentially a numerical solution of a complex differential equation. Since this numerical solution can have arbitrary initial conditions (i.e., delay time and initial velocity), a study was made to see how changes in the fragmentation delay times might affect the final transport position of a particle. The results of that study are summarized in Fig. 62. The figure illustrates the influence of delay time on the final distance a projectile travels. Case A is for a particle initially at 271 ft above ground surface, while Case B is for a particle at 31 ft above ground surface. As delay time is increased, the total distance a particle travels decreases. This decrease however, is insignificant for delay times which are physically meaningful(i.e., up to 0.1 sec) for frangible panels commonly found in structures. The delay time variation was made again with a zero initial velocity. Increasing initial velocity will tend to offset the delay time effect. As fragmentation time for an element increases, the strain energy within the element builds up. This strain energy is likely to impart some kinetic energy to the particle when it is free to fly. Therefore, an increase in fragmentation delay time tends to be counteracted by a corresponding increase in initial velocity and the entire effect on total particle displacement is negligible.

4.6 MODIFICATION OF BLAST LOADING DUE TO LOCAL SHIELDING

One companion problem associated with debris estimation is an accurate description of the blast loading. Most estimates of blast loading on structures are developed under the assumption that there are no obstructions between ground zero and the point of load application. In the real world problem this is far from true; the blast wave must interact with a variety of obstructions in its path to the structure of interest. This phenomenon is

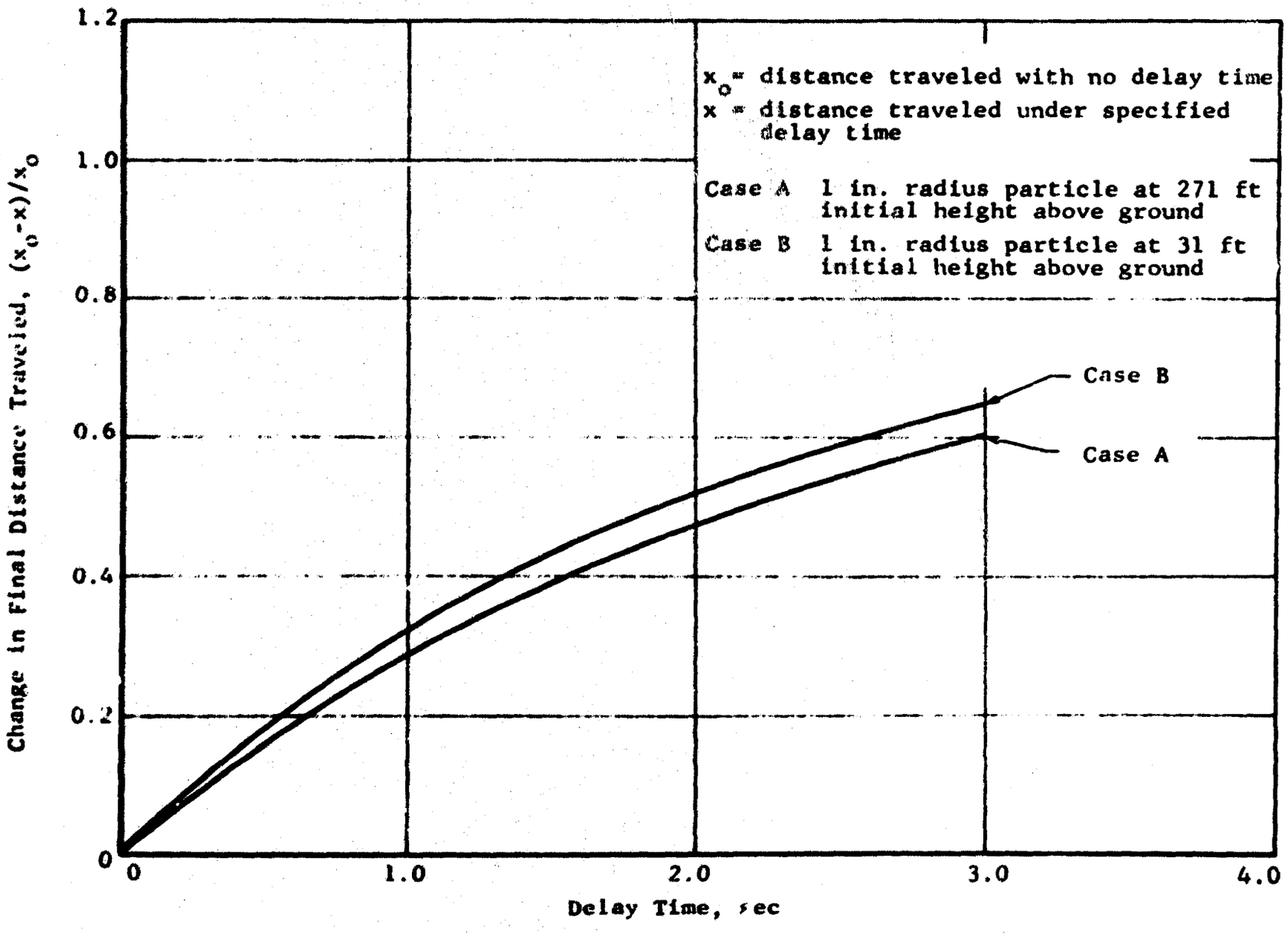

Fig. 62 INFLUENCE OF FRAGMENTATION DELAY TIME ON FINAL TRANSPORT DISTANCE

known as blast shielding. Blast shielding is accounted for in the SINBAD model by attenuating the free-field overpressure by a factor which is an empirical function of building height, length, and spacing from contiguous structures. This factor was determined in a previous experimental program (Ref. 15) and Fig. 63 illustrates the applied results. The three curves represent different ratios of exposed length to height for the structures investigated. The separation ratio is determined from the spacing between neighboring structures and the height of the structure. These curves, Fig. 63, are based on previous model studies and are the most appropriate data which could be found on attenuation due to structural shielding.

4.7 IMPINGEMENT OF DEBRIS FROM ONE STRUCTURE ON ANOTHER

Although it is conceivable that under the right set of circumstances the debris from one structure might collide in midflight with another structure, this result has not been observed in problems run to date. Such a result, in any case, is difficult to observe and still more difficult to analyze. This phenomenon has not been incorporated into SINBAD and can only be detected from intermediate results.

4.8 INTERIOR BUILDING CONTENTS AS POTENTIAL DEBRIS

After the blast wave interacts with the exterior walls of a structure, it enters the interior of the building. During the transition from the outside to the inside of the structure the blast overpressure undergoes still another attenuation. This attenuation is, again, determined from empirical results obtained from an experimental investigation (Ref. 16). As discussed previously, the SINBAD Code operates on an idealized space consisting of lumped particles at discrete initial heights.

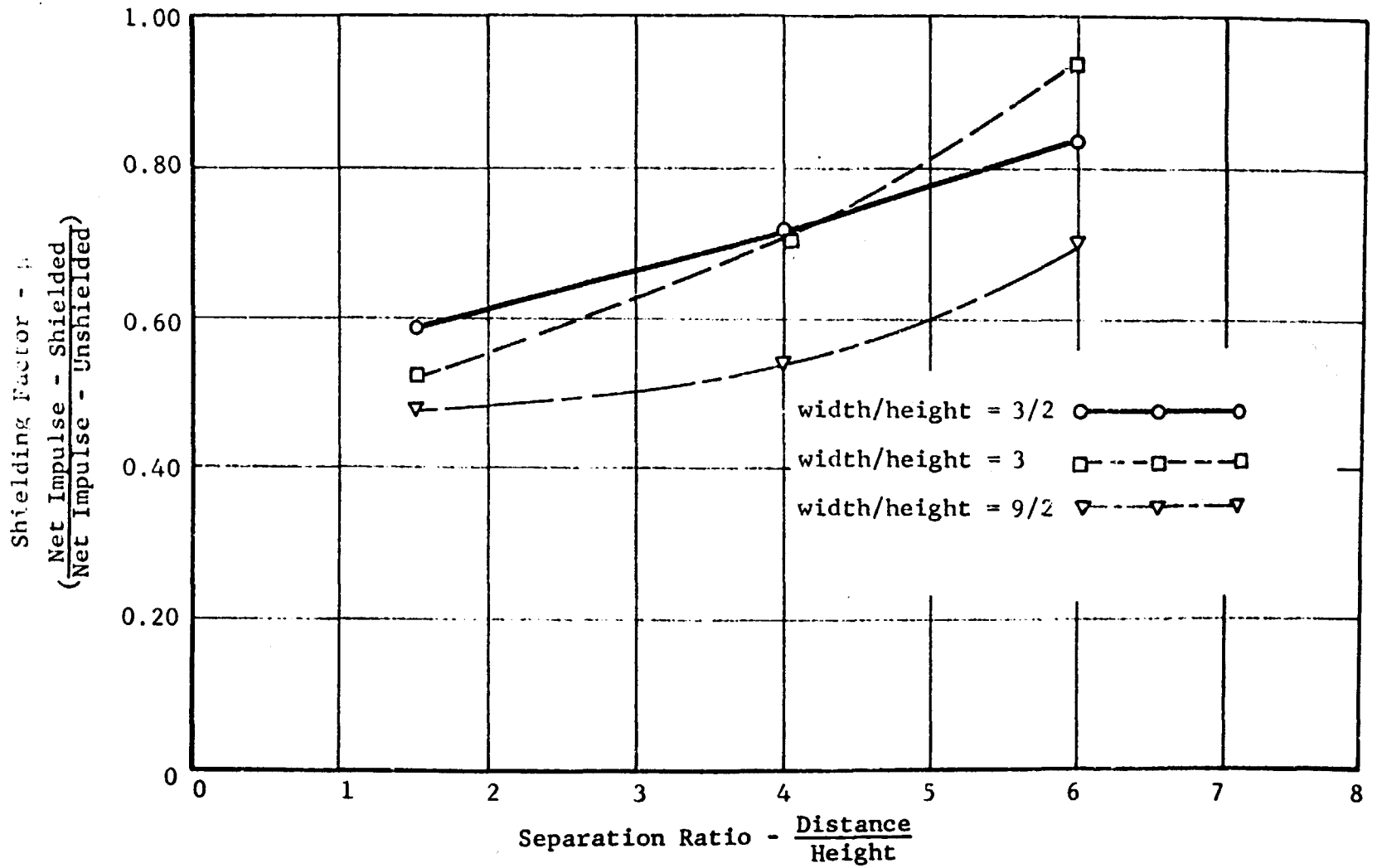

Fig. 63 SHIELDING FROM CONTIGUOUS STRUCTURES

These particles may be any size; however, at some finite size the model may not yield plausible results. For interior items such as furniture, ice boxes, etc., SINBAD will yield good results, however, large bulky objects such as might be found in a warehouse are another story. These objects are highly sensitive to diffraction loading and must gain some inertia before they can be picked up by drag loading. A more meaningful analysis for this type of interior debris item might include a sliding overturning study that would establish whether the debris can start moving or not. When it is established that the debris moves, the SINBAD analysis may be utilized.

REFERENCES

1. Guillard, E., The Ultimate Strength of Braced Frames, ARF Project No. K082, Physical Vulnerability Div., USAF, Contract No. AF 33(600)-27712, April 1958.
2. American Society of Civil Engineers - American Concrete Institute, Proceedings, International Symposium on Flexural Mechanics of Reinforced Concrete, November 1964.
3. Merchant, W., "The Failure Load of Rigidly Jointed Frameworks as Influenced by Stability", The Structural Engineer, London, England, Vol. 32, 1954.
4. Wood, R. H., "The Stability of Tall Buildings", Proceedings, Inst. of Civ. Engrs., London, Vol. 11, 1958.
5. Horne, M. R., "Elastic-Plastic Failure Loads of Plane Frames", Proceedings, Royal Soc. of London, Series A, Vol. 274, 1963.
6. Low, M. W., "Some Model Tests on Multi-story Rigid Steel Frames", Proceedings, Inst. of Civ. Engrs., London, England, Vol. 13, 1959.
7. Wang, C. K., "General Computer Program for Limit Analysis", Proceedings, ASCE, Vol. 89 No. ST6, December 1963.
8. Liber, T., Experimental Study of Fragmentation of Structural Wall Panels, for OCD, Contract No. OCD-PS-64-60, October 1966.
9. Ahlers, E. B., Debris Clearance Study, OCD Contract No. OCD-OS-62-202, Subtask 3322A; IIT Research Institute Project No. M264, September 1963.
10. Feinstein, D. I., Debris Distribution, Task 3372-B for Office of Civil Defense, Washington, D. C., August 1965.
11. Nowacki, W., Dynamics of Elastic Systems, Wiley, 1963.
12. Weibull, W., "A Structural Theory of the Strength of Materials", Ing. Vetenskaps Akad., 151, pp 1-45, 1939.
13. Ahlers, E. B., Parametric Study of Shelter Vulnerability, for OCD, Task 1614A, November 1965.
14. Hoerner, S. F., Fluid Dynamic Drag, Great Britain, 1958.
15. Experimental Observation of Interior Pressures in Hollow Models Blast Effects on Buildings and Structures Operation of Six Foot and Two Foot Shock Tubes, Final Test Report No. 5, Armour Research Foundation, No. D-087, March 12, 1956.
16. Experimental Observation of Interior Pressures in Hollow Models (Part II) Blast Effects on Buildings and Structures Operation of Six Foot and Two Foot Shock Tubes, Final Test Report No. 7 Armour Research Foundation, No. D-087, July 1956.

APPENDIX A

COMPUTER PROGRAM FOR LIMITED ROTATION ANALYSIS

```
C      LIMIT ANALYSIS OF FRAMES
      DIMENSION A(20,30),S(60),ASAT(20,20),INDEX(20),P(20)
      DIMENSION SATX(30),PM(30),ALF(30),CX(20)
      DIMENSION CM(30),D(60),H(30)
C
C
C        INPUT DATA- NP IS TOTAL DEGREES OF FREEDOM
C                    NF IS TWICE THE NUMBER OF MEMBERS
C                    A  IS THE INTERNAL-EXTERNAL FORCE MATRIX
C                    P  IS THE LOAD VECTOR
C                    PM IS THE PLASTIC MOMENT AT EACH NODE
C                    S  IS THE SLOPE-DELECTION STIFFNESS MATRIX (IN VECTOR FORM)
C
C
    1 READ (5,2) JJ
    2 FORMAT(1I5)
      IF (JJ) 4,4,3
    3 READ (5,101) NP,NF
  101 FORMAT (2I5)
      READ (5,102) ((A(I,J),J=1,NF),I=1,NP)
  102 FORMAT (8F10.4)
      NFT2=NF*2
      READ (5,102) (S(I),I=1,NFT2)
      NP1=NP+1
      READ (5,102) (P(I),I=1,NP)
      READ (5,102) (PM(I),I=1,NF)
      WRITE (6,103)
  103 FORMAT (31H1LIMIT ANALYSIS OF RIGID FRAMES//)
      WRITE(6,5) JJ
    5 FORMAT(8H1CASE NO,I3)
      WRITE (6,104)
  104 FORMAT (13HOTHE MATRIX A)
      DO 105 I=1,NP
  105 WRITE (6,106) I,(A(I,J),J=1,NF)
  106 FORMAT (4H ROW,I3,1X,1P4E16.7/(8X,1P4E16.7))
      WRITE (6,107)
  107 FORMAT (13HOTHE MATRIX S)
      DO 108 I=1,NF
      I1=(I-1)/2*2+1
      I2=(I+1)/2*2
      I3=2*I-1
      I4=2*I
  108 WRITE (6,109) I,I1,S(I3),I2,S(I4)
  109 FORMAT (4H ROW,I3,5X,3HCOL,I3,1PE16.7,5X,3HCOL,I3,1PE16.7)
      WRITE (6,110)
  110 FORMAT (13HOTHE MATRIX P)
      DO 221 I=1,NP
  221 WRITE (6,106) I,P(I)
      WRITE (6,111)
```

```
  111 FORMAT(14HOTHE MATRIX PM)
      DO 222 I=1,NP
  222 WRITE (6,106) I,PM(I)
      DO 112 I=1,NF
C
C


C         INVERT THE STIFFNESS MATRIX . D=(S**-1)
C
C
      IF (I/2*2-I) 113,112,112
  113 N1=2*I-1
      N2=2*I
      IP1=I+1
      N3=2*IP1-1
      N4=2*IP1
      IF (S(N1)) 711,712,711
  712 D(N4)=1./S(N4)
      D(N1)=0.
      D(N2)=0.
      D(N3)=0.
      GO TO 112
  711 IF(S(N4)) 710,713,710
  713 D(N1)=1./S(N1)
      D(N2)=0.
      D(N3)=0.
      D(N4)=0.
      GO TO 112
  710 TEMP=1./(S(N1)*S(N4)-S(N2)*S(N3))
      D(N1)=S(N4)*TEMP
      D(N4)=S(N1)*TEMP
      D(N2)=-S(N2)*TEMP
      D(N3)=D(N2)
  112 CONTINUE
C
C
C         PLASTIC ANALYSIS FOR UNIT LOADS
C
C
  500 NCYCL=0
      CLF=0.
      DO 24 I=1,NP
   24 CX(I)=0.
      DO 26 I=1,NF
   26 CM(I)=0.
   15 DO 116 I=1,NP
      DO 116 J=1,NP
      ASAT(I,J)=0.
      DO 116 K=1,NF
      K1=(K-1)/2*2+1
      K2=(K+1)/2*2
      K3=2*K-1
      K4=2*K
```

```
  116 ASAT(I,J)=ASAT(I,J)+A(I,K)*(S(K3)*A(J,K1)+S(K4)*A(J,K2))
      DO 151 I=1,NP
  151 ASAT (I,NP1)=P(I)
      DO 117 I=1,NP
  117 INDEX(I)=0
  118 AMAX=-1.
      DO 119 I=1,NP
      IF (INDEX(I)) 119,120,119
  120 TEMP=ABS(ASAT(I,I))
      IF (TEMP-AMAX) 119,119,121

  121 IROW=I
      AMAX=TEMP
  119 CONTINUE
C
C
C             CHECK FOR ZERO IN PIVOT ELEMENT OR EXCESSIVE DEFLECTION
C             THESE CONDITIONS ARE INSTABILITY CHECKS
C
C
      IF (AMAX) 122,147,124
  124 INDEX (IROW) =1
      PIVOT=1./(ASAT(IROW,IROW))
      DO 125 J=1,NP1
  125 ASAT(IROW,J)=ASAT(IROW,J)*PIVOT
      DO 126 I=1,NP
      IF(I-IROW) 127,126,127
  127 TEMP=ASAT(I,IROW)
      DO 128 J=1,NP1
  128 ASAT(I,J)=ASAT(I,J)-ASAT(IROW,J)*TEMP
  126 CONTINUE
      GO TO 118
  147 WRITE (6,347)
  347 FORMAT(24HOZERO PIVOT IN INVERSION)
      GO TO 47
  122 DO 311 I=1,NP
      IF (ABS(ASAT(I,NP1))-1.E+10) 311,647,647
  311 CONTINUE
      GO TO 303
  647 WRITE (6,847)
  847 FORMAT (21HODEFLECTION TOO LARGE)
      GO TO 47
C
C
C             COMPUTE THE MOMENTS
C
  303 DO 131 I=1,NF
      I1=(I-1)/2*2+1
      I2=(I+1)/2*2
      I3=2*I-1
      I4=2*I
```

```
      SATX(I)=0.
      DO 131 K=1,NP
  131 SATX(I)=SATX(I)+ASAT(K,NP1)*(S(I3)*A(K,I1)+S(I4)*A(K,I2))
C
C
C        FIND ADDITIONAL LOAD FACTOR REQUIRED TO BRING JOINT WITH LARGEST
C        MOMENT UNDER UNIT LOAD UP TO PLASTIC MOMENT
C     CHECK THAT MOMENT IS INCREASING IN MAGNITUDE UNDER UNIT LOAD
C
C
      DO 201 I=1,NF
      IF (ABS(SATX(I))-1.E-04) 202,202,203
  202 ALF(I)=1.E20
      GO TO 201
  203 ALF(I)=(PM(I)-ABS(CM(I)))/ABS(SATX(I))
  201 CONTINUE



      SALF=1.E20
      DO 204 I=1,NF
      TEST = CM(I)*SATX(I)
      IF (TEST) 204,205,205
  205 IF(ALF(I)-SALF) 1206,204,204
 1206 SALF = ALF(I)
      NPH=I
  204 CONTINUE
C
C
C        IF THERE IS NO INCREASE IN LOAD FACTOR,COLLAPSE MECHANISM EXISTS
C
C
      IF (SALF-1.E-07) 247,247,302
  247 WRITE (6,447)
  447 FORMAT(22HOLOAD FACTOR TOO SMALL)
      GO TO 47
C
C
C        COMPUTE MOMENTS UNDER CURRENT LOAD FACTOR
C
C
  302 DO 207 I=1,NF
      SATX(I)=SALF*SATX(I)
  207 CM(I)=CM(I)+SATX(I)
C
C
C        DOUBLE-CHECK ADMISSIBILITY OF SOLUTION,MOMENT.LE.PM AT ALL JOINTS
C
C
      DO 314 I=1,NF
      IF (PM(I)-ABS(CM(I))+1.E-03) 547,314,314
  314 CONTINUE
      GO TO 304
  547 WRITE (6,747)
  747 FORMAT(24HOPLASTIC MOMENT EXCEEDED)
      GO TO 47
C
C
```

```
C        WRITE MOMENTS AND DEFLECTIONS UNDER CURRENT LOAD FACTOR
C
C
  304 CLF=CLF+SALF
      DO 206 I=1,NP
      ASAT(I,NP1)=SALF*ASAT(I,NP1)
  206 CX(I)=CX(I)+ASAT(I,NP1)
      NCYCL=NCYCL+1
      WRITE (6,401) NCYCL,NPH
  401 FORMAT (18H1PLASTIC HINGE NO.,I3,2X,15HFORMED AT POINT,I3)
      WRITE (6,402)
  402 FORMAT(12HOLOAD FACTOR,3X,10HADDITIONAL,9X,10HCUMULATIVE)
      WRITE (6,403) NCYCL,SALF,CLF
  403 FORMAT(7HOSTAGE(,I3,1H),1PE18.7,1PE19.7)
      WRITE (6,404)
  404 FORMAT(11HODEFLECTION,4X,10HADDITIONAL,9X,10HCUMULATIVE/)
      DO 208 I=1,NP




  208 WRITE (6,405) I,ASAT(I,NP1),CX(I)
  405 FORMAT(3H X(,I3,1H),1PE22.7,1PE19.7)
      WRITE (6,406)
  406 FORMAT(7HOMOMENT8X,10HADDITIONAL,9X10HCUMULATIVE10X,8HPLAS MOM/)
      DO 209 I=1,NF
  209 WRITE (6,407) I,SATX(I),CM(I),PM(I)
  407 FORMAT(3H M(,I3,1H),F18.4,2F19.4)
C
C
C        COMPUTE INELASTIC HINGE ROTATIONS UNDER CURRENT LOAD FACTOR
C
C
      DO 933 I=1,NF
      I1=(I-1)/2*2+1
      I2=(I+1)/2*2
      I3=2*I-1
      I4=2*I
      H(I)=D(I3)*CM(I1)+D(I4)*CM(I2)
      DO 933 K=1,NP
  933 H(I)=H(I)-A(K,I)*CX(K)
      DO 501 I=1,NF
  501 IF(ABS(H(I)).LT.(1.E-07))H(I)=0.0
      WRITE (6,138)
  138 FORMAT(1HO,14X,15HHINGE ROTATIONS/)
      DO 939 I=1,NF
  939 WRITE (6,140) I,H(I)
  140 FORMAT(10H AT POINT(,I3,1H),1PE15.7)
C
C
```

```
C         MODIFY STIFFNESS MATRIX TO INCLUDE PLASTIC HINGE
C
C
      IF ((NPH/2*2)-NPH) 211,210,210
  211 N1=2*NPH-1
      N2=2*NPH
      NPHP1=NPH+1
      N3=2*NPHP1-1
      N4=2*NPHP1
      S(N4)=S(N4)*(1.-S(N2)*S(N3)/(S(N1)*S(N4)))
      S(N1)=0.
      S(N2)=0.
      S(N3)=0.
      GO TO 212
  210 NPHM1=NPH-1
      N1=2*NPHM1-1
      N2=2*NPHM1
      N3=2*NPH-1
      N4=2*NPH
      S(N1)=S(N1)*(1.-S(N2)*S(N3)/(S(N1)*S(N4)))
      S(N2)=0.
      S(N3)=0.
      S(N4)=0.
  212 GO TO 15
C
C
   47 WRITE (6,408)



  408 FORMAT(36HOCOLLAPSE MECHANISM HAS BEEN REACHED)
      GO TO 1
    4 STOP
      END
```

APPENDIX B

RESULTS OF SAMPLE PROBLEM

CASE NO 2

THE MATRIX A

ROW 1	-0.00000000E-39	1.00000000E 00	1.00000000E 00	-0.00000000E-39
	-0.00000000E-39	-0.00000000E-39	-0.00000000E-39	-0.00000000E-39
	-0.00000000E-39	-0.00000000E-39	-0.00000000E-39	-0.00000000E-39
	1.00000000E 00	-0.00000000E-39	-0.00000000E-39	-0.00000000E-39
	-0.00000000E-39	-0.00000000E-39	-0.00000000E-39	-0.00000000E-39
ROW 2	-0.00000000E-39	-0.00000000E-39	-0.00000000E-39	-0.00000000E-39
	-0.00000000E-39	1.00000000E 00	1.00000000E 00	-0.00000000E-39
	-0.00000000E-39	-0.00000000E-39	-0.00000000E-39	-0.00000000E-39
	-0.00000000E-39	1.00000000E 00	1.00000000E 00	-0.00000000E-39
	-0.00000000E-39	-0.00000000E-39	-0.00000000E-39	-0.00000000E-39
ROW 3	-0.00000000E-39	-0.00000000E-39	-0.00000000E-39	-0.00000000E-39
	-0.00000000E-39	-0.00000000E-39	-0.00000000E-39	-0.00000000E-39
	-0.00000000E-39	1.00000000E 00	1.00000000E 00	-0.00000000E-39
	-0.00000000E-39	-0.00000000E-39	-0.00000000E-39	1.00000000E 00
	-0.00000000E-39	-0.00000000E-39	-0.00000000E-39	-0.00000000E-39
ROW 4	-0.00000000E-39	-0.00000000E-39	-0.00000000E-39	1.00000000E 00
	-0.00000000E-39	-0.00000000E-39	-0.00000000E-39	-0.00000000E-39
	-0.00000000E-39	-0.00000000E-39	-0.00000000E-39	-0.00000000E-39
	-0.00000000E-39	-0.00000000E-39	-0.00000000E-39	-0.00000000E-39
	1.00000000E 00	-0.00000000E-39	-0.00000000E-39	-0.00000000E-39
ROW 5	-0.00000000E-39	-0.00000000E-39	-0.00000000E-39	-0.00000000E-39
	-0.00000000E-39	-0.00000000E-39	-0.00000000E-39	1.00000000E 00
	-0.00000000E-39	-0.00000000E-39	-0.00000000E-39	-0.00000000E-39
	-0.00000000E-39	-0.00000000E-39	-0.00000000E-39	-0.00000000E-39
	-0.00000000E-39	1.00000000E 00	1.00000000E 00	-0.00000000E-39
ROW 6	-0.00000000E-39	-0.00000000E-39	-0.00000000E-39	-0.00000000E-39
	-0.00000000E-39	-0.00000000E-39	-0.00000000E-39	-0.00000000E-39
	-0.00000000E-39	-0.00000000E-39	-0.00000000E-39	1.00000000E 00
	-0.00000000E-39	-0.00000000E-39	-0.00000000E-39	-0.00000000E-39
	-0.00000000E-39	-0.00000000E-39	-0.00000000E-39	1.00000000E 00
ROW 7	1.00000000E-01	1.00000000E-01	-1.00000000E-01	-1.00000000E-01
	1.00000000E-01	1.00000000E-01	-1.00000000E-01	-1.00000000E-01
	1.00000000E-01	1.00000000E-01	-1.00000000E-01	-1.00000000E-01
	-0.00000000E-39	-0.00000000E-39	-0.00000000E-39	-0.00000000E-39
	-0.00000000E-39	-0.00000000E-39	-0.00000000E-39	-0.00000000E-39
ROW 8	-0.00000000E-39	-0.00000000E-39	1.00000000E-01	1.00000000E-01
	-0.00000000E-39	-0.00000000E-39	1.00000000E-01	1.00000000E-01
	-0.00000000E-39	-0.00000000E-39	1.00000000E-01	1.00000000E-01
	-0.00000000E-39	-0.00000000E-39	-0.00000000E-39	-0.00000000E-39
	-0.00000000E-39	-0.00000000E-39	-0.00000000E-39	-0.00000000E-39

THE MATRIX S

ROW 1	COL 1	7.20000000E 05	COL 2	3.60000000E 05
ROW 2	COL 1	3.60000000E 05	COL 2	7.20000000E 05
ROW 3	COL 3	7.20000000E 05	COL 4	3.60000000E 05
ROW 4	COL 3	3.60000000E 05	COL 4	7.20000000E 05
ROW 5	COL 5	7.20000000E 05	COL 6	3.60000000E 05
ROW 6	COL 5	3.60000000E 05	COL 6	7.20000000E 05
ROW 7	COL 7	7.20000000E 05	COL 8	3.60000000E 05
ROW 8	COL 7	3.60000000E 05	COL 8	7.20000000E 05

ROW 9	COL 9	7.2000000E 05	COL 10	3.6000000E 05
ROW 10	COL 9	3.6000000E 05	COL 10	7.2000000E 05
ROW 11	COL 11	7.2000000E 05	COL 12	3.6000000E 05
ROW 12	COL 11	3.6000000E 05	COL 12	7.2000000E 05
ROW 13	COL 13	3.6000000E 05	COL 14	1.8000000E 05
ROW 14	COL 13	1.8000000E 05	COL 14	3.6000000E 05
ROW 15	COL 15	3.6000000E 05	COL 16	1.8000000E 05
ROW 16	COL 15	1.8000000E 05	COL 16	3.6000000E 05
ROW 17	COL 17	3.6000000E 05	COL 18	1.8000000E 05
ROW 18	COL 17	1.8000000E 05	COL 18	3.6000000E 05
ROW 19	COL 19	3.6000000E 05	COL 20	1.8000000E 05
ROW 20	COL 19	1.8000000E 05	COL 20	3.6000000E 05

THE MATRIX P

ROW 1	-0.0000000E-39
ROW 2	-0.0000000E-39
ROW 3	-0.0000000E-39
ROW 4	-0.0000000E-39
ROW 5	-0.0000000E-39
ROW 6	-0.0000000E-39
ROW 7	-0.0000000E-39
ROW 8	1.0000000E 00

THE MATRIX PM

ROW 1	6.0000000E 03
ROW 2	6.0000000E 03
ROW 3	6.0000000E 03
ROW 4	6.0000000E 03
ROW 5	6.0000000E 03
ROW 6	6.0000000E 03
ROW 7	6.0000000E 03
ROW 8	6.0000000E 03

PLASTIC HINGE NO. 1 FORMED AT POINT 8

LOAD FACTOR	ADDITIONAL	CUMULATIVE
STAGE(1)	2.3483869E 03	2.3483869E 03

DEFLECTION	ADDITIONAL	CUMULATIVE
X(1)	-9.2293903E-03	-9.2293903E-03
X(2)	-7.1684583E-03	-7.1684583E-03
X(3)	-9.2293903E-03	-9.2293903E-03
X(4)	-7.2281954E-03	-7.2281954E-03
X(5)	-4.7192351E-03	-4.7192351E-03
X(6)	-7.2281957E-03	-7.2281957E-03
X(7)	7.8952607E-02	7.8952607E-02
X(8)	1.8986459E-01	1.8986459E-01

MOMENT	ADDITIONAL	CUMULATIVE	PLAS MOM
M(1)	5204.3008	5204.3008	6000.0000
M(2)	1881.7204	1881.7204	6000.0000
M(3)	2731.1828	2731.1828	6000.0000
M(4)	3451.6130	3451.6130	6000.0000
M(5)	5946.2365	5946.2365	6000.0000
M(6)	3365.5915	3365.5915	6000.0000
M(7)	5118.2797	5118.2797	6000.0000
M(8)	5999.9999	5999.9999	6000.0000
M(9)	5204.3008	5204.3008	6000.0000
M(10)	1881.7204	1881.7204	6000.0000
M(11)	2731.1828	2731.1828	6000.0000
M(12)	3451.6128	3451.6128	6000.0000
M(13)	-4612.9030	-4612.9030	6000.0000
M(14)	-4241.9352	-4241.9352	6000.0000
M(15)	-4241.9352	-4241.9352	6000.0000
M(16)	-4612.9030	-4612.9030	6000.0000
M(17)	-3451.6126	-3451.6126	6000.0000
M(18)	-2999.9998	-2999.9998	6000.0000
M(19)	-2999.9998	-2999.9998	6000.0000
M(20)	-3451.6127	-3451.6127	6000.0000

HINGE ROTATIONS

AT POINT(1)	0.0000000E-39
AT POINT(2)	0.0000000E-39
AT POINT(3)	0.0000000E-39
AT POINT(4)	0.0000000E-39
AT POINT(5)	0.0000000E-39
AT POINT(6)	0.0000000E-39
AT POINT(7)	0.0000000E-39
AT POINT(8)	0.0000000E-39
AT POINT(9)	0.0000000E-39
AT POINT(10)	0.0000000E-39
AT POINT(11)	0.0000000E-39
AT POINT(12)	0.0000000E-39
AT POINT(13)	0.0000000E-39
AT POINT(14)	0.0000000E-39
AT POINT(15)	0.0000000E-39
AT POINT(16)	0.0000000E-39
AT POINT(17)	0.0000000E-39
AT POINT(18)	0.0000000E-39
AT POINT(19)	0.0000000E-39
AT POINT(20)	0.0000000E-39

PLASTIC HINGE NO. 2 FORMED AT POINT 5

LOAD FACTOR	ADDITIONAL	CUMULATIVE
STAGE(2)	1.8046505E 01	2.3664334E 03

DEFLECTION	ADDITIONAL	CUMULATIVE
X(1)	-9.4618827E-05	-9.3240091E-03
X(2)	-5.7648556E-05	-7.2261068E-03
X(3)	-9.4618829E-05	-9.3240091E-03

X(4)	-1.1446163E-04	-7.3426570E-03
X(5)	5.7230812E-05	-4.6620043E-03
X(6)	-1.1446162E-04	-7.3426573E-03
X(7)	6.8997251E-04	7.9642579E-02
X(8)	2.0546002E-03	1.9191919E-01

MOMENT	ADDITIONAL	CUMULATIVE	PLAS MOM
M(1)	40.4543	5244.7551	6000.0000
M(2)	6.3915	1888.1118	6000.0000
M(3)	38.0481	2769.2308	6000.0000
M(4)	30.9046	3482.5177	6000.0000
M(5)	53.7635	5999.9999	6000.0000
M(6)	33.0101	3398.6015	6000.0000
M(7)	42.5597	5160.8394	6000.0000
M(8)	0.0000	5999.9999	6000.0000
M(9)	40.4543	5244.7551	6000.0000
M(10)	6.3915	1888.1118	6000.0000
M(11)	38.0480	2769.2308	6000.0000
M(12)	30.9046	3482.5174	6000.0000
M(13)	-44.4395	-4657.3425	6000.0000
M(14)	-37.7849	-4279.7200	6000.0000
M(15)	-37.7849	-4279.7200	6000.0000
M(16)	-44.4395	-4657.3425	6000.0000
M(17)	-30.9046	-3482.5172	6000.0000
M(18)	-0.0000	-2999.9998	6000.0000
M(19)	-6.3915	-2999.9998	6000.0000
M(20)	-30.9046	-3482.5174	6000.0000

	HINGE ROTATIONS
AT POINT(1)	0.0000000E-39
AT POINT(2)	0.0000000E-39
AT POINT(3)	0.0000000E-39
AT POINT(4)	0.0000000E-39
AT POINT(5)	0.0000000E-39
AT POINT(6)	0.0000000E-39
AT POINT(7)	0.0000000E-39
AT POINT(8)	-2.3310143E-04
AT POINT(9)	0.0000000E-39
AT POINT(10)	0.0000000E-39
AT POINT(11)	0.0000000E-39
AT POINT(12)	0.0000000E-39
AT POINT(13)	0.0000000E-39
AT POINT(14)	0.0000000E-39
AT POINT(15)	0.0000000E-39
AT POINT(16)	0.0000000E-39
AT POINT(17)	0.0000000E-39
AT POINT(18)	0.0000000E-39
AT POINT(19)	0.0000000E-39
AT POINT(20)	0.0000000E-39

PLASTIC HINGE NO. 3 FORMED AT POINT 9

LOAD FACTOR	ADDITIONAL	CUMULATIVE
STAGE(3)	2.2768410E 02	2.5941175E 03

DEFLECTION	ADDITIONAL	CUMULATIVE
X(1)	-1.4603046E-03	-1.0784314E-02
X(2)	-6.1703011E-04	-7.8431369E-03
X(3)	-1.4603046E-03	-1.0784314E-02
X(4)	-1.4808722E-03	-8.8235291E-03
X(5)	7.4043609E-04	-3.9215682E-03
X(6)	-1.4808722E-03	-8.8235295E-03
X(7)	1.1860691E-02	9.1503262E-02
X(8)	3.0303036E-02	2.2222223E-01

MOMENT	ADDITIONAL	CUMULATIVE	PLAS MOM
M(1)	755.2449	5999.9999	6000.0000
M(2)	229.5353	2117.6471	6000.0000
M(3)	407.2399	3176.4707	6000.0000
M(4)	399.8356	3882.3532	6000.0000
M(5)	-0.0000	5999.9999	6000.0000
M(6)	307.2810	3705.8825	6000.0000
M(7)	662.6904	5823.5297	6000.0000
M(8)	0.0000	5999.9999	6000.0000
M(9)	755.2449	5999.9999	6000.0000
M(10)	229.5353	2117.6471	6000.0000
M(11)	407.2400	3176.4707	6000.0000
M(12)	399.8356	3882.3530	6000.0000
M(13)	-636.7751	-5294.1176	6000.0000
M(14)	-484.9857	-4764.7057	6000.0000
M(15)	-484.9857	-4764.7057	6000.0000
M(16)	-636.7751	-5294.1175	6000.0000
M(17)	-399.8355	-3882.3527	6000.0000
M(18)	-0.0000	-2999.9998	6000.0000
M(19)	-0.0000	-2999.9998	6000.0000
M(20)	-399.8355	-3882.3528	6000.0000

	HINGE ROTATIONS
AT POINT(1)	0.0000000E-39
AT POINT(2)	0.0000000E-39
AT POINT(3)	0.0000000E-39
AT POINT(4)	0.0000000E-39
AT POINT(5)	-1.4705887E-03
AT POINT(6)	0.0000000E-39
AT POINT(7)	0.0000000E-39
AT POINT(8)	-3.4313742E-03
AT POINT(9)	0.0000000E-39
AT POINT(10)	0.0000000E-39
AT POINT(11)	0.0000000E-39
AT POINT(12)	0.0000000E-39
AT POINT(13)	0.0000000E-39
AT POINT(14)	0.0000000E-39
AT POINT(15)	0.0000000E-39
AT POINT(16)	0.0000000E-39
AT POINT(17)	0.0000000E-39
AT POINT(18)	0.0000000E-39
AT POINT(19)	0.0000000E-39
AT POINT(20)	0.0000000E-39

PLASTIC HINGE NO. 4 FORMED AT POINT 1

LOAD FACTOR	ADDITIONAL	CUMULATIVE
STAGE(4)	1.2065213E-05	2.5941175E 03

DEFLECTION	ADDITIONAL	CUMULATIVE
X(1)	-9.5428928E-11	-1.0784314E-02
X(2)	-4.0570425E-11	-7.8431369E-03
X(3)	-7.5083876E-11	-1.0784314E-02
X(4)	-7.8787207E-11	-8.8235291E-03
X(5)	4.1089025E-11	-3.9215681E-03
X(6)	-8.5568894E-11	-8.8235295E-03
X(7)	8.8323677E-10	9.1503269E-02
X(8)	1.9207236E-09	2.2222223E-01

MOMENT	ADDITIONAL	CUMULATIVE	PLAS MOM
M(1)	0.0001	5999.9999	6000.0000
M(2)	0.0000	2117.6471	6000.0000
M(3)	0.0000	3176.4707	6000.0000
M(4)	0.0000	3882.3532	6000.0000
M(5)	-0.0001	5999.9999	6000.0000
M(6)	0.0000	3705.8825	6000.0000
M(7)	0.0000	5823.5297	6000.0000
M(8)	0.0000	5999.9999	6000.0000
M(9)	-0.0001	5999.9999	6000.0000
M(10)	0.0000	2117.6471	6000.0000
M(11)	0.0000	3176.4707	6000.0000
M(12)	0.0000	3882.3530	6000.0000
M(13)	-0.0000	-5294.1176	6000.0000
M(14)	-0.0000	-4764.7057	6000.0000
M(15)	-0.0000	-4764.7057	6000.0000
M(16)	-0.0001	-5294.1175	6000.0000
M(17)	-0.0000	-3882.3527	6000.0000
M(18)	0.0000	-2999.9997	6000.0000
M(19)	-0.0000	-2999.9998	6000.0000
M(20)	-0.0000	-3882.3528	6000.0000

HINGE ROTATIONS

AT POINT(1)	0.0000000E-39
AT POINT(2)	0.0000000E-39
AT POINT(3)	0.0000000E-39
AT POINT(4)	0.0000000E-39
AT POINT(5)	-1.4705887E-03
AT POINT(6)	0.0000000E-39
AT POINT(7)	0.0000000E-39
AT POINT(8)	-3.4313744E-03
AT POINT(9)	0.0000000E-39
AT POINT(10)	0.0000000E-39
AT POINT(11)	0.0000000E-39
AT POINT(12)	0.0000000E-39
AT POINT(13)	0.0000000E-39
AT POINT(14)	0.0000000E-39
AT POINT(15)	0.0000000E-39
AT POINT(16)	0.0000000E-39
AT POINT(17)	0.0000000E-39
AT POINT(18)	0.0000000E-39
AT POINT(19)	0.0000000E-39
AT POINT(20)	0.0000000E-39

PLASTIC HINGE NO. 5 FORMED AT POINT 7

LOAD FACTOR	ADDITIONAL	CUMULATIVE
STAGE(5)	6.8895929E 01	2.6630134E 03

DEFLECTION	ADDITIONAL	CUMULATIVE
X(1)	-6.3121024E-04	-1.1415524E-02
X(2)	-3.7604015E-04	-8.2191770E-03
X(3)	-6.3121024E-04	-1.1415524E-02
X(4)	-5.3720015E-04	-9.3607293E-03
X(5)	2.6860008E-04	-3.6529680E-03
X(6)	-5.3720015E-04	-9.3607296E-03
X(7)	9.7143713E-03	1.0121764E-01
X(8)	1.6742741E-02	2.3896497E-01

MOMENT	ADDITIONAL	CUMULATIVE	PLAS MOM
M(1)	-0.0000	5999.9999	6000.0000
M(2)	183.7225	2301.3696	6000.0000
M(3)	111.2005	3287.6711	6000.0000
M(4)	145.0441	4027.3973	6000.0000
M(5)	-0.0000	5999.9999	6000.0000
M(6)	321.5144	4027.3969	6000.0000
M(7)	176.4703	5999.9999	6000.0000
M(8)	0.0000	5999.9999	6000.0000
M(9)	-0.0000	5999.9999	6000.0000
M(10)	183.7225	2301.3696	6000.0000
M(11)	111.2005	3287.6712	6000.0000
M(12)	145.0441	4027.3971	6000.0000
M(13)	-294.9229	-5589.0405	6000.0000
M(14)	-248.9923	-5013.6979	6000.0000
M(15)	-248.9923	-5013.6979	6000.0000
M(16)	-294.9229	-5589.0404	6000.0000
M(17)	-145.044	-4027.3968	6000.0000
M(18)	-0.0000	-2999.9997	6000.0000
M(19)	-0.0000	-2999.9998	6000.0000
M(20)	-145.0440	-4027.3969	6000.0000

	HINGE ROTATIONS
AT POINT(1)	-1.1415508E-03
AT POINT(2)	0.0000000E-39
AT POINT(3)	0.0000000E-39
AT POINT(4)	0.0000000E-39
AT POINT(5)	-2.7397243E-03
AT POINT(6)	0.0000000E-39
AT POINT(7)	0.0000000E-39
AT POINT(8)	-4.5662099E-03
AT POINT(9)	-1.1415508E-03
AT POINT(10)	0.0000000E-39
AT POINT(11)	0.0000000E-39
AT POINT(12)	0.0000000E-39
AT POINT(13)	0.0000000E-39
AT POINT(14)	0.0000000E-39
AT POINT(15)	0.0000000E-39
AT POINT(16)	0.0000000E-39
AT POINT(17)	0.0000000E-39
AT POINT(18)	0.0000000E-39
AT POINT(19)	0.0000000E-39
AT POINT(20)	0.0000000E-39

PLASTIC HINGE NO. 6 FORMED AT POINT 13

LOAD FACTOR	ADDITIONAL	CUMULATIVE
STAGE(6)	9.4433264E 01	2.7574467E 03

DEFLECTION	ADDITIONAL	CUMULATIVE
X(1)	-9.9582392E-04	-1.2411348E-02
X(2)	-2.9146067E-04	-8.5106377E-03
X(3)	-9.9582391E-04	-1.2411348E-02
X(4)	-9.2295874E-04	-1.0283688E-02
X(5)	4.6147938E-04	-3.1914886E-03
X(6)	-9.2295874E-04	-1.0283688E-02
X(7)	1.3439576E-02	1.1465721E-01
X(8)	2.5219445E-02	2.6418442E-01

MOMENT	ADDITIONAL	CUMULATIVE	PLAS MOM
M(1)	-0.0000	5999.9999	6000.0000
M(2)	187.9922	2489.3617	6000.0000
M(3)	222.9674	3510.6385	6000.0000
M(4)	249.1989	4276.5962	6000.0000
M(5)	-0.0000	5999.9999	6000.0000
M(6)	568.3483	4595.7452	6000.0000
M(7)	0.0000	5999.9999	6000.0000
M(8)	0.0000	5999.9999	6000.0000
M(9)	-0.0000	5999.9999	6000.0000
M(10)	187.9922	2489.3617	6000.0000
M(11)	222.9674	3510.6386	6000.0000
M(12)	249.1989	4276.5959	6000.0000
M(13)	-410.9595	-5999.9999	6000.0000
M(14)	-284.1741	-5297.8721	6000.0000
M(15)	-284.1741	-5297.8721	6000.0000
M(16)	-410.9595	-5999.9999	6000.0000
M(17)	-249.1989	-4276.5956	6000.0000
M(18)	0.0000	-2999.9997	6000.0000
M(19)	0.0000	-2999.9998	6000.0000
M(20)	-249.1989	-4276.5957	6000.0000

	HINGE ROTATIONS
AT POINT(1)	-2.6595752E-03
AT POINT(2)	0.0000000E-39
AT POINT(3)	0.0000000E-39
AT POINT(4)	0.0000000E-39
AT POINT(5)	-4.6099302E-03
AT POINT(6)	0.0000000E-39
AT POINT(7)	-8.8652689E-04
AT POINT(8)	-6.2056759E-03
AT POINT(9)	-2.6595752E-03
AT POINT(10)	0.0000000E-39
AT POINT(11)	0.0000000E-39
AT POINT(12)	0.0000000E-39
AT POINT(13)	0.0000000E-39
AT POINT(14)	0.0000000E-39
AT POINT(15)	0.0000000E-39
AT POINT(16)	0.0000000E-39
AT POINT(17)	0.0000000E-39
AT POINT(18)	0.0000000E-39
AT POINT(19)	0.0000000E-39
AT POINT(20)	0.0000000E-39

PLASTIC HINGE NO. 7 FORMED AT POINT 16

LOAD FACTOR	ADDITIONAL	CUMULATIVE
STAGE(7)	1.9151234E-05	2.7574467E 03

DEFLECTION	ADDITIONAL	CUMULATIVE
X(1)	-3.7942877E-10	-1.2411348E-02
X(2)	-1.3346932E-10	-4.5106378E-03
X(3)	-2.7234954E-10	-1.2411348E-02
X(4)	-2.1890485E-10	-1.0283668E-02
X(5)	1.1837570E-10	-3.1914885E-03
X(6)	-2.5459793E-10	-1.0283669E-02
X(7)	3.7996672E-09	1.1465722E-01
X(8)	7.0561856E-09	2.6418442E-01

MOMENT	ADDITIONAL	CUMULATIVE	PLAS MOM
M(1)	-0.0000	5999.9999	6000.0000
M(2)	0.0000	2489.3617	6000.0000
M(3)	-0.0000	3510.6385	6000.0000
M(4)	0.0001	4276.5962	6000.0000
M(5)	-0.0000	5999.9999	6000.0000
M(6)	0.0001	4595.7453	6000.0000
M(7)	0.0000	5999.9999	6000.0000
M(8)	0.0000	5999.9999	6000.0000
M(9)	-0.0000	5999.9999	6000.0000
M(10)	0.0001	2489.3618	6000.0000
M(11)	0.0001	3510.6386	6000.0000
M(12)	0.0001	4276.5960	6000.0000
M(13)	-0.0000	-5999.9999	6000.0000
M(14)	-0.0000	-5297.8721	6000.0000
M(15)	-0.0001	-5297.8721	6000.0000
M(16)	-0.0001	-5999.9999	6000.0000
M(17)	-0.0001	-4276.5956	6000.0000
M(18)	0.0000	-2999.9997	6000.0000
M(19)	-0.0000	-2999.9998	6000.0000
M(20)	-0.0001	-4276.5958	6000.0000

	HINGE ROTATIONS
AT POINT(1)	-2.6595755E-03
AT POINT(2)	0.0000000E-39
AT POINT(3)	0.0000000E-39
AT POINT(4)	0.0000000E-39
AT POINT(5)	-4.6099306E-03
AT POINT(6)	0.0000000E-39
AT POINT(7)	-8.8652689E-04
AT POINT(8)	-6.2056761E-03
AT POINT(9)	-2.6595755E-03
AT POINT(10)	0.0000000E-39
AT POINT(11)	0.0000000E-39
AT POINT(12)	0.0000000E-39
AT POINT(13)	0.0000000E-39
AT POINT(14)	0.0000000E-39
AT POINT(15)	0.0000000E-39
AT POINT(16)	0.0000000E-39
AT POINT(17)	0.0000000E-39
AT POINT(18)	0.0000000E-39
AT POINT(19)	0.0000000E-39
AT POINT(20)	0.0000000E-39

PLASTIC HINGE NO. 8 FORMED AT POINT 6

LOAD FACTOR	ADDITIONAL	CUMULATIVE
STAGE(8)	1.4781631E 02	2.9052630E 03

DEFLECTION	ADDITIONAL	CUMULATIVE
X(1)	-5.1325095E-03	-1.7543857E-02
X(2)	-2.6004716E-03	-1.1111109E-02
X(3)	-5.1325095E-03	-1.7543857E-02
X(4)	-2.8742050E-03	-1.3157893E-02
X(5)	1.4371025E-03	-1.7543859E-03
X(6)	-2.8742050E-03	-1.3157894E-02
X(7)	5.2009434E-02	1.6666665E-01
X(8)	9.5464680E-02	3.5964910E-01

MOMENT	ADDITIONAL	CUMULATIVE	PLAS MOM
M(1)	-0.0000	5999.9999	6000.0000
M(2)	36.9543	2526.3160	6000.0000
M(3)	-36.9541	3473.6844	6000.0000
M(4)	776.0355	5052.6317	6000.0000
M(5)	-0.0000	5999.9999	6000.0000
M(6)	1404.2547	5999.9999	6000.0000
M(7)	0.0000	5999.9999	6000.0000
M(8)	0.0000	5999.9999	6000.0000
M(9)	-0.0000	5999.9999	6000.0000
M(10)	36.9543	2526.3160	6000.0000
M(11)	-36.9541	3473.6845	6000.0000
M(12)	776.0355	5052.6315	6000.0000
M(13)	-0.0000	-5999.9999	6000.0000
M(14)	-702.1273	-5999.9994	6000.0000
M(15)	-702.1273	-5999.9995	6000.0000
M(16)	-0.0000	-5999.9999	6000.0000
M(17)	-776.0353	-5052.6309	6000.0000
M(18)	0.0000	-2999.9996	6000.0000
M(19)	0.0000	-2999.9998	6000.0000
M(20)	-776.0353	-5052.6311	6000.0000

	HINGE ROTATIONS
AT POINT(1)	-7.8947357E-03
AT POINT(2)	0.0000000E-39
AT POINT(3)	0.0000000E-39
AT POINT(4)	0.0000000E-39
AT POINT(5)	-1.1111110E-02
AT POINT(6)	0.0000000E-39
AT POINT(7)	-2.6315800E-03
AT POINT(8)	-1.1988303E-02
AT POINT(9)	-7.8947357E-03
AT POINT(10)	0.0000000E-39
AT POINT(11)	0.0000000E-39
AT POINT(12)	0.0000000E-39
AT POINT(13)	6.4327457E-03
AT POINT(14)	0.0000000E-39
AT POINT(15)	0.0000000E-39
AT POINT(16)	6.4327456E-03
AT POINT(17)	0.0000000E-39
AT POINT(18)	0.0000000E-39
AT POINT(19)	0.0000000E-39
AT POINT(20)	0.0000000E-39

PLASTIC HINGE NO. 9 FORMED AT POINT 4

LOAD FACTOR	ADDITIONAL	CUMULATIVE
STAGE(9)	9.4736889E 01	2.9999998E 03

DEFLECTION	ADDITIONAL	CUMULATIVE
X(1)	-7.4561370E-03	-2.4999994E-02
X(2)	-0.0000000E-39	-1.1111109E-02
X(3)	-7.4561370E-03	-2.4999994E-02
X(4)	-3.5087701E-03	-1.6666663E-02
X(5)	1.7543851E-03	-8.4401108E-10
X(6)	-3.5087701E-03	-1.6666664E-02
X(7)	8.3333299E-02	2.4999995E-01
X(8)	1.4035082E-01	4.9999992E-01

MOMENT	ADDITIONAL	CUMULATIVE	PLAS MOM
M(1)	-0.0000	5999.9999	6000.0000
M(2)	473.6841	3000.0001	6000.0000
M(3)	-473.6837	3000.0007	6000.0000
M(4)	947.3683	5999.9999	6000.0000
M(5)	-0.0000	5999.9999	6000.0000
M(6)	-0.0000	5999.9999	6000.0000
M(7)	0.0000	5999.9999	6000.0000
M(8)	0.0000	5999.9999	6000.0000
M(9)	-0.0000	5999.9999	6000.0000
M(10)	473.6841	3000.0001	6000.0000
M(11)	-473.6837	3000.0008	6000.0000
M(12)	947.3683	5999.9998	6000.0000
M(13)	-0.0000	-5999.9999	6000.0000
M(14)	-0.0000	-5999.9994	6000.0000
M(15)	-0.0000	-5999.9995	6000.0000
M(16)	-0.0000	-5999.9999	6000.0000
M(17)	-947.3679	-5999.9988	6000.0000
M(18)	0.0000	-2999.9996	6000.0000
M(19)	0.0000	-2999.9998	6000.0000
M(20)	-947.3679	-5999.9990	6000.0000

HINGE ROTATIONS

AT POINT(1)	-1.6666662E-02
AT POINT(2)	0.0000000E-39
AT POINT(3)	0.0000000E-39
AT POINT(4)	0.0000000E-39
AT POINT(5)	-1.9444439E-02
AT POINT(6)	-8.3333300E-03
AT POINT(7)	-8.3333319E-03
AT POINT(8)	-1.9444440E-02
AT POINT(9)	-1.6666662E-02
AT POINT(10)	0.0000000E-39
AT POINT(11)	0.0000000E-39
AT POINT(12)	0.0000000E-39
AT POINT(13)	1.3888883E-02
AT POINT(14)	0.0000000E-39
AT POINT(15)	0.0000000E-39
AT POINT(16)	1.3888882E-02
AT POINT(17)	0.0000000E-39
AT POINT(18)	0.0000000E-39
AT POINT(19)	0.0000000E-39
AT POINT(20)	0.0000000E-39

PLASTIC HINGE NO. 10 FORMED AT POINT 12

LOAD FACTOR	ADDITIONAL	CUMULATIVE
STAGE(10)	1.2207035E-05	2.9999998E 03

DEFLECTION	ADDITIONAL	CUMULATIVE
X(1)	-1.4411074E-09	-2.4999996E-02
X(2)	0.0000000E-39	-1.1111109E-02
X(3)	-1.5541353E-09	-2.4999995E-02
X(4)	-1.1302803E-10	-1.6666663E-02
X(5)	2.2605605E-10	-6.1795503E-10
X(6)	-7.9119615E-10	-1.6666664E-02
X(7)	1.6106494E-08	2.4999996E-01
X(8)	2.8822148E-08	4.9999994E-01

MOMENT	ADDITIONAL	CUMULATIVE	PLAS MOM
M(1)	-0.0000	5999.9999	6000.0000
M(2)	0.0001	3000.0002	6000.0000
M(3)	-0.0001	3000.0006	6000.0000
M(4)	0.0001	5999.9999	6000.0000
M(5)	-0.0001	5999.9999	6000.0000
M(6)	-0.0000	5999.9999	6000.0000
M(7)	0.0000	5999.9999	6000.0000
M(8)	0.0000	5999.9999	6000.0000
M(9)	-0.0000	5999.9999	6000.0000
M(10)	0.0000	3000.0002	6000.0000
M(11)	-0.0000	3000.0008	6000.0000
M(12)	0.0002	5999.9999	6000.0000
M(13)	-0.0000	-5999.9999	6000.0000
M(14)	-0.0000	-5999.9994	6000.0000
M(15)	-0.0000	-5999.9995	6000.0000
M(16)	-0.0000	-5999.9999	6000.0000
M(17)	-0.0001	-5999.9988	6000.0000
M(18)	0.0001	-2999.9995	6000.0000
M(19)	-0.0001	-2999.9998	6000.0000
M(20)	-0.0002	-5999.9992	6000.0000

	HINGE ROTATIONS
AT POINT(1)	-1.6666663E-02
AT POINT(2)	0.0000000E-39
AT POINT(3)	0.0000000E-39
AT POINT(4)	0.0000000E-39
AT POINT(5)	-1.9444441E-02
AT POINT(6)	-8.3333314E-03
AT POINT(7)	-8.3333333E-03
AT POINT(8)	-1.9444442E-02
AT POINT(9)	-1.6666663E-02
AT POINT(10)	0.0000000E-39
AT POINT(11)	0.0000000E-39
AT POINT(12)	0.0000000E-39
AT POINT(13)	1.3888884E-02
AT POINT(14)	0.0000000E-39
AT POINT(15)	0.0000000E-39
AT POINT(16)	1.3888884E-02
AT POINT(17)	0.0000000E-39
AT POINT(18)	0.0000000E-39
AT POINT(19)	0.0000000E-39
AT POINT(20)	0.0000000E-39

APPENDIX C

COMPUTER INPUT AND OUTPUT LISTINGS FOR SAMPLE PROBLEM 1

```
*     SAMPLE PROBLEM I DEBRIS CHARACTERISTICS OF FOUR CONTIGINCUS WALLS
*     FIRST WALL (ALL DISTRIBUTIONS ARE TAKEN RELATIVE TO THE POSITION
*     CF THIS WALL)
WEAPCN PARAMETERS
YIELD 1CCO. KILO-TCNS
OVERPRESSURE 10. PSI
PREBLAST STRUCTURAL CONFIGURATICN
WALL HEIGHT 40 FLCCRS
HEIGHT BETWEEN FLCCRS 10. FEET
NORMALIZING FACTCR 3.333
FRAGMENTATION CHARACTERISTICS
NUMBER CF PARTICLE SIZES 5
PARTICLE SIZES 10.C,8.0,6.0,4.0,2.0 INCHES ECUIVALENT RADIUS
PERCENTAGE BY SIZE 0.13,C.05,0.45,0.32,0.C5
ACCELERATICN CCEFFICIENT 0.C
OUTPUT
PRCFILE DISTRIBUTICN 1
DISTRIBUTICN OF SIZES 1
LCCATICNS 3
DISTANCES FROM FIRST WALL 5C.,15C.,300. FEET
VELCCITY DESCRIPTICN 1
DEBRIS PROFILE PLCT 1
SCLVE
```

5PARTICLE SIZES

4CSTORY BUILDING

10.00FT. BETWEEN FLOORS

YIELD= 1000.0KT.

OVERPRESSURE= 10.[illegible]

PARTICLE RADIUS PERCENT OF PANEL

10.00 FT.	0.13 X100
8.00 FT.	0.05 X100
6.00 FT.	0.45 X100
4.00 FT.	0.32 X100
2.00 FT.	0.05 X100

DISTANCE OF CURRENT WALL FROM STARTING WALL 0. FT.

SIZE RANGE	1	8.00 IN. TO 10.00 IN.
SIZE RANGE	2	6.00 IN. TO 8.00 IN.
SIZE RANGE	3	4.00 IN. TO 6.00 IN.
SIZE RANGE	4	2.00 IN. TO 4.00 IN.
SIZE RANGE	5	0. IN. TO 2.00 IN.

DEBRIS HEIGHT (FT.) AT 1FT. INTERVALS FROM ORIGINAL POSITION

1FT.	0.	0.	0.	0.	0.
6FT.	0.330084	0.408156	0.078072	0.445253	0.367180
11FT.	0.528454	0.528454	0.625690	0.296915	0.255358
16FT.	0.255358	0.255358	0.438196	0.527403	0.407687
21FT.	0.407687	0.493983	0.517660	0.500055	0.539420
26FT.	0.582019	0.652413	0.445815	0.445815	0.644539
31FT.	0.542003	0.618976	0.604127	0.604127	0.773387

36FT.	0.775632	C.731747	C.775645	0.716664
41FT.	0.777205	C.92C992	C.79E85E	0.929227
46FT.	0.902788	1.031642	C.957461	1.034885
51FT.	1.006507	1.097313	1.085E67	1.113363
56FT.	1.113492	1.2C8325	1.197926	1.315751
61FT.	1.213985	1.3C3C46	1.3541EC	1.199628
66FT.	1.226740	1.215174	1.195C54	1.152172
71FT.	1.115349	1.123452	1.C59362	1.094257
76FT.	1.087330	1.C14116	1.07C25E	0.997177
81FT.	1.043305	1.027304	1.C72163	1.125356
86FT.	1.100669	1.152479	1.1C2C91	1.135814
91FT.	1.186171	1.154855	1.212355	1.189963
96FT.	1.238439	1.223616	1.232CC5	1.179748
1C1FT.	1.195582	1.16CC35	1.109746	1.125154
1C6FT.	1.076632	1.0E6346	1.C34585	0.987387
111FT.	1.002234	0.97C810	C.902486	0.917035
116FT.	0.871504	C.841C42	C.856C15	0.790615
121FT.	0.804747	C.731536	C.745E3E	0.703192
126FT.	0.717744	C.627358	C.64C541	0.613229
131FT.	0.573033	C.535525	C.499E95	0.513123
136FT.	0.487279	C.425209	C.4292C5	0.429209
141FT.	0.429800	C.411519	C.411515	0.41036C
146FT.	0.392554	C.392554	C.392554	0.393111
151FT.	0.375742	C.375742	C.376284	0.359279
156FT.	0.359279	C.355807	C.343141	0.343141
161FT.	0.343658	C.327273	C.327273	0.327778
166FT.	0.311690	C.312185	C.296346	0.296346
171FT.	0.296832	C.281200	C.281677	0.266269
176FT.	0.266269	C.2EE738	C.251542	0.251542
181FT.	0.252004	C.237441	C.222594	0.222594
186FT.	0.223042	C.2CE800	C.19425C	0.19425C
191FT.	0.194686	C.18C719	C.165151	0.165151
196FT.	0.165576	C.151864	C.137848	0.137848
2C1FT.	0.138264	C.124772	C.11C575	0.111386
2C6FT.	0.097699	C.0E4518	C.084516	0.071417
211FT.	0.071811	C.058801	C.C45475	0.045866
216FT.	0.032638	C.015E69	C.C15E65	0.019869
221FT.	0.019869	C.015E69	C.C15E65	0.019869
226FT.	0.019869	C.015E69	C.C19E65	0.019869
231FT.	0.019869	C.C1E79C	C.C1E79C	0.018790
236FT.	0.018790	C.01E790	C.01875C	0.01879C
241FT.	0.01879C	C.C1E79C	C.C1875C	0.01879C

246FT.	0.018790	0.018790	0.018790	0.018790	0.018790
251FT.	0.018790	0.018790	0.018790	0.018790	0.018790
256FT.	0.018790	0.018790	0.018790	0.018790	0.018790
261FT.	0.018790	0.018790	0.018790	0.018790	0.018790
266FT.	0.017846	0.017846	0.017846	0.017846	0.017846
271FT.	0.017846	0.017846	0.017846	0.017846	0.017846
276FT.	0.017846	0.017846	0.017846	0.017846	0.017846
281FT.	0.017846	0.017846	0.017846	0.017846	0.017846
286FT.	0.017846	0.017846	0.017846	0.017846	0.017846
291FT.	0.017846	0.016987	0.016987	0.016987	0.016987
296FT.	0.016987	0.016987	0.016987	0.016987	0.016987
301FT.	0.016987	0.016987	0.016987	0.016987	0.016987
306FT.	0.016987	0.016987	0.016987	0.016987	0.016987
311FT.	0.016987	0.016987	0.016987	0.016987	0.016987
316FT.	0.016987	0.016987	0.016199	0.016199	0.016199
321FT.	0.016199	0.016199	0.016199	0.016199	0.016199
326FT.	0.016199	0.016199	0.016199	0.016199	0.016199
331FT.	0.016199	0.016199	0.016199	0.016199	0.016199
336FT.	0.016199	0.016199	0.016199	0.015458	0.015458
341FT.	0.015458	0.015458	0.015458	0.015458	0.015458
346FT.	0.015458	0.015458	0.015458	0.015458	0.015458
351FT.	0.015458	0.015458	0.015458	0.015458	0.015458
356FT.	0.015458	0.015458	0.014759	0.014759	0.014759
361FT.	0.014759	0.014759	0.014759	0.014759	0.014759
366FT.	0.014759	0.014759	0.014759	0.014759	0.014759
371FT.	0.014759	0.014759	0.014759	0.014759	0.014759
376FT.	0.014759	0.014759	0.014095	0.014095	0.014095
381FT.	0.014095	0.014095	0.014095	0.014095	0.014095
386FT.	0.014095	0.014095	0.014095	0.014095	0.014095
391FT.	0.014095	0.014095	0.014095	0.013459	0.013459
396FT.	0.013459	0.013459	0.013459	0.013459	0.013459
401FT.	0.013459	0.013459	0.013459	0.013459	0.013459
406FT.	0.013459	0.013459	0.013459	0.012847	0.012847
411FT.	0.012847	0.012847	0.012847	0.012847	0.012847
416FT.	0.012847	0.012847	0.012847	0.012847	0.012847
421FT.	0.012847	0.012847	0.012255	0.012255	0.012255
426FT.	0.012255	0.012255	0.012255	0.012255	0.012255
431FT.	0.012255	0.012255	0.012255	0.012255	0.012255
436FT.	0.012255	0.011682	0.011682	0.011682	0.011682
441FT.	0.011682	0.011682	0.011682	0.011682	0.011682
446FT.	0.011682	0.011682	0.011682	0.011682	0.011126

451FT.	0.011126	0.C11126	C.011126	C.C11126	0.011126
456FT.	0.011126	0.C11126	C.011126	C.011126	0.011126
461FT.	0.011126	0.C10584	C.C1C584	C.01C584	C.010584
466FT.	0.010584	0.C10584	C.01C584	C.C1C584	0.010584
471FT.	0.01C584	0.C10584	C.01C584	C.C1CC55	0.010C55
476FT.	0.01C055	0.C10055	C.01CC55	C.01CC55	0.01CC55
481FT.	0.01C055	0.C10055	C.01CC55	C.C09538	C.009538
486FT.	C.009538	0.CC9538	C.0C9538	C.009538	0.009538
491FT.	0.009538	0.CC9538	C.0C9538	C.009538	0.009538
496FT.	0.009033	0.CC9033	C.0C9C33	C.0C9C33	0.009C33
5C1FT.	0.009033	0.CC9033	C.CC9C33	C.009C33	0.009033
5C6FT.	0.008538	0.CC8538	C.0CE538	C.C08538	0.008538
511FT.	0.008538	0.C08538	C.0CE538	C.C08538	0.008C51
516FT.	0.008051	0.C08051	C.0CE051	C.0CE051	0.008C51
521FT.	0.008051	0.C08051	C.0CE051	C.007574	0.007574
526FT.	0.007574	0.C07574	C.0C7574	C.007574	0.007574
531FT.	0.007574	0.CC7574	C.0C7574	C.0071C5	0.007105
536FT.	0.0071C5	0.CC7105	C.007105	C.0071C5	0.007105
541FT.	0.007105	0.CC7105	C.CC6643	C.CC6643	0.006643
546FT.	0.006643	0.C06643	C.CC6643	C.006643	0.006643
551FT.	0.006189	0.CC6189	C.006189	C.006189	0.006189
556FT.	0.006189	0.C06189	C.0C6189	C.005741	0.005741
561FT.	0.005741	0.C05741	C.0C5741	C.005741	0.005741
566FT.	0.005298	0.CC5298	C.0C5298	C.005298	0.005298
571FT.	0.005298	0.C05298	C.0C5298	C.004862	0.004862
576FT.	0.004862	0.CC4862	C.0C4862	C.004862	0.004862
581FT.	0.004432	0.C04432	C.0C4432	C.004432	0.004432
586FT.	0.004432	0.C04432	C.CC4[illegible]	C.C04CC7	0.004007
591FT.	0.004007	0.CC4007	C.0C4CC7	C.004CC7	0.004C07
596FT.	0.003587	0.CC3587	C.0C3587	C.003587	0.003587
6C1FT.	0.003587	0.CC3587	C.0C3172	C.003172	C.003172
6C6FT.	0.003172	0.C03172	C.0C3172	C.003172	0.002761
611FT.	0.002761	0.CC2761	C.0C2761	C.002761	0.002761
616FT.	0.002761	0.CC2355	C.0C2355	C.002355	0.002355
621FT.	0.C02355	0.CC2355	C.CC1953	C.001953	0.001953
626FT.	0.001953	0.CC1953	C.0C1953	C.001555	0.001555
631FT.	0.001555	0.CC1555	C.0C1555	C.001555	0.001161
636FT.	0.001161	0.CC1161	C.0C1161	C.001161	0.001161
641FT.	0.000770	0.CC0770	C.CCC77C	C.00C77C	0.000770
646FT.	0.000770	0.C00383	C.CCC383	C.C0C383	0.000383

DISTRIBUTION OF SIZES AT 50 FT. FROM ORIGINAL POSITION

SIZE RANGE	PERCENT
1	40.75
2	8.56
3	40.84
4	9.35
5	0.50

DISTRIBUTION OF SIZES AT 150 FT. FROM ORIGINAL POSITION

SIZE RANGE	PERCENT
1	0.
2	0.
3	0.
4	97.45
5	2.55

DISTRIBUTION OF SIZES AT 300 FT. FROM ORIGINAL POSITION

SIZE RANGE	PERCENT
1	0.
2	0.
3	0.
4	0.
5	100.00

CUMULATIVE DEBRIS MOMENTUM (FT./SEC.) AT 1FT INTERVALS FROM ORIGINAL POSITION
(MULTIPLY BY MASS OF ONE PANEL)

1FT.	0.	0.	C.	C.	C.	
6FT.	2.386594	3.C24842	C.63E248	4.335165	3.696922	
11FT.	5.405084	5.4C4084	E.863768	3.60C571	3.454173	
16FT.	3.454173	3.454173	5.79E788	7.248E43	5.687479	
21FT.	5.687479	7.145287	7.514506	7.505C77	8.083C16	
26FT.	9.117875	10.327536	7.949C13	7.949C13	11.618105	
31FT.	9.805254	11.565352	11.555785	11.555785	15.136837	
36FT.	15.474083	13.783531	15.56C373	16.977215	15.565096	
41FT.	17.333539	19.C91831	21.145230	19.269737	22.789785	
46FT.	22.465785	24.255568	2E.381796	25.212E9C	27.601C27	
51FT.	27.880796	27.571948	31.1C5674	31.147294	32.102242	
56FT.	33.655144	35.C42313	37.162220	37.211C14	41.381230	
61FT.	39.334664	44.420122	42.978363	44.184946	40.295345	
66FT.	40.936779	39.481692	4C.12EC47	39.206264	38.120965	
71FT.	36.656732	37.303761	3E.1CC884	34.907668	35.564526	
76FT.	34.988850	32.C74061	32.882643	34.86CC74	32.782650	
81FT.	34.587931	36.582033	34.497C25	36.3175C3	38.325420	
86FT.	38.068248	37.7C7194	4C.10E589	39.272143	40.763350	
91FT.	42.803449	42.566010	42.2CC307	44.622287	44.391C76	
96FT.	46.462622	46.250708	47.213742	47.397785	45.641564	
101FT.	46.200190	44.436951	45.0CC592	43.226792	43.794174	
106FT.	42.032731	41.483365	42.054354	4C.846346	39.054883	
111FT.	39.634661	37.835953	3E.437224	3E.08S1CS	36.677984	
116FT.	34.862829	35.455564	33.635C86	34.249589	31.883058	
121FT.	32.484025	31.255995	29.415133	3C.024E7C	28.176798	
126FT.	28.807395	27.C37483	25.176584	25.798467	24.558319	
131FT.	22.700323	22.796663	21.55C848	19.663C82	20.300566	
136FT.	19.067093	16.634137	16.634137	16.634137	16.634137	
141FT.	16.651051	16.115095	16.115C95	16.115C95	16.106304	
146FT.	15.568192	15.568192	15.568192	15.568192	15.585120	
151FT.	15.044865	15.C44865	15.044865	15.061843	14.518121	
156FT.	14.518121	14.518121	14.535141	13.988C9C	13.988090	
161FT.	14.005191	13.453710	13.453710	13.45371C	13.470839	
166FT.	12.916302	12.916302	12.933496	12.37487C	12.37487C	
171FT.	12.392164	11.828523	11.828523	11.845E6E	11.278487	
176FT.	11.278487	11.278487	11.295876	1C.724E87	10.724887	
181FT.	10.742355	10.1668RR	1C.184429	9.cC465C	9.604650	
186FT.	9.622257	9.C3H321	9.05EC27	8.467152	8.467152	

191FT.	8.484913	7.892177	7.910024	7.290958	7.290908
196FT.	7.308801	6.707835	6.725805	6.120487	6.120487
201FT.	6.138529	5.528992	5.547102	4.933469	4.951643
206FT.	4.334030	4.352263	3.730780	3.749101	3.123066
211FT.	3.141440	2.511749	2.530204	1.896184	1.914685
216FT.	1.277201	1.295776	0.654164	0.654164	0.654164
221FT.	0.654164	0.654164	0.654164	0.654164	0.654164
226FT.	0.654164	0.654164	0.654164	0.654164	0.654164
231FT.	0.654164	0.654164	0.634352	0.634352	0.634352
236FT.	0.634352	0.634352	0.634352	0.634352	0.634352
241FT.	0.634352	0.634352	0.634352	0.634352	0.634352
246FT.	0.634352	0.634352	0.634352	0.634352	0.634352
251FT.	0.634352	0.634352	0.634352	0.634352	0.634352
256FT.	0.634352	0.634352	0.634352	0.634352	0.634352
261FT.	0.634352	0.634352	0.634352	0.634352	0.634352
266FT.	0.615674	0.615674	0.615674	0.615674	0.615674
271FT.	0.615674	0.615674	0.615674	0.615674	0.615674
276FT.	0.615674	0.615674	0.615674	0.615674	0.615674
281FT.	0.615674	0.615674	0.615674	0.615674	0.615674
286FT.	0.615674	0.615674	0.615674	0.615674	0.615674
291FT.	0.615674	0.597603	0.597603	0.597603	0.597603
296FT.	0.597603	0.597603	0.597603	0.597603	0.597603
301FT.	0.597603	0.597603	0.597603	0.597603	0.597603
306FT.	0.597603	0.597603	0.597603	0.597603	0.597603
311FT.	0.597603	0.597603	0.597603	0.597603	0.597603
316FT.	0.597603	0.597603	0.580064	0.580064	0.580064
321FT.	0.580064	0.580064	0.580064	0.580064	0.580064
326FT.	0.580064	0.580064	0.580064	0.580064	0.580064
331FT.	0.580064	0.580064	0.580064	0.580064	0.580064
336FT.	0.580064	0.580064	0.580064	0.562728	0.562728
341FT.	0.562728	0.562728	0.562728	0.562728	0.562728
346FT.	0.562728	0.562728	0.562728	0.562728	0.562728
351FT.	0.562728	0.562728	0.562728	0.562728	0.562728
356FT.	0.562728	0.562728	0.545585	0.545585	0.545585
361FT.	0.545585	0.545585	0.545585	0.545585	0.545585
366FT.	0.545585	0.545585	0.545585	0.545585	0.545585
371FT.	0.545585	0.545585	0.545585	0.545585	0.545585
376FT.	0.545585	0.545585	0.528621	0.528621	0.528621
381FT.	0.528621	0.528621	0.528621	0.528621	0.528621
386FT.	0.528621	0.528621	0.528621	0.528621	0.528621
391FT.	0.528621	0.528621	0.528621	0.511689	0.511689

396FT.	0.511689	0.511689	C.511689	C.511689	0.511689
401FT.	0.511689	0.511689	C.511689	C.511689	0.511689
406FT.	0.511689	0.511689	C.511689	C.494794	0.494794
411FT.	0.494794	0.494794	C.494794	C.494794	0.494794
416FT.	0.494794	0.494794	C.494794	C.494794	0.494794
421FT.	0.494794	0.494794	C.477880	C.477880	0.477880
426FT.	0.477880	0.477880	C.477880	C.477880	0.477880
431FT.	0.477880	0.477880	C.477880	C.477880	0.477880
436FT.	0.477880	0.460956	C.460956	C.460956	0.460956
441FT.	0.460956	0.460956	C.460956	C.460956	0.460956
446FT.	0.460956	0.460956	C.460956	C.460956	0.444028
451FT.	0.444028	0.444028	C.444028	C.444028	0.444028
456FT.	0.444028	0.444028	C.444028	C.444028	0.444028
461FT.	0.444028	0.427049	C.427049	C.427049	0.427049
466FT.	0.427049	0.427049	C.427049	C.427049	0.427049
471FT.	0.427049	0.427049	C.427049	C.410029	0.410029
476FT.	0.410029	0.410029	C.410029	C.410029	0.410029
481FT.	0.410029	0.410029	C.410029	C.392928	0.392928
486FT.	0.392928	0.392928	C.392928	C.392928	0.392928
491FT.	0.392928	0.392928	C.392928	C.392928	0.392928
496FT.	0.375800	0.375800	C.375800	C.375800	0.375800
501FT.	0.375800	0.375800	C.375800	C.375800	0.375800
506FT.	0.358606	0.358606	C.358606	C.358606	0.358606
511FT.	0.358606	0.358606	C.358606	C.358606	0.341312
516FT.	0.341312	0.341312	C.341312	C.341312	0.341312
521FT.	0.341312	0.341312	C.341312	C.323967	0.323967
526FT.	0.323967	0.323967	C.323967	C.323967	0.323967
531FT.	0.323967	0.323967	C.323967	C.306578	0.306578
536FT.	0.306578	0.306578	C.306578	C.306578	0.306578
541FT.	0.306578	0.306578	C.289110	C.289110	0.289110
546FT.	0.289110	0.289110	C.289110	C.289110	0.289110
551FT.	0.271569	0.271569	C.271569	C.271569	0.271569
556FT.	0.271569	0.271569	C.271569	C.253962	0.253962
561FT.	0.253962	0.253962	C.253962	C.253962	0.253962
566FT.	0.236256	0.236256	C.236256	C.236256	0.236256
571FT.	0.236256	0.236256	C.236256	C.218496	0.218496
576FT.	0.218496	0.218496	C.218496	C.218496	0.218496
581FT.	0.200648	0.200648	C.200648	C.200648	0.200648
586FT.	0.200648	0.200648	C.200648	C.182755	0.182755
591FT.	0.182755	0.182755	C.182755	C.182755	0.182755
596FT.	0.164785	0.164785	C.164785	C.164785	0.164785
601FT.	0.164785	0.164785	C.146743	C.146743	0.146743

606FT.	0.146743	0.146743	C.146743	C.146743	0.128633
611FT.	0.128633	0.128633	C.128633	C.128633	0.128633
616FT.	0.128633	0.110460	C.110460	0.110460	0.110460
621FT.	0.110460	0.110460	C.092227	C.092227	0.092227
626FT.	0.092227	0.092227	C.092227	C.073905	0.073905
631FT.	0.073905	0.073905	C.073905	C.073905	0.055531
636FT.	0.055531	0.055531	C.055531	C.055531	0.055531
641FT.	0.037076	0.037076	C.037076	C.037076	C.037076
646FT.	0.037076	0.018575	C.018575	C.018575	0.018575

MINIMUM DEBRIS MOMENTUM (FT./SEC.) AT 1FT. INTERVALS FROM ORIGINAL POSITION
(MULTIPLY BY MASS OF ONE PANEL)

1FT.	0.	0.	C.	C.	0.
6FT.	0.	0.638248	C.	C.	0.
11FT.	1.708162	1.708162	1.456684	C.434124	0.434124
16FT.	0.434124	0.434124	C.434124	C.389408	0.389408
21FT.	0.389408	0.389408	C.369219	C.041708	0.369219
26FT.	0.369219	0.358099	C.358099	C.358099	0.353427
31FT.	0.353427	0.347978	C.347978	C.347978	0.347439
36FT.	0.347439	0.346072	C.346072	0.344207	0.344207
41FT.	0.344207	0.344207	C.344207	0.344207	0.344207
46FT.	0.344207	0.344207	C.025715	C.025715	0.025715
51FT.	0.025715	0.025715	C.025715	C.025715	0.025715
56FT.	0.025715	0.025715	C.025715	C.025715	0.025715
61FT.	0.025715	0.025715	C.025715	C.021756	0.021756
66FT.	0.021756	0.021756	C.021756	C.021756	0.021756
71FT.	0.021756	0.021756	C.021756	C.021756	0.021756
76FT.	0.021756	0.019812	C.019812	C.019812	0.019812
81FT.	0.019812	0.019812	C.019812	C.019812	0.019812
86FT.	0.019812	0.019812	C.018678	C.018678	0.018678
91FT.	0.018678	0.018678	C.018678	C.018678	0.018678
96FT.	0.018678	0.018071	C.018071	C.018071	0.018071
101FT.	0.018071	0.018071	C.018071	C.018071	0.018071
106FT.	0.017539	0.017539	C.017539	C.017539	0.017539
111FT.	0.017539	0.017539	C.017336	C.017336	0.017336
116FT.	0.017336	0.017336	C.017336	C.017143	0.017143
121FT.	0.017143	0.017143	C.017143	C.017143	0.017143
126FT.	0.016964	0.016964	C.016964	C.016964	0.016964
131FT.	0.016932	0.016932	C.016932	C.016932	0.016932
136FT.	0.016895	0.016895	C.016895	C.016895	0.016895
141FT.	0.016895	0.016895	C.016895	C.016895	0.016895
146FT.	0.016895	0.016895	C.016895	C.016895	0.016895
151FT.	0.016895	0.016895	C.016895	C.016895	0.016895
156FT.	0.016895	0.016895	C.016895	C.016895	0.016895
161FT.	0.016895	0.016895	C.016895	C.016895	0.016895
166FT.	0.016895	0.016895	C.016895	C.016895	0.016895
171FT.	0.016895	0.016895	C.016895	C.016895	0.016895
176FT.	0.016895	0.016895	C.016895	C.016895	0.016895
181FT.	0.016895	0.016895	C.016895	C.016895	0.016895
186FT.	0.016895	0.016895	C.016895	C.016895	C.016895

191FT.	0.016895	0.016895	0.016895	0.016895	0.016895
196FT.	0.016895	0.016895	0.016895	0.016895	0.016895
201FT.	0.016895	0.016895	0.016895	0.016895	0.016895
206FT.	0.016895	0.016895	0.016895	0.016895	0.016895
211FT.	0.016895	0.016895	0.016895	0.016895	0.016895
216FT.	0.016895	0.016895	0.016895	0.016895	0.016895
221FT.	0.016895	0.016895	0.016895	0.016895	0.016895
226FT.	0.016895	0.016895	0.016895	0.016895	0.016895
231FT.	0.016895	0.016895	0.016895	0.016895	0.016895
236FT.	0.016895	0.016895	0.016895	0.016895	0.016895
241FT.	0.016895	0.016895	0.016895	0.016895	0.016895
246FT.	0.016895	0.016895	0.016895	0.016895	0.016895
251FT.	0.016895	0.016895	0.016895	0.016895	0.016895
256FT.	0.016895	0.016895	0.016895	0.016895	0.016895
261FT.	0.016895	0.016895	0.016895	0.016895	0.016895
266FT.	0.016895	0.016895	0.016895	0.016895	0.016895
271FT.	0.016895	0.016895	0.016895	0.016895	0.016895
276FT.	0.016895	0.016895	0.016895	0.016895	0.016895
281FT.	0.016895	0.016895	0.016895	0.016895	0.016895
286FT.	0.016895	0.016895	0.016895	0.016895	0.016895
291FT.	0.016895	0.016895	0.016895	0.016895	0.016895
296FT.	0.016895	0.016895	0.016895	0.016895	0.016895
301FT.	0.016895	0.016895	0.016895	0.016895	0.016895
306FT.	0.016895	0.016895	0.016895	0.016895	0.016895
311FT.	0.016895	0.016895	0.016895	0.016895	0.016895
316FT.	0.016895	0.016895	0.016895	0.016895	0.016895
321FT.	0.016895	0.016895	0.016895	0.016895	0.016895
326FT.	0.016895	0.016895	0.016895	0.016895	0.016895
331FT.	0.016895	0.016895	0.016895	0.016895	0.016895
336FT.	0.016895	0.016895	0.016895	0.016895	0.016895
341FT.	0.016895	0.016895	0.016895	0.016895	0.016895
346FT.	0.016895	0.016895	0.016895	0.016895	0.016895
351FT.	0.016895	0.016895	0.016895	0.016895	0.016895
356FT.	0.016895	0.016895	0.016895	0.016895	0.016895
361FT.	0.016895	0.016895	0.016895	0.016895	0.016895
366FT.	0.016895	0.016895	0.016895	0.016895	0.016895
371FT.	0.016895	0.016895	0.016895	0.016895	0.016895
376FT.	0.016895	0.016895	0.016895	0.016895	0.016895
381FT.	0.016895	0.016895	0.016895	0.016895	0.016895
386FT.	0.016895	0.016895	0.016895	0.016895	0.016895
391FT.	0.016895	0.016895	0.016895	0.	0.

MAXIMUM DEBRIS MOMENTUM (FT./SEC.) AT 1FT. INTERVALS FROM ORIGINAL POSITION
(MULTIPLY BY MASS OF ONE PANEL)

1FT.	0.	0.	C.	C.	0.
6FT.	2.386594	2.386594	C.63E248	3.696922	3.696922
11FT.	3.696922	3.696922	3.696922	1.708162	1.561364
16FT.	1.561364	1.561364	2.344616	2.344616	2.344616
21FT.	2.344616	2.344616	2.344616	2.344616	2.344616
26FT.	2.344616	2.344616	2.036624	2.036624	2.036624
31FT.	2.036624	2.036624	2.036624	2.036624	2.036624
36FT.	2.036624	1.896301	1.896301	1.896301	1.896301
41FT.	1.896301	1.896301	1.896301	1.818809	1.818809
46FT.	1.818809	1.818809	1.818809	1.818809	1.818809
51FT.	1.782281	1.782281	1.782281	1.782281	1.782281
56FT.	1.747065	1.747065	1.747065	1.747065	1.747065
61FT.	1.739187	1.739187	1.739187	1.739187	1.738668
66FT.	1.743933	1.743933	1.753C17	1.753C17	1.756222
71FT.	1.756222	1.763239	1.773EOC	1.773ECC	1.778982
76FT.	1.778982	1.783475	1.7914c3	1.798709	1.798709
81FT.	1.805281	1.815155	1.815155	1.82C479	1.829078
86FT.	1.833348	1.833348	1.84C862	1.847872	1.854405
91FT.	1.860499	1.866183	1.866183	1.874929	1.879836
96FT.	1.887766	1.891980	1.895187	1.899187	1.899187
101FT.	1.899187	1.899187	1.895187	1.899187	1.899187
106FT.	1.899187	1.899187	1.895187	1.899187	1.899187
111FT.	1.899187	1.899187	1.895187	1.899187	1.899187
116FT.	1.899187	1.899187	1.895187	1.899187	1.899187
121FT.	1.899187	1.899187	1.895187	1.899187	1.899187
126FT.	1.899187	1.899187	1.895187	1.899187	1.899187
131FT.	1.899187	1.899187	1.895187	1.899187	1.899187
136FT.	1.899187	0.641611	C.641611	C.641611	0.641611
141FT.	0.641611	0.641611	C.641611	C.641611	0.641611
146FT.	0.641611	0.641611	C.641611	C.641611	0.641611
151FT.	0.641611	0.641611	C.641611	0.641611	0.641611
156FT.	0.641611	0.641611	C.641611	C.641611	0.641611
161FT.	0.641611	0.641611	C.641611	C.641611	0.641611
166FT.	0.641611	0.641611	C.641611	C.641611	0.641611
171FT.	0.641611	0.641611	C.641611	0.641611	0.641611
176FT.	0.641611	0.641611	C.641611	C.641611	0.641611
181FT.	0.641611	0.641611	C.641611	C.641611	0.641611
186FT.	0.641611	C.641611	C.641611	C.641611	0.641611

191FT.	0.641611	0.641611	C.641611	C.641611	0.641611
196FT.	0.641611	0.641611	C.641611	C.641611	0.641611
201FT.	0.641611	0.641611	C.641611	C.641611	0.641611
206FT.	0.641611	0.641611	C.641611	0.641611	0.641611
211FT.	0.641611	0.641611	C.641611	C.641611	0.641611
216FT.	0.641611	0.641611	C.019812	C.019812	0.019812
221FT.	0.019812	0.C19812	C.019812	C.019812	0.019812
226FT.	0.019812	0.C19812	C.019812	C.019812	0.019812
231FT.	0.019812	0.C19812	C.018678	C.018678	0.018678
236FT.	0.018678	0.C18678	C.018678	C.018678	0.018678
241FT.	0.018678	0.C18678	C.018678	C.018678	0.018678
246FT.	0.018678	0.C18678	C.018678	C.018678	0.018678
251FT.	0.018678	0.C18678	C.018678	C.018678	0.018678
256FT.	0.018678	0.C18678	C.018678	C.018678	0.018678
261FT.	0.018678	0.C18678	C.018678	C.018678	0.018678
266FT.	0.018575	0.C18575	C.018575	C.018575	0.018575
271FT.	0.018575	0.C18575	C.018575	C.018575	0.018575
276FT.	0.018575	0.C18575	C.018575	C.018575	0.018575
281FT.	0.018575	0.C18575	C.018575	C.018575	0.018575
286FT.	0.018575	0.C18575	C.018575	C.018575	0.018575
291FT.	0.018575	0.C18575	C.018575	C.018575	0.018575
296FT.	0.018575	0.C18575	C.018575	C.018575	0.018575
301FT.	0.018575	0.C18575	C.018575	0.018575	0.018575
306FT.	0.018575	0.C18575	C.018575	C.018575	0.018575
311FT.	0.018575	0.C18575	C.018575	C.018575	0.018575
316FT.	0.018575	0.C18575	C.018575	C.018575	0.018575
321FT.	0.018575	0.C18575	C.018575	0.018575	0.018575
326FT.	0.018575	0.C18575	C.018575	C.018575	0.018575
331FT.	0.018575	0.C18575	C.018575	C.018575	0.018575
336FT.	0.018575	0.C18575	C.018575	C.018575	0.018575
341FT.	0.018575	0.C18575	C.018575	C.018575	0.018575
346FT.	0.018575	0.C18575	C.018575	C.018575	0.018575
351FT.	0.018575	0.C18575	C.018575	C.018575	0.018575
356FT.	0.018575	0.C18575	C.018575	C.018575	0.018575
361FT.	0.018575	0.C18575	C.018575	C.018575	0.018575
366FT.	0.018575	0.C18575	C.018575	C.018575	0.018575
371FT.	0.018575	0.C18575	C.018575	C.018575	0.018575
376FT.	0.018575	0.C18575	C.018575	C.018575	0.018575
381FT.	0.018575	0.C18575	C.018575	C.018575	0.018575
386FT.	0.018575	0.C18575	C.018575	C.018575	0.018575
391FT.	0.018575	0.C18575	C.018575	C.018575	0.018575

396FT.	0.018575	0.018575	0.018575	0.018575	0.018575
401FT.	0.018575	0.018575	0.018575	0.018575	0.018575
406FT.	0.018575	0.018575	0.018575	0.018575	0.018575
411FT.	0.018575	0.018575	0.018575	0.018575	0.018575
416FT.	0.018575	0.018575	0.018575	0.018575	0.018575
421FT.	0.018575	0.018575	0.018575	0.018575	0.018575
426FT.	0.018575	0.018575	0.018575	0.018575	0.018575
431FT.	0.018575	0.018575	0.018575	0.018575	0.018575
436FT.	0.018575	0.018575	0.018575	0.018575	0.018575
441FT.	0.018575	0.018575	0.018575	0.018575	0.018575
446FT.	0.018575	0.018575	0.018575	0.018575	0.018575
451FT.	0.018575	0.018575	0.018575	0.018575	0.018575
456FT.	0.018575	0.018575	0.018575	0.018575	0.018575
461FT.	0.018575	0.018575	0.018575	0.018575	0.018575
466FT.	0.018575	0.018575	0.018575	0.018575	0.018575
471FT.	0.018575	0.018575	0.018575	0.018575	0.018575
476FT.	0.018575	0.018575	0.018575	0.018575	0.018575
481FT.	0.018575	0.018575	0.018575	0.018575	0.018575
486FT.	0.018575	0.018575	0.018575	0.018575	0.018575
491FT.	0.018575	0.018575	0.018575	0.018575	0.018575
496FT.	0.018575	0.018575	0.018575	0.018575	0.018575
501FT.	0.018575	0.018575	0.018575	0.018575	0.018575
506FT.	0.018575	0.018575	0.018575	0.018575	0.018575
511FT.	0.018575	0.018575	0.018575	0.018575	0.018575
516FT.	0.018575	0.018575	0.018575	0.018575	0.018575
521FT.	0.018575	0.018575	0.018575	0.018575	0.018575
526FT.	0.018575	0.018575	0.018575	0.018575	0.018575
531FT.	0.018575	0.018575	0.018575	0.018575	0.018575
536FT.	0.018575	0.018575	0.018575	0.018575	0.018575
541FT.	0.018575	0.018575	0.018575	0.018575	0.018575
546FT.	0.018575	0.018575	0.018575	0.018575	0.018575
551FT.	0.018575	0.018575	0.018575	0.018575	0.018575
556FT.	0.018575	0.018575	0.018575	0.018575	0.018575
561FT.	0.018575	0.018575	0.018575	0.018575	0.018575
566FT.	0.018575	0.018575	0.018575	0.018575	0.018575
571FT.	0.018575	0.018575	0.018575	0.018575	0.018575
576FT.	0.018575	0.018575	0.018575	0.018575	0.018575
581FT.	0.018575	0.018575	0.018575	0.018575	0.018575
586FT.	0.018575	0.018575	0.018575	0.018575	0.018575
591FT.	0.018575	0.018575	0.018575	0.018575	0.018575
596FT.	0.018575	0.018575	0.018575	0.018575	0.018575
601FT.	0.018575	0.018575	0.018575	0.018575	0.018575

€C6FT.	0.018575	0.C18575	C.018575	C.018575	C.018575
€11FT.	0.018575	0.C18575	C.018575	C.018575	0.018575
€16FT.	0.018575	0.C18575	C.018575	C.018575	0.018575
€21FT.	0.018575	0.C18575	C.018575	C.018575	0.018575
€26FT.	0.018575	0.C18575	C.018575	C.018575	0.018575
€31FT.	0.018575	0.C18575	C.018575	C.018575	0.018575
€36FT.	0.018575	0.C18575	C.018575	C.018575	0.018575
€41FT.	0.018575	0.C18575	C.018575	C.018575	0.018575
€46FT.	0.018575	0.C18575	C.018575	C.018575	C.018575

- WALL 2 SUPERIMPOSED ON WALL 1
- THERE ARE 50 FT. BETWEEN WALLS 1 AND 2

PREBLAST STRUCTURAL CONFIGURATION

SPACE BETWEEN WALLS 50. FT.

SOLVE

0PARTICLE SIZE:

4CSTORY BUILDING

10.CCFT. BETWEEN FLOORS

WIELD= 1CCC.CKT.

(VERPRESSURE= 10.0PSI

PARTICLE RADIUS	PERCENT OF PANEL
1C.CO FT.	C.13 X1CC
8.CO FT.	C.05 X1CC
6.CC FT.	C.45 X1CC
4.CC FT.	C.32 X1CC
2.CC FT.	C.05 X1CC

DISTANCE OF CURRENT WALL FROM STARTING WALL 5C.0 FT.

SIZE RANGE	1	8.00 IN. TO 1C.00 IN.
SIZE RANGE	2	6.00 IN. TO 8.00 IN.
SIZE RANGE	3	4.0C IN. TO 6.00 IN.
SIZE RANGE	4	2.0C IN. TO 4.00 IN.
SIZE RANGE	5	C. IN. TO 2.00 IN.

DEBRIS HEIGHT (FT.) AT 1FT. INTERVALS FROM CRICITAL POSITION

1FT.	C.	C.	C.	C.	C.
6FT.	0.33C0R4	0.4CR1?6	C.07EC72	C.445251	0.36718C
11FT.	0.528454	0.528454	C.6255C4C	C.296515	0.255358
16FT.	0.255358	0.255358	C.43E196	C.5274C3	0.407687
21FT.	0.407687	0.4939-3	C.51766C	C.5CCC55	0.53942C
26FT.	0.582C19	.C52413	C.445F15	C.445F15	0.644539
31FT.	0.542?C3	....	C.4C4127	C.4C4127	0.773387

36FT.	0.775632	0.654074	C.731747	C.775645	C.716664
41FT.	0.777205	0.849109	C.92C592	C.796858	0.929227
46FT.	0.902788	0.955474	1.C31642	C.957461	1.034885
51FT.	1.006507	0.983730	1.C97313	1.C85667	1.113363
56FT.	1.443976	1.553040	1.2EE397	1.643178	1.682931
61FT.	1.742439	1.872304	1.926735	1.651C55	1.454986
66FT.	1.482098	1.443774	1.653369	1.726457	1.559858
71FT.	1.524636	1.445767	1.691112	1.565416	1.633677
76FT.	1.669349	1.6C0065	1.4CC531	1.52CC71	1.641716
81FT.	1.586208	1.716903	1.631431	1.672250	1.898743
86FT.	1.876301	1.746087	1.885226	1.877741	1.852478
91FT.	1.963375	2.C12082	2.C75847	2.C09211	2.119190
96FT.	2.141227	2.172979	2.255258	2.189470	2.214633
101FT.	2.202095	2.128132	2.257347	2.195413	2.238518
106FT.	2.190524	2.198035	2.276671	2.232911	2.303137
111FT.	2.216219	2.299235	2.273856	2.256666	2.116663
116FT.	2.098244	2.074317	2.056216	2.055C6E	1.942787
121FT.	1.920696	1.916873	1.9C5388	1.8152CC	1.797449
126FT.	1.80[illegible]78	1.676686	1.641474	1.711197	1.610406
131FT.	1.616337	1.666722	1.567229	1.572C58	1.638480
136FT.	1.587948	1.521222	1.582687	1.5313CC	1.565C23
141FT.	1.615971	1.574492	1.566374	1.623873	1.600322
146FT.	1.630994	1.610059	1.616170	1.624564	1.572859
151FT.	1.571330	1.520144	1.535777	1.486C3C	1.484434
156FT.	1.435911	1.412430	1.428154	1.378126	1.330527
161FT.	1.345892	1.282658	1.298C83	1.229758	1.244813
166FT.	1.183193	1.197591	1.153227	1.15236C	1.086961
171FT.	1.101579	1.C56288	1.C13136	1.027516	0.969461
176FT.	0.983917	0.935303	C.894C96	C.8924E3	0.864772
181FT.	0.825031	0.803982	C.777367	C.722485	0.735717
186FT.	0.710320	0.637566	C.638C08	C.623459	0.623459
191FT.	0.624487	0.591807	C.592238	C.576669	0.575510
196FT.	0.558130	0.543998	C.544418	C.53C4C3	0.530959
2C1FT.	0.514006	0.500104	C.50C514	0.487263	0.470665
2C6FT.	0.456978	0.457380	C.444326	0.42EC57	0.414558
211FT.	0.415469	0.385683	C.38EC73	C.372752	0.373644
216FT.	0.344327	0.344711	C.332C53	C.316214	0.316214
221FT.	0.316701	0.3C1068	C.3C1C68	0.301546	0.286137
226FT.	0.286137	0.286137	C.286606	C.271411	0.271411
231FT.	0.271873	0.256855	C.256232	C.241384	0.241384
236FT.	0.241832	0.227148	C.22759C	C.213C41	0.213041
241FT.	0.213477	0.194079	C.195509	C.183541	0.183541

246FT.	0.184366	0.170234	C.170654	C.156639	0.156639
251FT.	0.157054	0.143152	C.143562	C.129770	0.130176
256FT.	0.116490	0.116892	C.103309	C.103707	0.090208
261FT.	0.090602	0.077201	C.077591	0.064270	0.064657
266FT.	0.050483	0.050867	C.037714	C.037714	0.037714
271FT.	0.037714	0.037714	C.037714	C.037714	0.037714
276FT.	0.037714	0.037714	C.037714	C.037714	0.037714
281FT.	0.037714	0.037714	C.036636	C.036636	0.036636
286FT.	0.036636	0.036636	C.036636	C.036636	0.036636
291FT.	0.036636	0.035778	C.035778	C.035778	0.035778
296FT.	0.035778	0.035778	C.035778	C.035778	0.035778
301FT.	0.035778	0.035778	C.035778	C.035778	0.035778
306FT.	0.035778	0.035778	C.035778	C.035778	0.035778
311FT.	0.035778	0.035778	C.035778	C.035778	0.035778
316FT.	0.034833	0.034833	C.034044	C.034044	0.034044
321FT.	0.034044	0.034044	C.034044	0.034044	0.034044
326FT.	0.034044	0.034044	C.034044	C.034044	0.034044
331FT.	0.034044	0.034044	C.034044	C.034044	0.034044
336FT.	0.034044	0.034044	C.034044	C.033304	0.033304
341FT.	0.033304	0.032446	C.032446	C.032446	0.032446
346FT.	0.032446	0.032446	C.032446	C.032446	0.032446
351FT.	0.032446	0.032446	C.032446	C.032446	0.032446
356FT.	0.032446	0.032446	C.031746	C.031746	0.031746
361FT.	0.031746	0.031746	C.031746	C.031746	0.031746
366FT.	0.031746	0.031746	C.030958	C.030958	0.030958
371FT.	0.030958	0.030958	C.030958	C.030958	0.030958
376FT.	0.030958	0.030958	C.030294	C.030294	0.030294
381FT.	0.030294	0.030294	C.030294	C.030294	0.030294
386FT.	0.030294	0.030294	C.030294	C.029554	0.029554
391FT.	0.029554	0.029554	C.029554	C.028917	0.028917
396FT.	0.028917	0.028917	C.028917	C.028917	0.028917
401FT.	0.028917	0.028917	C.028917	C.028917	0.028917
406FT.	0.028917	0.028917	C.028218	C.027606	0.027606
411FT.	0.027606	0.027606	C.027606	C.027606	0.027606
416FT.	0.027606	0.027606	C.027606	C.027606	0.027606
421FT.	0.027606	0.027606	C.027014	C.027014	0.027014
426FT.	0.027014	0.027014	C.026350	C.026350	0.026350
431FT.	0.026350	0.026350	C.026350	C.026350	0.026350
436FT.	0.026350	0.025777	C.025777	C.025777	0.025777
441FT.	0.025777	0.025777	C.025777	C.025141	0.025141
446FT.	0.025141	0.025141	C.025141	C.025141	0.024585

451FT.	0.024585	0.C24585	C.024585	C.024585	0.024585
456FT.	0.024585	0.C24585	C.024585	C.023973	0.023973
461FT.	0.023973	0.C23431	C.023431	C.023431	0.023431
466FT.	0.023431	0.C23431	C.023431	C.023431	0.023431
471FT.	0.023431	0.C23431	C.022839	C.022311	0.022311
476FT.	0.022311	0.C22311	C.022311	C.022311	0.022311
481FT.	0.022311	0.C22311	C.022311	C.021793	0.021793
486FT.	0.021793	0.C21223	C.021220	C.021220	0.021220
491FT.	0.021220	0.C21220	C.021220	C.021220	0.021220
496FT.	0.020715	0.C20715	C.020715	C.020715	0.020159
501FT.	0.020159	0.C20159	C.020159	C.020159	0.020159
506FT.	0.019664	0.C19664	C.019664	C.019664	0.019664
511FT.	0.019664	0.C19122	C.019122	C.019122	0.018635
516FT.	0.018635	0.C18635	C.018635	C.018635	0.018635
521FT.	0.018635	0.C18635	C.018635	C.017629	0.017629
526FT.	0.017629	0.C17629	C.017629	C.017629	0.017629
531FT.	0.017629	0.C17629	C.017629	C.016643	0.016643
536FT.	0.016643	0.C16643	C.016643	C.016643	0.016643
541FT.	0.016643	0.C16643	C.016182	C.016182	0.016182
546FT.	0.015676	0.C15676	C.015676	C.015676	0.015676
551FT.	0.015222	0.C15222	C.015222	C.015222	0.015222
556FT.	0.014727	0.C14727	C.014727	C.014279	0.014279
561FT.	0.014279	0.C14279	C.014279	C.014279	0.013792
566FT.	0.013350	0.C13350	C.013350	C.013350	0.013350
571FT.	0.013350	0.C13350	C.013350	C.012436	0.012436
576FT.	0.012436	0.C12436	C.012436	C.012436	0.012436
581FT.	0.012005	0.C12005	C.012005	C.011536	0.011536
586FT.	0.011536	0.C11536	C.011536	C.011112	0.011112
591FT.	0.011112	0.C11112	C.010650	C.010650	0.010650
596FT.	0.010230	0.C10230	C.010230	C.010230	0.010230
601FT.	0.009775	0.CC9775	C.009360	C.009360	0.009360
606FT.	0.009360	0.CC9360	C.009360	C.008912	0.008502
611FT.	0.008502	0.CC8502	C.008502	C.008502	0.008502
616FT.	0.008059	0.CC7653	C.007653	C.007653	0.007653
621FT.	0.007653	0.CC7653	C.007251	C.006815	0.006815
626FT.	0.006815	0.CC6815	C.006815	C.006417	0.006417
631FT.	0.005986	0.CC5986	C.005986	C.005986	0.005592
636FT.	0.005592	0.CC5592	C.005592	C.005168	0.005168
641FT.	0.004777	0.CC4777	C.004777	C.004777	0.004777
646FT.	0.004357	0.CC3970	C.003970	C.003970	0.003970
651FT.	0.003970	0.CC3970	C.003172	C.003172	0.003172
656FT.	0.003172	0.CC3172	C.003172	C.003172	0.002761

661FT.	0.002761	0.002761	C.002761	C.002761	0.002761
666FT.	0.002761	0.002355	C.002355	C.002355	0.002355
671FT.	0.002355	0.002355	C.001953	C.001953	0.001953
676FT.	0.001953	0.001953	C.001953	C.001555	0.001555
681FT.	0.001555	0.001555	C.001555	C.001555	0.001161
686FT.	0.001161	0.001161	C.001161	C.001161	0.001161
691FT.	0.000770	0.000770	C.000770	C.000770	0.000770
696FT.	0.000770	0.000383	C.000383	C.000383	0.000383

DISTRIBUTION OF SIZES AT 50 FT. FROM ORIGINAL POSITION

SIZE RANGE	PERCENT
1	40.75
2	8.56
3	40.84
4	9.35
5	0.50

DISTRIBUTION OF SIZES AT 150 FT. FROM ORIGINAL POSITION

SIZE RANGE	PERCENT
1	0.
2	0.
3	59.07
4	39.92
5	1.01

DISTRIBUTION OF SIZES AT 300 FT. FROM ORIGINAL POSITION

SIZE RANGE	PERCENT
1	0.
2	0.
3	0.
4	0.
5	100.00

CUMULATIVE DEBRIS MOMENTUM (FT./SEC.) AT 1FT INTERVALS FROM CRIGINAL POSITION
(MULTIPLY BY MASS OF ONE PANEL)

1FT.	0.	0.	C.	C.	0.	
6FT.	2.386594	3.C24842	C.638248	4.335165	3.696922	
11FT.	5.405084	5.405084	6.863768	3.60C971	3.454173	
16FT.	3.454173	3.454173	5.798788	7.248E43	5.687479	
21FT.	5.687479	7.145287	7.514SC6	7.505C77	8.083C16	
26FT.	9.117875	10.327536	7.949C13	7.949C13	11.618105	
31FT.	9.805254	11.565352	11.555785	11.555785	15.136837	
36FT.	15.474083	13.783531	15.566373	16.977215	15.565C96	
41FT.	17.333539	19.C91831	21.145230	19.269737	22.789765	
46FT.	22.465785	24.255568	26.381796	25.21289C	27.601C27	
51FT.	27.880796	27.571948	31.1C5674	31.147294	32.102242	
56FT.	35.941738	38.C67154	37.8CC467	41.546183	45.078152	
61FT.	44.739747	49.825205	49.842131	47.785916	43.749517	
66FT.	44.390951	42.935864	45.926836	46.4551C6	43.808444	
71FT.	42.344210	44.449048	45.615389	42.412744	43.647541	
76FT.	44.106723	42.401595	4C.831654	42.809C84	44.400753	
81FT.	44.393182	48.147382	46.052807	47.873285	53.462255	
86FT.	53.542328	51.490723	55.673360	56.249356	56.328443	
91FT.	60.136985	61.657838	63.349534	63.892C22	67.180837	
96FT.	68.928402	70.506271	73.595532	72.61C67C	73.242584	
1C1FT.	74.08C979	72.CC8894	76.1C6259	74.374C8C	75.896408	
1C6FT.	75.587868	76.525670	79.216564	78.057352	80.436105	
111FT.	78.969316	82.256065	81.415579	8C.274C46	76.973321	
116FT.	75.799600	74.937249	73.763126	73.455845	70.004C16	
121FT.	69.14C748	68.559748	67.516C1C	64.932331	63.741319	
126FT.	63.796240	59.111539	5E.059622	6C.658536	57.340965	
131FT.	57.288249	59.378694	56.047869	55.98C5E2	58.625983	
136FT.	57.135338	54.341329	5E.741124	55.906277	57.397484	
141FT.	59.454496	58.681102	5E.315399	6C.737379	60.497377	
146FT.	62.030810	61.818896	62.781930	62.965574	61.226681	
151FT.	61.245051	59.481812	6C.C45454	58.298632	58.312292	
156FT.	56.55C849	56.CC1483	5E.589491	54.934433	53.042569	
161FT.	53.639849	51.289660	51.89C931	49.542816	50.148819	
166FT.	47.779128	48.371863	46.568579	46.62445E	44.257925	
171FT.	44.876186	43.C84515	41.243653	41.87C534	39.455282	
176FT.	40.085879	38.315966	36.472857	36.523351	35.283204	
181FT.	33.442675	32.963549	31.735274	29.26773C	29.905214	
186FT.	28.689348	25.672457	25.69C162	25.1C1287	25.101287	

191FT.	25.135961	24.CC727C	24.025117	23.4C6CC2	23.397211
196FT.	22.876992	22.276025	22.293595	21.688678	21.705606
2C1FT.	21.183393	20.573856	2C.591966	19.995311	19.469763
2C6FT.	18.852150	18.870383	18.265920	17.737191	17.111156
211FT.	17.146631	15.965459	15.983914	15.349854	15.385523
216FT.	14.193503	14.212078	13.58766C	13.029C34	13.029C34
221FT.	13.046328	12.482687	12.482687	12.50CC32	11.932651
226FT.	11.932651	11.932651	11.95CC40	11.379C51	11.379051
231FT.	11.396520	10.821052	1C.818781	1C.239CC2	10.239C02
236FT.	10.256610	9.672674	9.69C379	9.1015C4	9.101504
241FT.	9.119265	8.526529	8.544377	7.92526C	7.925260
246FT.	7.943154	7.342187	7.36C157	6.754839	6.754839
251FT.	6.772882	6.163345	6.181454	5.567822	5.585995
256FT.	4.968382	4.986615	4.365132	4.383454	3.757418
261FT.	3.775792	3.146101	3.164556	2.53C537	2.549037
266FT.	1.892874	1.911449	1.269838	1.269838	1.269838
271FT.	1.269838	1.269838	1.269838	1.269838	1.269838
276FT.	1.269838	1.269838	1.269838	1.269838	1.269838
281FT.	1.269838	1.269838	1.25CC26	1.25CC26	1.250026
286FT.	1.250026	1.250026	1.25CC26	1.25CC26	1.250026
291FT.	1.250026	1.231955	1.231955	1.231955	1.231955
296FT.	1.231955	1.231955	1.231955	1.231955	1.231955
3C1FT.	1.231955	1.231955	1.231955	1.231955	1.231955
306FT.	1.231955	1.231955	1.231955	1.231955	1.231955
311FT.	1.231955	1.231955	1.231955	1.231955	1.231955
316FT.	1.213276	1.213276	1.195737	1.195737	1.195737
321FT.	1.195737	1.195737	1.195737	1.195737	1.195737
326FT.	1.195737	1.195737	1.195737	1.195737	1.195737
331FT.	1.195737	1.195737	1.195737	1.195737	1.195737
336FT.	1.195737	1.195737	1.195737	1.178402	1.178402
341FT.	1.178402	1.160330	1.16C330	1.16C33C	1.160330
346FT.	1.16C330	1.160330	1.16C330	1.16C33C	1.160330
351FT.	1.160330	1.160330	1.16C330	1.16C33C	1.160330
356FT.	1.160330	1.160330	1.143187	1.143187	1.143187
361FT.	1.143187	1.143187	1.143187	1.143187	1.143187
366FT.	1.143187	1.143187	1.125648	1.125648	1.125648
371FT.	1.125648	1.125648	1.125648	1.125648	1.125648
376FT.	1.125648	1.125648	1.1C8684	1.108684	1.108684
381FT.	1.108684	1.1C8684	1.1C8684	1.1C8684	1.108684
386FT.	1.108684	1.108684	1.1C8684	1.C91348	1.091348
391FT.	1.091348	1.C91348	1.091348	1.074416	1.074416

356FT.	1.074416	1.074416	1.074416	1.074416	1.074416
401FT.	1.074416	1.074416	1.074416	1.074416	1.074416
406FT.	1.074416	1.074416	1.057273	1.040379	1.040379
411FT.	1.040379	1.040379	1.040379	1.040379	1.040379
416FT.	1.040379	1.040379	1.040379	1.040379	1.040379
421FT.	1.040379	1.040379	1.023465	1.023465	1.023465
426FT.	1.023465	1.023465	1.006501	1.006501	1.006501
431FT.	1.006501	1.006501	1.006501	1.006501	1.006501
436FT.	1.006501	0.989577	0.989577	0.989577	0.989577
441FT.	0.989577	0.989577	0.989577	0.972645	0.972645
446FT.	0.972645	0.972645	0.972645	0.972645	0.955716
451FT.	0.955716	0.955716	0.955716	0.955716	0.955716
456FT.	0.955716	0.955716	0.955716	0.938821	0.938821
461FT.	0.938821	0.921843	0.921843	0.921843	0.921843
466FT.	0.921843	0.921843	0.921843	0.921843	0.921843
471FT.	0.921843	0.921843	0.904929	0.887909	0.887909
476FT.	0.887909	0.887909	0.887909	0.887909	0.887909
481FT.	0.887909	0.887909	0.887909	0.870808	0.870808
486FT.	0.870808	0.853884	0.853884	0.853884	0.853884
491FT.	0.853884	0.853884	0.853884	0.853884	0.853884
496FT.	0.836756	0.836756	0.836756	0.836756	0.819827
501FT.	0.819827	0.819827	0.819827	0.819827	0.819827
506FT.	0.802634	0.802634	0.802634	0.802634	0.802634
511FT.	0.802634	0.785655	0.785655	0.785655	0.768361
516FT.	0.768361	0.768361	0.768361	0.768361	0.768361
521FT.	0.768361	0.768361	0.768361	0.733996	0.733996
526FT.	0.733996	0.733996	0.733996	0.733996	0.733996
531FT.	0.733996	0.733996	0.733996	0.699506	0.699506
536FT.	0.699506	0.699506	0.699506	0.699506	0.699506
541FT.	0.699506	0.699506	0.682037	0.682037	0.682037
546FT.	0.664909	0.664909	0.664909	0.664909	0.664909
551FT.	0.647369	0.647369	0.647369	0.647369	0.647369
556FT.	0.630175	0.630175	0.630175	0.612568	0.612568
561FT.	0.612568	0.612568	0.612568	0.612568	0.595274
566FT.	0.577568	0.577568	0.577568	0.577568	0.577568
571FT.	0.577568	0.577568	0.577568	0.542463	0.542463
576FT.	0.542463	0.542463	0.542463	0.542463	0.542463
581FT.	0.524615	0.524615	0.524615	0.507226	0.507226
586FT.	0.507226	0.507226	0.507226	0.489333	0.489333
591FT.	0.489333	0.489333	0.471864	0.471864	0.471864
596FT.	0.453894	0.453894	0.453894	0.453894	0.453894
601FT.	0.436354	0.436354	0.418312	0.418312	0.418312

606FT.	0.418312	0.418312	C.41E312	C.40C7C4	0.382595
611FT.	0.382595	0.382595	C.382595	C.382595	0.382595
616FT.	0.364889	0.346716	C.346716	C.346716	0.346716
621FT.	0.346716	0.346716	C.328483	C.31C722	0.310722
626FT.	0.31C722	0.310722	C.31C722	C.2924CC	0.29240C
631FT.	0.274553	0.274553	C.274553	C.274553	0.256179
636FT.	0.256179	0.256179	C.256179	C.238286	0.238286
641FT.	C.219830	0.21983C	C.21983C	C.21983C	C.21983C
646FT.	0.20186C	0.183360	C.18336C	C.18336C	0.18336C
651FT.	0.183360	0.183360	C.146743	C.146743	0.146743
656FT.	0.146743	0.146743	C.146743	C.146743	0.128633
661FT.	0.128633	0.128633	C.12E633	C.128633	0.128633
666FT.	0.128633	0.110460	C.11C46C	C.11C46C	0.11046C
671FT.	0.110460	0.110460	C.092227	C.092227	0.092227
676FT.	0.092227	0.C92227	C.092227	C.C739C5	0.073905
681FT.	0.073905	0.C73905	C.073905	C.0739C5	0.055531
686FT.	0.055531	0.C55531	C.055531	0.055531	0.055531
691FT.	0.037076	0.C37076	C.037C76	C.037C76	0.037C76
696FT.	0.037076	0.C18575	C.018575	C.018575	0.018575

MINIMUM DEBRIS MOMENTUM (FT./SEC.) AT 1FT. INTERVALS FROM ORIGINAL POSITION
(MULTIPLY BY MASS OF ONE PANEL)

1FT.	0.	0.	C.	C.	0.
6FT.	0.	0.639248	C.	C.	C.
11FT.	1.708162	1.708162	1.498684	C.434124	0.434124
16FT.	0.434124	0.434124	C.434124	C.389408	0.389408
21FT.	0.389408	0.389408	C.369219	C.0417C8	0.369219
26FT.	0.369219	0.359099	C.358C99	C.358C99	0.353427
31FT.	0.353427	0.347978	C.347978	C.347978	0.347439
36FT.	0.347439	0.346072	C.346C72	C.3442C7	0.344207
41FT.	0.344207	0.344207	C.344207	C.3442C7	0.3442C7
46FT.	0.344207	0.344207	C.025715	C.025715	C.025715
51FT.	0.025715	0.C25715	C.025715	C.025715	C.025715
56FT.	0.025715	0.C25715	C.025715	C.025715	0.025715
61FT.	0.025715	0.C25715	C.025715	C.021756	0.021756
66FT.	0.021756	0.C21756	C.021756	C.021756	C.021756
71FT.	0.021756	0.C21756	C.021756	C.021756	C.021756
76FT.	0.021756	0.C19812	C.019812	C.019812	0.019812
81FT.	0.019812	0.C19812	C.019812	C.019812	0.019812
86FT.	0.019812	0.C19812	C.018678	C.018678	C.018678
91FT.	0.018678	0.C18678	C.018678	C.018678	0.018678
96FT.	0.018678	0.C18071	C.018C71	C.018C71	0.018C71
101FT.	0.018071	0.C18071	C.018C71	C.018C71	0.018C71
106FT.	0.017539	0.C17539	C.017539	C.017539	C.017539
111FT.	0.017539	0.C17539	C.017336	C.017336	0.017336
116FT.	0.017336	0.C17336	C.017336	C.017143	0.017143
121FT.	0.017143	0.C17143	C.017143	C.017143	0.017143
126FT.	C.016964	0.C16964	C.016964	C.016964	C.016964
131FT.	0.016932	0.C16932	C.016932	C.016932	C.016932
136FT.	0.016895	0.C16895	C.016895	C.016895	0.016895
141FT.	0.016895	0.C16895	C.016895	C.016895	0.016895
146FT.	0.016895	0.C16895	C.016895	C.016895	C.016895
151FT.	0.016895	0.C16895	C.016895	C.016895	0.016895
156FT.	0.016895	0.C16895	C.016895	C.016895	0.016895
161FT.	0.016895	0.C16895	C.016895	C.016895	0.016895
166FT.	0.016895	0.C16895	C.016895	C.016895	0.016895
171FT.	0.016895	0.C16895	C.016895	C.016895	0.016895
176FT.	0.016895	0.C16895	C.016895	C.016895	0.016895
181FT.	0.016895	0.C16895	C.016895	C.016895	0.016895
186FT.	0.016895	0.C16895	C.016895	C.016895	C.016895

191FT.	0.016895	0.016895	0.016895	0.016895	0.016895
196FT.	0.016895	0.016895	0.016895	0.016895	0.016895
201FT.	0.016895	0.016895	0.016895	0.016895	0.016895
206FT.	0.016895	0.016895	0.016895	0.016895	0.016895
211FT.	0.016895	0.016895	0.016895	0.016895	0.016895
216FT.	0.016895	0.016895	0.016895	0.016895	0.016895
221FT.	0.016895	0.016895	0.016895	0.016895	0.016895
226FT.	0.016895	0.016895	0.016895	0.016895	0.016895
231FT.	0.016895	0.016895	0.016895	0.016895	0.016895
236FT.	0.016895	0.016895	0.016895	0.016895	0.016895
241FT.	0.016895	0.016895	0.016895	0.016895	0.016895
246FT.	0.016895	0.016895	0.016895	0.016895	0.016895
251FT.	0.016895	0.016895	0.016895	0.016895	0.016895
256FT.	0.016895	0.016895	0.016895	0.016895	0.016895
261FT.	0.016895	0.016895	0.016895	0.016895	0.016895
266FT.	0.016895	0.016895	0.016895	0.016895	0.016895
271FT.	0.016895	0.016895	0.016895	0.016895	0.016895
276FT.	0.016895	0.016895	0.016895	0.016895	0.016895
281FT.	0.016895	0.016895	0.016895	0.016895	0.016895
286FT.	0.016895	0.016895	0.016895	0.016895	0.016895
291FT.	0.016895	0.016895	0.016895	0.016895	0.016895
296FT.	0.016895	0.016895	0.016895	0.016895	0.016895
301FT.	0.016895	0.016895	0.016895	0.016895	0.016895
306FT.	0.016895	0.016895	0.016895	0.016895	0.016895
311FT.	0.016895	0.016895	0.016895	0.016895	0.016895
316FT.	0.016895	0.016895	0.016895	0.016895	0.016895
321FT.	0.016895	0.016895	0.016895	0.016895	0.016895
326FT.	0.016895	0.016895	0.016895	0.016895	0.016895
331FT.	0.016895	0.016895	0.016895	0.016895	0.016895
336FT.	0.016895	0.016895	0.016895	0.016895	0.016895
341FT.	0.016895	0.016895	0.016895	0.016895	0.016895
346FT.	0.016895	0.016895	0.016895	0.016895	0.016895
351FT.	0.016895	0.016895	0.016895	0.016895	0.016895
356FT.	0.016895	0.016895	0.016895	0.016895	0.016895
361FT.	0.016895	0.016895	0.016895	0.016895	0.016895
366FT.	0.016895	0.016895	0.016895	0.016895	0.016895
371FT.	0.016895	0.016895	0.016895	0.016895	0.016895
376FT.	0.016895	0.016895	0.016895	0.016895	0.016895
381FT.	0.016895	0.016895	0.016895	0.016895	0.016895
386FT.	0.016895	0.016895	0.016895	0.016895	0.016895
391FT.	0.016895	0.016895	0.016895	0.016895	0.016895

396FT.	0.016895	0.016895	C.C16E95	C.C16E95	C.016895
401FT.	0.016895	0.016895	C.016895	C.016895	C.016895
406FT.	0.016895	0.016895	C.016E95	C.016E95	0.016E95
411FT.	0.016895	0.016895	C.016E95	C.016E95	0.016895
416FT.	0.016895	0.016895	C.016E95	C.016E95	C.016895
421FT.	0.016895	0.016895	C.016E95	C.016E95	C.016895
426FT.	C.016895	0.016895	C.016E95	C.016E95	C.016895
431FT.	0.016895	0.016895	C.016E95	C.016E95	0.016895
436FT.	0.016895	0.016895	C.016E95	C.016E95	0.016895
441FT.	0.016895	0.016895	C.016E95	C.016E95	0.016895
446FT.	C.016895	0.016895	C.016E95	C.016E95	0.016895
451FT.	0.016895	0.016895	C.016E95	C.016E95	C.016895
456FT.	0.016895	0.016895	C.016E95	C.016914	0.016914
461FT.	0.016914	0.016914	C.016914	C.016914	C.016914
466FT.	0.016914	0.016914	C.016914	C.016914	0.016914
471FT.	0.016914	0.016914	C.016924	C.016924	0.016924
476FT.	0.016924	0.016924	C.016924	C.016924	0.016924
481FT.	0.016924	0.016924	C.016924	C.016924	C.016924
486FT.	C.016924	0.016928	C.016928	C.016928	0.016928
491FT.	0.016928	0.016928	C.016928	C.016928	0.016928
496FT.	0.016928	0.016928	C.016928	C.016928	0.016978
501FT.	0.016978	0.016974	C.016978	C.016978	C.016978
506FT.	C.016978	0.016978	C.016978	C.016978	0.016978
511FT.	0.016976	C.017020	C.017020	C.017020	0.017020
516FT.	0.017020	0.017020	C.017020	C.017020	0.017020
521FT.	0.017020	0.017020	C.017020	C.017101	C.017101
526FT.	C.017101	0.017101	C.017101	C.017101	C.017101
531FT.	0.017101	0.017101	C.017101	C.017128	0.017128
536FT.	0.017128	0.017128	C.017128	C.017128	0.017128
541FT.	0.017128	0.017128	C.017128	C.017128	C.017128
546FT.	0.017194	0.017194	C.017194	C.017194	0.017194
551FT.	0.017194	0.017194	C.017194	C.017194	0.017194
556FT.	0.017294	0.017294	C.017294	C.017294	0.017294
561FT.	0.017294	0.017294	C.017294	C.017294	C.017345
566FT.	C.017345	C.017345	C.017345	C.017345	0.017345
571FT.	0.017345	0.017345	C.017345	C.017389	0.017389
576FT.	0.017389	0.017389	C.017389	C.017389	0.017389
581FT.	0.017389	0.017389	C.017389	C.017468	C.017468
586FT.	0.017468	0.017468	C.017468	C.017468	0.017468
591FT.	0.017468	0.017468	C.017541	C.017541	0.017541
596FT.	0.017541	0.017541	C.017541	C.017541	0.017541
601FT.	0.017607	0.017607	C.017607	C.017607	0.017607

606FT.	0.017607	0.017607	0.017607	0.017706	0.017706
611FT.	0.017706	0.017706	0.017706	0.017706	0.017706
616FT.	0.017761	0.017761	0.017761	0.017761	0.017761
621FT.	0.017761	0.017761	0.017761	0.017848	0.017848
626FT.	0.017848	0.017848	0.017848	0.017848	0.017848
631FT.	0.017893	0.017893	0.017893	0.017893	0.017893
636FT.	0.017893	0.017893	0.017893	0.017970	0.017970
641FT.	0.017970	0.017970	0.017970	0.017970	0.017970
646FT.	0.018042	0.018042	0.018042	0.018042	0.018042
651FT.	0.018042	0.018042	0.	0.	0.
656FT.	0.	0.	0.	0.	0.
661FT.	0.	0.	0.	0.	0.
666FT.	0.	0.	0.	0.	0.
671FT.	0.	0.	0.	0.	0.
676FT.	0.	0.	0.	0.	0.
681FT.	0.	0.	0.	0.	0.
686FT.	0.	0.	0.	0.	0.
691FT.	0.	0.	0.	0.	0.
696FT.	0.	0.	0.	0.	0.

MAXIMUM DEBRIS MOMENTUM (FT./SEC.) AT 1FT. INTERVALS FROM ORIGINAL POSITION
(MULTIPLY BY MASS OF ONE PANEL)

1FT.	0.	0.	C.	C.	0.
6FT.	2.386594	2.386594	C.638248	3.696922	3.696922
11FT.	3.696922	3.696922	3.696922	1.708162	1.561364
16FT.	1.561364	1.561364	2.344616	2.344616	2.344616
21FT.	2.344616	2.344616	2.344616	2.344616	2.344616
26FT.	2.344616	2.344616	2.036624	2.036624	2.036624
31FT.	2.036624	2.036624	2.036624	2.036624	2.036624
36FT.	2.036624	1.896301	1.896301	1.896301	1.896301
41FT.	1.896301	1.896301	1.896301	1.818809	1.818809
46FT.	1.818809	1.818809	1.818809	1.818809	1.818809
51FT.	1.782281	1.782281	1.782281	1.782281	1.782281
56FT.	2.386594	2.386594	1.747065	3.696922	3.696922
61FT.	3.696922	3.696922	3.696922	1.739187	1.738668
66FT.	1.743933	1.743933	2.344616	2.344616	2.344616
71FT.	2.344616	2.344616	2.344616	2.344616	2.344616
76FT.	2.344616	2.344616	2.036624	2.036624	2.036624
81FT.	2.036624	2.036624	2.036624	2.036624	2.036624
86FT.	2.036624	1.896301	1.896301	1.896301	1.896301
91FT.	1.896301	1.896301	1.896301	1.874929	1.879836
96FT.	1.887766	1.891980	1.899187	1.899187	1.899187
101FT.	1.899187	1.899187	1.899187	1.899187	1.899187
106FT.	1.899187	1.899187	1.899187	1.899187	1.899187
111FT.	1.899187	1.899187	1.899187	1.899187	1.899187
116FT.	1.899187	1.899187	1.899187	1.899187	1.899187
121FT.	1.899187	1.899187	1.899187	1.899187	1.899187
126FT.	1.899187	1.899187	1.899187	1.899187	1.899187
131FT.	1.899187	1.899187	1.899187	1.899187	1.899187
136FT.	1.899187	1.833348	1.840862	1.847872	1.854405
141FT.	1.860499	1.866183	1.866183	1.874929	1.879836
146FT.	1.887766	1.891980	1.899187	1.899187	1.899187
151FT.	1.899187	1.899187	1.899187	1.899187	1.899187
156FT.	1.899187	1.899187	1.899187	1.899187	1.899187
161FT.	1.899187	1.899187	1.899187	1.899187	1.899187
166FT.	1.899187	1.899187	1.899187	1.899187	1.899187
171FT.	1.899187	1.899187	1.899187	1.899187	1.899187
176FT.	1.899187	1.899187	1.899187	1.899187	1.899187
181FT.	1.899187	1.899187	1.899187	1.899187	1.899187
186FT.	1.899187	0.641611	C.641611	C.641611	0.641611

191FT.	0.641611	0.641611	C.641611	C.641611	0.641611
196FT.	0.641611	0.641611	C.641611	C.641611	0.641611
201FT.	0.641611	0.641611	C.641611	C.641611	0.641611
206FT.	C.641611	0.641611	C.641611	C.641611	0.641611
211FT.	0.641611	0.641611	C.641611	C.641611	0.641611
216FT.	C.641611	0.641611	C.641611	C.641611	0.641611
221FT.	0.641611	0.641611	C.641611	C.641611	0.641611
226FT.	0.641611	0.641611	C.641611	C.641611	0.641611
231FT.	C.641611	0.641611	C.641611	C.641611	0.641611
236FT.	0.641611	0.641611	C.641611	C.641611	0.641611
241FT.	0.641611	0.641611	C.641611	C.641611	0.641611
246FT.	C.641611	0.641611	C.641611	C.641611	0.641611
251FT.	0.641611	0.641611	C.641611	C.641611	0.641611
256FT.	0.641611	C.641611	C.641611	C.641611	0.641611
261FT.	0.641611	0.641611	C.641611	C.641611	0.641611
266FT.	0.641611	0.641611	C.019812	C.019812	0.019812
271FT.	0.019812	0.019812	C.019812	C.019812	0.019812
276FT.	0.019812	0.019812	C.019812	C.019812	0.019812
281FT.	0.019812	0.019812	C.018678	C.018678	0.018678
286FT.	0.018678	0.018678	C.018678	C.018678	0.018678
291FT.	0.018678	0.018678	C.018678	C.018678	C.018678
296FT.	C.018678	0.018678	C.018678	C.018678	C.018678
301FT.	0.018678	0.018678	C.018678	C.018678	0.018678
306FT.	0.018678	0.018678	C.018678	C.018678	C.018678
311FT.	0.018678	0.018678	C.018678	C.018678	C.018678
316FT.	C.018575	0.018575	C.018575	C.018575	0.018575
321FT.	0.018575	0.018575	C.018575	C.018575	0.018575
326FT.	0.018575	0.018575	C.018575	C.018575	C.018575
331FT.	C.018575	0.018575	C.018575	C.018575	0.018575
336FT.	C.018575	0.018575	C.018575	C.018575	0.018575
341FT.	0.018575	0.018575	C.018575	C.018575	0.018575
346FT.	0.018575	C.018575	C.018575	C.018575	C.018575
351FT.	0.018575	0.018575	C.018575	C.018575	0.018575
356FT.	0.018575	0.018575	C.018575	C.018575	0.018575
361FT.	0.018575	0.018575	C.018575	C.018575	0.018575
366FT.	0.018575	0.018575	C.018575	C.018575	0.018575
371FT.	0.018575	0.018575	C.018575	C.018575	0.018575
376FT.	C.018575	C.018575	C.018575	C.018575	0.018575
381FT.	0.018575	C.018575	C.018575	C.018575	0.018575
386FT.	0.018575	0.018575	C.018575	C.018575	0.018575
391FT.	0.018575	0.018575	C.018575	C.018575	0.018575

396FT.	0.018575	0.018575	0.018575	0.018575	0.018575
401FT.	0.018575	0.018575	0.018575	0.018575	0.018575
406FT.	0.018575	0.018575	0.018575	0.018575	0.018575
411FT.	0.018575	0.018575	0.018575	0.018575	0.018575
416FT.	0.018575	0.018575	0.018575	0.018575	0.018575
421FT.	0.018575	0.018575	0.018575	0.018575	0.018575
426FT.	0.018575	0.018575	0.018575	0.018575	0.018575
431FT.	0.018575	0.018575	0.018575	0.018575	0.018575
436FT.	0.018575	0.018575	0.018575	0.018575	0.018575
441FT.	0.018575	0.018575	0.018575	0.018575	0.018575
446FT.	0.018575	0.018575	0.018575	0.018575	0.018575
451FT.	0.018575	0.018575	0.018575	0.018575	0.018575
456FT.	0.018575	0.018575	0.018575	0.018575	0.018575
461FT.	0.018575	0.018575	0.018575	0.018575	0.018575
466FT.	0.018575	0.018575	0.018575	0.018575	0.018575
471FT.	0.018575	0.018575	0.018575	0.018575	0.018575
476FT.	0.018575	0.018575	0.018575	0.018575	0.018575
481FT.	0.018575	0.018575	0.018575	0.018575	0.018575
486FT.	0.018575	0.018575	0.018575	0.018575	0.018575
491FT.	0.018575	0.018575	0.018575	0.018575	0.018575
496FT.	0.018575	0.018575	0.018575	0.018575	0.018575
501FT.	0.018575	0.018575	0.018575	0.018575	0.018575
506FT.	0.018575	0.018575	0.018575	0.018575	0.018575
511FT.	0.018575	0.018575	0.018575	0.018575	0.018575
516FT.	0.018575	0.018575	0.018575	0.018575	0.018575
521FT.	0.018575	0.018575	0.018575	0.018575	0.018575
526FT.	0.018575	0.018575	0.018575	0.018575	0.018575
531FT.	0.018575	0.018575	0.018575	0.018575	0.018575
536FT.	0.018575	0.018575	0.018575	0.018575	0.018575
541FT.	0.018575	0.018575	0.018575	0.018575	0.018575
546FT.	0.018575	0.018575	0.018575	0.018575	0.018575
551FT.	0.018575	0.018575	0.018575	0.018575	0.018575
556FT.	0.018575	0.018575	0.018575	0.018575	0.018575
561FT.	0.018575	0.018575	0.018575	0.018575	0.018575
566FT.	0.018575	0.018575	0.018575	0.018575	0.018575
571FT.	0.018575	0.018575	0.018575	0.018575	0.018575
576FT.	0.018575	0.018575	0.018575	0.018575	0.018575
581FT.	0.018575	0.018575	0.018575	0.018575	0.018575
586FT.	0.018575	0.018575	0.018575	0.018575	0.018575
591FT.	0.018575	0.018575	0.018575	0.018575	0.018575
596FT.	0.018575	0.018575	0.018575	0.018575	0.018575
601FT.	0.018575	0.018575	0.018575	0.018575	0.018575

606FT.	0.018575	0.018575	0.018575	0.018575	0.018575
611FT.	0.018575	0.018575	0.018575	0.018575	0.018575
616FT.	0.018575	0.018575	0.018575	0.018575	0.018576
621FT.	0.018575	0.018575	0.018575	0.018575	0.018575
626FT.	0.018575	0.018575	0.018575	0.018575	0.018575
631FT.	0.018575	0.018575	0.018575	0.018575	0.018575
636FT.	0.018575	0.018575	0.018575	0.018575	0.018575
641FT.	0.018575	0.018575	0.018575	0.018575	0.018575
646FT.	0.018575	0.018575	0.018575	0.018575	0.018575
651FT.	0.018575	0.018575	0.018575	0.018575	0.018575
656FT.	0.018575	0.018575	0.018575	0.018575	0.018575
661FT.	0.018575	0.018575	0.018575	0.018575	0.018575
666FT.	0.018575	0.018575	0.018575	0.018575	0.018575
671FT.	0.018575	0.018575	0.018575	0.018575	0.018575
676FT.	0.018575	0.018575	0.018575	0.018575	0.018575
681FT.	0.018575	0.018575	0.018575	0.018575	0.018575
686FT.	0.018575	0.018575	0.018575	0.018575	0.018575
691FT.	0.018575	0.018575	0.018575	0.018575	0.018575
696FT.	0.018575	0.018575	0.018575	0.018575	0.018575

* WALL 3 SUPERIMPOSED ON WALLS 1 AND 2

* THERE ARE 100 FT. BETWEEN WALLS 2 AND 3

* WALL 3 IS ONLY 30 FLOORS HIGH

PREBLAST STRUCTURAL CONFIGURATION

WALL HEIGHT 30 FLOORS

SPACE BETWEEN WALLS 100. FEET

SOLVE

SPARTICLE SIZES

30STORY BUILDING

10.00FT. BETWEEN FLOORS

YIELD= 1000.0KT.

OVERPRESSURE= 10.0PSI

PARTICLE RADIUS	PERCENT OF PANEL
10.00 FT.	0.13 X100
8.00 FT.	0.05 X100
6.00 FT.	0.40 X100
4.00 FT.	0.32 X100
2.00 FT.	0.09 X100

DISTANCE OF CURRENT WALL FROM STARTING WALL 150.0 FT.

SIZE RANGE	1	8.00 IN. TO	10.00 IN.
SIZE RANGE	2	6.00 IN. TO	8.00 IN.
SIZE RANGE	3	4.00 IN. TO	6.00 IN.
SIZE RANGE	4	2.00 IN. TO	4.00 IN.
SIZE RANGE	5	0. IN. TO	2.00 IN.

DEBRIS HEIGHT (FT.) AT 1FT. INTERVALS FROM ORIGINAL POSITION

1FT.	0.	0.	0.	0.	0.
6FT.	0.330084	0.408156	0.078072	0.445252	0.367180
11FT.	0.528454	0.528454	0.625690	0.296515	0.255358
16FT.	0.255358	0.255358	0.438196	0.527403	0.407687
21FT.	0.407687	0.493983	0.517660	0.500055	0.539420
26FT.	0.582019	0.652413	0.449815	0.449815	0.644539
31FT.	0.542903	0.618976	0.604127	0.604127	0.773387

* WALL 4 SUPERIMPOSED ON WALLS 1,2, AND 3

* THERE ARE 35 FT. BETWEEN WALLS 3 AND 4

* WALL 4 IS THE SAME HEIGHT AS WALL 3

PREPLAST STRUCTURAL CONFIGURATION

SPACE BETWEEN WALLS 35. FEET

SOLVE

5PARTICLE SIZES

3CSTORY BUILDING

1C.CCFT. BETWEEN FLCORS

YIELD= 1CCC.CKT.

CVERPRESSURE= 10.0PSI

PARTICLE RADIUS	PERCENT OF PANEL
1C.CC FT.	C.13 X1CC
8.CC FT.	C.05 X1CC
6.CC FT.	C.45 X1CC
4.CC FT.	C.32 X1CC
2.CC FT.	C.05 X1CC

DISTANCE OF CURRENT WALL FROM STARTING WALL 185.0 FT.

SIZE RANGE	1	8.0C IN. TO 1C.CO IN.
SIZE RANGE	2	6.00 IN. TO 8.CO IN.
SIZE RANGE	3	4.00 IN. TO 6.CO IN.
SIZE RANGE	4	2.0C IN. TO 4.CO IN.
SIZE RANGE	5	C. IN. TO 2.CO IN.

PARTS PER FOOT (SQ.) AT 5 FT. INTERVALS FROM ORIGINAL POSITION

1FT.	0.	0.	C.	C.	0.
6FT.	0.330084	0.408156	C.C78C72	C.445253	0.367180
11FT.	0.529454	0.528454	C.625690	C.296915	0.255358
16FT.	0.255358	0.255358	C.43E196	C.5274C3	0.407687
21FT.	C.407687	0.493983	C.517660	C.5CCC55	0.539420
26FT.	C.582019	0.652413	C.449815	C.449815	0.644539
31FT.	0.542903	0.618976	C.6C4127	C.604127	0.773387
36FT.	0.775632	0.654074	C.731747	C.775649	0.716664

```
*     SAMPLE PROBLEM II VARIATION OF AERODYNAMIC COEFFICIENTS FOR A
*     SINGLE MASONRY BRICK WITH 2.25 X 3.75 X 8 INCH NOMINAL DIMENSIONS
*     CASE 1 EQUIVALENT SPHERICAL RADIUS = 2.53 INCHES
WEAPON PARAMETERS
YIELD (CCC. MEGATONS
OVERPRESSURE 10. PSI
FREEBLAST STRUCTURAL CONFIGURATION
WALL HEIGHT 40 FLOORS
HEIGHT BETWEEN FLOORS 10. FEET
SPACE BETWEEN WALLS C.C FEET
NORMALIZING FACTOR 3.333
FRAGMENTATION CHARACTERISTICS
NUMBER OF PARTICLE SIZES 1
PARTICLE SIZES 2.53
PERCENTAGE BY SIZE 1.0
ACCELERATION COEFFICIENT C.C
CLIPLT
PROFILE DISTRIBUTION 1
DISTRIBUTION OF SIZES 1
LOCATIONS 3
```

DISTANCES FROM FIRST WALL 5C.,6O.,7C.,8C.,1CC. FEET

VELCCITY DESCRIPTICN 1

DEBRIS PROFILE PLCT 1

SCLVE

UNCLASSIFIED

Security Classification

DOCUMENT CONTROL DATA - R&D

(Security classification of title, body of abstract and indexing annotation must be entered when the overall report is classified)

1 ORIGINATING ACTIVITY *(Corporate author)*
IIT Research Institute
Technology Center
Chicago, Illinois 60616

2a. REPORT SECURITY CLASSIFICATION
N/A

2b GROUP
N/A

3 REPORT TITLE

DEBRIS FORMATION AND TRANSLATION

4 DESCRIPTIVE NOTES *(Type of report and inclusive dates)*
Final Report

5 AUTHOR(S) *(Last name, first name, initial)*

Barnett, Ralph L. Costello, James F. Feinstein, David F.

6 REPORT DATE	7a TOTAL NO OF PAGES	7b NO OF REFS
November 1966	186	16

8a CONTRACT OR GRANT NO.
OCD-PS-64-201

b PROJECT NO
M6103

c
Subcontract No.
d B-70942(4949 A-34)-US

9a ORIGINATOR'S REPORT NUMBER(S)
Work Unit 33228

9b OTHER REPORT NO(S) *(Any other numbers that may be assigned this report)*

10 AVAILABILITY/LIMITATION NOTICES

Distribution of this document is unlimited.

11 SUPPLEMENTARY NOTES

12 SPONSORING MILITARY ACTIVITY
Department of the Army
Office of Secretary of the Army
Office of Civil Defense

13 ABSTRACT

A comprehensive view is taken of the physical models required to estimate volumes and heights of blast-initiated debris. Particular emphasis and development is directed toward three areas: the fragmentation of frangible elements, the failure of elements with limited ductility, and the transport of debris particles by blast winds. Computer programs to handle the computations involved in these three models have been written.

DD FORM 1473

UNCLASSIFIED

Security Classification